

11-17-2017

Selective Sensing of Ions and Ion Pairs of Environmental and Forensic Significance

Tosin Mobolaji Jonah

Florida International University, tjona002@fiu.edu

DOI: 10.25148/etd.FIDC004059

Follow this and additional works at: <https://digitalcommons.fiu.edu/etd>

 Part of the [Life Sciences Commons](#)

Recommended Citation

Jonah, Tosin Mobolaji, "Selective Sensing of Ions and Ion Pairs of Environmental and Forensic Significance" (2017). *FIU Electronic Theses and Dissertations*. 3498.

<https://digitalcommons.fiu.edu/etd/3498>

This work is brought to you for free and open access by the University Graduate School at FIU Digital Commons. It has been accepted for inclusion in FIU Electronic Theses and Dissertations by an authorized administrator of FIU Digital Commons. For more information, please contact dcc@fiu.edu.

FLORIDA INTERNATIONAL UNIVERSITY

Miami, Florida

SELECTIVE SENSING OF IONS AND ION PAIRS OF ENVIRONMENTAL AND
FORENSIC SIGNIFICANCE

A dissertation submitted in partial fulfillment of the

requirements for the degree of

DOCTOR OF PHILOSOPHY

in

CHEMISTRY

by

Tosin Mobolaji Jonah

2017

To: Dean Michael R. Heithaus
College of Arts, Sciences and Education

This dissertation, written by Tosin Mobolaji Jonah, and entitled Selective Sensing of Ions and Ion Pairs of Environmental and Forensic Significance, having been approved in respect to style and intellectual content, is referred to you for judgment.

We have read this dissertation and recommend that it be approved.

José R. Almirall

Bruce R. McCord

Francisco A. Fernandez-Lima

Chenzhong Li

Konstantinos Kavallieratos, Major Professor

Date of Defense: November 17, 2017

The dissertation of Tosin Mobolaji Jonah is approved.

Dean Michael R. Heithaus
College of Arts, Sciences and Education

Andrés G. Gil
Vice President for Research and Economic Development
and Dean of the University Graduate School

Florida International University, 2017

© Copyright 2017 by Tosin Mobolaji Jonah
All rights reserved.

DEDICATION

I dedicate this dissertation to my family, most especially Tola and Ewaoluwa for all of their love and support.

ACKNOWLEDGMENTS

I would like to thank my PhD advisor, Dr. Konstantinos Kavallieratos for his advice, support and guidance during my PhD studies. I would like to thank my committee members: Dr. José Almirall, Dr. Bruce McCord, Dr. Francisco Fernandez-Lima, and Dr. Chenzhong Li for providing me with useful feedback during my studies.

I would like to thank all the past and present members of Dr. Kavallieratos's lab. I would also like to thank the University Graduate School for awarding me the Doctoral Evidence Acquisition (DEA) Fellowship Award, which allowed me to collect the data used in this work. I would like to thank the Department of Chemistry & Biochemistry for providing me funding through teaching assistantships. I would also like to thank my friends: Sauday, Deborah and Olubunmi for all their moral support. I would also want to thank my WOLBM family, without you guys surviving the last two years of my PhD would have been impossible. You guys are my rock.

Lastly, I would like to express my deepest gratitude to my family, my mother Esther and father Emmanuel Afolabi, and my siblings: Ope, Yemisi, Tobi and Damilare. I thank you all for the advice, support and unconditional love.

ABSTRACT OF THE DISSERTATION

SELECTIVE SENSING OF IONS AND ION PAIRS OF ENVIRONMENTAL AND FORENSIC SIGNIFICANCE.

by

Tosin Mobolaji Jonah

Florida International University, 2017

Miami, Florida

Professor Konstantinos Kavallieratos, Major Professor

Dual-host combinations of cation and anion sensors have unique potential for selective detection of ion pairs, such as NH_4NO_3 , via solvent extraction. Selective sensors for NH_4^+ and NO_3^- were synthesized and used together for ion-pair sensing of ammonium nitrate both in organic solvents (using $\text{Bu}_4\text{N}^+\text{NO}_3^-$ and $\text{NH}_4^+\text{PF}_6^-$) and in extraction of NH_4NO_3 from water into dichloromethane. A fluorescent sensor for NH_4^+ based on 1,3,5-triethylbenzene framework shows remarkable binding and sensing selectivity for NH_4^+ vs. K^+ . Fluorescence and $^1\text{H-NMR}$ titrations reveal surprising differences in sensing properties and binding constants for the tris-(3,5-dimethyl)pyrazole vs. the tris-(3,5-diphenyl)pyrazole. X-ray and theoretical DFT studies reveals the role of ion pairing and solvation is revealed by (Chapter 2). We have also demonstrated a unique dual-host extraction-based ion-pair sensing paradigm using Förster Resonance Energy Transfer (FRET), showing selectivity for NH_4NO_3 . The fluorescence emission of the NH_4^+ sensor tris-(3,5-dimethyl)pyrazole (305-340 nm), is compatible with the excitation wavelength of the dansyl fluorophore of the nitrate sensor 1,3,5-Tris-(5-dimethylamino-1-naphthalenesulfonamido)methyl]-2,4,6-triethylbenzene, thus resulting in FRET emission

upon combined use of these two sensors for the NH_4NO_3 ion pair. Contact of dichloromethane solutions containing the two hosts with aqueous solutions of NH_4NO_3 ($1 \times 10^{-5} \text{ M}$ to $1 \times 10^{-4} \text{ M}$), resulted in FRET fluorescence enhancements at 510 nm, with increasing concentrations of NH_4NO_3 , while NaNO_3 , KNO_3 , NaCl and KCl showed only minimal fluorescence responses, under identical conditions (Chapter 3). The ability of the tris-pyrazole framework to bind cations, such as NH_4^+ , was also exploited in a detailed fluorescence and $^1\text{H-NMR}$ Ln(III) binding study using tris-pyrazole ligands with varying substitution patterns. The dependence of fluorescence responses on pyrazole substitution that had been observed for NH_4^+ (Chapter 2), was also observed for several Ln(III), indicating the significant role of ion pairing for Ln(III) binding and fluorescence sensing (Chapter 4). These findings can lead to new selective Lanthanide (Ln) and Actinide (An) extractants and sensors, which are important for nuclear separation and extraction processes and detection of fission products. Likewise, the tris-dansyl nitrate receptor (Chapter 3) was also found to be an efficient Hg(II) fluorescent sensor, in its deprotonated form, showing fluorescence quenching, with no responses for Ca(II), Ag(I), Co(II), Cu(II), and Cd(II), and a fluorescence enhancement for Zn(II). The responses to Hg(II) were also observed in the presence of those competing cations, in competitive titration experiments. An X-ray crystal structure showed the ability of this receptor in its trianionic version to bind three Hg(II) atoms, also containing three CH_3COO^- counteranions. The X-ray crystal structure of the same receptor with HgCl_2 showed instead a 2:1 complexation pattern, with one Hg atom complexed by two bis-deprotonated receptor molecules (Chapter 5).

TABLE OF CONTENTS

CHAPTER	PAGE
I.	A Review: Ion pair receptors and fluorescence sensing.....1
	1.1. Ion pair sensing.....2
	1.2. Ion pair receptors.....2
	1.3. Ditopic ion pair receptors.....4
	1.3.1. Ditopic receptors based on spatially separated ion.....4
	1.3.2. Ditopic Receptors based on contact ion pairs.....6
	1.4. Dual-host ion pair receptors.....8
	1.5. Ion-pair receptors as sensors.....10
	1.6. Ion pair extraction.....12
	1.7. Solvation effects in ion pairing.....13
	1.8. Fluorescence sensors.....14
	1.8.1. The charge transfer processes.....15
	1.8.2. Photoinduced electron transfer (PET)....16
	1.8.3. Electronic energy transfer (EET).....17
	1.9. Methodology for quantifying supramolecular interactions18
	1.10. Overview of NH_4^+ receptors.....21
	1.11. Overview of nitrate receptors.....23
	1.12. Overview of mercury (II) sensors.....25
	1.13. Overview of lanthanide receptors.....26
	1.14. References.....27
II.	Remarkably selective NH_4^+ binding and fluorescence sensing by tripodal tris(pyrazolyl) receptors derived from 1,3,5-triethylbenzene.....38
	2.1. Abstract.....39
	2.2. Introduction.....39
	2.3. Results and discussion.....41
	2.4. Conclusion.....47
	2.5. Experimental.....48
	2.6. References.....72
III.	Selective ion-pair fluorescent sensing of ammonium nitrate by a combination of pyrazolyl and dansyl tripodal extractants.....76
	3.1. Abstract.....77
	3.2. Introduction.....77
	3.3. Results and discussion.....80
	3.4. Conclusion.....90
	3.5. Experimental.....90
	3.6. References.....93

IV.	Tripodal pyrazole ligands and analogs for selective Ln(III) sensing.....	96
	4.1. Abstract.....	97
	4.2. Introduction	97
	4.3. Results and discussion	99
	4.4. Conclusion	110
	4.5. Experimental	110
	4.6. References.....	112
V.	Hg(II) complexation and sensing by a tris-dansylamide derivative of 1,3,5-Tris(2-aminomethyl) -2,4,6-triethylbenzene.....	114
	5.1. Abstract.....	115
	5.2. Introduction.....	115
	5.3. Results and discussion	117
	5.4. Conclusion	128
	5.5. Experimental.....	129
	5.6. References.....	151
VI.	General Conclusion.....	154
	APPENDIX	156
	VITA.....	170

LIST OF TABLES

TABLE		PAGE
2.1.	Average distances (in Å) and corresponding standard deviations.....	53
2.2.	Crystallographic data.	71
5.1.	Crystallographic data for Hg ₃ (L)(CH ₃ COO) ₃	132
5.2.	Fractional atomic coordinates (×10 ⁴) and equivalent isotropic displacements parameters (Å ² ×10 ³) for Hg ₃ (L)(CH ₃ COO) ₃ . U _{eq} is defined as 1/3 of the trace of the orthogonalised U _{ij}	135
5.3.	Anisotropic displacement parameters (×10 ⁴) Hg ₃ (L)(CH ₃ COO) ₃ . The anisotropic displacement factor exponent takes the form: -2π ² [h ² a* ² × U ₁₁ + ... +2hka* × b* × U ₁₂].....	137
5.4.	Bond lengths in Å for Hg ₃ (L)(CH ₃ COO) ₃	139
5.5.	Bond angles in Å for Hg ₃ (L)(CH ₃ COO) ₃	141
5.6.	Hydrogen fractional atomic coordinates (×10 ⁴) and equivalent isotropic displacement parameters (Å ² ×10 ³) for Hg ₃ (L)(CH ₃ COO) ₃ . U _{eq} is defined as 1/3 of the trace of the orthogonalised U _{ij}	145
5.7.	Atomic occupancies for all atoms that are not fully occupied in Hg ₃ (L)(CH ₃ COO) ₃	147
5.8.	Crystal data and structure refinement for [Hg(L.H ₂) ₂ (H ₂ O)].....	148
5.9.	Bond lengths for [Hg(L.H ₂) ₂ (H ₂ O)].....	149
5.10.	Bond angles for [Hg(L.H ₂) ₂ (H ₂ O)].....	150
A.1.	Hydrogen bond information for RGR534_a.....	165

LIST OF FIGURES

FIGURE	PAGE
1.1 Structure of crown ether-type ditopic receptors 1 ²² and 2 ¹⁴	5
1.2 Structure of alkylammonium chloride ion pair receptor 3 reported by Gellman et al. ²³	5
1.3 Structure of NaF receptor 4a ²⁶ and 4b ²⁵	6
1.4 Structure of ion pair receptor 5 reported by Reinhoudt that binds NaCl	6
1.5 Structure of ion pair receptor 6 ¹⁸ for KF binding.....	7
1.6 Structure of ion pair receptor 7a ³⁰ and 7b ³¹	8
1.7 Structure of dual-host ion pair receptors reported by Das and his group.	9
1.8 Structure of 18-crown-6 and calix[6]pyrrole receptors for effective binding of ion-paired (n-Bu)NH ₃ ⁺ Cl ⁻	9
1.9 Structures of 18-crown-6, tripodal amide and the single crystal structure of the encapsulated F ⁻ in the cavity of the tripodal amide ³⁴	10
1.10 Structure of ferrocene-based amidopyridine receptor 10 reported by Tucker et al.....	11
1.11 Structure of ferrocene/imidazopyrene receptor ³⁷ 11 reported by Molina et al.....	11
1.12 Structure of ferrocene/imidazopyrene receptor 12 reported by De Silva et al. ³⁸	12
1.13 Metal sulfate binding with a salen-based receptor reported by Tasker ⁴²	13
1.14 An all-organic internal charge transfer (ICT) based fluorescent sensor.....	16
1.15 A twisted internal charge transfer (TICT) based fluorescent sensor.....	16
1.16 A metal-to-ligand charge transfer (MLCT) based fluorescent sensor.....	16
1.17 Photoinduced electron transfer (PET)-based fluorescent sensors.....	17

1.18	Calix[4]arene-based electronic energy transfer (EET)-based fluorescent probe for Hg(II).....	18
1.19	Chemical structure of nonactin.....	22
1.20	The cage-type NH ₄ ⁺ receptor reported by Kim et al. based on cation- π interaction and hydrogen bonding ⁶³	23
1.21	A fluorescent probe bearing a diazostilbene chromophore and a benzo-15-crown-5 ether moiety reported by Bekiari et al.	27
1.22	A tripodal N-anthracen-9-ylmethyl-N7,N7-bis-[2-(anthracen-9-ylmethyl-thiophen-2-ylmethylamino)ethyl]-N- thiophen-2-ylmethyl-ethane with selective fluorescence enhancement for Ce ³⁺ in dry tetrahydrofuran (THF) reported by Aoki et al.	27
2.1	Chemical structure of ligands 1 and 2	40
2.2	Fluorescence titration ($\lambda_{exc} = 272$ nm) of 1 (1.0 X 10 ⁻⁴ M) with NH ₄ ⁺ PF ₆ ⁻ or K ⁺ PF ₆ ⁻ in CH ₃ CN/CH ₂ Cl ₂ (1:1).	42
2.3	Fluorescence titration ($\lambda_{exc} = 262$ nm) of 2 with NH ₄ ⁺ PF ₆ ⁻ in CH ₃ CN/CH ₂ Cl ₂ (1:1)	42
2.4	¹ H-NMR titration plot of 1 (for CH ₃ CH ₂ -) with M ⁺ PF ₆ ⁻ (M ⁺ = NH ₄ ⁺ , K ⁺) in acetone-d ₆ . The concentration of 1 was kept constant at 2 mM.....	43
2.5	¹ H-NMR titration of 1 with M ⁺ PF ₆ ⁻ in CD ₃ OD (X = NH ₄ ⁺ , Na ⁺ , or K ⁺). The concentration of 1 was kept constant at 2 mM.....	43
2.6	Jobs plot of 1 (CH ₃ CH ₂ -) with NH ₄ ⁺ PF ₆ ⁻ in acetone-d ₆ . 0.002 M Stock solutions of 1 and NH ₄ ⁺ PF ₆ ⁻ were used.....	44
2.7	Jobs plot for 2 with NH ₄ ⁺ PF ₆ ⁻ in acetone-d ₆ . 0.002 M Stock solutions of 2 and NH ₄ ⁺ PF ₆ ⁻ were used.....	44
2.8	Crystal structure of [2] (left) and [2·NH ₄] ⁺ PF ₆ ⁻ (right). H-atoms and disorders on phenyl rings are not shown for clarity.....	46
2.9	Crystal structure of [2·NH ₄] ⁺ PF ₆ ⁻ showing NH ₄ ⁺ H-bonded to the 2 host. N(pz)···N(NH ₄) distance: 2.950(3) Å. The disordered PF ₆ ⁻ is not shown for clarity.....	46
2.10	DFT calculated structure of [1·NH ₄] ⁺ PF ₆ ⁻	52

2.11	DFT calculated structure of $[2 \cdot \text{NH}_4]^+\text{PF}_6^-$	53
3.1	Chemical structure of ligands 1 and 2	80
3.2	$^1\text{H-NMR}$ titration of 2 with $(\text{n-Bu})_4\text{N}^+\text{NO}_3^-$ in CDCl_2 . The concentration of 2 was kept constant at 2 mM	81
3.3	Fluorescence titration ($\lambda_{\text{exc}} = 352 \text{ nm}$) of 2 ($1.0 \times 10^{-6} \text{ M}$) with ($1.0 \times 10^{-3} \text{ M}$) of $(\text{n-Bu})_4\text{N}^+\text{NO}_3^-$ in CH_2Cl_2 . The concentration of 2 was kept constant.....	82
3.4	Fluorescence emission of an equimolar mixture of 1 and 2 ($5.0 \times 10^{-5} \text{ M}$) with an equimolar mixture of $\text{NH}_4^+\text{PF}_6^-$ and $(\text{n-Bu})_4\text{N}^+\text{NO}_3^-$ in $\text{CH}_3\text{OH}/\text{CH}_2\text{Cl}_2$ (2:8).....	83
3.5	Fluorescence titration curve of 1 & 2 with $\text{NH}_4^+\text{PF}_6^-$ & $(\text{n-Bu})_4\text{N}^+\text{NO}_3^-$ $\lambda_{\text{exc}} = 272 \text{ nm}$, $\lambda_{\text{em}} = 352 \text{ nm}$	84
3.6	Fluorescence emission ($\lambda_{\text{exc}} = 272 \text{ nm}$) of an organic phase (CH_2Cl_2) containing 1 & 2 (0.05 mM) after extraction with NH_4NO_3 . NH_4NO_3 concentrations are 0 mM (black), 0.01 mM (red), 0.05 mM (blue) and 0.1 mM (green)	85
3.7	Fluorescence emission of 1 & 2 (0.05 mM) after extraction with KNO_3 from water into CH_2Cl_2 following 272 nm excitation.....	86
3.8	Fluorescence emission of 1 & 2 (0.05 mM) after extraction with NaNO_3 . Concentration range of 0 mM - 0.10 mM in CH_2Cl_2 following 272 nm excitation.....	86
3.9	Fluorescence emission of 1 & 2 (0.05 mM) after extraction with KCl in CH_2Cl_2 following 272 nm excitation.....	87
3.10	Fluorescence emission of 1 & 2 (0.05 mM) after extraction with NaCl in CH_2Cl_2 following 272 nm excitation	87
3.11.	Fluorescence emission ($\lambda_{\text{exc}} = 272 \text{ nm}$) of organic phases (CH_2Cl_2) containing 1 & 2 (0.05 mM) after extraction with various concentrations of MNO_3 ($\text{M} = \text{NH}_4^+, \text{K}^+$) showing selective FRET sensing for NH_4NO_3	88
3.12.	Fluorescence emission ($\lambda_{\text{exc}} = 272 \text{ nm}$) of organic phases (CH_2Cl_2) containing 1 & 2 (0.05 mM) after extraction with various concentrations of NH_4NO_3 and KCl , showing selective FRET sensing for NH_4NO_3	89

3.13	Fluorescence emission ($\lambda_{\text{exc}} = 272 \text{ nm}$) of organic phases (CH_2Cl_2) containing 1 & 2 (0.05 mM) after extraction with various concentrations of NH_4NO_3 and NaCl	89
4.1	Fluorescence emission for receptor 1 ($\lambda_{\text{exc}} = 272 \text{ nm}$) and 2 ($\lambda_{\text{exc}} = 262 \text{ nm}$) in $\text{CH}_3\text{CN}/\text{CH}_2\text{Cl}_2$ (1:1).....	99
4.2	Fluorescence emission of receptor 3 in CH_3CN at $\lambda_{\text{exc}} = 230 \text{ nm}$	100
4.3	Fluorescence titrations of 1, 2 and 3 ($1.0 \times 10^{-4} \text{ M}$) with $\text{Nd}(\text{NO}_3)_3$ in CH_3CN	101
4.4	Fluorescence titrations of 1, 2 and 3 ($1.0 \times 10^{-4} \text{ M}$) with $\text{Eu}(\text{NO}_3)_3$ in CH_3CN	102
4.5	Fluorescence titrations of 1, 2 and 3 ($1.0 \times 10^{-4} \text{ M}$) with $\text{Lu}(\text{NO}_3)_3$ in CH_3CN	102
4.6	Fluorescence titrations of 1, 2 and 3 ($1.0 \times 10^{-4} \text{ M}$) with $\text{Ce}(\text{NO}_3)_3$ in CH_3CN	103
4.7	Fluorescence titrations of 1, 2 and 3 ($1.0 \times 10^{-4} \text{ M}$) with $\text{Sm}(\text{NO}_3)_3$ in CH_3CN	103
4.8	Fluorescence titrations of 1, 2 and 3 ($1.0 \times 10^{-4} \text{ M}$) with $\text{La}(\text{NO}_3)_3$ in CH_3CN	104
4.9	Benesi-Hildebrand plot of receptor 1 in acetonitrile in the presence of La^{3+}	105
4.10	Benesi-Hildebrand plot of receptor 1 in acetonitrile in the presence of Sm^{3+}	105
4.11	Stern-Volmer plot of 3 ($1.0 \times 10^{-4} \text{ M}$) with low concentration of $\text{Sm}(\text{NO}_3)_3$ in CH_3CN	107
4.12	Stern-Volmer plot of 3 ($1.0 \times 10^{-4} \text{ M}$) with low concentration of $\text{Lu}(\text{NO}_3)_3$ in CH_3CN	107
4.13	Stern-Volmer plot of 3 ($1.0 \times 10^{-4} \text{ M}$) with low concentration of $\text{Nd}(\text{NO}_3)_3$ in CH_3CN	108
4.14	^1H -NMR titration plot of 1 with $\text{La}(\text{NO}_3)_3 \cdot 6\text{H}_2\text{O}$ in acetone- d_6 . The concentration of 1 was kept constant at 2 mM.....	109

4.11	¹ H-NMR titration plot of 3 with La(NO ₃) ₃ ·6H ₂ O in acetonitrile-d ₃ . The concentration of 3 was kept constant at 2 mM.....	110
5.1	Chemical and crystal structures of receptor LH ₃	116
5.2	Fluorescence titration of LH ₃ (1.0 x 10 ⁻⁶ M) with Hg(CH ₃ COO) ₂ in methanol.....	118
5.3	Fluorescence titration of LH ₃ (1.0 x 10 ⁻⁶ M) with HgCl ₂ in methanol.....	118
5.4	Stern-Volmer plot of LH ₃ (1.0 x 10 ⁻⁶ M) with low concentrations of HgCl ₂ in methanol.....	119
5.5	Fluorescence titration of LH ₃ (1.0 x 10 ⁻⁶ M) with ZnCl ₂ in CH ₃ OH.....	119
5.6	Fluorescence titration of LH ₃ (λ _{exc} = 350 nm, 1 μM) with Hg ²⁺ , Ag ⁺ , Co ²⁺ , Ca ²⁺ , Cu ²⁺ and Cd ²⁺ (500 μM) in CH ₃ OH.....	120
5.7	Fluorescence titrations of LH ₃ (1 μM) and Et ₃ N (3 μM) with Hg ²⁺ in the presence of other cations in methanol (λ _{exc} = 350 nm). The concentration of 1 was stable at all experiments (1 μM). Titration with Hg(II) in the absence of competing ions (red rhombus), in constant concentration of Ca(II) at 1 x 10 ⁻⁵ M, (blue triangles), and in constant concentration 1.0 x 10 ⁻⁵ M each of 100 μM Ag ⁺ , Co ²⁺ , and Ca ²⁺ (green triangles).....	121
5.8	¹ H-NMR titration experiments of LH ₃ with HgCl ₂ in DMSO-d ₆ . (i) LH ₃ ; (ii) LH ₃ with 1 equivalent of Hg(II); (iii) LH ₃ with 18 equivalent of Hg(II).....	122
5.9	X-ray crystal structure of Hg ₃ (L)(CH ₃ COO) ₃ highlighting the chair conformation of the Hg ₃ O ₃ unit.....	124
5.10	X-ray crystal structure of Hg ₃ (L)(CH ₃ COO) ₃ . Hydrogen atoms are not shown for clarity. Color coding: silver, Hg; red, O; yellow, S; blue, N; dark gray, C.....	124
5.11	X-ray crystal structure of Hg(LH ₂) ₂ . Hydrogen atoms are not shown for clarity. Color coding: silver, Hg; red, O; yellow, S; blue, N; dark gray, C.....	125
5.12	Ball and stick representation showing intermolecular π-π interaction between two centroids.....	125
5.13	FT-IR spectrum of LH ₃	126
5.14	FT-IR spectrum of crystals of Hg ₃ (L)(CH ₃ COO) ₃	127

5.15	FT-IR spectrum of crystals of Hg(L.H ₂) ₂	127
5.16	Overlay of the FT-IR spectra (crystals) of Hg(L.H ₂) ₂ and LH ₃	128
A.1	Chemical structure of receptor 1.....	157
A.2	Fluorescence titration of 1 with NH ₄ ⁺ PF ₆ ⁻ in CD ₃ OD (λ _{exc} = 272 nm).....	159
A.3	Fluorescence titration curve of 1 with NH ₄ ⁺ PF ₆ ⁻ (λ _{exc} = 272 nm).....	159
A.4	Fluorescence titration curve of 1 with K ⁺ PF ₆ ⁻ (λ _{exc} = 272 nm).....	160
A.5	¹ H-NMR titration plot of 1 with NH ₄ ⁺ PF ₆ ⁻ in CD ₃ OD. The concentration of 1 was kept constant at 2 mM.....	161
A.6	¹ H-NMR titration plot of 1 with K ⁺ PF ₆ ⁻ in CD ₃ OD. The concentration of 1 was kept constant at 2 mM.....	162
A.7	¹ H-NMR titration plot showing selective binding of NH ₄ ⁺ over K ⁺ by 1 in CD ₃ OD.....	162
A.8	Job plot of 1 with NH ₄ ⁺ PF ₆ ⁻ in CD ₃ OD. 0.002 M Stock solutions of 1 and NH ₄ ⁺ PF ₆ ⁻ were used.....	163
A.9	50% probability ORTEP thermoellipsoid (left) and PLATO (right) representations of the crystal structure of 2,4,6-triethylbenzene-1,3,5-triacetic acid, with NH ₄ ⁺ and alaninol, showing NH ₄ ⁺ binding to tricarboxylic acid via H-bonding and cation-π interactions.....	164
A.10	Packing diagram of the crystal structure of alaninol/NH ₄ ⁺ /2,4,6-triethylbenzene-1,3,5-triacetic acid, showing alternate layers of hydrophilic H-bonding networks and organic networks stabilized by hydrophobic interactions and crystal packing.....	164

ABBREVIATIONS AND ACRONYMS

1,2-DCE	1,2-dichloroethane
An	Actinides
DFT	Density functional theory
EET	Electronic energy transfer
FRET	Förster resonance energy transfer
FSR	Fluorophore spacer receptor
FT-IR	Fourier transform infrared spectroscopy
ICT	Internal charge transfer
Ln	Lanthanides
MeOH	Methanol
MLCT	Metal-to-ligand charge transfer
NMR	Nuclear magnetic resonance
PET	Photoinduced electron transfer
TICT	Twisted internal charge transfer
UV-Vis	Ultraviolet-visible

CHAPTER I

A Review: Ion pair receptors and fluorescence sensing

1.1 Ion pair sensing.

Ion-pair sensing is the simultaneous complexation and detection of both the cationic and anionic components of a salt. Investigations on ion pairing and specific ion-pair interactions have led to an increased recent interest in extraction, separation, and sensing systems that involve co-operative cation and anion binding.¹⁻³ The rapid expansion in the field of supramolecular chemistry has opened routes for the uncovering of efficient and selective binding agents for application in ion pair separations and analysis. Ion pairing has found potential applications in salt extraction,^{4,5} membrane transport,⁶ catalysis⁷ and has also been utilized in sensing by ditopic hosts.⁸⁻¹¹ Despite their simplicity, dual-host approaches that combine separate anion and cation receptors in co-extraction¹² and sensing of ionic components have received much less attention, as there are challenges in deriving systems for which the signal response for the ion pair is unique and distinct from the signals for the individual anionic and cationic components.

1.2 Ion pair receptors

Ion pair binding and sensing has often involved ditopic host molecules that bind both ionic species within the same molecule.¹³⁻¹⁸ The design of ditopic host receptors comes with unique synthetic challenges: The cation-binding site must be separated from the anion binding site in a way that the two sites do not interfere with each other. Selectivity of these sites for the target ion-pair over possible interfering ion pairs must also be considered, when designing a ditopic receptor. The design of the individual binding sites is relatively straightforward, and the methods for creating individual hosts can be applied here. The difficulty lies in linking of the two binding sites, which could be a complex process and a synthetic challenge.

Another approach to ion pair binding which has been explored by fewer researchers is the dual-host strategy,^{12,19,20} in which two different receptors specific for each ion pair component are used together to achieve combined extraction. The use of the dual host receptors for ion pair recognition can produce synergistic effects and in the case of fluorescent sensing, provide unique sensing signals for the pair, as opposed to the individual components, through close contact of the complexed pair components, presumably because of the lower dielectric constant of the organic solvent. One of the advantages of using the dual-host strategy over the heteroditopic receptor strategy is the avoidance of the laborious steps in synthesis of ditopic receptors.

Aside from the single ditopic host *vs.* the dual host distinction, ion pair receptors have also been classified, structurally, on the basis of how the ion pair is bound within the receptor structure. There may be: i) contact ion-pairing, ii) solvent-bridged ion pairing and iii) host-separated ion pairing. Contact ion pairing allows direct contact of the two components of the ion pair, in contrast to the solvent-separated bridge in which the solvent forms a bridge between the two component ions of the pair. In host-separated ion pairing there is no contact between the bound cation and the co-bound anion of the ion pair.

In terms of mechanism, ion pair receptors can bind the ion pair components sequentially, or in a concurrent fashion. The sequential binding involves initial binding of one of the ionic components. Once bound, the affinity of the receptor for the other ion is increased. The increase in affinity of the receptor for the other ion component in the ion pair can be as a result of either allosteric effects, or a direct or solvent-mediated electrostatic interaction with the counter ion.⁹ The concurrent bind mode involves the receptor forming a complex simultaneously with both the cation and the anion. In this work, we will be

emphasizing the dual host approach, with binding by two separate hosts, which can form contact ion pairs of the complexed ions upon extraction into an organic phase. The dual-host extraction sensing strategy can take advantage of dehydration-resolvation energetics leading to selective extraction for some anions or cations from the aqueous into the organic medium. As an example, a relatively less hydrophilic anion, such as nitrate, is expected to be more extractable than the more hydrophilic chloride into organic solvents, because the higher the hydrophilicity of the anion, the higher the hydration energy barrier that needs to be overcome for anion transfer from water into an organic solvent.^{2,21}

1.3 Ditopic ion-pair receptors.

1.3.1 Ditopic receptors based on spatially separated ions.

There are several examples of ditopic hosts, often combining crown ether sites for cation binding and hydrogen-bond donor sites for anion binding. In 1994, Reinhoudt and co-workers reported receptor **1**, which contains a uranyl center, acting as a Lewis acid, which is covalently linked to two crown ether sites. Reinhoudt and co-workers showed that the receptor **1**, is able to bind to K^+ and $H_2PO_4^-$ in a concurrent fashion. A single K^+ ion binds to both crown ether moieties in a sandwich fashion, while the anion binds to the uranyl center.²²

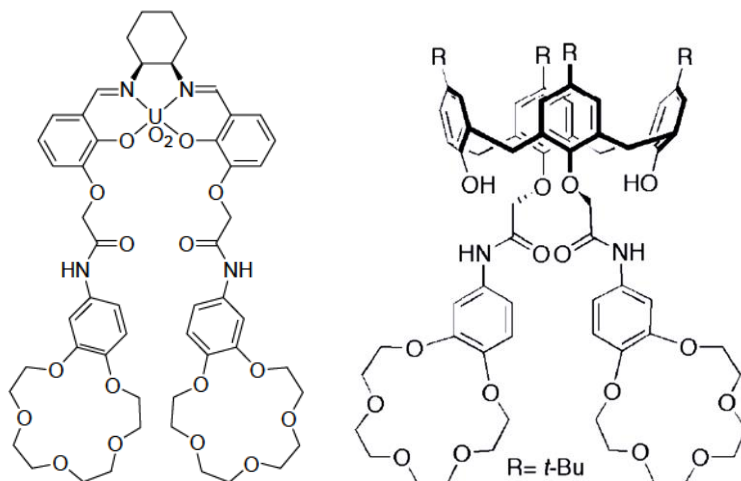


Figure 1.1. Structure of crown ether-type ditopic receptors **1**²² and **2**¹⁴

An analogous ditopic receptor was synthesized by the Beer group (receptor **2**).¹⁴ The receptor **2** was found to bind potassium and ammonium cations together with several counteranions, such as Cl^- , NO_3^- , HSO_4^- , or H_2PO_4^- . In 1994, Gellman et al.²³ reported a phosphine oxide-disulfoxide system (receptor **3**) that binds to monoalkylammonium cations together with halide anions. The receptor binds to the alkylammonium ion through hydrogen bonding with the three P=O and S=O groups. The binding of the alkylammonium ion to the three P=O and S=O groups led to the polarization and preorganization of the receptor, thereby allowing the cavity to be better suited for binding of the chloride anion on the opposite side of the receptor.

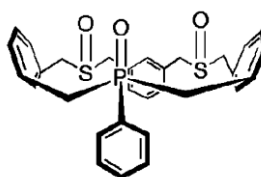


Figure 1.2. Structure of alkylammonium chloride ion pair receptor **3** reported by Gellman et al.²³

An organotin-substituted crown ether receptor $\text{Ph}_2(\text{I})\text{SnCH}_2\text{Sn}(\text{Ph})(\text{I})\text{CH}_2$ -[16]-crown-5 capable of binding NaF in acetonitrile was reported in 2007.²⁴ The structure reveals that in CH_3CN , the ion pair is spatially separated by the receptor, whereas in methanol, a solvent separated ion pair was observed, instead, in which the Na^+ and the F^- ions are separated by a molecule of methanol (Figure 1.3).²⁴⁻²⁶

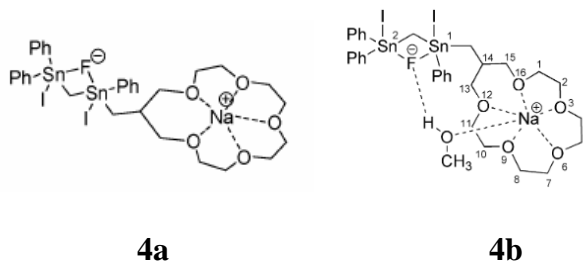


Figure 1.3. Structure of NaF receptor **4a**²⁶ and **4b**²⁵

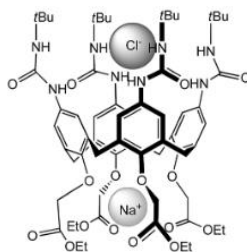


Figure 1.4. Structure of ion pair receptor **5** reported by Reinhoudt that binds NaCl ²⁷

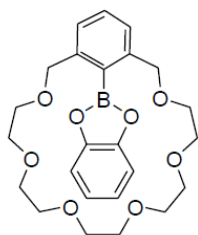
A calix[4]-arene based ditopic receptor **5**^{27,28} reported by Reinhoudt and coworkers was shown to bind NaCl as a separated ion pair: The sodium ion is bound to the ester cavity of the receptor. The binding of the sodium ion causes the molecule to pre-organize the urea groups for binding of the chloride counteranion.

1.3.2 Ditopic receptors based on contact ion pairs.

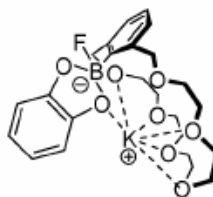
Ion pair receptors that bind contact ion pairs usually show higher binding affinities than ditopic receptors that separate the ion-pair components. The higher binding affinities

for contact ion pairs arises from the reduction of the coulombic penalty associated with ion separation due to binding of the ion pair to the host molecule.²⁹

Reetz and co-workers demonstrated one of the first examples of a ditopic host, receptor (**6**) on the basis of binding of an associated ion pair by coupling a crown ether moiety designed for K^+ recognition to a Lewis-acidic boron center designed for F^- recognition.¹⁸ The receptor **6** contains a crown ether moiety, which is used to coordinate K^+ , together with a Lewis acidic boron center for covalent binding of the fluoride anion, forming a 1:1 complex with KF. X-ray diffraction revealed close contact between the bound K^+ and F^- , even though the K^+ is also bound to the crown ether moiety.



6



6·KF

Figure 1.5. Structure of ion pair receptor **6** for KF binding reported by Reetz et al.¹⁸

Another example of a ditopic receptor reported by Kilburn et al,³⁰ combining crown ether and diamide sites (**7a**), was shown to bind mono-potassium salts of dicarboxylic acids as contact ion pairs in chloroform. The crystal structures show hydrogen bonding interactions and an electrostatic association between the carboxylate anion and the crown ether bound potassium cation.

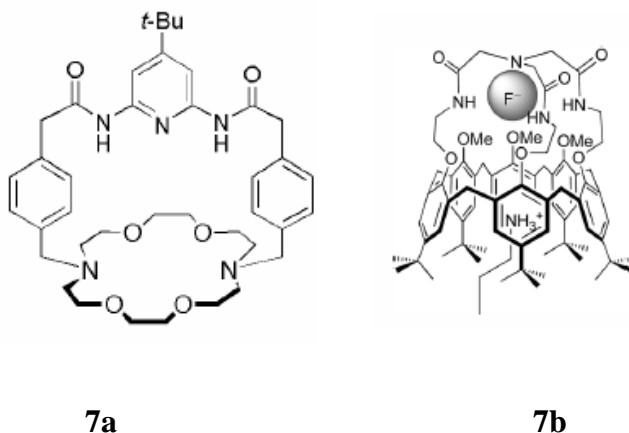


Figure 1.6. Structure of pair receptors **7a**³⁰ and **7b**³¹

A reversible and selective contact ion-pair receptor **7b** that binds alkyl ammonium fluoride as an ion pair was reported in 2010 by Jabin et al.³¹ The receptor is a calix[6]cryptamide with the ammonium ion binding inside the calixarene cavity and the fluoride ion binding to the tris- amino cap present in the receptor. The observed selectivity was attributed to the size compatibility with fluoride and preorganization of the hydrogen bond donor sites.

1.4 Dual-host ion-pair receptors.

The dual-host strategy is another approach proposed for ion-pair recognition and sensing. This strategy employs two different receptors, each specific for the cation and anion component. These dual-host systems have found use in membrane transport and extraction of alkali metal salts.^{12,20} Das et al.³² have reported a dual host for K_2CO_3 . In the K_2CO_3 system, a crown ether (**8**) coordinates the potassium ion while a tripodal urea receptor **9** binds carbonate. X-ray diffraction analysis revealed the coordination of the potassium ion to all the ethereal oxygen atoms in the crown ether molecule and also with

a carbonyl group and a nitro group of the tripodal urea receptor in order to satisfy an 8-coordinate environment for the potassium ion.

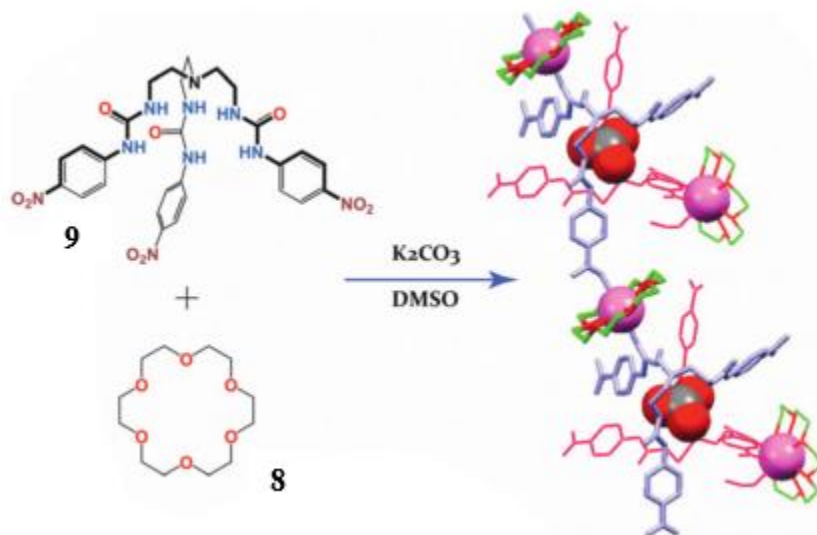


Figure 1.7. Structure of dual-host ion pair receptors reported by Das and his group.³²

Cafeo³³ et al. reported a dual-host combination of cationic (18-crown-6) and anionic (calix-[6]-pyrrole) receptors for effective binding of $(n\text{-Bu})\text{NH}_3^+\text{Cl}^-$ organic salts. Small downfield shifts occurred in the pyrrole NH resonances when 0.5 eq. of $(n\text{-Bu})\text{NH}_3^+\text{Cl}^-$ was added to a calix-[6]-pyrrole solution in CH_2Cl_2 , indicating a weak host-guest interaction.



Figure 1.8. Structure of 18-crown-6 and calix-[6]-pyrrole receptors for effective binding of ion-paired $(n\text{-Bu})\text{NH}_3^+\text{Cl}^-$.³³

Ghosh et al. have reported KF and KCl liquid-liquid extraction into CHCl_3 by equimolar amounts of 18-crown-6 and a tripodal amide.³⁴ The X-ray crystal structure shows that upon binding, the potassium salts self-assemble to form a 1-D coordination polymer.

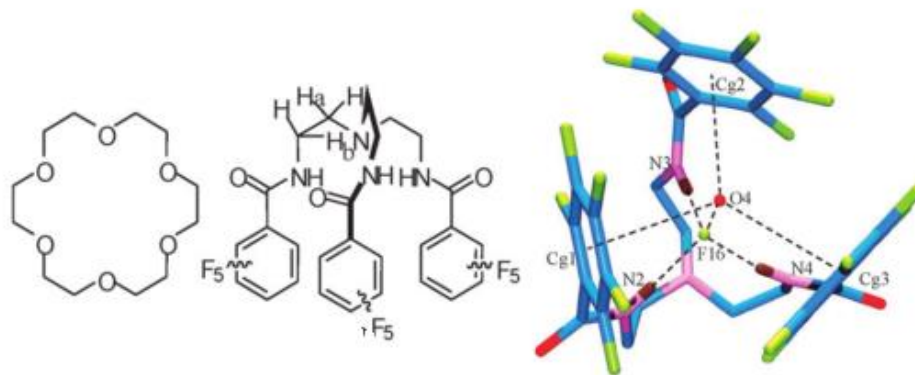


Figure 1.9. Structures of 18-crown-6, tripodal amide and the single crystal structure of the encapsulated F^- in the cavity of the tripodal amide.³⁴

1.5 Ion-pair receptors as sensors

The utilization of ion pair receptors as sensors has found use in both biological and environmental systems, yet it comes with some challenges: An optical or electrochemical output is needed to be incorporated into the host design in order for a signal to be obtained. A few ditopic receptors have been utilized in ion-pair sensing.³⁵⁻³⁷ These include the ferrocene/amidopyridine type electrochemical L-phenylalanine sensor **10**,³⁵ that is capable of binding the carboxylate group through the crown ether moiety and the ammonium group through the amidopyridine moiety. Large $^1\text{H-NMR}$ chemical shifts changes in CD_3CN were observed upon L-phenylalanine binding.

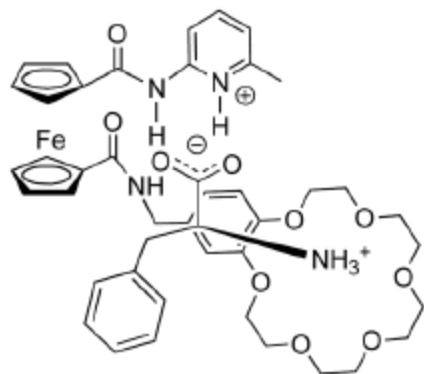


Figure 1.10. Structure of ferrocene-based amidopyridine receptor³⁵ **10** reported by Tucker et al.

Another ion-pair receptor that acts as both a fluorescent and electrochemical sensor is the ferrocene/imidazopyrene compound³⁷ **11**, which is capable of binding $\text{Zn}(\text{H}_2\text{PO}_4)_2$ through the imidazole moiety in the receptor. The electrochemical output signal upon binding was the result of change in the oxidation potential for the ferrocene/ferrocinium redox couple.

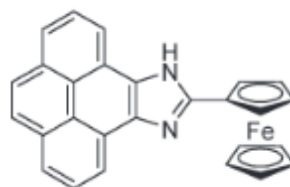


Figure 1.11 Structure of ferrocene/imidazopyrene receptor³⁷ **11** reported by Molina et al.

De Silva et al. published in the structure of the fluorescent sensor **12** that is able to detect the presence of sodium and phosphate ion pair simultaneously.³⁸ The fluorescent receptor consists of a crown ether known for its high selectivity towards the sodium ion together with a polyamine moiety for phosphate binding. Fluorescence enhancement of the

anthracene fluorophore was observed at acidic pH when the NaH_2PO_4 ion pair was introduced to the receptor.

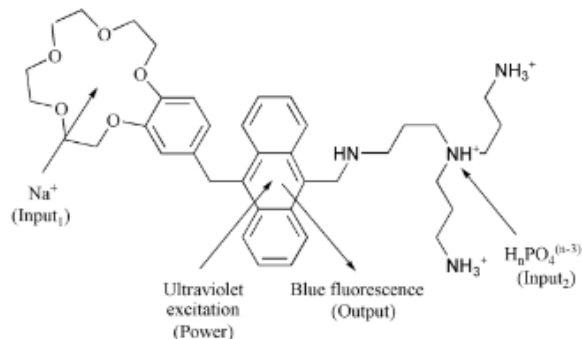


Figure 1.12. Structure of ferrocene/imidazopyrene receptor **12** reported by De Silva et al.³⁸

1.6 Ion-pair extraction

Ion pair extraction involves three components: The aqueous layer, the organic layer and the interface between the two phases.³⁹ Unlike ion-exchange extraction, in which one of the ions is exchanged, in ion-pair extraction the cation and its counteranion are both transported into the organic phase. Two approaches can be utilized in ion pair extraction: One is the use of a ligand system that can extract both the cation and the anion into the organic layer, such as in the salen-type ditopic receptor reported by Tasker et al.⁴⁰⁻⁴² (Figure 1.13), in which the binding site for the sulfate anion is covalently attached to the salen metal-complexing moiety. The other approach is the dual host by individual cation and anion receptors. Unlike ditopic receptors, in which binding for both cation and the anion is achieved with a single extractant, in dual-host systems two individual cation and anion hosts, are used together. An example of ion pair extraction using a dual-host system was reported by Moyer et al.²⁰, where the combination of an anion host that used the tripodal

1,3,5-tricarboxamide framework with the Cs⁺ host tetrabenzo-24-crown-8, showed extraction of CsNO₃ as an ion pair from water into 1,2-dichloroethane. The Cs⁺ extraction was enhanced by a factor of 4.4 in the presence of the nitrate receptor. The same authors⁴³ reported an analogous system using a Cs(I)-selective calix-crown extractant as the cation host together with a disulfonamide anion host for extraction of cesium salts. When the anion host is used together with the selective calix-crown cation receptor it strongly synergizes the extraction of cesium salts in 1,2-dichloroethane. Bates et al.⁴⁴ have also used the dual-host approach in extracting nickel sulfate.⁴²

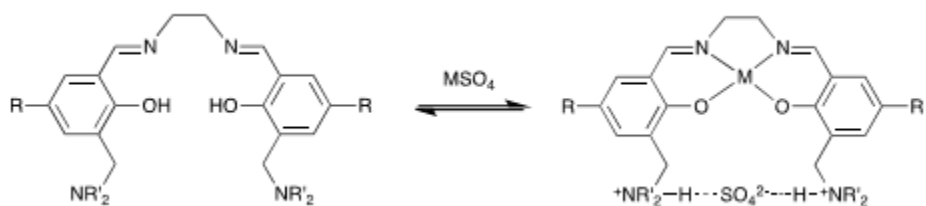


Figure 1.13 Metal sulfate binding with a salen-based receptor reported by Tasker.⁴²

1.7 Solvation effects in ion pairing

Solvent effects in ion pairing have been studied right from the introduction of the concept of ion pairing. Bjerrum in 1926 has studied the effects of solvation in ion pairing in strong electrolytes. The choice of solvent can affect the energetics of host-guest binding in molecular recognition. Bulk permittivity of the solvent, ϵ , (the electrostatic attraction between oppositely charged ions in solution that causes them to form ion pairs) has been considered as the main effect solvation has on ion pairing. Another solvent effect on ion pairing is the competition between the solvent and the counterion for space in the presence of an ion in an electrolyte solution.⁴⁵ Diederich and his group have reported the effects of solvent on hydrophobic binding interactions.⁴⁶ Solvent effects can have notable influence

on the binding propensities of host-guest complexes, which are promoted by electrostatic or hydrophobic interactions. When salts are in aqueous media, they exist as free ions, in organic medium because of the low dielectric constants and because they are charged, we can achieve distinct ion pairing, and can take advantage of intermolecular effects like FRET, which could be unique of the ion pair compared to the signal seen from the individual ions. Ion pair extraction can occur because of low dielectric constant, and having the right fluorophore, unique fluorescence effects can be achieved for the ion pair as opposed to the individual ions.

1.8. Fluorescence sensors

In the design of a fluorescent sensor, several approaches can be undertaken. In the fluorophore-spacer-receptor (FSR) approach, a light-emitting fragment is covalently linked to a receptor subunit, which is also a quencher. In the presence of an analyte the quenching no longer occurs and the fluorescence turns on. In the chemosensing ensemble, a fluorescence indicator binds in solution to the receptor through noncovalent interactions. The chemosensing approach⁴⁷⁻⁴⁹ is based on competition between the bound indicator and the competing analyte for binding to the receptor. For the chemosensing approach, the interaction between the receptor and the indicator must not be too strong and the optical properties of the indicator when bound to the receptor and when dispersed in solution must be different. Fabbrizzi and coworkers⁵⁰ reported an example in which displacement of the indicator by the competing carbonate ion from the dinuclear Cu(II) macrobicyclic complex receptor core results in visible light emission. The same group used a dicopper(II) host for sensing pyrophosphate in water at pH 7. Coupling of the fluorescent indicator to the

dicopper(II) receptor led to complete quenching of the emission when titrating a solution of the indicator with a standard receptor solution.

There are also other approaches that use fluorescence enhancement or quenching through both covalent or non-covalent interactions, as a result of electron transfer, and other phenomena, such as formation of excimers. Apart from the design considerations, other factors need to be taken into account when designing fluorescent sensors, especially with regard to the fluorophore properties. The choice of fluorophore must show reproducible and quantitative change in the fluorescence properties upon ion binding. Charge-transfer processes, photoinduced electron transfer (PET) processes, or electronic energy transfer (EET) processes could be used to attain this effect.

1.8.1 The charge transfer processes

The charge transfer processes include an all-organic internal charge transfer (ICT),^{51a} a metal-to-ligand charge transfer (MLCT),^{51b} a twisted internal charge transfer (TICT)^{51c} and through-bond charge transfer. ICT (figure 1.14) and TICT (figure 1.15) processes involve non-hydrocarbon π -electron systems where the ground state has a very different dipole moment compared to the lowest energy singlet excited state. Molecules that use TICT have their donor and acceptor portion connected by a single bond. The twisted internal charge transfer (TICT) differs from the MLCT process in that for TICT system, the full charge separation is achieved in systems by twisting the donor and acceptor components of the system by 90°. For the metal-to-ligand charge transfer (MLCT) process, significant changes in the luminescence properties of the receptor are induced when a guest species is bound. MLCT processes are mostly seen in organometallic complexes.^{51c}

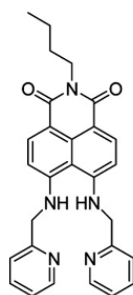


Figure 1.14. An all-organic internal charge transfer (ICT) based fluorescent sensor

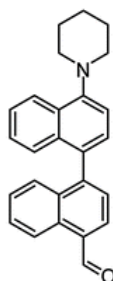


Figure 1.15. A twisted internal charge transfer (TICT) based fluorescent sensor

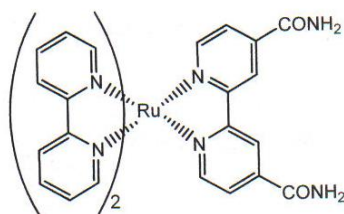


Figure 1.16. A metal-to-ligand charge transfer (MLCT) based fluorescent sensor

1.8.2 Photoinduced electron transfer (PET)

Photoinduced electron transfer (PET) process involves the transfer of an electron from a donor to an acceptor photochemically. PET sensors are generally designed using

fluorophore-spacer-receptor units. The spacer unit links the fluorophore to the guest binding site and acts to preserve the independence of the chromophore and the receptor in the electronic ground state. PET-based sensors are designed as either off-/on- or on-/off-fluorescence switches. Fluorescence enhancement is seen in “off-on” switches when guest binding leads to the opening of the fluorescence pathways, while fluorescence quenching is observed in “on-off” switches, when guest binding leads to the closure of fluorescence pathways. Examples of PET fluorescence sensors that use the bis-(2-picoly) amine receptor, capable of generating a fluorescence signal upon binding zinc ions were previously reported by De Silva and coworkers.^{52,53} The same group has reported a fluorescent PET off-on switch sensor that uses a coumarin chromophore capable of sensing Zn^{2+} , Cd^{2+} , and Pb^{2+} .

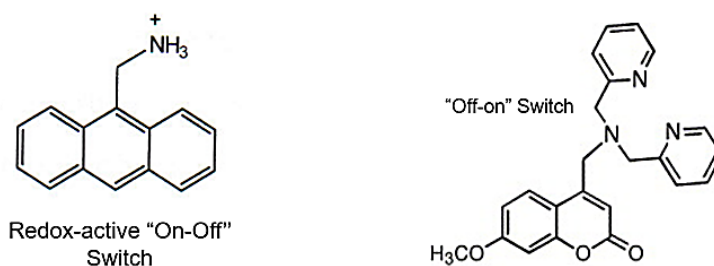


Figure 1.17. Photoinduced electron transfer (PET)-based fluorescent sensors.

1.8.3 Electronic Energy Transfer or Förster Resonance Energy transfer (FRET)

Electronic energy transfer (EET) or Förster resonance energy transfer (FRET), involves the transfer of energy between multiple fluorophores. It is a distance dependent non-radiative transfer of energy between a donor fluorophore initially in its electronic excited state, to an acceptor fluorophore.^{54-56a} FRET is sensitive to slight changes in distance. The

FRET process requires the donor and acceptor molecules to be in nanoscale distances to each other and the alignment of dipole moments. A critical factor in the process is the overlapping of the excitation and emission spectra of the donor and acceptor fluorophores respectively. FRET efficiency is inversely proportional to the sixth power of the distance between donor and acceptor. These systems frequently depend on guest recognition-induced conformational changes in the host molecule for the EET process to work efficiently (Fig. 1.18).

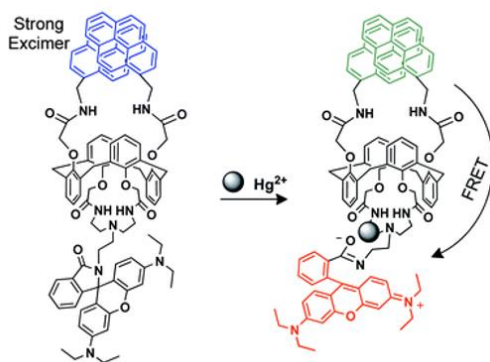


Figure 1.18. Calix[4]arene-based electronic energy transfer (EET)-based fluorescent probe for Hg(II).^{56b}

1.9 Methodology for quantifying supramolecular interactions

There are several methods available for the determination of association constants K_a . The general problem is determining accurately a property (variable) of the supramolecular complex and its components that shows a regular variation upon binding, and measure it as a function of the total concentration of the one of the components. In a simple 1:1 equilibrium system, where the receptor S is complexing the ligand L resulting in the 1:1 supramolecular complex SL, we have:



The 1:1 binding isotherm can be derived from the equilibrium constant to give:

$$f_{11} = \frac{K_a [L]}{1 + K_a [L]} \quad (\text{eq. 2})$$

f_{11} represents the fraction of the receptor that has been complexed:

$$f_{11} = \frac{[SL]}{[S]_t} = \frac{[L]_t - [L]}{[S]_t} \quad (\text{eq. 3})$$

The value L from equation (3) is substituted into equation (2) and solving for f_{11} we get equation 4 that contains total ligand concentration $[L]_t$, as the only variable. The equation 4 is possible if we assume that experimental conditions $[S]_t$ is kept stable:

$$f_{11} = \frac{[S]_t + [L]_t + K_a^{-1} - \left(\left([S]_t + [L]_t + K_a^{-1} \right)^2 - 4[L]_t[S]_t \right)^{1/2}}{2[S]_t} \quad (\text{eq. 4})$$

The f_{11} value is directly related to the measured property, and therefore non-linear fitting of the expression $f_{11} = f([L]_t)$ via equation (4) allows direct determination of the association constant.

In an NMR titration experiment in which the complex and the components are in fast exchange, the chemical shift c observed is the weighted average of the chemical shifts of the components.

Let a = chemical shift of a specific resonance at the start of the titration when $[L]_t = 0$

Then, $[S] = [S]_t$ or $f_{11} = 0$

Let b = the chemical shift of the same resonance at the end of the titration when $[L]_t = \infty$

Then, $[S] = 0$ or $f_{11} = 1$.

By defining $\Delta\delta_{\max} = b - a$

And defining $\Delta\delta = c - a$

And substituting f_{11} (equation 4) into equation 5,

Equation 6 can be used in order to fit the data which allows for the calculation of K_a as and $\Delta\delta_{\max}$. This model can also be used for complicated equilibrium systems.⁵⁷

$$f_{11} = \Delta\delta/\Delta\delta_{\max} = (c-a)/(b-a) \quad (\text{eq. 5})$$

$$\Delta\delta = \frac{([S]_t + [L]_t + K_a^{-1} - ((([S]_t + [L]_t + K_a^{-1})^2 - 4[L]_t[S]_t)^{1/2}))}{(2[S]_t)} \Delta\delta_{\max} \quad (\text{eq. 6})$$

For fluorescence spectroscopy, in the case of enhancements the Benesi-Hildebrand analysis can be applied: In a typical fluorescence titrations experiment, the receptor was titrated with the analyte at constant receptor concentration. When addition of analyte to receptor showed an increase in fluorescence upon cation binding, the Benesi-Hildebrand equation was used to fit the data.

$$I_0/I - I_0 = b/(a - b)[1/K_a[M] + 1] \quad (\text{eq. 7})$$

Where I_0 is the fluorescence intensity of the sensor in the absence of guest; I is the fluorescence intensity of the sensor in the presence of guest; $[M]$ is the concentration of the substrates; and K_a is the association constant between the receptor and the substrate. In the equation, a and b are constants. The value of $b/(a - b)$ can be found out by plotting

$I_0/(I - I_0)$ against the inverse of the concentration term, M^{-1} . The intercept of the graph gives $b/(a - b)$; I_0 and I are found out experimentally.

In the case of fluorescence quenching, at lower concentrations of the analyte, a plot of I_0/I vs $[Q]$ is plotted and the slope obtained gives the Stern-Volmer constant (K_{sv}). Fluorescence quenching is measured quantitatively with the Stern-Volmer equation (8) where, the quencher concentration is $[Q]$, the Stern-Volmer constant is K_{sv} , I_0 is the measured fluorescence intensity without quencher present, and I is the measured fluorescence intensity with $[Q]$ present.

$$I_0/I = 1 + K_{sv}[Q] \quad (\text{eq. 8})$$

1.10 Overview of NH_4^+ receptors

Cations and anions play key role in biology and in the environment. Cations play major roles such as maintenance of life processes such as the transmission of nerve impulses and muscle contraction. Synthetic receptors for NH_4^+ have found uses both in the biological (measuring the urea and creatine levels) and the environmental systems. Several ammonium ion receptors have been designed ranging from the crown ethers to nonactin, an antibiotic that can detect ammonium ions at molecular levels.⁵⁸ The major goal in designing these receptors is to overcome the selectivity of NH_4^+ over K^+ . The selectivity issue arises from the similarity in diameter between these two ions (286 pm for ammonium and 266 pm). Kim et al. reported a thiazolo dibenzo-crown ether that is capable of binding ammonium selectively over sodium or potassium.⁵⁹

There are three main forces behind the binding of ammonium ion. These are ion pairs and salt bridges, hydrogen bonds, and cation- π interactions.⁶⁰ An example of ammonium binding via hydrogen bonding is nonactin.⁶¹ Binding is achieved via the four ethereal and four carbonyl oxygen atoms that bind to NH_4^+ through hydrogen bonding.

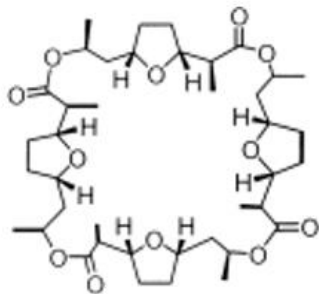


Figure 1.19. Chemical structure of nonactin

Hydrogen bonding has been utilized extensively in recognition of ammonium, with some receptors also utilizing cation- π interactions. Kim et al.⁶² reported a tris-(pyrazol-1-ylmethyl)-triethylbenzene NH_4^+ receptor exploiting cation- π interactions. The receptor, was shown to be selective for binding NH_4^+ over K^+ . The receptor selectivity towards ammonium was a result of cation- π interactions between the substrate and the central benzene ring of the receptor. Kim et al. published a cage-type NH_4^+ receptor⁶³ that used cation- π interactions and hydrogen bonding. This cage-type NH_4^+ receptor was shown to have sensitivity and selectivity comparable or superior to nonactin over a wide range of pH. Some of these families of receptors have also been shown to sense NH_4^+ by fluorescence with notable selectivity vs. K^+ (See Chapter 2). Specifically, tripodal oxazolines derived from the analogous 1,3,5-trimethylbenzene framework^{64,65} showed

significant fluorescence response upon binding to NH_4^+ with little response to K^+ , Na^+ , and Mg^{2+} in the 305-340 nm range ($\lambda_{\text{exc}} = 272\text{nm}$).

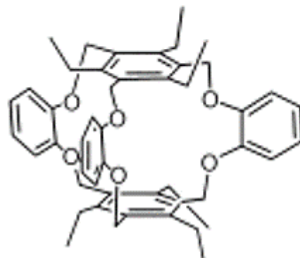


Figure 1.20. A cage-type NH_4^+ receptor reported by Kim et al. based on cation- π interactions and hydrogen bonding.⁶³

1.11 Overview of nitrate receptors

The design and synthesis of anion receptors has garnered extensive interest over the recent years. In particular, selective recognition, sensing and separation of nitrate is important because of the presence of nitrate salts in many common explosives¹² as well as for its environmental significance of nitrate as a pollutant.⁶⁶ Building selectivity for nitrate into an anion binding host framework poses a significant challenge. The primary force behind anion-receptor binding is hydrogen bonding. Therefore, the design of an anion host should include appropriately arranged hydrogen bonding sites. A nitrate-specific host should contain hydrogen bond donor sites specifically arranged so that all three oxygen atoms of the nitrate will be bound. An example is the amide-linked C_3 -symmetric bicyclic neutral cyclophane published by Bisson et al. which is capable of binding nitrate exclusively through hydrogen bonding.⁶⁷ Hydrogen bonds between the geometrically matched host and nitrate led to enhanced binding, overcoming the weak coordinative ability of this anion. In order for an anion host to be used as sensor, a molecular group

whose properties change upon binding must be introduced into the framework, without interference with the actual binding site. Different examples of electrochemical and optical based anion sensors are available in the literature.⁶⁸ For optical sensing the most common approach is to modify the receptor with a fluorophore, whose fluorescence intensity and/or emission wavelength changes upon binding.⁶⁹⁻⁷¹

Nitrate-responsive membrane development^{72,73} and other nitrate-selective optical sensors^{74,75} have also been reported. A nitrate-responsive optical membrane was developed by combining a highly fluorescent rhodamine-B octadecylester perchlorate (RBOE), as a dye, together with tridodecylmethylammonium chloride (TDMACl) as an anion exchanger incorporated into PVC or a PVC co-polymer.⁷² The nitrate-responsive optical membrane gave a limit of detection (LOD) of 1 ppm for nitrate ion with a selectivity factor of 200 for nitrate over chloride. The use of various betaine salts in polystyrene-*block*-polybutadiene-*block*-polystyrene (SBS) polymeric membranes as nitrate-selective electrodes has also been investigated.⁷³ The most effective of these membranes worked over a pH range of 2-8, with an LOD of 0.02 ppm for nitrate. The selectivity coefficient ($K_{potNO_3^-,Cl^-}$) for nitrate over chloride was 3.4×10^{-3} . Fluorescent fiber-optic sensors for nitrate have been developed using the fluorescence quenching induced by the irreversible nitration of fluorescein upon exposure to nitrates.⁷⁵ A system has also been reported by Huber et al. which contains a cationic potential-sensitive fluorescent dye incorporated into a hydrogel-plasticizer matrix.⁷⁴ This system showed strong fluorescence enhancement upon nitrate exposure and was effective in sensing nitrate in the 0.1 - 50 mM range, while showing no response to the presence of chloride, even at 200 mM. These receptors have a collective effectiveness in the mM range and considerable selectivity over chloride.

1.12 Overview of mercury (II) sensors

Over the last few decades, many efforts have been undertaken for the design and synthesis of selective Hg(II) receptors and sensors. The effort, arises from the toxic nature of mercury to both the human health and the environment^{76,77} Mercury is ranked among the priority metals that are of public health significance.⁷⁸ These metallic elements are considered systemic toxicants that are known to induce multiple organ damage. Mercury pollution has been shown to originate from both natural and anthropogenic sources. Minamata diseases⁷⁹ and prenatal brain damage are some of the effects that arise from mercury exposure in humans.⁸⁰⁻⁸⁴

Numerous methods have been employed in recent years for the detection of Hg(II). These include colorimetric sensing techniques, atomic absorption, X-ray fluorescence spectroscopy, and electrochemical sensing. The use of colorimetric and fluorescence sensors for Hg(II) detection stems from their low cost, operational simplicity and high selectivity. An example is the highly selective and sensitive colorimetric method that uses gold nanoparticles that utilize Au amalgamation and grown AuNPs for rapid Hg(II) detection.⁸⁵⁻⁸⁸ A number of fluorescence chemosensors have been reported in the literature for Hg(II) detection: Che et al.⁸⁹ reported a fluorescent 5-bromoindole-3-carboxaldehyde ethylthiosemicarbazone receptor that can detect and remove Hg(II) from water by extraction. This ligand coordinates directly to Hg through its N and S atoms, and is selective towards Hg(II), with a detection limit of 1.31×10^{-7} M. The rhodamine fluorophore⁹⁰⁻⁹⁴ has found a lot of use for Hg detection because of its emissive performance⁹⁵ and emission turn-on effect. The dansylamide fluorophore has also found uses as fluorescent probe

because it possesses high fluorescence quantum yield and large Stokes shifts. Some dansyl-based receptors have been reported for Hg(II) detection.⁹⁶⁻¹⁰⁰

1.13 Overview of lanthanide receptors

The processing and removal of high heat emitters from nuclear waste continuously poses a concern because nuclear waste streams typically contain long-lived radiotoxic minor actinides and fission products.¹⁰¹⁻¹⁰³ The radiotoxicity and high heat generation in these streams is mainly a consequence of actinide presence.¹⁰³⁻¹¹⁰ There is a continuous effort in generating ligands that can separate these high heat emitters from lanthanides and fission products. Selectively separating the actinides (An) from lanthanides (Ln) in used nuclear fuel presents an important challenge in closing the nuclear fuel cycle. The challenge comes from the chemical similarities between the actinides and the less harmful lanthanides in their ionic radii and identical oxidation states. Several ligands for selective separation of trivalent actinides from lanthanides, and fission products have been reported: Gullu et al.¹¹¹ have synthesized macrocyclic receptors based on the lactam ionophore. The observed change in the emission and absorption spectra of these compounds upon lanthanide addition was attributed to intramolecular energy transfer process. A fluorescent diazostilbene/benzo-15-crown sensor¹¹² capable of detecting lanthanide ions with high sensitivity and resolution has also been reported. Change in ligand fluorescence was observed when equimolar amounts of lanthanide was added to a ligand solution in THF. A cyclen-based fluorescent ligand capable of detecting micromolar concentrations of Y(III) and La(III) ions in aqueous solutions was reported by Aoki et al.¹¹³

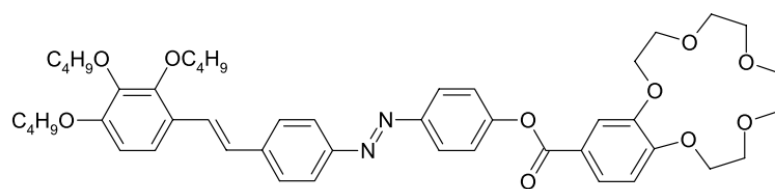


Figure 1.21. A fluorescent probe bearing a diazostilbene chromophore and a benzo-15-crown-5 ether moiety reported by Bekiari et al.

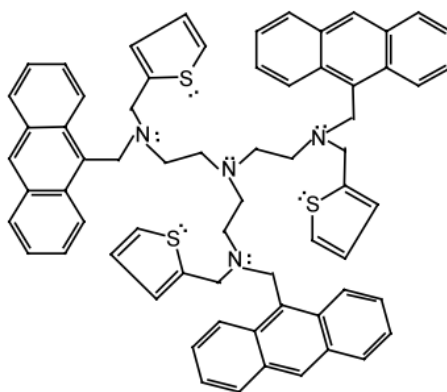


Figure 1.22. A tripodal N-anthracen-9-ylmethyl-N7,N7-bis-[2-(anthracen-9-ylmethylthiophen-2-ylmethylamino)ethyl]-N-thiophen-2-ylmethyl-ethane-1,2-diamine with Selective fluorescence enhancement for Ce^{3+} in dry tetrahydrofuran (THF) reported by Aoki et al .

The coordination chemistry of lanthanide ions with tripodal ligands has also been explored.¹⁰⁴ A tripodal fluoroionophore reported by Das et al.¹⁰⁴ shows selective fluorescence enhancement with Ce(III) in dry THF. The tripodal ligand, tris-(2-benzimidazolylmethyl) amine complexed Ln(III) with 2:1 ligand-to-metal ratio via intramolecular π - π interactions.¹¹⁴

1.14. References

- (1) Munshi, M. K.; Gade, S. M.; Rane, V. H.; Kelkar, A. A. Role of Cation-Anion Cooperation in the Selective Synthesis of Glycidol from Glycerol Using DABCO-DMC Ionic Liquid as Catalyst. *RSC Adv.* **2014**, *4*, 32127–32133.
- (2) Moyer, B. A. Complexation and transport, in: *Comprehensive Supramolecular*

Chemistry, edited by Gokel, G.W. Pergamon, Elsevier, Oxford, **1996**, Chap. 10, vol. 1, pp. 401-405.

- (3) Evans, N. H.; Rahman, H.; Davis, J. J.; Beer, P. D. Surface-Attached Sensors for Cation and Anion Recognition. *Anal. Bioanal. Chem.* **2012**, *402*, 1739-1748.
- (4) Akhuli, B.; Ghosh, P. Selective Recognition and Extraction of KBr via Cooperative Interactions with a Urea Functionalized Crown Ether Dual-Host. *Chem. Commun.* **2015**, *51*, 1-4.
- (5) Wintergerst, M. P.; Levitskaia, T. G.; Moyer, B. A.; Sessler, J. L.; Delmau, L. H. Calix[4]pyrrole: A New Ion-Pair Receptor As Demonstrated by Liquid-Liquid Extraction. *J. Am. Chem. Soc.* **2008**, *130*, 4129-4139.
- (6) Haynes, C. J. E.; Gale, P. A. Transmembrane Anion Transport by Synthetic Systems. *Chem. Commun. (Camb)*. **2011**, *47*, 8203-8209.
- (7) Brak, K.; Jacobsen, E. N. Asymmetric Ion-Pairing Catalysis. *Angew. Chemie - Int. Ed.* **2013**, *52*, 534-561.
- (8) Molina, P.; Tarraga, A.; Alfonso, M. Ferrocene-Based Multichannel Ion-Pair Recognition Receptors. *Dalt. Trans.* **2014**, *43*, 18-29.
- (9) B.D, S. In Ion Pair Recognition by Ditopic Receptors, *Macrocyclic Chemistry: Current Trends and Future Perspectives.*; Gloe K, A. B., Ed.; Kluwer, London, 2005.
- (10) Kirkovits, G. J.; Shriver, J. A.; Gale, P. A.; Sessler, J. L. Synthetic Ditopic Receptors. *J. Incl. Phenom. Macrocycl. Chem.* **2001**, *41*, 69-75.
- (11) Antonisse, M. M. G.; Reinhoudt, D. N. Neutral Anion Receptors: Design and Application. *Chem. Commun.* **1998**, 443-448.
- (12) Kavallieratos, K.; Danby, A.; Berkel, G. J. Van; Kelly, M. A; Sachleben, R. A; Moyer, B. A; Bowman-James, K. Enhancement of CsNO₃ Extraction in 1,2-Dichloroethane by Tris (2-Aminoethyl) Amine Triamide Derivatives via a Dual-Host Strategy Pairwise Anion / Cation Separations. **2008**, *72*, 5258-5264.
- (13) Beer, P. D.; Bernhardt, P. V. ferrocene functionalised macrocyclic receptor for cations and anions. *J. Chem. Soc., Dalt. Trans.* **2001**, 1428-1431.
- (14) Beer, P. D.; Drew, M. G. B.; Knubley, R. J.; Ogden, M. I. Synthesis and coordination chemistry of a novel bis(benzo crown ether) substituted calix[4]arene that can simultaneously complex cations and anions.. *J. Chem. Soc., Dalt. Trans.* **1995**, 3117-3123.
- (15) Cooper, J. B.; Drew, M. G. B.; Beer, P. D. Alkali Metal Cation Cooperative Anion Recognition by Heteroditopic bis(calix[4]arene) rhenium(I) Bipyridyl and Ferrocene Receptor Molecules. *J. Chem. Soc. Dalt. Trans.* **2000**, 2721-2728.

- (16) Cooper, J. B.; Drew, M. G. B.; Beer, P. D. Heteroditopic rhenium(I) and ruthenium(II) bipyridyl calix[4]arene receptors for binding cation–anion ion pairs. *J. Chem. Soc., Dalt. Trans.* **2001**, 392-401.
- (17) Rudkevich, D. M.; Mercer-Chalmers, J. D.; Verboom, W.; Ungaro, R.; de Jong, F.; Reinhoudt, D. N. Bifunctional Recognition: Simultaneous Transport of Cations and Anions through a Supported Liquid Membrane. *J. Am. Chem. Soc.* **1995**, *117*, 6124-6125.
- (18) Reetz, M. T.; Niemeyer, C. M.; Harms, K. Crown Ethers with a Lewis Acidic Center: A New Class of Heterotopic Host Molecules. *Angew. Chemie Int. Ed. English* **1991**, *30*, 1472-1474.
- (19) D. Beer, P.; K. Hopkins, P.; D. McKinney, J. Cooperative Halide, Perrhenate Anion-Sodium Cation Binding and Pertechnetate Extraction and Transport by a Novel Tripodal Tris(amido Benzo-15-Crown-5) Ligand. *Chem. Commun.* **1999**, 1253-1254.
- (20) Kavallieratos, K.; Sachleben, R. A.; Van Berkel, G. J.; Moyer, B. A. Novel Dual-Host Approach in Ion Pair Extraction: A Simple Tripodal Nitrate Host Facilitates CsNO₃ Transfer to 1,2-Dichloroethane by a Large Crown Ether. *Chem. Commun.* **2000**, 187-188.
- (21) Moyer, B. A., Bonnesen, P. V. *Supramolecular Chemistry of Anions*, edited by Bianchi, A.; Bowman-James, K.; Garcia-Espafia E. Wiley-VCH.; Wiley-VCH: New York, 1997.
- (22) Rudkevich, D.M., Brzozka, Z., Palys, M., Visser, H.C., Verboom, W.; and Reinhoudt, D.N. A Difunctional Receptor for the Simultaneous Complexation of Anions and Cations; Recognition of KH₂PO₄. *Angew Chem, Int Ed Engl.* **1994**, *33*, 467-469.
- (23) Savage, P. B.; Holmgren, S. K.; Gellman, S. H. Anion and Ion Pair Complexation by a Macrocyclic Phosphine Oxide Disulfoxide. *J. Am. Chem. Soc.* **1994**, *116*, 4069-4070.
- (24) Reeske, G.; Bradtmöller, G.; Schürmann, M.; Jurkschat, K. Solubilizing Sodium Fluoride in Acetonitrile: Synthesis, Molecular Structure, and Complexation Behavior of Bis(organostannyl)methyl-Substituted Crown Ethers. *Chem. - A Eur. J.* **2007**, *13*, 10239-10245.
- (25) Reeske, G.; Schurmann, M.; Jurkschat, K. Charge Separation by Ditopic Complexation in the Solid State: Molecular Structure of {Ph₂(I)SnCH₂Sn(Ph)(I)CH₂-[16]-Crown-5}NaFCH₃OH. *Dalt. Trans.* **2008**, 3398-3400.

- (26) Reeske, G.; Schürmann, M.; Costisella, B.; Jurkschat, K. Ph(3-n)XnSnCH2-16-Crown-5 (X = F, Cl, Br, I, SCN; N = 1, 2): Intramolecular O → Sn Coordination versus Ditopic Complexation of Sodium Thiocyanate. *Organometallics* **2007**, *26*, 4170-4179.
- (27) Scheerder, J.; Duynhoven, J. P. M. van; Engbersen, J. F. J.; Reinhoudt, D. N. Solubilization of NaX Salts in Chloroform by Bifunctional Receptors. *Angew. Chemie Int. Ed. English* **1996**, *35*, 1090-1093.
- (28) Scheerder, J.; Duynhoven, J. P. M. Van; Engbersen, J. F. J.; Reinhoudt, D. N. Solubilisierung von NaXSalzen in Chloroform Durch Difunktionelle Rezeptoren. *Angew. Chemie* **1996**, *108*, 1172-1175.
- (29) Mahoney, J. M.; Beatty, A. M.; Smith, B. D. Selective Recognition of an Alkali Halide Contact Ion-Pair. *J. Am. Chem. Soc.* **2001**, *123*, 5847-5848.
- (30) Flack, S. S.; Chaumette, J.-L.; Kilburn, J. D.; Langley, G. J.; Webster, M. A Novel Receptor for Dicarboxylic Acid Derivatives. *Chem. Commun.* **1993**, 399-401.
- (31) Lascaux, A.; Le Gac, S.; Wouters, J.; Luhmer, M.; Jabin, I. An Allosteric Heteroditopic Receptor for Neutral Guests and Contact Ion Pairs with a Remarkable Selectivity for Ammonium Fluoride Salts. *Org. Biomol. Chem.* **2010**, *8*, 4607-4616.
- (32) Chutia, R.; Dey, S. K.; Das, G. A Supramolecular Dual-Host Based Ion-Pair Induced Formation of 1D Coordination Polymer. *Cryst. Eng. Comm* **2013**, *15*, 9641-9647.
- (33) Cafeo, G.; Gattuso, G.; Kohnke, F. H.; Notti, A.; Occhipinti, S.; Pappalardo, S.; Parisi, M. F. Remarkable Boosting of the Binding of Ion-Paired Organic Salts by Binary Host Systems. *Angew. Chemie Int. Ed.* **2002**, *41*, 2122-2126.
- (34) Ravikumar, I.; Saha, S.; Ghosh, P. Dual-Host Approach for Liquid-Liquid Extraction of Potassium Fluoride/chloride via Formation of an Integrated 1-D Polymeric Complex. *Chem. Commun.* **2011**, 4721-4723.
- (35) Miyaji, H.; Gasser, G.; Green, S. J.; Molard, Y.; Strawbridge, S. M.; Tucker, J. H. R. Selective Electrochemical Sensing of Acidic Organic Molecules via a Novel Guest-to-Host Proton Transfer Reaction. *Chem. Commun.* **2005**, 5355-5357.
- (36) McConnell, A. J.; Beer, P. D. Heteroditopic Receptors for Ion-Pair Recognition. *Angew. Chemie - Int. Ed.* **2012**, *51*, 5052-5061.
- (37) Alfonso, M.; Espinosa, A.; Tárraga, A.; Molina, P. A Simple but Effective Dual Redox and Fluorescent Ion Pair Receptor Based on a Ferrocene-Imidazopyrene Dyad. *Org. Lett.* **2011**, *13*, 2078-2081.
- (38) De Silva, A. P.; McClean, G. D.; Pagliari, S. Direct Detection of Ion Pairs by Fluorescence Enhancement. *Chem. Commun.* **2003**, 2010-2011.
- (39) Brandstrom, A. Ion-Pair Extraction as a Tool for the Study of Mechanisms of Reactions Related to Phase Transfer Catalysis. *Pure Appl. Chem.* **1982**, *54*, 1769-1782.

- (40) White, D. J.; Laing, N.; Miller, H.; Parsons, S.; Tasker, P. A. Ditopic Ligands for the Simultaneous Solvent Extraction of Cations and Anions Incorporation of a Dianionic Binding Site for Transition Metal Cations and a Dicationic Binding Site for Anions into a Lipophilic Molecule Has Produced a Ligand with a High. *Chem. Commun.* **1999**, 2077-2078.
- (41) Galbraith, S. G.; Plieger, P. G.; Tasker, P. A. Cooperative Sulfate Binding by Metal Salt Extractants Containing 3-Dialkylaminomethylsalicylaldimine Units. *Chem. Commun.* **2002**, 2662-2663.
- (42) Coxall, R. A.; Lindoy, L. F.; Miller, H. A.; Parkin, A.; Parsons, S.; Tasker, P. A.; White, D. J. Solvent Extraction of Metal Sulfates by Zwitterionic Forms of Ditopic Ligands. *Dalt. Trans.* **2003**, 55-64.
- (43) Kavallieratos, K.; Moyer, B. A. Attenuation of Hofmeister Bias in Ion-Pair Extraction by a Disulfonamide Anion Host Used in Strikingly Effective Synergistic Combination with a Calix-Crown Cs⁺ Host. *Chem. Commun.* **2001**, 1620-1621.
- (44) Bates, G. W.; Davidson, J. E.; Forgan, R. S.; Gale, P. A.; Henderson, D. K.; King, M. G.; Light, M. E.; Moore, S. J.; Tasker, P. A.; Tong, C. C. A Dual Host Approach to NiSO₄ Extraction. *Supramol. Chem.* **2012**, 24, 117-126.
- (45) Stockhausen, M. J. M. G. Barthel, H. Krienke, and W. Kunz: Physical Chemistry of Electrolyte Solutions: Modern Aspects (Topics in Physical Chemistry, Vol. 5, Ed. by Deutsche Bunsengesellschaft), Steinkopff, Darmstadt/Springer, New York, 1998, ISBN 3-7985-1076-8, XVII+401. *Berichte der Bunsengesellschaft für Phys. Chemie* **1998**, 102, 1521.
- (46) Smithrud D. B., Sanford, E. M., Chao, I., Ferguson, S. B., Carcanague, D. R., Evanseck, J. D., Houk, K. N., Diederich, F. Solvent Effects in Molecular Recognition. *Pure Appl. Chem* **1990**, 62, 2227.
- (47) Niikura, K.; Metzger, A.; Anslyn, E. V. Chemosensor Ensemble with Selectivity for Inositol-Trisphosphate. *J. Am. Chem. Soc.* **1998**, 120, 8533-8534.
- (48) Metzger, A.; Anslyn, E. V. A Chemosensor for Citrate in Beverages. *Angew. Chem., Int. Ed.* **1998**, 37, 649-652.
- (49) Lavigne, J.; Anslyn, E. V. Teaching Old Indicators New Tricks: A Colorimetric Chemosensing Ensemble for Tartrate/Malate in Beverages. *Angewandte Chemie International Edition, Angew. Chemie, Int. Ed.* **1999**, 38, 3666-3669.
- (50) Fabbrizzi, L., Marcotte, N., Stomeo, F. and Taglietti, A. Pyrophosphate Detection in Water by Fluorescence Competition Assays: Inducing Selectivity through the Choice of the Indicator. *Angew. Chemie Int. Ed.* **2002**, 41, 3811-3814.
- (51) (a) Xu, Z.; Xiao, Y.; Qian, Z.; Cui, J.; Cui, D. Ratiometric and Selective Fluorescent Sensor for CuII Based on Internal Charge Transfer (ICT). *Org. Lett.* **2005**, 7, 889-892. (b) de Silva, A. P.; Gunaratne, H. Q. N.; Gunnlaugsson, T.; Huxley, A. J. M.; McCoy, C. P.; Rademacher, J. T.; Rice, T. E. Signaling

- Recognition Events with Fluorescent Sensors and Switches. *Chem. Rev.* **1997**, *97*, 1515–1566. (c) Sasaki, S.; Niko, Y.; Igawa K.; Konishi, G. Aggregation-induced emission active D- π -A binaphthyl luminophore with dual-mode fluorescence *RSC Adv.*, **2014**, *4*, 33474–33477
- (52) De Silva, S. A., Kasner, M. L., Whitener, M. A. and Pathirana, S. L. A Computational Study of a Fluorescent Photoinduced Electron Transfer (PET) Sensor for Cations. *Int. J. Quantum Chem.* **2004**, *100*, 753–757.
- (53) de Silva, S.A.; Zavaleta, A. Fluorescent Photoinduced Electron Transfer Sensor for Cations with an off-on-off Proton Switch. *Tetrahedron Lett.* **1997**, *38*, 2237–2240.
- (54) Harris, D. “Applications of Spectrophotometry”. Quantitative Chemical Analysis 8th ed.; W. H. Freeman and Co.: New York, 2010.
- (55) Cheng, P.-C. “The Contrast Formation in Optical Microscopy”. In Pawley, James B. Handbook Of Biological Confocal Microscopy; Springer.: New York, 2006; pp. 162-206.
- (56) (a) Helms, V. “Fluorescence Resonance Energy Transfer”. *Principles of Computational Cell Biology.*; Wiley-VCH: New York, 2008. (b) Lee, Y. H.; Lee, M. H.; Zhang J. F.; Kim, J. S. Pyrene Excimer-Based Calix [4] arene FRET Chemosensor for Mercury (II). *J. Org. Chem.*, **2010**, *75*, 7159
- (57) Connors, K. A. *Binding Constants*; Wiley: New York, 1987.
- (58) Chin, J.; Oh, J.; Jon S.Y.; Park, S. H.; Walsdorff, C.; Stranix, B.; Ghossoub, A.; Lee, S. K.; Chung, H. J.; Park, S. M.; Kim, K. Tuning and Dissecting Electronic and Steric Effects in Ammonium Receptors: Nonactin vs Artificial Receptors. *J. Am. Chem. Soc.* **2002**, *124*, 5374-5379.
- (59) Kim, H. S.; Do, K. S.; Kim, K. S.; Shim, J. H.; Cha, G. S.; Nam, H. Ammonium Ion Binding Property of Naphtho-Crown Ethers Containing Thiazole as Sub-Cyclic Unit. *Bull. Korean Chem. Soc.* **2004**, *25*, 1465-1470.
- (60) Späth, A.; König, B. Molecular Recognition of Organic Ammonium Ions in Solution Using Synthetic Receptors. *Beilstein J. Org. Chem.* **2010**, *6*, 1-111.
- (61) Neupert-Laves, K.; Dobler, M. The Crystal Structure of the NH₄NCS Complex of Nonactin. *Helv. Chim. Acta.* **1976**, *59*, 614–623.
- (62) Chin, J.; Walsdorff, C.; Stranix, B.; Oh, J.; Chung, H. J.; Park, S. M.; Kim, K. A Rational Approach to Selective Recognition of NH₄⁺ over K⁺. *Angew. Chemie - Int. Ed.* **1999**, *38*, 2756-2759.
- (63) Jon, S. Y.; Kim, J.; Kim, M.; Park, S.; Jeon, W. S.; Heo, J.; Kim, K. A Rationally Designed NH₄⁺ Receptor Based on Cation- π Interaction and Hydrogen Bonding. *Angew. Chemie* **2001**, *113*, 2174-2177.

- (64) Ahn, K. H.; Kim, S.-G.; Jung, J.; Kim, K.-H.; Kim, J.; Chin, J.; Kim, K. Selective Recognition of NH_4^+ over K^+ with Tripodal Oxazoline Receptors. *Chem. Lett.* **2000**, 29, 170-171.
- (65) Ahn, K. H.; Ku, H. Y.; Kim, Y.; Kim, S. G.; Kim, Y. K.; Son, H. S.; Ku, J. K. Fluorescence Sensing of Ammonium and Organoammonium Ions with Tripodal Oxazoline Receptors. *Org. Lett.* **2003**, 5, 1419-1422.
- (66) Cho, S. J.; Sasaki, S.; Ikebukuro, K.; Karube, I. A Simple Nitrate Sensor System Using Titanium Trichloride and an Ammonium Electrode. *Sensors Actuators B Chem.* **2002**, 85, 120-125.
- (67) Bisson, A. P.; Lynch, V. M.; Monahan, M.-K. C.; Anslyn, E. V. Recognition of Anions through $\text{NH}-\pi$ Hydrogen Bonds in a Bicyclic Cyclophane Selectivity for Nitrate. *Angew. Chemie Int. Ed. English* **1997**, 36, 2340-2342.
- (68) Valiyaveetil, S.; Engbersen, J. F. J.; Verboom, W.; Reinhoudt, D. N. Synthesis and Complexation Studies of Neutral Anion Receptors. *Angew. Chemie Int. Ed. English* **1993**, 32, 900-901.
- (69) Corradini, R.; Dossena, A.; Galaverna, G.; Marchelli, R.; Panagia, A.; Sartor, G. Fluorescent Chemosensor for Organic Guests and Copper(II) Ion Based on Dansyldiethylenetriamine-Modified β -Cyclodextrin. *J. Org. Chem.* **1997**, 62, 6283-6289.
- (70) Ikeda, H.; Nakamura, M.; Ise, N.; Toda, F.; Ueno, A. NMR Studies of Conformations of N-Dansyl-L-Leucine-Appended and N-Dansyl-D-Leucine-Appended β -Cyclodextrin as Fluorescent Indicators for Molecular Recognition. *J. Org. Chem.* **1997**, 62, 1411-1418.
- (71) Hamasaki, K.; Ikeda, H.; Nakamura, A.; Ueno, A.; Toda, F.; Suzuki, I.; Osa, T. Fluorescent Sensors of Molecular Recognition. Modified Cyclodextrins Capable of Exhibiting Guest-Responsive Twisted Intramolecular Charge Transfer Fluorescence. *J. Am. Chem. Soc.* **1993**, 115, 5035-5040.
- (72) Effects of the Polymer Matrix on an Optical Nitrate Sensor Based on a Polarity-Sensitive Dye. *Sensors Actuators B Chem.* **1996**, 37, 103-109.
- (73) Le Goff, T.; Braven, J.; Ebdon, L.; Scholefield, D. High-Performance Nitrate-Selective Electrodes Containing Immobilized Amino Acid Betaines as Sensors. *Anal. Chem.* **2002**, 74, 2596-2602.
- (74) Huber, C., Klimant, I., Krause, C., Werner, T., Wolfbeis, O. Nitrate-Selective Optical Sensor Applying a Lipophilic Fluorescent Potential-Sensitive Dye. *Anal. Chim. Acta* **2001**, 449, 81-93.
- (75) Mahieux, B.; Carré, M. C.; Viriot, M. L.; André, J. C.; Donner, M. Fiber-Optic Fluorescing Sensors for Nitrate and Nitrite Detection. *J. Fluoresc.* **1994**, 4, 7-10.

- (76) Renzoni, A.; Zino, F.; Franchi, E. Mercury Levels along the Food Chain and Risk for Exposed Populations. *Environ. Res.* **1998**, *77*, 68-72.
- (77) Harris, H. H.; Pickering, I. J.; George, G. N. The Chemical Form of Mercury in Fish. *Science.* **2003**, *301*, 1203.
- (78) Tchounwou, P. B.; Yedjou, C. G.; Patlolla, A. K.; Sutton, D. J. Heavy Metals Toxicity and the Environment. *EXS* **2012**, *101*, 133-164.
- (79) Akagi, H.; Grandjean, P.; Takizawa, Y.; Weihe, P. Methylmercury Dose Estimation from Umbilical Cord Concentrations in Patients with Minamata Disease. *Environ. Res.* **1998**, *77*, 98-103.
- (80) Cavalleri, A.; Gobba, F. Reversible Color Vision Loss in Occupational Exposure to Metallic Mercury. *Environ. Res.* **1998**, *77*, 173-177.
- (81) Grandjean, P.; Weihe, P.; White, R. F.; Debes, F. Cognitive Performance of Children Prenatally Exposed to “Safe” Levels of Methylmercury. *Environ. Res.* **1998**, *77*, 165-172.
- (82) Henriksson, J.; Tjälve, H. Uptake of Inorganic Mercury in the Olfactory Bulbs via Olfactory Pathways in Rats. *Environ. Res.* **1998**, *77*, 130-140.
- (83) Mahaffey, K. R.; Mergler, D. Blood Levels of Total and Organic Mercury in Residents of the Upper St. Lawrence River Basin, Québec: Association with Age, Gender, and Fish Consumption. *Environ. Res.* **1998**, *77*, 104-114.
- (84) Shenker, B. J.; Guo, T. L.; Shapiro, I. M. Low-Level Methylmercury Exposure Causes Human T-Cells to Undergo Apoptosis: Evidence of Mitochondrial Dysfunction. *Environ. Res.* **1998**, *77*, 149-159.
- (85) Zhou, Y.; Ma, Z. Colorimetric Detection of Hg²⁺ by Au Nanoparticles Formed by H₂O₂ Reduction of HAuCl₄ Using Au Nanoclusters as the Catalyst. *Sensors Actuators B Chem.* **2017**, *241*, 1063-1068.
- (86) Tan, L.; Zhang, Y.; Qiang, H.; Li, Y.; Sun, J.; Hu, L.; Chen, Z. A Sensitive Hg(II) Colorimetric Sensor Based on Synergistic Catalytic Effect of Gold Nanoparticles and Hg. *Sensors Actuators B Chem.* **2016**, *229*, 686-691.
- (87) Zhao, Y.; Gui, L.; Chen, Z. Colorimetric Detection of Hg²⁺ Based on Target-Mediated Growth of Gold Nanoparticles. *Sensors Actuators B Chem.* **2017**, *241*, 262-267.
- (88) Tian, K.; Siegel, G.; Tiwari, A. A Simple and Selective Colorimetric Mercury (II) Sensing System Based on Chitosan Stabilized Gold Nanoparticles and 2,6-Pyridinedicarboxylic Acid. *Mater. Sci. Eng. C* **2017**, *71*, 195-199.
- (89) Che, Y.; Wu, D.; Deng, C.; Liu, L.; Jia, D. 5-Bromoindole-3-Carboxaldehyde Ethylthiosemicarbazone for Hg(II) Sensing and Removal. *Chem. Phys. Lett.* **2016**, *644*, 171-175.

- (90) Angupillai, S.; Hwang, J.-Y.; Lee, J.-Y.; Rao, B. A.; Son, Y.-A. Efficient Rhodamine-Thiosemicarbazide-Based Colorimetric/fluorescent “Turn-On” Chemodosimeters for the Detection of Hg²⁺ in Aqueous Samples. *Sensors Actuators B Chem.* **2015**, *214*, 101-110.
- (91) Song, K.; Mo, J.; Lu, C. Hg(II) Sensing Platforms with Improved Photostability: The Combination of Rhodamine Derived Chemosensors and up-Conversion Nanocrystals. *Spectrochim. Acta Part A Mol. Biomol. Spectrosc.* **2017**, *179*, 125-131.
- (92) Wan, D.; Li, Y.; Zhu, P. A Series of Emission “turn-On” Probes Derived from Rhodamine for Hg(II) Recognition and Sensing: Synthesis, Characterization and Performance. *Sensors Actuators B Chem.* **2015**, *221*, 1271-1278.
- (93) Nutiu, R.; Li, Y. Structure-Switching Signaling Aptamers. *J. Am. Chem. Soc.* **2003**, *125*, 4771.
- (94) Jun, W.; Kai, R.; Beijing, H. Synthesis and Sensing Behavior of Fluorescence “turn-On” Chemosensors Based on Rhodamine for Hg(II) Detection. *Sensors Actuators B Chem.* **2016**, *224*, 465-477.
- (95) Ramette, R. W.; Sandell, E. B. Rhodamine B Equilibria. *J. Am. Chem. Soc.* **1956**, *78*, 4872-4878.
- (96) Zhou, S.; Zhou, Z.-Q.; Zhao, X.-X.; Xiao, Y.-H.; Xi, G.; Liu, J.-T.; Zhao, B.-X. A Dansyl Based Fluorescence Chemosensor for Hg(II) and Its Application in the Complicated Environment Samples. *Spectrochim. Acta Part A Mol. Biomol. Spectrosc.* **2015**, *148*, 348-354.
- (97) Srivastava, P.; Ali, R.; Razi, S. S.; Shahid, M.; Patnaik, S.; Misra, A. A Simple Blue Fluorescent Probe to Detect Hg²⁺ in Semiaqueous Environment by Intramolecular Charge Transfer Mechanism. *Tetrahedron Lett.* **2013**, *54*, 3688-3693.
- (98) Wanichacheva, N.; Kumsorn, P.; Sangsuwan, R.; Kamkaew, A.; Lee, V. S.; Grudpan, K. A New Fluorescent Sensor Bearing Three Dansyl Fluorophores for Highly Sensitive and Selective Detection of mercury(II) Ions. *Tetrahedron Lett.* **2011**, *52*, 6133-6136.
- (99) Li, H.-W.; Wang, B.; Dang, Y.-Q.; Li, L.; Wu, Y. A Highly Selective Fluorescent Sensor for Mercury Ions in Aqueous Solution: Detection Based on Target-Induced Aggregation. *Sensors Actuators B Chem.* **2010**, *148*, 49-53.
- (100) Métivier, R.; Leray, I.; Valeur, B. Lead and Mercury Sensing by Calixarene-Based Fluoroionophores Bearing Two or Four Dansyl Fluorophores. *Chem. - A Eur. J.* **2004**, *10*, 4480-4490.
- (101) Hudson, M. J.; Harwood, L. M.; Laventine, D. M.; Lewis, F. W. Use of Soft Heterocyclic N-Donor Ligands To Separate Actinides and Lanthanides. *Inorg. Chem.* **2013**, *52*, 3414-3428.

- (102) Bhattacharyya, A.; Mohapatra P.K.; Manchanda, V. K. Separation of Americium(III) and Europium(III) from Nitrate Medium Using a Binary Mixture of Cyanex-301 with N-donor Ligands. *Solvent Extr. Ion Exch.* **2006**, *24*, 1-17.
- (103) Radioactive Waste Partitioning and Transmutation within Advanced Fuel Cycles: Achievements and Challenges. *Prog. Part. Nucl. Phys.* **2011**, *66*, 144-166.
- (104) Ghosh, P.; Shukla, A. D.; Das, A. Cerium Ion-Induced Fluorescence Enhancement of a Tripodal Fluoroionophore. *Tetrahedron Lett.* **2002**, *43*, 7419-7422.
- (105) Panak, P. J.; Geist, A. Complexation and Extraction of Trivalent Actinides and Lanthanides by Triazinylpyridine N-Donor Ligands. *Chem. Rev.* **2013**, *113*, 1199-1236.
- (106) Demir, S.; Brune, N. K.; Van Humbeck, J. F.; Mason, J. A.; Plakhova, T. V.; Wang, S.; Tian, G.; Minasian, S. G.; Tyliczszak, T.; Yaita, T.; Kobayashi, T.; Kalmykov, S. N.; Shiwaku, H.; Shuh, D. K.; Long, J. R. Extraction of Lanthanide and Actinide Ions from Aqueous Mixtures Using a Carboxylic Acid-Functionalized Porous Aromatic Framework. *ACS Cent. Sci.* **2016**, *2*, 253-265.
- (107) Edwards, A. C.; Wagner, C.; Geist, A.; Burton, N. A.; Sharrad, C. A.; Adams, R. W.; Pritchard, R. G.; Panak, P. J.; Whitehead, R. C.; Harwood, L. M. Exploring Electronic Effects on the Partitioning of actinides(III) from lanthanides(III) Using Functionalised Bis-Triazinyl Phenanthroline Ligands. *Dalton Trans.* **2016**, *45*, 18102-18112
- (108) Macerata, E.; Mossini, E.; Scaravaggi, S.; Mariani, M.; Mele, A.; Panzeri, W.; Boubals, N.; Berthon, L.; Charbonnel, M.-C.; Sansone, F.; Arduini, A.; Casnati, A. Hydrophilic Clicked 2,6-Bis-Triazolyl-Pyridines Endowed with High Actinide Selectivity and Radiochemical Stability: Toward a Closed Nuclear Fuel Cycle. *J. Am. Chem. Soc.* **2016**, *138*, 7232-7235.
- (109) Geist, A.; Müllich, U.; Magnusson, D.; Kaden, P.; Modolo, G.; Wilden, A.; Zevaco, T. Actinide(III)/Lanthanide(III) Separation Via Selective Aqueous Complexation of Actinides(III) Using a Hydrophilic 2,6-Bis(1,2,4-Triazin-3-Yl)-Pyridine in Nitric Acid. *Solvent Extr. Ion Exch.* **2012**, *30*, 433-444.
- (110) Zalupski, P. R.; Nash, K. L.; Martin, L. R. Thermodynamic Features of the Complexation of Neodymium(III) and Americium(III) by Lactate in Trifluoromethanesulfonate Media. *J. Solut. Chem.* **2010**, *39*, 1213-1229.
- (111) Güllü, F.; Bayrakçı, M.; Kursunlu, A. N.; Yiğiter, Ş.; Ertul, Ş. Synthesis and Trivalent Lanthanide Ion Complexation Studies of New Macrocyclic Receptors Based Lactam Ionophores. *J. Incl. Phenom. Macrocycl. Chem.* **2014**, *80*, 303-312.
- (112) Bekiari, V.; Judeinstein, P.; Lianos, P. A Sensitive Fluorescent Sensor of Lanthanide Ions. *J. Lumin.* **2003**, *104*, 13-15.
- (113) Aoki, S.; Kawatani, H.; Goto, T.; Kimura, E.; Shiro, M. A Double-Functionalized Cyclen with Carbamoyl and Dansyl Groups (Cyclen = 1,4,7,10-

Tetraazacyclododecane): A Selective Fluorescent Probe for Y^{3+} and La^{3+} . *J. Am. Chem. Soc.* **2001**, *123*, 1123-132.

- (114) Wietzke, R.; Mazzanti, M. Strong Intramolecular $[\pi]$ - $[\pi]$ Interactions Favor the Formation of 2:1 (L:M) Lanthanide Complexes of tris(2-Benzimidazolylmethyl)amine. *Chem. Commun.* **1999**, 209-210.

CHAPTER II

Remarkably selective NH₄⁺ binding and fluorescence sensing by tripodal tris(pyrazolyl) receptors derived from 1,3,5-triethylbenzene.

Tosin M. Jonah, Logesh Mathivathanan, Alexander N. Morozov, Alexander M. Mebel,
Raphael G. Raptis and Konstantinos Kavallieratos*

Department of Chemistry and Biochemistry and the Biomolecular Sciences Institute,
Florida International University, 11200 SW 8th St, Miami, FL 33199, USA

(New J. Chem. **2017**, *41*, 14835-14838; DOI: 10.1039/c7nj03213g)

2.1. ABSTRACT

A tripodal fluorescent sensor for NH_4^+ based on 1,3,5-triethylbenzene shows remarkable binding and sensing selectivity for NH_4^+ vs. K^+ . Fluorescence and NMR titrations reveal surprising differences in sensing properties and binding constants for the tris-(3,5-dimethyl)pyrazole **1** vs. the tris(3,5-diphenyl)pyrazole **2**. The X-ray structure of **2**. NH_4^+ and DFT calculations for **1**, **2** and their ammonium complexes highlight the role of ion pairing of NH_4^+ with the PF_6^- counteranion, in explaining these differences.

2.2. Introduction

The design and synthesis of selective NH_4^+ receptors and sensors is of biological and environmental importance.¹ Synthetic NH_4^+ receptors have found uses in measuring the urea and creatinine levels and in environmental applications.²⁻⁴ However, achieving selectivity for NH_4^+ over K^+ remains a challenge due to their similar ionic radii (286 vs. 266 pm, respectively).⁵ Receptors that bind NH_4^+ via hydrogen bonding, including crown ethers and nonactin derivatives, have been reported.⁵⁻⁹ Some remarkable examples include a cryptand/crown ether system reported by Shim et al. that binds NH_4^+ with a K_a two orders of magnitude greater than that for K^+ ($K_{a,\text{NH}_4^+}/K_{a,\text{K}^+} = 2.3 \times 10^2$)^{10a} and a cryptand family with pre-organized tetrahedral donor sites developed by Lehn et al. with a NH_4^+/K^+ selectivity of up to 500.^{10b} Tripodal 1,3,5-trisubstituted benzene frameworks have found application in supramolecular chemistry for cation and anion binding and sensing:^{11,12} A polyether cryptand-type receptor derived from 1,3,5-triethylbenzene has shown high sensitivity and selectivity for NH_4^+ , comparable to nonactin in an

ion-selective electrode; the high selectivity was ascribed to cation- π interactions.¹³ Oxazolines derived from the analogous 1,3,5-trimethylbenzene framework,^{14,15} showed selective fluorescence response for NH_4^+ over K^+ , Na^+ , and Mg^{2+} in the 305-340 nm range ($\lambda_{\text{exc}} = 272$ nm). Tripodal pyrazoles have been reported as redox-activated MRI contrast agents,¹⁶ and ion-selective electrodes modified with tripodal pyrazolyl¹⁷ analogs, such as 1,3,5-tris-(3,5-dimethylpyrazolyl)-2,4,6-triethylbenzene (**1**), have shown selectivity for NH_4^+ over K^+ . However, NMR and fluorescence studies of NH_4^+ binding with pyrazolyl hosts have not been previously undertaken.

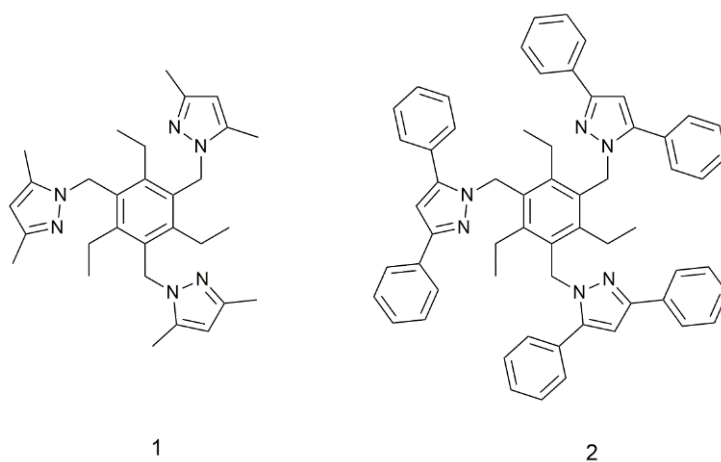


Figure 2.1. Chemical structure of ligands **1** and **2**.

Herein, we report a new pyrazole receptor (**2**), based on the 1,3,5-triethylbenzene framework, and for the first time selective fluorescence sensing of NH_4^+ vs. K^+ by any pyrazole-type receptor. $^1\text{H-NMR}$ titrations reveal remarkable binding strength and selectivity for NH_4^+ over K^+ for **1**, and a surprising difference in binding constants between trispyrazoles **1** and **2**. The X-ray structure of $\mathbf{2}\cdot\text{NH}_4^+$ and DFT calculations for **1**, **2** and their corresponding NH_4^+ complexes provide consistent

information related to the lack of ion pairing of NH_4^+ with the PF_6^- counteranion for **2** that may explain the dramatic NH_4^+ binding differences between **1** and **2**.

2.3. Results and Discussion

Both compounds were prepared by modification of previously reported methods.^{17,18} Fluorescence titrations of **1** and **2** with NH_4PF_6 at constant receptor concentration ($1.0 \times 10^{-4} \text{ M}$) were carried out in $\text{CH}_3\text{CN}/\text{CH}_2\text{Cl}_2(1:1)$ with $\lambda_{\text{exc}} = 272 \text{ nm}$ for **1** and $\lambda_{\text{exc}} = 262 \text{ nm}$ for **2**. Addition of NH_4PF_6 to tris-(3,5-dimethylpyrazole) **1** showed an increase in fluorescence upon cation binding, which is significantly higher for NH_4^+ vs. K^+ (Fig. 2.2), a pattern similar to the one observed for analogous tripodal oxazolines.¹⁵ The diphenyl analog **2** did not show such increases and instead showed fluorescence quenching (Fig 2.3). This sharp difference in sensing behavior between the dimethyl and diphenyl analogy is striking.

The cation binding properties of **1** and **2** were determined in acetone- d_6 by ^1H -NMR titrations with M^+PF_6^- ($\text{M}^+ = \text{NH}_4^+, \text{K}^+$, Fig. 2.4). The association constants for the formation of 1:1 complex (K_a), were determined by non-linear regression analysis using the 1:1 binding isotherm. For **1**, downfield shifts for all proton resonances were observed except for the $-\text{CH}_2-$ of the ethyl group, which shifted upfield. Non-linear regression analysis of the binding isotherms obtained from these shifts gave a 1:1 association constant K_a of $74000 (\pm 900) \text{ M}^{-1}$ for the formation of $\mathbf{1} \cdot \text{NH}_4^+$ and a K_a of $22 \text{ M}^{-1} (\pm 1)$ for $\mathbf{1} \cdot \text{K}^+$. In order to include Na^+ in the comparison, and due to the limited solubility of NaPF_6 in acetone- d_6 , the experiments were repeated in CD_3OD (Fig. 2.5). The association constants, K_a obtained by NMR show

the preference of **1** for NH_4^+ ($K_a = 163 \text{ M}^{-1}$) over Na^+ ($K_a = 4 \text{ M}^{-1}$) and K^+ (for which the chemical shift changes were too small to give a reliable binding curve fit).

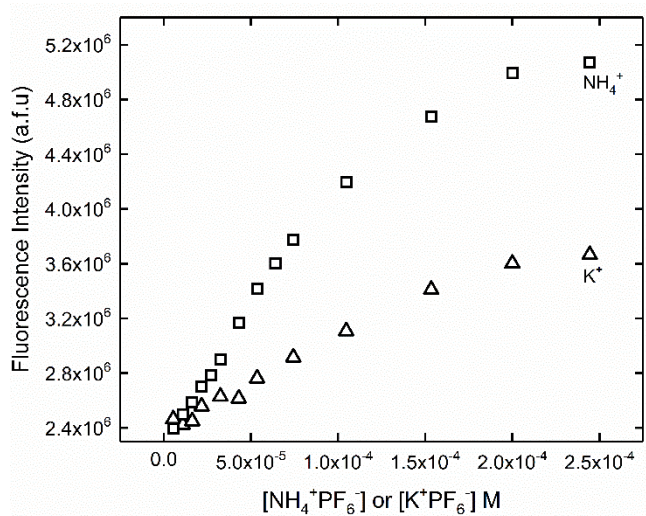


Figure 2.2. Fluorescence titration ($\lambda_{\text{exc}} = 272\text{nm}$) of **1** ($1.0 \times 10^{-4} \text{ M}$) with $\text{NH}_4^+\text{PF}_6^-$ or K^+PF_6^- in $\text{CH}_3\text{CN}/\text{CH}_2\text{Cl}_2$ (1:1).

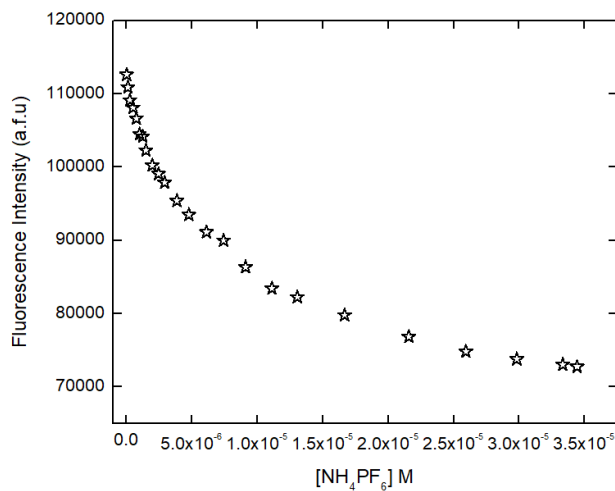


Figure 2.3. Fluorescence titration ($\lambda_{\text{exc}} = 262 \text{ nm}$) of **2** with $\text{NH}_4^+\text{PF}_6^-$ in $(\text{CH}_3\text{CN}/\text{CH}_2\text{Cl}_2$ (1:1)).

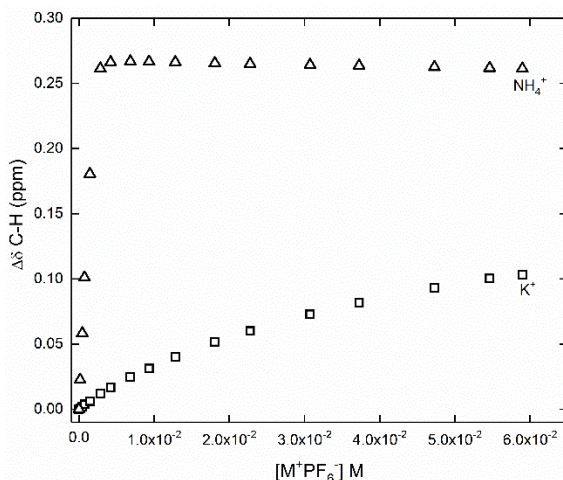


Figure 2.4. ¹H-NMR titration plot of **1** (for CH₃CH₂) with M⁺PF₆⁻ (M⁺ = NH₄⁺, K⁺) in acetone-d₆. The concentration of **1** was kept constant at 2 mM.

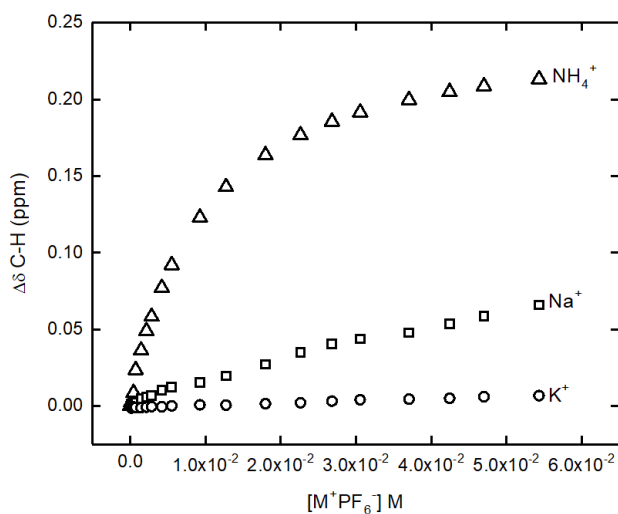


Figure 2.5. ¹H-NMR titration of **1** with M⁺PF₆⁻ in CD₃OD (M = NH₄⁺, Na⁺, or K⁺). The concentration of **1** was kept constant at 2 mM.

For **2**, (unlike for **1**) the CH₃ protons of the ethyl group shift downfield upon addition of NH₄PF₆ instead of upfield. The association constant for the **2**·NH₄⁺ complex in acetone-d₆ was found to be only 15 M⁻¹, which is almost four orders of magnitude lower than those of the dimethyl analog **1**. This dramatic difference in binding cannot be simply explained by electronic and steric effects, as the cavity of

the tris(diphenyl)pyrazole can comfortably accommodate the NH_4^+ (as seen in the X-ray structure). The 1:1 complexation stoichiometry indicated by the titration curve fits, was also verified by the continuous variation method¹⁹ with Job plot maxima at mol fraction of 0.5 for both **1** and **2** (Fig. 2.6 & 2.7).

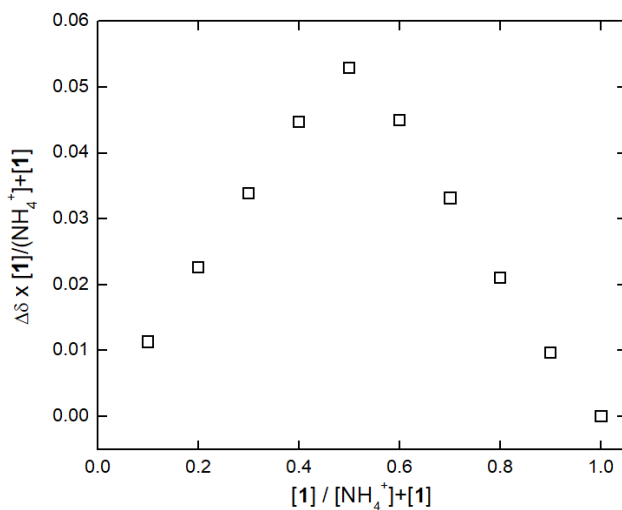


Figure 2.6. Jobs plot of **1** (CH_3CH_2^-) with $\text{NH}_4^+\text{PF}_6^-$ in acetone- d_6 . 0.002 M Stock solutions of **1** and $\text{NH}_4^+\text{PF}_6^-$ were used.

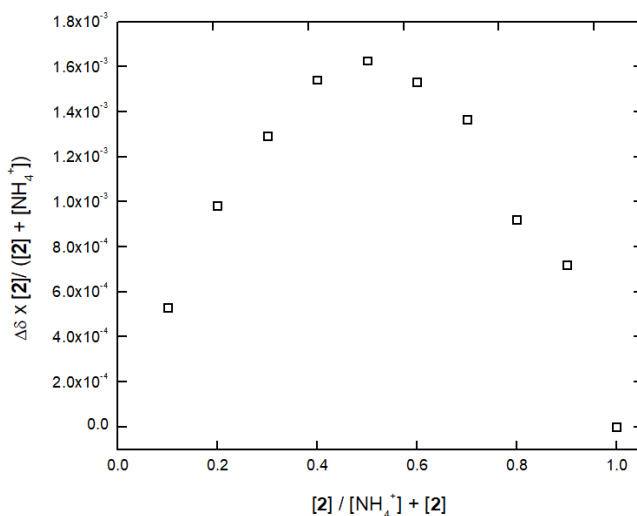


Figure 2.7. Jobs plot for **2** with $\text{NH}_4^+\text{PF}_6^-$ in acetone- d_6 . 0.002 M Stock solutions of **2** and $\text{NH}_4^+\text{PF}_6^-$ were used.

X-ray structural analysis of the crystals of $[\mathbf{2}\cdot\text{NH}_4]^+\text{PF}_6^-$ (Fig. 2.8 & 2.9) obtained by diffusion of Et_2O into a methanol solution of $\mathbf{2}$ and $\text{NH}_4^+\text{PF}_6^-$ (1:1 molar ratio) shows important similarities and differences with the $[\mathbf{1}\cdot\text{NH}_4]^+\text{PF}_6^-$ X-ray structure previously published by Chin et al.^{17b} All three pyrazole rings are directed towards the bound NH_4^+ , but unlike the X-ray structure of $[\mathbf{1}\cdot\text{NH}_4]^+\text{PF}_6^-$ all three ethyl groups are now directed on the opposite side of the central aromatic ring. A crystallographic 3-fold symmetry axis now runs through the ammonium N-atom and the aromatic centroid. The three symmetry-related H-bonded N...N distances between the ammonium and the pyrazole are 2.950(2) Å, indicating strong hydrogen bonding. In the published structure of $[\mathbf{1}\cdot\text{NH}_4]^+\text{PF}_6^-$ however,^{17b} the three N...N distances of 2.948(5) Å, 3.001(4) Å, and 3.053(4) Å are longer - on average, 3.00(4) Å. Both $[\mathbf{2}\cdot\text{NH}_4]^+\text{PF}_6^-$ and $[\mathbf{1}\cdot\text{NH}_4]^+\text{PF}_6^-$ show cation- π interactions between NH_4^+ and the central aromatic ring, with the $[\mathbf{2}\cdot\text{NH}_4]^+\text{PF}_6^-$ structure showing a slightly stronger interaction with an N-centroid distance of 3.030(6) Å vs. 3.131(3) Å in $[\mathbf{1}\cdot\text{NH}_4]^+\text{PF}_6^-$. The small difference in the N-H...N distances between $[\mathbf{1}\cdot\text{NH}_4]^+\text{PF}_6^-$ and $[\mathbf{2}\cdot\text{NH}_4]^+\text{PF}_6^-$ indicates that neither the strength of the hydrogen bonding interaction between ammonium and $\mathbf{1}$ or $\mathbf{2}$, nor the differences in cation- π interactions, can explain the remarkable four orders of magnitude difference in the binding affinities of these ligands with NH_4^+ . On the contrary, both the H-bonding distances and the N-centroid distances suggest that $\mathbf{2}$ should bind NH_4^+ stronger than $\mathbf{1}$, which is in direct contrast to the measured NMR binding constants. However, a key observation in the crystal structure of $[\mathbf{2}\cdot\text{NH}_4]^+\text{PF}_6^-$ may explain this discrepancy: The lack of any interaction between the complexed NH_4^+ and the PF_6^- counteranion, presumably because the NH_4^+ cation is “buried” among the phenyl rings of the pyrazoles, prevents the approach of PF_6^- , leading

to a well-separated ion pair. This is unlike the crystal structure of $[1 \cdot \text{NH}_4]^+\text{PF}_6^-$,^{17b} which shows weak H-bonding between the complexed NH_4^+ and the F of the PF_6^- counteranion ($\text{F} \cdots \text{N}$ distance of 3.031(4) Å). This difference between **1** and **2** in facilitating ion pairing between NH_4^+ and PF_6^- can explain the binding constant trends, as the thermodynamic contribution of second-sphere coordination²⁰⁻²¹ to overall binding by ion pair interactions is very substantial.²²⁻²⁵

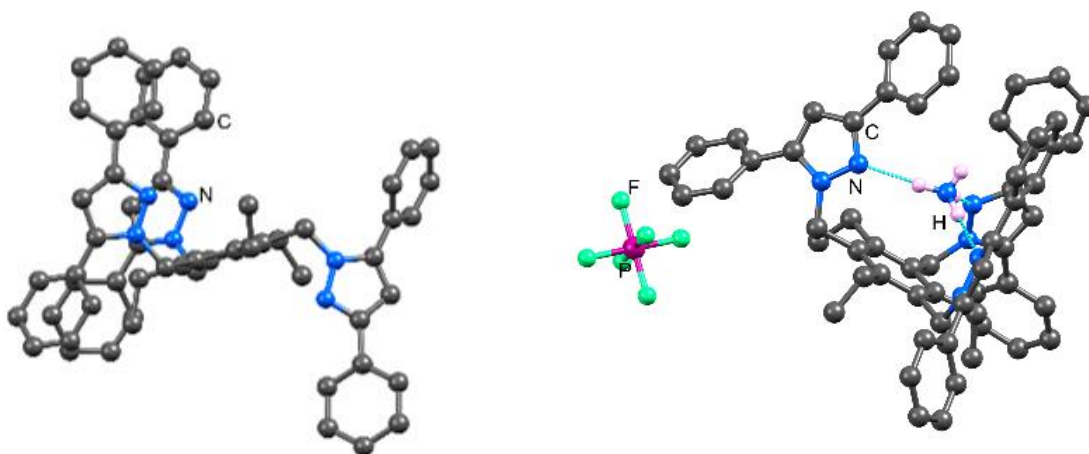


Figure 2.8. Crystal structure of **[2]** (left) vs. **2.NH₄PF₆** (right). H-atoms and disorders on phenyl rings are not shown for clarity.

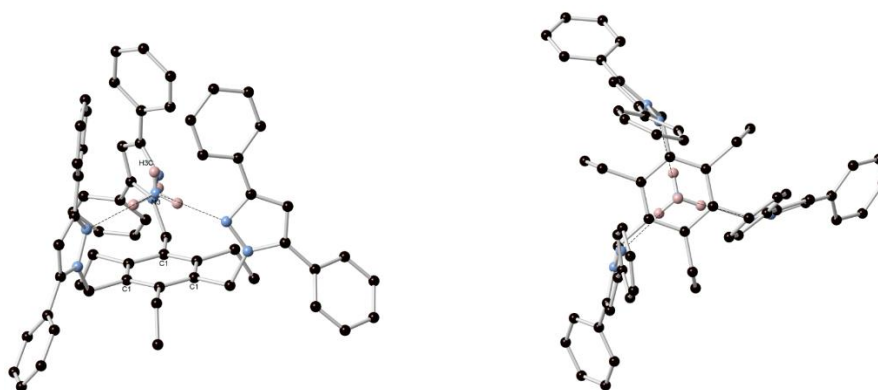


Figure 2.9. Crystal structure of $[2 \cdot \text{NH}_4]^+\text{PF}_6^-$ showing NH_4^+ H-bonded to the **2** host. $\text{N}(\text{pz}) \cdots \text{N}(\text{NH}_4)$ distance: 2.950(3) Å. The disordered PF_6^- is not shown for clarity.

In order to further understand the NH_4^+ binding properties for **1** and **2** and the roles of ion pairing and solvation *vs.* chelation,²⁶ DFT 6-31G**/B3LYP calculations of Gibbs free energies (ΔG) for NH_4^+ , PF_6^- , **L**, $[\text{L}\cdot\text{NH}_4]^+$ and $[\text{L}\cdot\text{NH}_4]^+\text{PF}_6^-$ (**L** = **1**, **2**) were conducted. In the gas phase, the complex formation reaction $\text{L} + \text{NH}_4^+ \rightarrow [\text{L}\cdot\text{NH}_4]^+$ is exergonic by -60.8 kcal/mol and -61.9 kcal/mol for **1** and **2**, respectively at ambient temperature. When acetone solvation is taken into account, the corresponding ΔG values change to -12.2 kcal/mol and -9.3 kcal/mol, respectively. The DFT results are in line with the experimental data and indicate that solvation effect decisively contributes to the measured difference in NH_4^+ binding by **1** and **2**. The $[\text{2}\cdot\text{NH}_4]^+$ complex creates a larger cavity in solvent than $[\text{1}\cdot\text{NH}_4]^+$, making solvation less favorable. The calculated ΔG for the formation of $[\text{1}\cdot\text{NH}_4]^+\text{PF}_6^-$ is exergonic both in the gas phase (-68.2 kcal/mol) and in acetone (-0.8 kcal/mol). This agrees with the presence of ion pairing in the crystal structure.^{17b} Alternatively, the ΔG for the formation of $[\text{2}\cdot\text{NH}_4]^+\text{PF}_6^-$ is exergonic in the gas phase (-43.8 kcal/mol), but endergonic in acetone (8.2 kcal/mol), which again agrees with the absence of ion pairing in the $[\text{2}\cdot\text{NH}_4]^+\text{PF}_6^-$ crystal structure. Thus, the DFT results (Fig. 2.11) corroborate our hypothesis that the lack of ion pairing^{25b} in $[\text{2}\cdot\text{NH}_4]^+\text{PF}_6^-$ strongly contributes to the observed difference in the NH_4^+ binding properties between **1** and **2**.

2.4. Conclusion

In conclusion, selective NH_4^+ binding and fluorescence sensing by tripodal pyrazolyl receptors were demonstrated. Spectroscopic studies in solution, X-ray structural information, and DFT calculations all point to the importance of ion pairing and solvation

in determining binding strength and selectivity, with pyrazole substitution leading to remarkable differences. We are currently probing the binding properties of these ligand platforms by further structural, spectroscopic and theoretical investigations involving other ion pairs.

2.5 Experimental Section

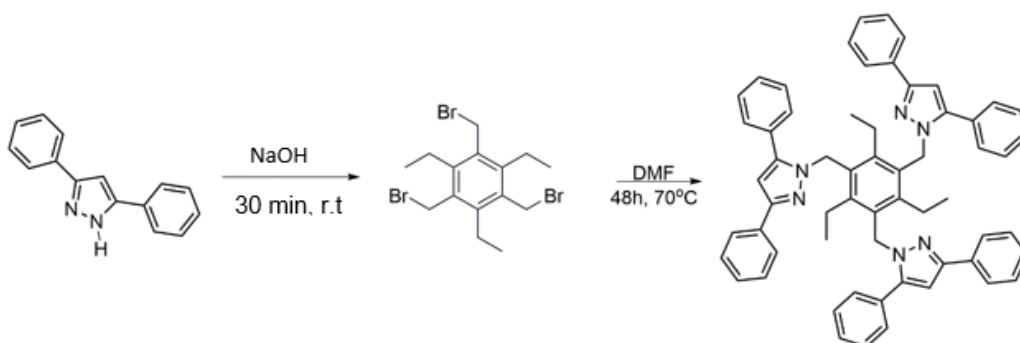
2.5.1 Materials and Methods

All chemicals were purchased from Aldrich Chemical Company or ACROS Organics, were standard reagent grade and were used without further purification unless otherwise noted. 1,3,5-trisbromomethyl-2,4,6-triethylbenzene was either purchased from Aldrich Chemicals, or synthesized as previously reported.²⁷ The tris-(pyrazolyl) ammonium receptor **1** was prepared from 1,3,5-tris-(bromomethyl)-2,4,6-triethylbenzene, NaH and 3,5-dimethylpyrazole, according to a previously published procedure, and was found spectroscopically to be identical to the reported compound.^{17b} ¹H and ¹³C NMR spectra were recorded on a 400 MHz Bruker NMR spectrometer and were referenced to the residual solvent resonance. All chemical shifts, δ , are reported in ppm. Fluorescence spectra were recorded on a Jobin-Yvon Horiba Fluoromax-3 instrument, or a Photon Technologies Model PTI- QuantaMaster UV-Vis QM-4 steady state spectrofluorometer. Elemental analysis was obtained at Galbraith Labs, Knoxville, TN.

2.5.2 Synthesis of 1,3,5- tris(3,5-diphenyl-1H-pyrazole) -2,4,6-triethylbenzene (2)

The tris-(3,5-diphenyl) analog **2** was synthesized as described below by a modification of a previously published procedure by Arunachalam et al.²⁸ NaOH (72 mg, 1.81 mmol) was dissolved in 5 mL of DMF (dried with 4A molecular sieves). 3,5-diphenyl pyrazole

(398 mg 1.81 mmol) was added to the stirring solution and was allowed to react for 30 min, at room temperature. 1,3,5-tris(bromomethyl)-2,4,6-triethylbenzene (198 mg, 0.45 mmol) was added to the resulting solution and the reaction mixture was stirred for 48 h at 70 °C under N₂. The reaction was allowed to cool to room temperature and then poured into ice/water. The formed solid was filtered, dried, and recrystallized from dichloromethane/hexane. Further purification by silica column chromatography EtOAc/Hexane (1:9) gave 350 mg of the pure product (yield, 90%). ¹H NMR (400 MHz, acetone-d₆) δ 7.75 (d, *J* = 6.7 Hz, 6H), 7.58 (d, *J* = 6.6 Hz, 6H), 7.54 - 7.38 (m, 9H), 7.39 - 7.10 (m, 9H), 6.74 (s, 3H), 5.39 (s, 6H), 2.65 (q, *J* = 7.5 Hz, 6H), 0.67 (t, *J* = 7.5 Hz, 9H). ¹³C-NMR (400 MHz, acetone-d₆) δ 150.2, 144.2, 135.5, 130.5, 128.7, 129.2, 127.5, 10.0, 52.1, 23.8, 15.1. Anal. Calcd. For C₆₀H₅₄N₆: C, 83.80, H, 6.34, N, 9.78, Found C, 83.70, H, 6.32, N, 9.66.



Scheme 2.1. Synthesis of receptor 2

2.5.3. Fluorescence titrations

Fluorescence titrations were performed in solutions of constant concentration of receptors **1** or **2** with KPF₆, and NH₄PF₆. Fluorescence emission was measured at

increments of 0.5 nm, and integration time of 0.1 s, excitation slit width of 10 nm, emission slit width of 5 nm. For **1**, the emission was measured at 298 nm ($\lambda_{\text{exc}} = 272$ nm) and for **2**, the emission was measured at 335 nm ($\lambda_{\text{exc}} = 262$ nm). In a typical experiment, solution A (1.0×10^{-4} M) in $\text{CH}_3\text{CN}/\text{CH}_2\text{Cl}_2$ (1:1) of receptor **2** was titrated with solution B of with $\text{NH}_4^+\text{PF}_6^-$ (1.0×10^{-2} M). Solution B was prepared by dilutions with solution A, thus keeping a constant concentration of **2** upon titration of solution A with solution B. 2.0 mL of solution A were added to the fluorescence cuvette and solution B was added in increments until a total of 1000 μL . Figure 2.3 shows the results for fluorescence titration of ligand **2** with $\text{NH}_4^+\text{PF}_6^-$ indicating fluorescence quenching.

2.5.4. $^1\text{H-NMR}$ Titration Experiments

The association constants^{19,29} for the formation of cation-receptor complexes were determined by titration of solutions of **1** or **2** in acetone- d_6 (for $\text{NH}_4^+\text{PF}_6^-$ and K^+PF_6^-) or methanol- d_4 , for all salts (2×10^{-3} M - solution A) with solutions of $\text{NH}_4^+\text{PF}_6^-$ (1.0×10^{-1}) K^+PF_6^- (1.0×10^{-1}), or Na^+PF_6^- (0.5 M) in the same receptor concentration (solution B). Solution B was prepared by dilutions with solution A, thus keeping a constant concentration of **1** or **2** upon titration of solution A with solution B. In a typical experiment, solution A (0.700 mL) was placed in an NMR tube. Solution B was added in increments with a μL syringe until a total of 950 μL was added. The chemical shift changes were monitored, with the results plotted and fitted to the 1:1 binding isotherm (Eq.1) using non-linear regression analysis:

$$\Delta\delta = \delta_{\text{obs}} - \delta_2 = ([\mathbf{R}]_t + [\mathbf{X}^-]_t + K_a^{-1} - ((([\mathbf{R}]_t + [\mathbf{X}^-]_t + K_a^{-1})^2 - 4[\mathbf{X}^-]_t [\mathbf{R}]_t)^{1/2})) \Delta\delta_{\text{max}} / (2[\mathbf{R}]_t) \text{ (Eq.1)}$$

2.5.5. Continuous Variation Method (Jobs plots):

Stock solutions of the receptors **1** or **2** (0.002 M) and $\text{NH}_4^+\text{PF}_6^-$ (0.002 M) in acetone- d_6 were prepared. Ten NMR tubes were filled with 500 μl solutions of the host and guest in the following volume ratios (in μl). 500:0, 450:50, 400:100, 350:150, 300:200, 250:250, 200:300, 150:350, 100:400, 50:450. ^1H -NMR spectra were recorded and jobs plot was obtained by plotting against $[\text{L}]/([\text{NH}_4^+]+[\text{L}])$ (where **L** is receptor **1** or **2**). Jobs plot curve maxima at mol. fraction of 0.5 were observed for host:guest indicating a 1:1 complex stoichiometry.

2.5.6. Computational Details.

DFT calculations of the gas phase molecular structures were carried out without symmetry restrictions using the B3LYP³⁰⁻³¹ hybrid density functional (B3LYP) with the double-6-31G** basis set for H, C, N, O, F³² and P³³ atoms (basis set B0). Stability checks, optimizations, frequency and hydration energy calculations with basis set B0 were performed using Gaussian-09.³⁴ All optimized molecular structures have only real frequencies. The calculated frequencies were used to obtain free energies at room temperature. Solvent contributions to the gas-phase free energies were estimated as single-point hydration energy for a gas-phase optimized molecular structure within the self-consistent reaction field (SCRF) using PCM³⁵ model with Gaussian-09³⁴ default parameters for acetone.

2.5.6.1.1. $L + NH_4^+ \rightarrow [L \cdot NH_4^+]$

The calculated free energy of $1 + NH_4^+ \rightarrow [1 \cdot NH_4^+]$ gas phase complexation is -60.8 kcal/mol.

The calculated free energy of $[1]_{\text{acetone}} + [NH_4^+]_{\text{acetone}} \rightarrow [1 \cdot NH_4^+]_{\text{acetone}}$ complexation is -12.2 kcal/mol.

The calculated free energy of $2 + NH_4^+ \rightarrow [2 \cdot NH_4^+]$ gas phase complexation is -61.9 kcal/mol.

The calculated free energy of $[1]_{\text{acetone}} + [NH_4^+]_{\text{acetone}} \rightarrow [1 \cdot NH_4^+]_{\text{acetone}}$ complexation is -9.3 kcal/mol.

2.5.6.1.2. $[L \cdot NH_4]^+ + PF_6^- \rightarrow [L \cdot NH_4]^+ PF_6^-$

The calculated free energy of $[1 \cdot NH_4]^+ + PF_6^- \rightarrow [1 \cdot NH_4]^+ PF_6^-$ gas phase complexation is -68.2 kcal/mol. The optimized molecular structure of $[1 \cdot NH_4]^+ PF_6^-$ has C_3 symmetry with 3-fold axis running through the phenyl ring, N of the NH_4^+ and P of PF_6^- . The calculated free energy of $[1 \cdot NH_4]^+_{\text{acetone}} + [PF_6^-]_{\text{acetone}} \rightarrow [[1 \cdot NH_4]^+ PF_6^-]_{\text{acetone}}$ complexation is -0.8 kcal/mol.

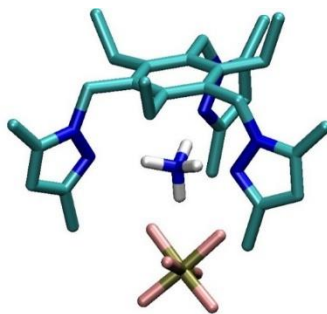


Figure 2.10. DFT calculated structure of $[1 \cdot NH_4]^+ PF_6^-$.

The calculated free energy of $[2 \cdot \text{NH}_4]^+ + \text{PF}_6^- \rightarrow [2 \cdot \text{NH}_4]^+ \text{PF}_6^-$ gas phase complexation is -43.8 kcal/mol. The optimized molecular structure of $[2 \cdot \text{NH}_4]^+ \text{PF}_6^-$ has C_3 symmetry with 3-fold axis running through the phenyl ring, N of the NH_4^+ and P of PF_6^- . The calculated free energy of $[2 \cdot \text{NH}_4]^+_{\text{acetone}} + [\text{PF}_6^-]_{\text{acetone}} \rightarrow [[2 \cdot \text{NH}_4]^+ \text{PF}_6^-]_{\text{acetone}}$ complexation is 8.2 kcal/mol.

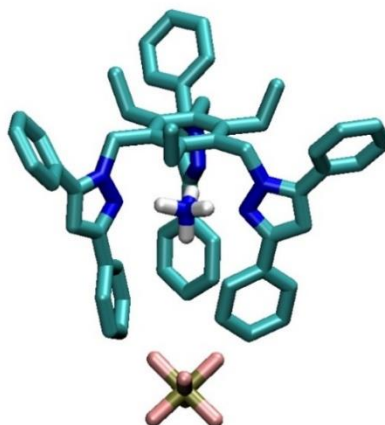


Figure 2.11. DFT calculated structure of $[2 \cdot \text{NH}_4]^+ \text{PF}_6^-$.

2.5.6.2. $\text{N}(\text{pz}) \cdots \text{N}(\text{NH}_4)$, $\text{N}(\text{NH}_4) \cdots \text{C}(\text{phenyl})$ and $\text{N}(\text{NH}_4) \cdots \text{P}$ distances.

Table 2.1. Averaged distances (in Å) and corresponding standard deviations.

	$\text{N}(\text{pz}) \cdots \text{N}(\text{NH}_4)$	$\text{N}(\text{NH}_4) \cdots \text{C}(\text{phenyl})$	$\text{N}(\text{NH}_4) \cdots \text{P}$
$[\mathbf{1} \cdot \text{NH}_4]^+$	2.89(5)	3.42(8)	-
$[\mathbf{2} \cdot \text{NH}_4]^+$	2.94(1)	3.43(1)	-
$[\mathbf{1} \cdot \text{NH}_4]^+ \text{PF}_6^-$	3.00(3)	3.50(6)	3.66
$[\mathbf{1} \cdot \text{NH}_4]^+ \text{PF}_6^-$ *	3.00(5)	3.43(7)	4.16
$[\mathbf{2} \cdot \text{NH}_4]^+ \text{PF}_6^-$	2.99(1)	3.47(1)	7.25

*Crystal structure from J.Chin et al.

2.5.6.3. Cartesian coordinates of the optimized molecular structures.

Compound 1

78

N	-2.998802	-1.556318	0.858378
N	-3.556019	-0.914080	-0.198103
C	-4.851690	-0.545188	0.043861
C	-5.126129	-0.952864	1.337059
C	-3.942173	-1.575959	1.799480
C	-2.815476	-0.823108	-1.459120
C	-1.357151	-0.405554	-1.310967
C	-0.346816	-1.388873	-1.294362
C	1.002300	-0.984043	-1.246031
C	1.337987	0.381160	-1.164786
C	0.317460	1.351037	-1.154214
C	-1.035078	0.962827	-1.220041
C	0.681413	2.829464	-1.097955
N	0.910402	3.341316	0.256263
C	1.877141	4.214243	0.676243
C	1.593530	4.482597	2.003674
C	0.425506	3.740581	2.301853
N	0.013104	3.058917	1.233302
C	2.797671	0.804804	-1.090747
C	3.444967	1.057484	-2.466653
C	2.110179	-2.028398	-1.311552
N	2.671317	-2.400481	-0.009974
C	3.983473	-2.628162	0.307295
C	3.983711	-3.076042	1.616246
C	2.623979	-3.105128	2.009353
N	1.834712	-2.702613	1.013776
C	-0.710900	-2.866747	-1.299864
C	-0.828649	-3.489971	-2.702614
C	-2.139476	2.009487	-1.179992
C	-2.536219	2.565442	-2.560934
C	2.970773	4.738182	-0.201638
C	-0.327485	3.647517	3.594000
C	5.119719	-2.429214	-0.647262

C	2.034287	-3.505445	3.327394
C	-5.726677	0.141035	-0.958317
C	-3.665497	-2.198266	3.134113
H	-2.883143	-1.785140	-1.972517
H	-3.349981	-0.107007	-2.083619
H	-0.099726	3.431260	-1.568056
H	1.593974	3.021420	-1.661868
H	2.940803	-1.661369	-1.915037
H	1.750432	-2.933511	-1.806031
H	2.161474	5.122554	2.664102
H	4.851780	-3.339025	2.204151
H	6.063872	-2.628014	-0.135405
H	5.167093	-1.406201	-1.039162
H	5.059541	-3.107255	-1.507003
H	0.946605	-3.416170	3.285604
H	2.400472	-2.868737	4.140686
H	2.288577	-4.540182	3.583643
H	-1.193842	2.994503	3.468612
H	-0.678674	4.630838	3.926949
H	0.298503	3.236942	4.394229
H	3.613054	5.405772	0.377159
H	2.581500	5.310259	-1.052298
H	3.606401	3.941177	-0.605496
H	-1.832859	2.823695	-0.519530
H	-3.020708	1.584099	-0.695125
H	-3.339836	3.303715	-2.465395
H	-2.885560	1.776103	-3.235762
H	-1.693178	3.055122	-3.059560
H	-1.645407	-2.996973	-0.749972
H	0.026333	-3.412882	-0.707256
H	3.371454	0.048123	-0.551403
H	2.887931	1.704239	-0.477630
H	4.493123	1.356679	-2.356576
H	2.926947	1.849292	-3.018108
H	3.415944	0.163466	-3.098143
H	-1.107449	-4.546763	-2.633535
H	0.113591	-3.429767	-3.258998
H	-1.585948	-2.984240	-3.311569
H	-6.054979	-0.811098	1.871404
H	-2.650409	-2.601000	3.148421
H	-4.365929	-3.012879	3.350888
H	-3.756125	-1.466227	3.944590

H	-6.701751	0.343704	-0.509995
H	-5.893708	-0.472573	-1.851598
H	-5.311276	1.099479	-1.290420

Compound 2

120

N	3.327104	-1.124201	-0.707982
C	1.375160	-0.419319	-2.095126
N	2.960105	-0.298814	0.291318
C	1.059987	0.953223	-2.101710
C	2.164617	2.000239	-2.071810
H	1.818682	2.890116	-1.542452
H	2.994724	1.630500	-1.466566
C	2.665728	2.415330	-3.467702
H	3.444210	3.180915	-3.386902
H	1.857029	2.826206	-4.081434
H	3.083202	1.565978	-4.019377
C	2.832051	-0.857165	-2.067835
H	2.976323	-1.773281	-2.638121
H	3.469941	-0.100457	-2.529005
C	4.097094	-2.170416	-0.260100
C	3.490129	-0.815073	1.407470
C	4.213659	-1.994182	1.110323
H	4.753604	-2.638512	1.787434
C	4.646725	-3.242084	-1.108392
C	5.338718	-2.971709	-2.301690
H	5.487645	-1.942999	-2.615578
C	5.865392	-4.010342	-3.068356
H	6.399843	-3.782922	-3.986261
C	5.721826	-5.334689	-2.652311
H	6.134520	-6.141898	-3.250168
C	5.049169	-5.615304	-1.461427
H	4.933009	-6.643122	-1.130146
C	4.514341	-4.579850	-0.697688
H	3.974682	-4.798199	0.218609
C	3.256911	-0.177134	2.714073
C	2.231340	0.770954	2.871256
H	1.617800	1.029640	2.014925
C	1.993758	1.357322	4.111930

H	1.186903	2.076144	4.217178
C	2.775642	1.011107	5.216841
H	2.586083	1.466522	6.184597
C	3.799527	0.073886	5.070691
H	4.416259	-0.198209	5.922849
C	4.039049	-0.515183	3.829823
H	4.847149	-1.233003	3.723217
N	-2.629445	-2.301647	-0.790715
C	-0.988965	-0.979732	-2.129403
N	-1.766321	-2.422566	0.236208
C	0.356994	-1.392621	-2.092854
C	0.713235	-2.871281	-2.042086
H	1.634820	-3.008314	-1.472829
H	-0.042283	-3.405733	-1.462962
C	0.877830	-3.519127	-3.429235
H	1.161872	-4.572090	-3.334030
H	1.650995	-3.016574	-4.019852
H	-0.048429	-3.470671	-4.012490
C	-2.098953	-2.020847	-2.133986
H	-2.941956	-1.689668	-2.738215
H	-1.750271	-2.958085	-2.572782
C	-3.937545	-2.404713	-0.383610
C	-2.518998	-2.602051	1.329201
C	-3.892529	-2.595136	0.989114
H	-4.746149	-2.712803	1.639145
C	-5.110867	-2.317869	-1.270455
C	-5.208883	-3.066325	-2.456328
H	-4.403375	-3.738245	-2.737228
C	-6.345496	-2.980062	-3.259433
H	-6.404933	-3.568080	-4.170831
C	-7.408223	-2.155364	-2.888145
H	-8.293624	-2.091373	-3.513798
C	-7.328496	-1.416859	-1.706140
H	-8.151170	-0.772745	-1.409381
C	-6.190496	-1.494915	-0.905671
H	-6.122272	-0.907825	0.005102
C	-1.892043	-2.750012	2.653376
C	-0.553442	-2.370886	2.852272
H	0.008406	-1.967373	2.016986
C	0.040555	-2.499080	4.105292
H	1.072092	-2.188702	4.241572
C	-0.689024	-3.008514	5.182419

H	-0.225586	-3.104541	6.160088
C	-2.019044	-3.388777	4.995711
H	-2.593733	-3.789870	5.826054
C	-2.616201	-3.261212	3.742040
H	-3.646682	-3.575797	3.604151
N	-0.669756	3.414078	-0.781957
C	-0.291598	1.348181	-2.130358
N	-1.247033	2.715439	0.215173
C	-1.322555	0.388695	-2.136386
C	-2.781342	0.821778	-2.148622
H	-3.390969	0.087744	-1.618654
H	-2.892272	1.736898	-1.563834
C	-3.351528	1.018890	-3.565817
H	-4.405361	1.312231	-3.523278
H	-3.282762	0.099619	-4.157081
H	-2.806366	1.793166	-4.116862
C	-0.638961	2.829202	-2.132080
H	0.091657	3.400521	-2.701577
H	-1.607075	2.999336	-2.607264
C	-0.124252	4.595208	-0.339161
C	-1.072064	3.445551	1.323958
C	-0.368527	4.636081	1.025137
H	-0.072864	5.426880	1.697680
C	0.581026	5.574130	-1.184355
C	0.052452	6.030462	-2.404559
H	-0.913645	5.667700	-2.742439
C	0.740008	6.970864	-3.170680
H	0.314783	7.311937	-4.110193
C	1.959111	7.484535	-2.726661
H	2.492418	8.218509	-3.323499
C	2.486258	7.052499	-1.508084
H	3.433956	7.447422	-1.153637
C	1.806451	6.105181	-0.745369
H	2.227284	5.755123	0.192178
C	-1.560754	2.964131	2.627062
C	-1.908141	1.613752	2.804364
H	-1.814778	0.931882	1.966165
C	-2.348183	1.152805	4.042768
H	-2.597375	0.102849	4.164277
C	-2.451277	2.029712	5.125619
H	-2.789652	1.667011	6.091992
C	-2.111768	3.373439	4.959668

H	-2.192865	4.064179	5.794444
C	-1.670348	3.837145	3.721045
H	-1.421425	4.887228	3.598799

[1·NH₄⁺]

83

N	-2.864931	-1.124299	0.932088
N	-3.517089	-0.654233	-0.170350
C	-4.845786	-0.458005	0.078207
C	-5.048436	-0.790784	1.407404
C	-3.791025	-1.204015	1.896006
C	-2.872849	-0.708434	-1.490665
C	-1.398961	-0.341764	-1.467584
C	-0.420158	-1.358776	-1.456096
C	0.942154	-0.992527	-1.454157
C	1.325721	0.361480	-1.415030
C	0.333253	1.358774	-1.364346
C	-1.033078	1.019683	-1.411747
C	0.758184	2.801486	-1.175644
N	1.090337	3.094657	0.228758
C	1.947152	4.058964	0.681364
C	1.737866	4.154024	2.047658
C	0.718257	3.223691	2.347184
N	0.325077	2.581498	1.238834
C	2.799193	0.742126	-1.445085
C	3.333188	0.936647	-2.878447
C	2.025383	-2.054209	-1.423930
N	2.578672	-2.260657	-0.077275
C	3.818982	-2.739634	0.234991
C	3.788349	-3.043251	1.586135
C	2.482767	-2.734969	2.022724
N	1.750252	-2.264115	1.005946
C	-0.823577	-2.827198	-1.419479
C	-0.988350	-3.472081	-2.807722
C	-2.105870	2.099503	-1.419880
C	-2.443446	2.595363	-2.840212
C	2.901815	4.802866	-0.205006
C	0.102698	2.928253	3.686664

C	4.923445	-2.872713	-0.766781
C	1.907792	-2.877748	3.402795
C	-5.810127	0.032361	-0.955806
C	-3.431643	-1.668617	3.276369
H	-3.019172	-1.708668	-1.900084
H	-3.419756	-0.024033	-2.138357
H	-0.018615	3.493655	-1.505254
H	1.646870	3.024331	-1.766300
H	2.854030	-1.764074	-2.068837
H	1.659694	-3.010795	-1.800107
H	2.261958	4.809707	2.731049
H	4.603425	-3.439132	2.175051
H	5.840522	-3.179680	-0.261457
H	5.131400	-1.928921	-1.284454
H	4.695229	-3.624546	-1.529765
H	0.828905	-2.694326	3.400020
H	2.377969	-2.185141	4.111418
H	2.064984	-3.891757	3.787235
H	-0.772735	2.279206	3.585625
H	-0.226954	3.853752	4.172729
H	0.816837	2.446014	4.366004
H	3.547520	5.436725	0.407551
H	2.385067	5.450277	-0.923604
H	3.550467	4.127397	-0.777343
H	-1.795949	2.943122	-0.799153
H	-3.011687	1.726421	-0.938728
H	-3.232362	3.353291	-2.811975
H	-2.786987	1.777056	-3.482077
H	-1.568380	3.037130	-3.327975
H	-1.750197	-2.933359	-0.850703
H	-0.089078	-3.392510	-0.841219
H	3.391151	-0.019682	-0.934574
H	2.969193	1.651952	-0.866210
H	4.395107	1.199261	-2.863164
H	2.796041	1.731383	-3.406462
H	3.219013	0.026504	-3.475591
H	-1.284937	-4.520732	-2.709520
H	-0.057055	-3.438726	-3.383117
H	-1.752154	-2.959610	-3.401130
H	-5.983618	-0.738036	1.947986
H	-2.403682	-2.041574	3.305243
H	-4.089002	-2.484016	3.596940

H	-3.529022	-0.863874	4.014385
H	-6.787138	0.189169	-0.496203
H	-5.938423	-0.681796	-1.776291
H	-5.491535	0.984624	-1.394757
N	-0.230851	-0.310782	1.670693
H	0.480949	-0.987435	1.284769
H	-0.037454	0.674173	1.385938
H	-0.200582	-0.352387	2.687685
H	-1.187469	-0.607798	1.334615

[1·NH₄⁺] PF₆⁻

90

N	0.018118	-2.001018	-2.095262
N	1.241092	-2.547261	-2.362374
C	1.129924	-3.797098	-2.903380
C	-0.222814	-4.074011	-2.957783
C	-0.877806	-2.932178	-2.443843
C	2.458110	-1.731480	-2.317839
C	2.422853	-0.632991	-1.269454
C	2.150335	0.696758	-1.651651
C	2.170221	1.708571	-0.669403
C	2.373887	1.394310	0.689037
C	2.614624	0.056283	1.055052
C	2.658032	-0.958644	0.079602
C	1.968031	3.158652	-1.074762
N	0.610661	3.664356	-0.850315
N	-0.474752	2.845560	-0.972238
C	-1.542619	3.651222	-0.925416
C	-1.135526	4.996990	-0.793136
C	0.246408	4.977578	-0.756465
C	1.230128	6.099411	-0.647064
C	-2.937167	3.110929	-0.978026
C	1.790417	1.027622	-3.093751
C	2.996221	1.369419	-3.989266
C	2.957609	-2.395340	0.482333
C	4.464014	-2.720851	0.482594
C	2.801125	-0.309253	2.516600
N	1.591944	-0.874823	3.123401

C	1.538083	-1.638158	4.255434
C	0.201798	-1.724864	4.597487
C	-0.499511	-0.970923	3.630428
N	0.352312	-0.444822	2.742323
C	2.313220	2.490508	1.743208
C	3.689535	3.083665	2.101284
C	2.750408	-2.209557	4.920004
C	-1.978290	-0.767356	3.517176
C	2.308149	-4.613829	-3.331792
C	-2.346627	-2.721355	-2.250784
N	-0.775283	0.037375	-0.034248
H	2.230657	3.296843	-2.126342
H	2.641534	3.802249	-0.505034
H	3.116497	0.559654	3.098648
H	3.591667	-1.053478	2.627989
H	3.288121	-2.412547	-2.121387
H	2.638586	-1.308692	-3.308779
H	-0.218031	-2.271190	5.429444
H	-0.680724	-4.986195	-3.311723
H	1.966515	-5.588248	-3.686114
H	3.011055	-4.788095	-2.508672
H	2.866321	-4.139740	-4.147859
H	-2.621494	-1.672620	-2.364074
H	-2.669683	-3.016414	-1.248757
H	-2.912064	-3.312884	-2.975720
H	-2.220519	0.233306	3.155093
H	-2.454626	-0.910818	4.490461
H	-2.431978	-1.467167	2.810383
H	2.444064	-2.841344	5.755863
H	3.412586	-1.431232	5.318039
H	3.343766	-2.828299	4.236690
H	1.829237	2.103967	2.643955
H	1.654008	3.290871	1.401303
H	3.587761	3.874593	2.851142
H	4.182673	3.513560	1.222812
H	4.366556	2.323635	2.505051
H	1.079103	1.856942	-3.102260
H	1.235063	0.190894	-3.525195
H	2.435858	-3.085362	-0.184407
H	2.539591	-2.596006	1.471565
H	4.636270	-3.761003	0.776681
H	5.016329	-2.078872	1.176551

H	4.909568	-2.573200	-0.506673
H	2.664747	1.629814	-4.999263
H	3.693526	0.528801	-4.072376
H	3.565246	2.216521	-3.592578
H	-1.771018	5.867822	-0.722242
H	-3.018411	2.275680	-1.674728
H	-3.633685	3.894340	-1.287241
H	-3.261241	2.729555	-0.005859
H	0.693381	7.047653	-0.578125
H	1.895493	6.156864	-1.516706
H	1.861454	6.012014	0.245421
H	-0.417804	-0.642300	-0.735822
H	-0.307884	-0.100741	0.882835
H	-1.782454	-0.121453	0.078959
H	-0.617457	1.007604	-0.378184
P	-4.386511	-0.467206	0.265348
F	-3.513181	0.018986	-1.068650
F	-5.141760	-0.948039	1.608197
F	-3.129488	-1.517220	0.599354
F	-5.097357	-1.613408	-0.625283
F	-5.532288	0.613023	-0.080372
F	-3.551009	0.678109	1.130027

[2·NH₄⁺]

125

N	-2.248914	-2.676503	-0.770972
C	-0.823192	-1.100697	-2.082077
N	-1.531686	-2.420609	0.352230
C	0.576216	-1.262621	-2.070597
C	1.202993	-2.650737	-2.064983
H	2.161675	-2.622159	-1.542368
H	0.585270	-3.330384	-1.471698
C	1.418885	-3.237649	-3.473406
H	1.878985	-4.228126	-3.409267
H	2.074348	-2.602832	-4.078248
H	0.476469	-3.338020	-4.021269
C	-1.719758	-2.324120	-2.099350
H	-2.583896	-2.170961	-2.745799
H	-1.185198	-3.184825	-2.502636

C	-3.425974	-3.318692	-0.489690
C	-2.265812	-2.904115	1.371095
C	-3.465561	-3.464926	0.889428
H	-4.236690	-3.967890	1.452453
C	-4.416128	-3.737576	-1.498887
C	-4.054794	-4.487488	-2.630610
H	-3.019811	-4.780476	-2.777624
C	-5.022587	-4.892380	-3.548334
H	-4.730640	-5.477322	-4.415116
C	-6.363552	-4.561770	-3.346434
H	-7.115762	-4.880286	-4.061422
C	-6.735013	-3.827044	-2.219040
H	-7.776896	-3.569726	-2.055049
C	-5.769806	-3.417647	-1.301221
H	-6.057228	-2.838178	-0.429154
C	-1.788832	-2.823015	2.761384
C	-0.415357	-2.749838	3.049688
H	0.299733	-2.789887	2.233451
C	0.031457	-2.668714	4.367629
H	1.095721	-2.603143	4.569960
C	-0.885296	-2.683134	5.420999
H	-0.536823	-2.631684	6.447856
C	-2.251368	-2.775491	5.147186
H	-2.969922	-2.795862	5.961190
C	-2.701163	-2.837536	3.828742
H	-3.766431	-2.889096	3.624887
N	-1.214906	3.296441	-0.661226
C	-0.564971	1.316334	-2.041157
N	-1.326997	2.514745	0.442464
C	-1.403446	0.184649	-2.062924
C	-2.918494	0.336968	-2.070166
H	-3.383538	-0.515286	-1.570805
H	-3.208275	1.201083	-1.466566
C	-3.507161	0.472465	-3.488172
H	-4.595550	0.574403	-3.446893
H	-3.274114	-0.402594	-4.102994
H	-3.103919	1.345659	-4.010884
C	-1.174877	2.705474	-2.010184
H	-0.607423	3.398036	-2.631943
H	-2.187468	2.688310	-2.414098
C	-1.199562	4.628394	-0.342505
C	-1.380533	3.362857	1.485965

C	-1.291992	4.696681	1.039876
H	-1.347275	5.599389	1.628884
C	-1.089568	5.723776	-1.324810
C	-1.965605	5.834308	-2.417539
H	-2.758623	5.105094	-2.553723
C	-1.850696	6.898409	-3.310534
H	-2.538251	6.975085	-4.147269
C	-0.866540	7.869923	-3.121728
H	-0.780177	8.699019	-3.817215
C	0.000303	7.777136	-2.031561
H	0.764246	8.532876	-1.877060
C	-0.109207	6.712575	-1.138714
H	0.570438	6.635113	-0.295412
C	-1.520966	2.864825	2.863925
C	-2.134676	1.627233	3.122637
H	-2.544014	1.055952	2.294731
C	-2.255243	1.152166	4.427595
H	-2.724075	0.189869	4.607476
C	-1.785552	1.916153	5.497891
H	-1.889617	1.551637	6.515177
C	-1.192356	3.156596	5.254230
H	-0.832665	3.760591	6.081994
C	-1.053835	3.624939	3.948079
H	-0.573578	4.581734	3.765963
N	3.467417	-0.571398	-0.727168
C	1.398348	-0.116935	-2.057956
N	2.860125	-0.122608	0.400674
C	0.838363	1.175243	-2.032222
C	1.728589	2.409980	-1.994340
H	1.223053	3.215418	-1.457639
H	2.622844	2.202192	-1.400910
C	2.135740	2.917109	-3.391625
H	2.768658	3.805472	-3.308250
H	1.260890	3.183082	-3.993170
H	2.690057	2.158689	-3.953518
C	2.906553	-0.280358	-2.058578
H	3.212671	-1.101848	-2.706349
H	3.386700	0.615903	-2.452261
C	4.617836	-1.259935	-0.445708
C	3.634241	-0.534011	1.421017
C	4.740316	-1.260107	0.936182
H	5.558623	-1.680416	1.500382

C	5.504030	-1.865147	-1.457597
C	5.992079	-1.133714	-2.553456
H	5.725830	-0.087649	-2.670262
C	6.852555	-1.729481	-3.473956
H	7.227582	-1.150364	-4.312229
C	7.245007	-3.058773	-3.310104
H	7.917795	-3.519635	-4.026686
C	6.775926	-3.790849	-2.217956
H	7.080616	-4.824073	-2.083099
C	5.911580	-3.200063	-1.298176
H	5.537150	-3.773080	-0.455333
C	3.290969	-0.213953	2.816271
C	2.544049	0.933778	3.132562
H	2.257570	1.615505	2.337367
C	2.210872	1.223482	4.454865
H	1.625086	2.109351	4.679345
C	2.641115	0.385860	5.485960
H	2.391840	0.617846	6.516763
C	3.404570	-0.744163	5.185832
H	3.751896	-1.394462	5.983232
C	3.719988	-1.047524	3.861967
H	4.294732	-1.940316	3.635004
N	0.011983	-0.013657	1.072070
H	0.016255	-0.032131	2.093758
H	1.004114	-0.003700	0.734074
H	-0.481385	-0.868088	0.722624
H	-0.489396	0.849635	0.752877

[2·NH₄⁺] PF₆⁻

132

N	-1.774303	3.553518	0.149159
C	-3.036515	1.389675	0.199833
N	-0.595058	2.886819	0.281244
C	-3.032470	0.528045	1.312644
C	-3.026494	1.082567	2.731081
H	-2.530219	0.379599	3.401463
H	-2.409949	1.984865	2.771381
C	-4.433697	1.387625	3.280581
H	-4.372830	1.764346	4.306097

H	-5.062599	0.491660	3.289922
H	-4.954227	2.137191	2.675664
C	-3.060287	2.892336	0.411304
H	-3.789717	3.361442	-0.251558
H	-3.376636	3.127077	1.427308
C	-1.585307	4.841397	-0.281037
C	0.360978	3.766025	-0.068308
C	-0.218087	4.999362	-0.436093
H	0.293944	5.906717	-0.716724
C	-2.661841	5.820210	-0.519197
C	-3.683224	6.057554	0.416153
H	-3.693484	5.512227	1.354597
C	-4.663157	7.017793	0.168617
H	-5.441754	7.192778	0.905057
C	-4.634956	7.763092	-1.011009
H	-5.397209	8.512604	-1.200702
C	-3.617888	7.545064	-1.942241
H	-3.587114	8.122997	-2.860973
C	-2.640714	6.581792	-1.700278
H	-1.856427	6.404804	-2.429652
C	1.791973	3.424327	-0.057099
C	2.332117	2.531202	0.885152
H	1.686887	2.108664	1.651162
C	3.691837	2.223266	0.867976
H	4.111354	1.524558	1.582463
C	4.538669	2.812942	-0.075657
H	5.586282	2.542276	-0.088689
C	4.010885	3.712702	-1.003058
H	4.661062	4.170741	-1.742656
C	2.650054	4.014092	-0.999055
H	2.242688	4.694412	-1.741743
N	-1.773549	-1.646938	-3.151921
C	-3.036310	-0.520510	-1.304139
N	-0.594355	-1.199274	-2.640409
C	-3.031788	0.874037	-1.114331
C	-3.025370	1.825257	-2.303724
H	-2.529468	2.757413	-2.029838
H	-2.408323	1.409142	-3.104971
C	-4.432355	2.148308	-2.843370
H	-4.371225	2.848168	-3.682280
H	-5.061771	2.604117	-2.072385
H	-4.952482	1.249552	-3.190395

C	-3.059491	-1.088587	-2.711305
H	-3.789338	-1.896757	-2.786889
H	-3.374796	-0.325780	-3.422738
C	-1.584580	-2.664174	-4.051326
C	0.361669	-1.942180	-3.226384
C	-0.217428	-2.877837	-4.110081
H	0.294550	-3.575225	-4.754871
C	-2.661203	-3.360050	-4.779614
C	-3.681542	-2.668795	-5.454558
H	-3.690787	-1.583398	-5.453287
C	-4.661723	-3.363525	-6.161794
H	-5.439520	-2.813373	-6.682889
C	-4.634797	-4.757880	-6.215135
H	-5.397246	-5.297097	-6.768939
C	-3.618733	-5.455232	-5.559043
H	-3.588955	-6.539937	-5.598421
C	-2.641298	-4.763800	-4.846391
H	-1.857803	-5.306828	-4.327087
C	1.792677	-1.761975	-2.935900
C	2.333164	-0.499629	-2.633154
H	1.688183	0.375219	-2.650111
C	3.692874	-0.361088	-2.357521
H	4.112759	0.606744	-2.109214
C	4.539350	-1.473396	-2.396470
H	5.586885	-1.349708	-2.155028
C	4.011268	-2.726152	-2.712551
H	4.661168	-3.595889	-2.739510
C	2.650442	-2.872858	-2.975874
H	2.242837	-3.856015	-3.194085
N	-1.775332	-1.906219	3.001416
C	-3.037107	-0.867882	1.102129
N	-0.596031	-1.687244	2.358104
C	-3.032610	-1.400799	-0.200475
C	-3.027241	-2.906445	-0.429470
H	-2.531046	-3.135721	-1.373414
H	-2.410951	-3.392860	0.331767
C	-4.434758	-3.534089	-0.440180
H	-4.374498	-4.610526	-0.627159
H	-5.063410	-3.093473	-1.220576
H	-4.955149	-3.385051	0.511513
C	-3.061235	-1.802421	2.297678
H	-3.790648	-1.462916	3.035377

H	-3.377736	-2.799584	1.992802
C	-1.586468	-2.177439	4.331908
C	0.359922	-1.824089	3.294401
C	-0.219276	-2.122202	4.546345
H	0.292647	-2.332805	5.472524
C	-2.663122	-2.460508	5.298558
C	-3.684386	-3.389358	5.036421
H	-3.694400	-3.929623	4.095056
C	-4.664487	-3.654974	5.991639
H	-5.442996	-4.380336	5.774963
C	-4.636576	-3.005775	7.226771
H	-5.398968	-3.216144	7.970602
C	-3.619627	-2.090174	7.503589
H	-3.589093	-1.583286	8.463356
C	-2.642289	-1.818205	6.548521
H	-1.858128	-1.097914	6.759931
C	1.790952	-1.662825	2.993122
C	2.331286	-2.031496	1.748366
H	1.686150	-2.483269	0.999136
C	3.691023	-1.862315	1.490496
H	4.110596	-2.131035	0.527976
C	4.537693	-1.340408	2.473383
H	5.585305	-1.193404	2.245726
C	4.009723	-0.987980	3.716451
H	4.659777	-0.576909	4.483256
C	2.648886	-1.142462	3.975248
H	2.241444	-0.840091	4.935937
N	0.141173	0.000684	-0.000042
H	1.164710	0.000085	0.000713
H	-0.195741	-0.606338	0.781664
H	-0.194420	0.981675	0.134695
H	-0.194362	-0.372800	-0.917113
P	7.393855	-0.000152	0.001061
F	8.303927	-0.709804	-1.140351
F	8.303512	-0.633770	1.186695
F	8.303483	1.343487	-0.042657
F	6.419679	0.705188	1.137309
F	6.420154	0.631152	-1.178314
F	6.420192	-1.337262	0.043734

2.5.7 Crystallographic data

X-ray quality colorless crystals of **2** were obtained by slow evaporation of a CH₂Cl₂ solution of **2**, while colorless crystals of [2·NH₄]⁺PF₆⁻ were obtained by slow Et₂O vapor diffusion into a MeOH solution of the compound. Single crystal X-ray data were collected on a Bruker D8 Quest instrument equipped with a CMOS detector and integrated using the APEX3 suite.³⁶ The structures were solved by intrinsic phasing methods available with SHELXT and were refined by full-matrix least-squares using SHELXL and SHELXS packages³⁷ using Olex2³⁸ or ShelXle³⁹. Multi-scan absorption correction was performed using SADABS.⁴⁰ Crystallographic data have been submitted to the Cambridge Crystallographic Data Center (CCDC numbers: 1550637 (**2**) and 1550636 ([2·NH₄]PF₆)) and can be obtained free of charge from www.ccdc.cam.ac.uk/data_request/cif. Crystallographic data are provided in Table 2, and the X-ray crystal structures are shown in Figures 2.8 and 2.9. The phenyl rings on the diphenyl pyrazole were thermally disordered and were refined using the SPLIT routine available within Olex2 program and using PARTS.³⁸ The PF₆⁻ ion was disordered over two positions and was refined using PARTS using ShelXle.³⁹

Table 2.2. Crystallographic data.

	2.NH₄PF₆	2
Chemical formula	C ₆₀ H ₅₈ N ₇ ·PF ₆	C ₆₀ H ₅₄ N ₆
<i>M_r</i>	1022.10	859.09
Crystal system, space group	Trigonal, <i>R</i> -3 (No. 148)	Triclinic, <i>P</i> -1 (No. 2)
Temperature (K)	301	297
<i>a</i> , <i>b</i> , <i>c</i> (Å)	14.7935 (5), 14.7935(5), 42.5752 (16)	10.5434(4), 12.4141(5), 19.6118(8)
<i>α</i> , <i>β</i> , <i>γ</i> (°)	90, 90, 120	94.867(1), 102.526(1), 106.638(1)
<i>V</i> (Å ³)	8069.2 (6)	2371.1(2)
<i>Z</i>	6	2
Radiation type	Mo <i>Kα</i>	Mo <i>Kα</i>
<i>μ</i> (mm ⁻¹)	0.12	0.071
Crystal size (mm)	0.16 × 0.14 × 0.11	0.327 x 0.227 x 0.046
Diffractometer	Bruker D8 Quest	Bruker D8 Quest
Absorption correction	SADABS	SADABS
No. of measured and independent reflections	32938, 3756	41715, 9430
<i>R</i> _{int}	0.0700	0.0701
<i>R</i> [<i>F</i> ² > 2σ(<i>F</i> ²)], <i>wR</i> (<i>F</i> ²), <i>S</i>	0.082, 0.212, 1.033	0.0672, 0.1287, 1.007
No. of observed reflections (<i>I</i> > 2σ(<i>I</i>))	2196	4462
Δρ _{max} , Δρ _{min} (e Å ⁻³)	0.75, -0.27	0.29/-0.17

2.6. References

1. Späth, A.; König, B. Molecular recognition of organic ammonium ions in solution using synthetic receptors. *Beilstein J. Org. Chem.* **2010**, *6*, 1-111.
2. Wolfbeis, O. S.; Li, H. Fluorescence optical urea biosensor with ammonium optrode as transducer. *Biosens. Bioelectron.* **1993**, *8*, 161-166.
3. Rhines, T. D.; Arnold, M. A. Fiber-Optic biosensor for urea based on sensing of ammonia gas. *Anal. Chim. Acta*, **1989**, *227*, 387-396.
4. Bühlmann, P.; Pretsch E.; Bakker, E. Carrier-Based Ion-Selective Electrodes and Bulk Optodes. 2. Ionophores for Potentiometric and Optical Sensors. *Chem. Rev.* **1998**, *98*, 1593-1688.
5. Rueda-Zubiaurre, A.; Herrero-García, N.; del Rosario Torres, M.; Fernández, I.; Osío Barcina, J. Rational design of a nonbasic molecular receptor for selective NH_4^+/K^+ complexation in the gas phase. *Chem. Eur. J.* **2012**, *18*, 16884–16889.
6. Kim H. S.; Kim D.H.; Kim K. S.; Choi H. J.; Shim J. H.; Jeong I. S.; Cha G. S.; Nam H. Synthesis and properties of 1,3,5-tris(phenoxymethyl)-2,4,6-triethylbenzenes as NH_4^+ ionophores. *J. Incl. Phenom. Macrocycl. Chem.* **2003**, *46*, 201–205.
7. Suzuki, K.; Siswanta, D.; Otsuka, K.; Amano, T.; Ikeda, T.; Hisamoto, H.; Yoshihara, R. Ohba, S. Design and Synthesis of a highly selective ammonium ionophore than nonactin and its application as an ion-sensing Component for an ion-selective electrode. *Anal. Chem.* **2000**, *72*, 2200-2205.
8. Kim, H. S.; Park, H. J.; Oh, H. J.; Koh, Y. K.; Choi, J.H.; Lee, D.H.; Cha, G.S.; Nam, H. Thiazole-Containing Benzo-Crown Ethers: A New Class of Ammonium-Selective Ionophores. *Anal. Chem.* **2000**, *72*, 4683-4688.
9. (a) Kim, H.S.; Kim, D.H.; Kim, K. S.; Choi, J. H.; Choi, H. J.; Kim, S. H.; Shim, J. H.; Cha G. S.; Nam, H. Cation selectivity of ionophores based on tripodal thiazole derivatives on benzene scaffold. *Talanta*, **2007**, *71*, 1986-1992. (b) Rüdiger, V.; Schneider, H. J.; Solov'ev, V. P.; Kazachenko, V. P.; Raevsky, O. A. Crown Ether–Ammonium Complexes: Binding Mechanisms and Solvent Effects. *Eur. J. Org. Chem.*, **1999**, *1999*, 1847-1856.
10. (a) Rahman, A.; Kwon, N. H.; Won, M.S.; Hyun, M.H.; Shim, Y. B. Selective Binding of NH_4^+ by Redox-Active Crown Ethers: Application to a NH_4^+ Sensor. *Anal. Chem.* **2004**, *76*, 3660-3665. (b) Graf, E.; Kintzinger, J. P.; Lehn, J. M.; LeMoigne, J. Molecular recognition: Selective ammonium cryptates of synthetic

- receptor molecules possessing a tetrahedral recognition site. *J. Am. Chem. Soc.* **1982**, *104*, 1672-1678.
11. Kuswandi, B.; Nuriman, Verboom, W.; Reinhoudt, D. N. Tripodal receptors for cation and anion sensors. *Sensors*, **2006**, *6*, 978-1017.
 12. Bill, N. L.; Kim, D. S.; Kim, S. K.; Park, J. S.; Lynch, V. M.; Young, N.J.; Hay, B. P.; Yang, Y.; Anslyn, E. V.; Sessler, J.L. Oxoanion recognition by benzene-based tripodal pyrrolic receptors. *Supramol. Chem.* **2012**, *24*, 72-76.
 13. Jon, S. Y.; J. Kim, M. Kim, S. Park, W. S. Jeon, J. Heo and K. Kim, A Rationally Designed NH_4^+ Receptor Based on Cation- π Interaction and Hydrogen Bonding. *Angew. Chem. Int. Ed.*, **2001**, *40*, 2116-2119.
 14. Ahn, K. H.; Kim, S. G.; Jung, J.; Kim, K.-H.; Kim, J.; Chin, J.; Kim, K. Selective Recognition of NH_4^+ over K^+ with Tripodal Oxazoline Receptors. *Chem. Lett.*, **2000**, *29*, 170-171.
 15. Ahn, K. H.; Ku, H. Y.; Kim, Y.; Kim, S. G.; Kim, Y. K.; Son H. S.; Ku, J. K. Fluorescence Sensing of Ammonium and Organoammonium Ions with Tripodal Oxazoline Receptors. *Org. Lett.*, **2003**, *5*, 1419-1422.
 16. Tsitovich, P. B.; Sperryak, J. A.; Morrow J. R.; A Redox-Activated MRI Contrast Agent that Switches Between paramagnetic and Diamagnetic States. *Angew. Chem. Int. Ed.*, **2013**, *52*, 13997-14000.
 17. (a) Chin, J.; Oh, J.; Jon, S. Y.; Park, S. H.; Walsdorff, C.; Stranix, B.; Ghousoub, A.; Lee, S.J.; Chung, H. J.; Park, S-M.; Kim, K. Tuning and Dissecting Electronic and Steric Effects in Ammonium Receptors: Nonactin vs Artificial Receptors. *J. Am. Chem. Soc.* **2002**, *124*, 5374-5379. (b) Chin, J.; Walsdorff, C.; Stranix, B.; Oh, J.; Chung, H. J.; Park, S. M.; Kim, K. A Rational Approach to Selective Recognition of NH_4^+ over K^+ . *Angew. Chemie - Int. Ed.* **1999**, *38*, 2756-2759.
 18. Koch, N.; Mazik, M. Synthesis of Tripodal and Hexapodal Pyrazole- and Benzimidazole-Bearing Compounds. *Synthesis (Stuttg)*. **2013**, *45*, 3341-3348.
 19. K. A. Connors, Binding Constants, John Wiley & Sons, New York, 1st ed., 1987.
 20. Mercer, D. J.; Loeb, S. J.; Metal-based Anion Receptors; An Application of Second Sphere Coordination. *Chem. Soc. Rev.* **2010**, *39*, 3612-3620.
 21. Mäkelä, T.; Kalenius, E.; Rissanen, K.; Cooperatively Enhanced Ion pair Binding with a Hybrid Receptor. *Inorg. Chem.* **2015**, *54*, 9154-9165.
 22. Higuchi, T.; Rytting, J. H. Thermodynamic group contributions from ion pair extraction equilibria for use in the prediction of partition coefficients.

- Correlation of surface area with group contributions. *J. Phys. Chem.*, **1973**, *77*, 2694-2703.
23. Levitskaia , T. G.; Bryan , J. C.; Sachleben , R. A.; Lamb , J. D.; Moyer, B. A. A Surprising Host-Guest Relationship between 1,2-Dichloroethane and the Cesium Complex of Tetrabenzo-24-Crown-8. *J. Am. Chem. Soc.*, **2000**, *122*, 554-562.
 24. Kim, S. K.; Sessler, J. L.; Gross, D. E.; Lee, C.; Kim, J. S.; Lynch, V. M.; Delmau , L. H.; Hay, B. P. A calix[4]arene strapped calix[4]pyrrole: An ion-pair receptor displaying three different cesium cation recognition modes. *J. Am. Chem. Soc.*, **2010**, *132*, 5827-5836.
 25. Levitskaia, T.G.; Maya, L.; Van Berkel, G. J.; Moyer, B. A.; Anion Partitioning and Ion-Pairing Behavior of Anions in the Extraction of Cesium Salts by 4,5"-bis(tert-octylbenzo)dibenzo-24-crown-8 in 1,2-Dichloroethane. *Inorg. Chem.*, **2007**, *46*, 261-272.
 26. Jia, C.; Wang, Q.-Q.; Begum, R. A.; Day, V. W.; Bowman-James, K.; Chelate effects in sulfate binding by amide/urea-based ligands; *Org. Biomol. Chem.* **2015**, *13*, 6953-6957.
 27. Vacca, A.; Nativi, C.; Cacciarini, M.; Pergoli R.; Roelens, S. A New Tripodal Receptor for Molecular Recognition of Monosaccharides. A Paradigm for Assessing Glycoside Binding Affinities and Selectivities by ¹H NMR Spectroscopy. *J. Am. Chem. Soc.*, **2004**, *126*, 16456-16465.
 28. Arunachalam, M.; B. N.; Ahamed, Ghosh, P. Binding of Ammonium Hexafluorophosphate and Cation-Induced Isolation of Unusual Conformers of a Hexapodal Receptor *Org. Lett.*, **2010**, *12*, 2742-2745.
 29. KaleidaGraph, Version 3.0.2. Synergy Software (PCS Inc.), Reading, PA 19606. Developed by Abelbeck Software Inc.
 30. Becke, A. D. Density-Functional Thermochemistry. III. The Role of Exact Exchange. *J. Chem. Phys.* **1993**, *98*, 5648-5652
 31. Lee, C.; Yang, W.; Parr, R. G. Development of the Colle-Salvetti Correlation-Energy Formula into a Functional of the Electron Density. *Phys. Rev. B* **1988**, *37*, 785-789.
 32. Hehre, W.J.; Ditchfield, R.; Pople, J.A. Self-consistent molecular orbital methods. XII. Further extensions of gaussian-type basis sets for use in molecular orbital studies of organic molecules. *J. Chem. Phys.* **1972**, *56*, 2257-2261.
 33. Francl, M. M.; Pietro, W. J.; Hehre, W. J.; Binkley, J. S.; Gordon, M. S.; DeFrees, D. J.; Pople, J. A. Self-Consistent Molecular Orbital Methods. XXIII. A

- Polarization-type Basis Set for Second-Row Elements. *J. Chem. Phys.* **1982**, *77*, 3654–3665
34. Frisch, M. J.; Trucks, G. W.; Schlegel, H. B.; Scuseria, G. E.; Robb, M. A.; Cheeseman, J. R.; Scalmani, G.; Barone, V.; Mennucci, B.; Petersson, G. A. *Gaussian 09*, Revision A.1; Gaussian, Inc., Wallingford CT, **2009**
 35. Tomasi, J.; Mennucci, B.; Cammi, R. Quantum mechanical continuum solvation models. *Chem. Rev.* **2005**, *105*, 2999-3094.
 36. APEX3, Bruker Inc., Madison, WI, 2017.
 37. Sheldrick, G. M. Crystal structure refinement with SHELXL. *Acta Crystallogr. Sect. C*, **2015**, *C71*, 3-8.
 38. Dolomanov, O. V.; Bourhis, L. J.; Gildea, R. J.; Howard J. A. K.; Puschmann. H. OLEX2: A complete structure solution, refinement and analysis program. *J. Appl. Cryst.* **2009**, *42*, 339-341.
 39. Hubschle, C. B.; Sheldrick, G. M.; Dittrich, B. ShelXle: a Qt graphical user interface for SHELXL. *J. Appl. Crystal.* **2011**, *44*, 1281-1284.
 40. Krause, L.; Herbst-Irmer, R.; Sheldrick, G. M.; Stalke, D. Comparison of silver and molybdenum microfocus X-ray sources for single-crystal structure determination. *J. Appl. Crystal.* **2015**, *48*, 3-10.

Chapter III
Selective ion-pair fluorescent sensing of
ammonium nitrate by a combination of pyrazolyl and dansyl tripodal extractants

Tosin M. Jonah, Richild A. Currie and Konstantinos Kavallieratos*

*Department of Chemistry and Biochemistry, Florida International University,
11200 SW 8th Street, CP 326, Miami, Florida 33199*

3.1. Abstract

Dual-host combination of cation and anion sensors is used for the detection of ion pairs via solvent extraction. Selective sensors for each ion were synthesized and used together for ion-pair sensing both in organic solvents (using $(n\text{-Bu})_4\text{N}^+\text{NO}_3^-$ and $\text{NH}_4^+\text{PF}_6^-$) and in extraction of ammonium nitrate from water, into dichloromethane. We have demonstrated a unique extraction-based ion pair sensing method using FRET, which is selective for NH_4NO_3 at the 1.0×10^{-5} M to 1.0×10^{-4} M concentration range. The pendant pyrazolyl fluorophore groups of **1** which emit at 305-340 nm range are compatible with the excitation wavelength of the dansyl fluorophore in **2**, thus resulting in FRET upon combined use of these receptors. Extraction results revealed FRET fluorescence enhancements at 510 nm, with increasing concentration of NH_4NO_3 while NaNO_3 , KNO_3 , NaCl and KCl showed no fluorescence responses.

3.2. Introduction

Ion-pair sensing, which is concurrent complexation and detection of both the cation and anion species is an area that faces challenges in supramolecular chemistry.¹ Selective receptors have been developed for the sensing of cationic and anionic species separately but the challenge faced by chemists is the combined co-extraction and selective sensing of both ionic components of inorganic salts simultaneously.

Ion pairing has found many uses in the development of membrane transport, salt extraction and sensors.² Ion-pair receptors can be classified on the basis of how they bind to the ion pair components, which can be either independently or in a combined fashion. Ditopic receptors bind both salt components within the same molecule.^{1,3-7} Reetz and coworkers demonstrated this by coupling a crown ether moiety designed for K^+ recognition

to a Lewis-acidic boron center designed for F^- recognition.⁸ The design of ditopic receptors comes with some unique synthetic challenges. The cation-binding site must be separated from the anion-binding site in a way that the two sites do not interfere with each other. Selectivity of these sites for the target ion-pair over all possible interfering ion pairs must also be considered when designing the ditopic receptor. The design of the individual binding sites is somewhat straightforward, and the methods for creating individual hosts can be applied here. The difficulty lies in the linking of the two binding sites, which could be a complex process and a synthetic challenge. Another approach to ion-pair sensing which has been explored by fewer researchers is the dual-host strategy,⁹⁻¹¹ in which two different receptors specific for each ion are used to achieve combined sensing. The ion pairing in an organic solvent of relatively low dielectric constant can produce synergistic effects and in the case of fluorescent sensing, provide unique sensing effects for the pair as opposed to the individual components, through close contact of the complexed pair components in the organic solvent. For example if a fluorophore in the cation binding host has an emission band compatible with the excitation wavelength of the fluorophore attached to the anion receptor, close contact of the two complexed ions in the organic phase should -in principle- result in unique FRET emissions. Another advantage of the dual host strategy over the heteroditopic receptor is the avoidance of the laborious steps in synthesis of ditopic receptors. The dual host approach involves the combined extraction and sensing of the ion pair by two separate receptors using an organic solvent, such as 1,2-dichloroethane.

Different dual host receptors have been used for the extraction of alkali metal salts. An example is the liquid-liquid extraction of KF or KCl into $CHCl_3$ from an aqueous phase

containing equimolar amounts of cation and anion receptors.¹² 18-Crown-6 and a tripodal amide were the receptor choices for cation and anion binding, respectively. From the X-ray crystal structure obtained, it was shown that upon ion-pair complexation, the potassium salts self assemble to form a 1-D coordination polymer. In another example, Das et al. combined a N-bridged tripodal urea receptor for anions with 18-crown for binding and self-assembly of a K_2CO_3 complex.¹³ Despite these and other efforts, the dual-host strategy has not yet to our knowledge been applied successfully for sensing specific ion pairs.

In our effort to expand this dual host approach into selective sensing, we chose the ammonium nitrate ion pair, as a prototype. Ammonium nitrate was chosen because it is a sought-after material by terrorists for making improvised explosive devices, and it is commonly obtained in large quantities by commercial vendors, because ammonium salts are often used as fertilizers. Fluorescence detection presents a sensitive, inexpensive, and potentially portable method for in-field explosive detection. The pyrazolyl and dansyl fluorophores in receptors **1** and **2** (Fig. 3.1) for NH_4^+ and NO_3^- , respectively, were chosen because of the compatibility of their fluorescence excitation and emission wavelengths respectively, so that FRET will be observed upon salt extraction in the organic phase. The pendant pyrazolyl fluorophore groups of **1** which emit at 305-340 nm range are compatible with the excitation wavelength of the dansyl fluorophore in **2** thus resulting in FRET upon combined use of these receptors. The low dielectric constant of the organic medium assures close contact of the complexed anion and cation after extraction, which may lead to unique sensing effects as a result of FRET.

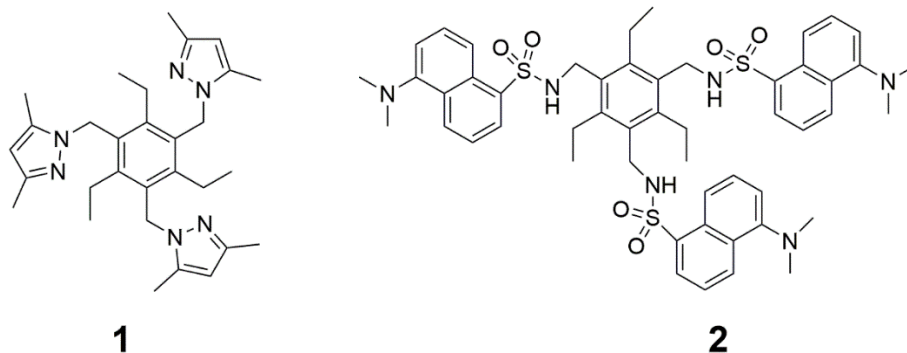


Figure 3.1 Chemical structures of ligands **1** and **2**.

3.3. Results and Discussion

There have been a few reported receptors for NH_4^+ cation binding and sensing.¹⁴⁻²⁰ The selected ammonium receptor is a fluorescent tripodal pyrazole, **1**, previously synthesized by J. Chin and co-workers.¹⁴ In our effort to understand the dual-host system, we studied the NH_4^+ binding properties of **1** by fluorescence and $^1\text{H-NMR}$ titrations. Fluorescence titration of **1** in $\text{CH}_3\text{CN}/\text{CH}_2\text{Cl}_2$ (1:1) with NH_4PF_6 at constant receptor concentration (1.0×10^{-4} M) showed an increase in fluorescence upon addition of NH_4PF_6 , which is significantly higher for NH_4^+ vs. K^+ , a pattern similar to the one observed for analogous tripodal oxazolines.^{15a} The results obtained from the $^1\text{H-NMR}$ titrations revealed remarkably strong and selective binding for NH_4^+ ($K_a = 74000 \text{ M}^{-1}$), over K^+ ($K_a = 15 \text{ M}^{-1}$) and 1:1 binding stoichiometry. (See Chapter 2 for details).

For the nitrate ion, we utilized **2**, a rigid 1,3,5-tris-(dansylsulfonamidomethyl)-2,4,6-triethylbenzene framework previously synthesized in our group.^{15b} The anion binding properties of **2** were determined in CDCl_3 by $^1\text{H-NMR}$ titration experiments using $(n\text{-Bu})_4\text{N}^+\text{NO}_3^-$. Significant downfield shifts of the N-H proton resonance were observed, indicating anion binding via hydrogen bonding. The titration studies were also performed

for other anions, such as Cl^- , Br^- and I^- . The ^1H -NMR titration results indicate that receptor **2** binds stronger to NO_3^- compared to Cl^- , Br^- and I^- . A single N-H resonance was observed, in all the experiments, indicating the involvements of all three N-H protons in anion binding or a fast exchange of $\text{NH}\cdots\text{X}^-$ anion complexes with number of hydrogen bonds. Non-linear regression analysis using the 1:1 binding isotherm (Eq. 1), was used in the determination the association constant K_a , which showed the formation of a 1:1 complex, where $\Delta\delta$ is the change in the N-H resonance, δ_{obs} is the observed change in the N-H resonance, δ_{R} is the actual change in the N-H resonance, $[\text{R}]_t$ is the total concentration of **R**, $[\text{X}^-]_t$ is the total concentration of $(n\text{-Bu})_4\text{N}^+\text{X}^-$, K_a is the association constant, and $\Delta\delta_{\text{max}}$ is the maximum chemical shift change. Non-linear regression analysis of the binding isotherms obtained from these shifts gave a 1:1 association constant K_a of $146 (\pm 3.9) \text{ M}^{-1}$ for the formation of $\mathbf{2}\cdot\text{NO}_3^-$ vs. 43 M^{-1} for $\mathbf{2}\cdot\text{Cl}^-$ and 91 M^{-1} for $\mathbf{2}\cdot\text{I}^-$.

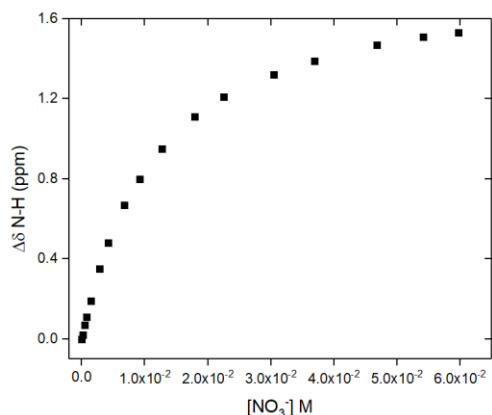


Figure 3.2. ^1H -NMR titration of **2** with $(n\text{-Bu})_4\text{N}^+\text{NO}_3^-$ in CD_2Cl_2 . The concentration of **2** was kept constant at 2 mM.

The dansyl group present in the structure of **2** provides the avenue for performing sensing studies with the receptor and the nitrate ion. Fluorescence titrations of **2** with $(n\text{-Bu})_4\text{N}^+\text{NO}_3^-$ at constant receptor concentration (1.0×10^{-6} M) were carried out in CH_2Cl_2 with $\lambda_{\text{exc}} = 352$ nm. Addition of $(n\text{-Bu})_4\text{N}^+\text{NO}_3^-$ to **2** showed a decrease in fluorescence upon nitrate binding (Figure 3.3).

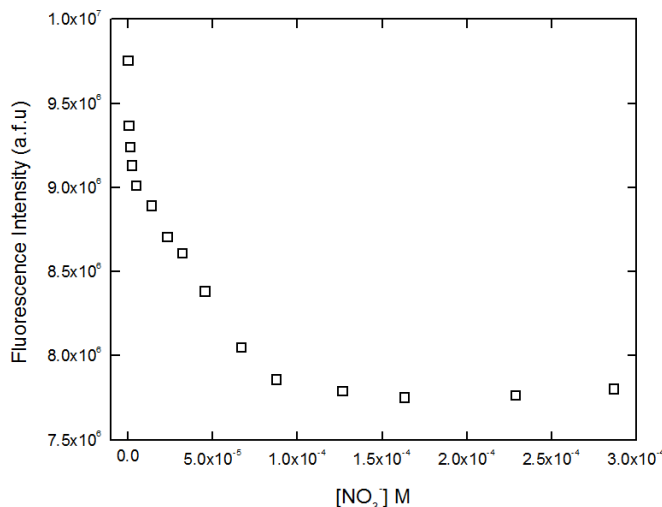


Figure 3.3. Fluorescence titration ($\lambda_{\text{exc}} = 352\text{nm}$) of **2** (1.0×10^{-6} M) with (1.0×10^{-3} M) of $(n\text{-Bu})_4\text{N}^+\text{NO}_3^-$ in CH_2Cl_2 . The concentration of **2** was kept constant.

The dual-host approach for sensing ion pairs involves the use of two separate receptors each for the individual ions in the ion pair. We used two approaches in investigating the dual-host sensing: We initially carried out fluorescence titrations studies in mixed solutions of **1** and **2**, in an organic solvent ($\text{CH}_3\text{OH}/\text{CH}_2\text{Cl}_2$ 2:8) with mixed solutions of $(n\text{-Bu})_4\text{N}^+\text{NO}_3^-$ and $\text{NH}_4^+\text{PF}_6^-$. The fluorescence emission spectra were collected at $\lambda_{\text{exc}} = 272$ nm, which corresponds to the excitation wavelength of **1**. Excitation of **1** at $\lambda_{\text{exc}} = 272$ nm resulted in the transfer of energy from excited **1** to **2** raising the energy state of an electron in **2** to higher vibrational levels of the excited singlet state. As a result, the energy level of the **1** returns to the ground state, without emitting its own fluorescence. The

resulted fluorescence quenching signal is shown below in figure 3.4 while figure 3.5 shows quenching at 506 nm wavelength. What is notable from these experiments is that dansyl FRET fluorescence is clearly observed upon excitation at 272 nm, only in the presence of the pyrazolyl fluorophore. As the excitation of the dansyl fluorophore is in the 310-352nm range, this experiment shows that in principle FRET fluorescence by the interaction of the two fluorophores in the organic phase could be used to monitor NH_4NO_3 quantities. Yet the presence of FRET fluorescence even in the absence of any NH_4NO_3 , presumably because of association between the two receptors, may present a potential problem. In the event that only the dansyl receptor **2** is used no fluorescence emission is observed upon excitation at 272 nm. Likewise, in the absence of the dansyl receptor **2**, excitation of solutions of **1**, gave fluorescence at 298 nm, but no FRET emissions at 506 nm.

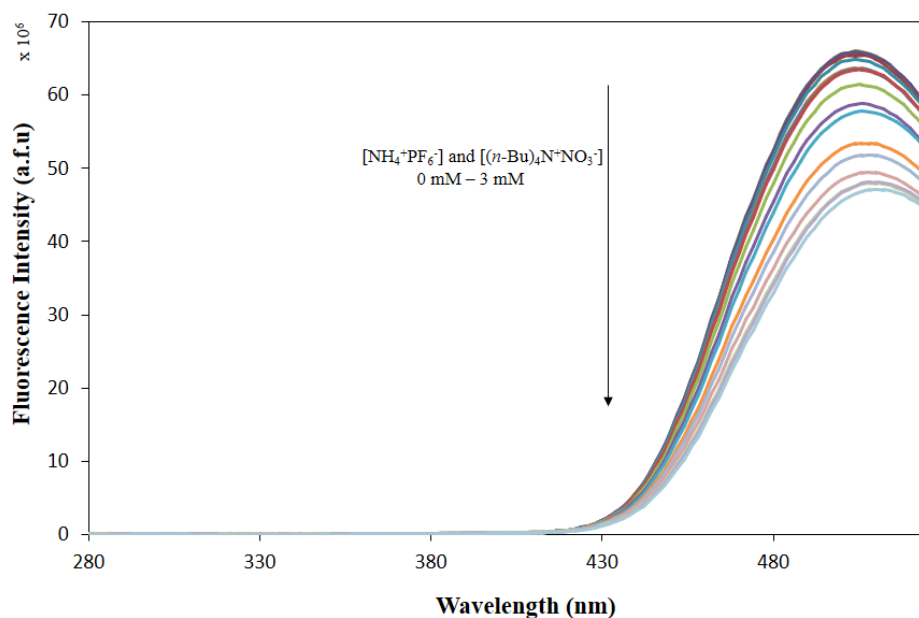


Figure 3.4. Fluorescence titrations of an equimolar mixture of **1** and **2** (5.0×10^{-5} M) with an equimolar mixture of $\text{NH}_4^+\text{PF}_6^-$ and $(n\text{-Bu})_4\text{N}^+\text{NO}_3^-$ in $\text{CH}_3\text{OH}/\text{CH}_2\text{Cl}_2$ (2:8).

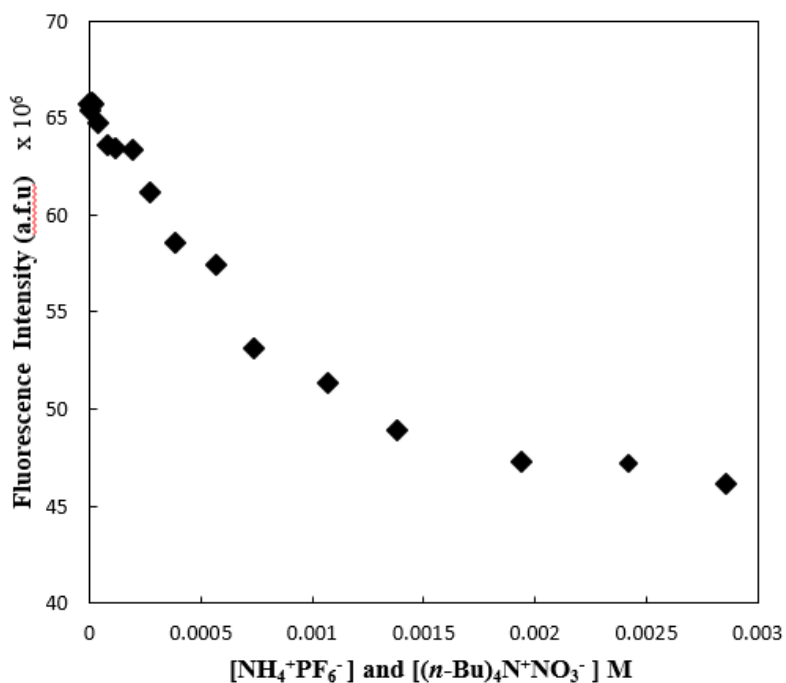


Figure 3.5. Fluorescence Titration curve of **1** & **2** with $\text{NH}_4^+\text{PF}_6^-$ & $(n\text{-Bu})_4\text{N}^+\text{NO}_3^-$
 $\lambda_{\text{exc}} = 272 \text{ nm}$, $\lambda_{\text{em}} = 506 \text{ nm}$.

Our investigation was expanded into the combined extraction and sensing of NH_4NO_3 by **1** and **2** using an organic solvent, dichloromethane. A dual-host extraction experiment was designed in which the tripodal pyrazolyl receptor **1** for NH_4^+ and the dansylated sulfonamide **2**, for NO_3^- were used in the organic phase to extract different alkali metal salts from aqueous phases, and the fluorescence spectra were recorded after contact, phase separation, and drying of the organic phase with granular Na_2SO_4 . Specifically, the organic phases contained both **1** and **2** ($5.0 \times 10^{-5} \text{ M}$) in CH_2Cl_2 . Stock solutions of NaNO_3 , KNO_3 , NH_4NO_3 , KCl , and NaCl , in ultrapure water ($1.0 \times 10^{-2} \text{ M}$) were brought in contact with the organic phases. The organic layers were separated from the aqueous layer after 3h. The fluorescence intensity of the organic layers was measured after separation and drying of the organic phases. All the solutions were excited at 272 nm with the slit at 1 nm. Extraction

results revealed fluorescent enhancements with increasing concentration of NH_4NO_3 (Fig. 3.6). The control extraction experiments repeated for NaNO_3 , KNO_3 , NaCl and KCl (Fig. 3.7- 3.10) showed no significant fluorescence responses when this salts were extracted by receptor **1** & **2**.

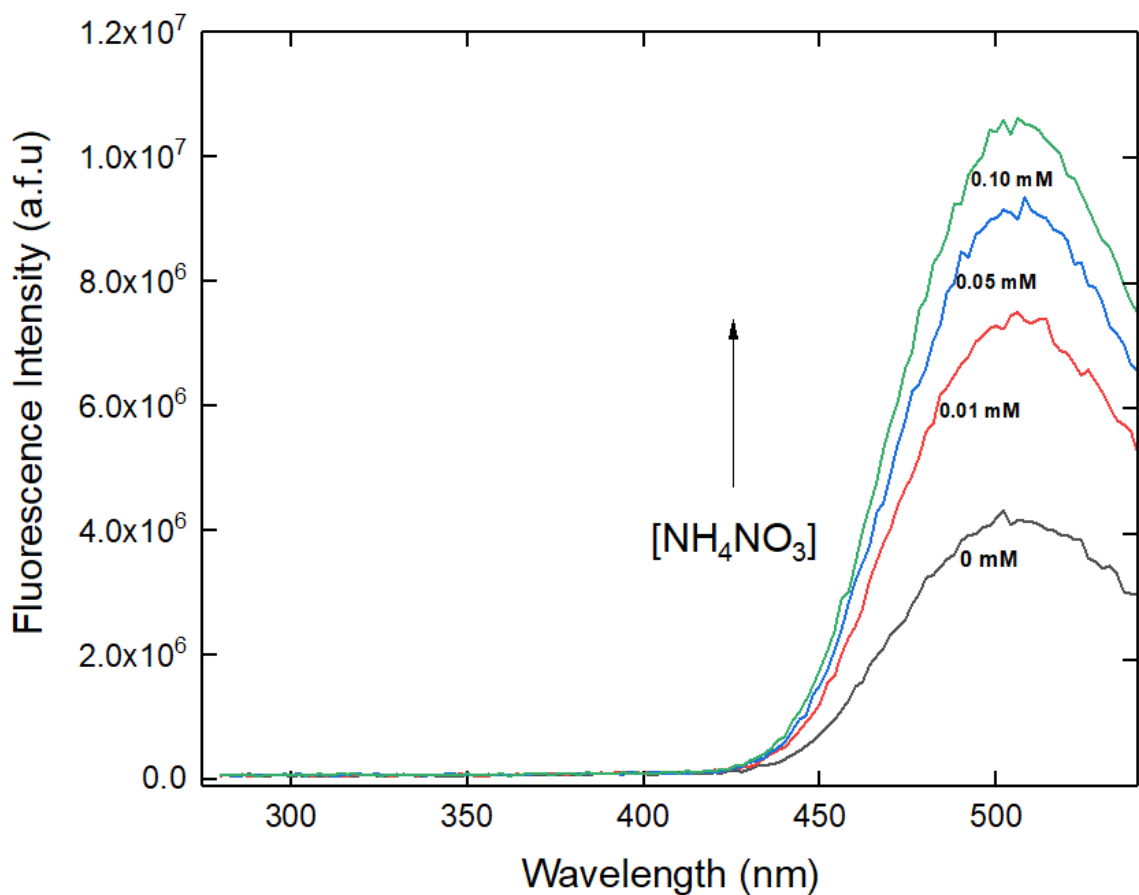


Figure 3.6. Fluorescence emission ($\lambda_{\text{exc}} = 272 \text{ nm}$) of an organic phase (CH_2Cl_2) containing **1** & **2** (0.05 mM) after extraction with NH_4NO_3 . NH_4NO_3 concentrations are 0 mM (black), 0.01 mM (red), 0.05 mM (blue) and 0.1 mM (green).

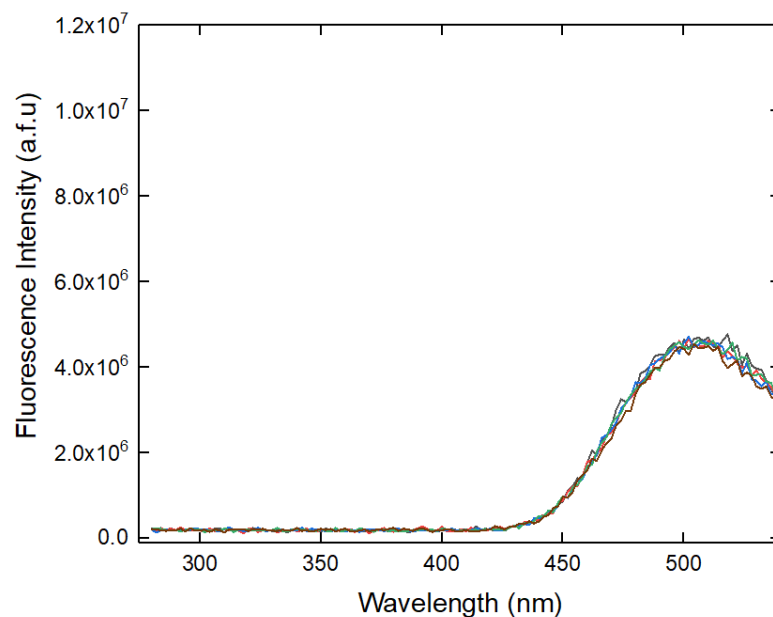


Figure 3.7. Fluorescence emission of **1** & **2** (0.05 mM) after extraction with KNO₃ from water into CH₂Cl₂ following 272 nm excitation.

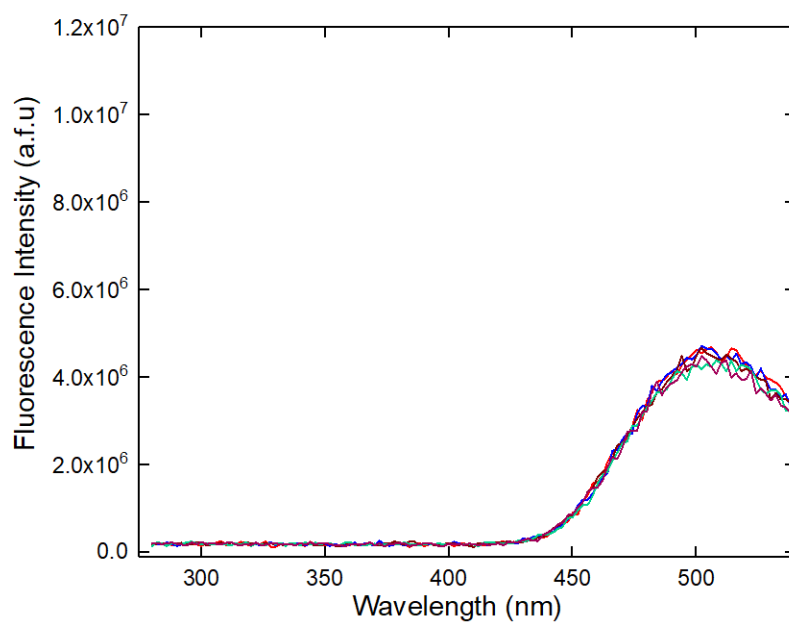


Figure 3.8. Fluorescence emission of **1** & **2** (0.05 mM) after extraction with NaNO₃. Concentration range of 0 mM - 0.10 mM in CH₂Cl₂ following 272 nm excitation.

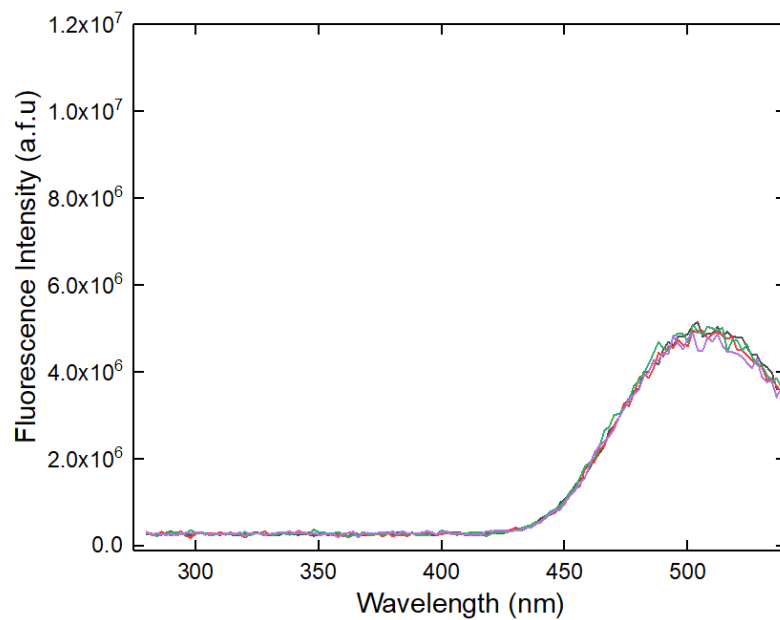


Figure 3.9. Fluorescence emission of **1** & **2** (0.05 mM) after extraction with KCl in CH_2Cl_2 following 272 nm excitation.

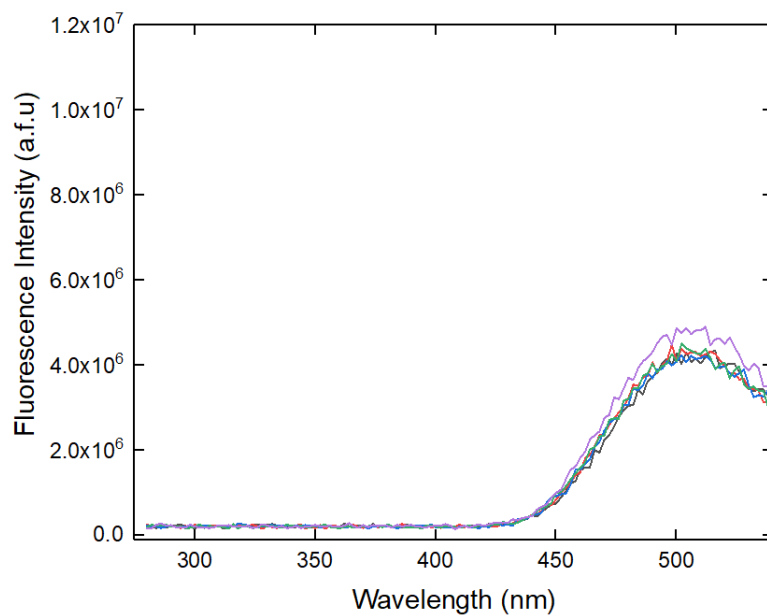


Figure 3.10. Fluorescence emission of **1** & **2** (0.05 mM) after extraction with NaCl in CH_2Cl_2 following 272 nm excitation.

The remarkable FRET response selectivity for NH_4NO_3 vs. other alkali metal nitrate salts (Fig 3.11) and other halide salts (Fig. 3.12 and 3.13) demonstrates that our hypothesis of using FRET for selective dual-host extraction and sensing of NH_4NO_3 is a valid one. However, a point of concern is that FRET is not zero at zero concentration of added salts, thus implying that some association of **1** and **2** in the organic phase is taking place leading to FRET, even in the absence of the extracted salt. As receptor **2** has hydrogen bond donor SO_2NH sites, and receptor **1** has pyrazole acceptor sites, this is a reasonable hypothesis.

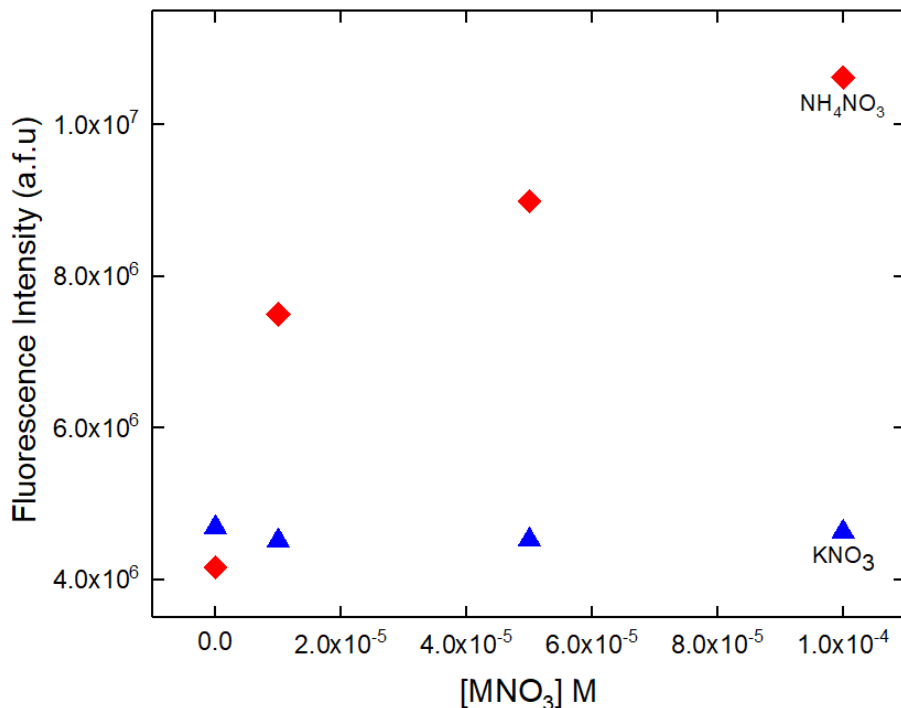


Figure 3.11. Fluorescence emission ($\lambda_{\text{exc}} = 272$ nm) of organic phases (CH_2Cl_2) containing **1** & **2** (0.05 mM) after extraction with various concentrations of MNO_3 ($\text{M} = \text{NH}_4^+$, K^+), showing selective FRET sensing for NH_4NO_3 .

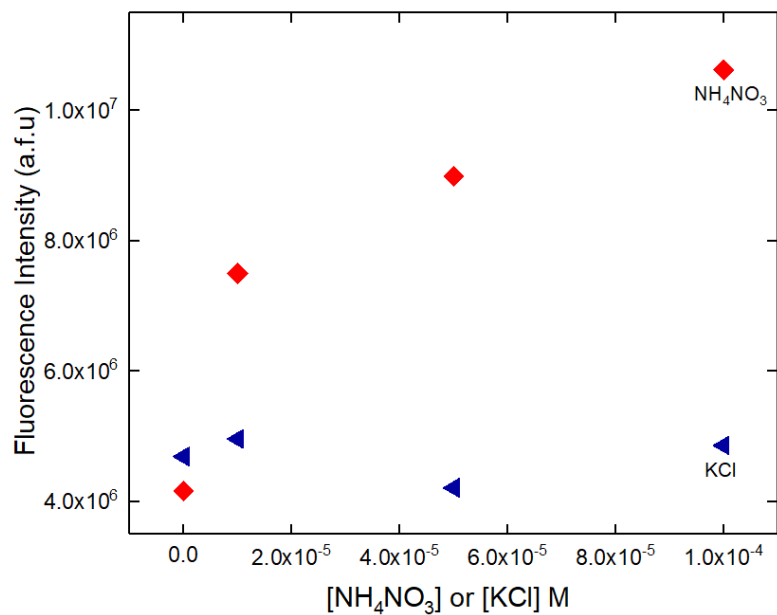


Figure 3.12. Fluorescence emission ($\lambda_{exc} = 272$ nm) of organic phases (CH_2Cl_2) containing **1** & **2** (0.05 mM) after extraction with various concentrations of NH_4NO_3 and KCl, showing selective FRET sensing for NH_4NO_3 .

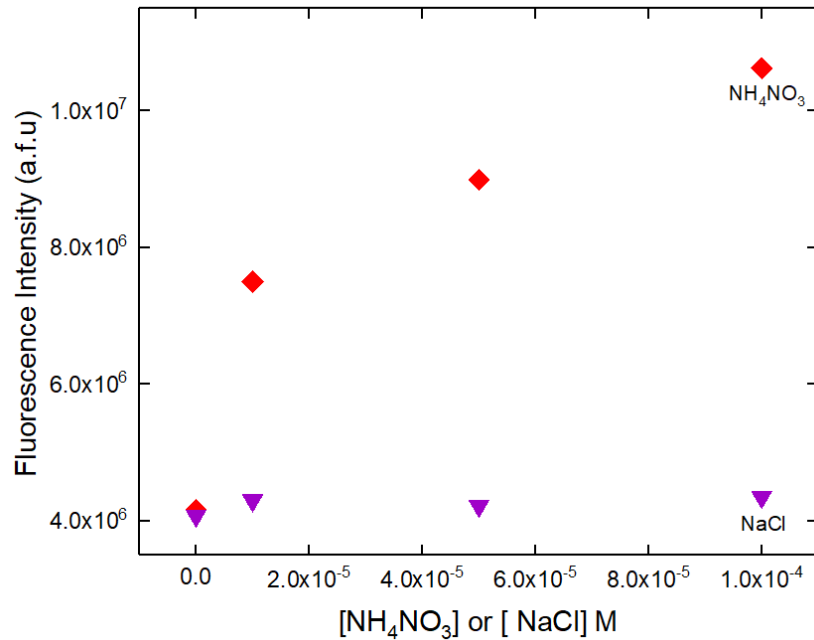


Figure 3.13. Fluorescence emission ($\lambda_{exc} = 272$ nm) of organic phases (CH_2Cl_2) containing **1** & **2** (0.05 mM) after extraction with various concentrations of NH_4NO_3 and NaCl.

3.4 Conclusion

In conclusion, we have performed ion pair extraction and ammonium nitrate sensing studies in organic solvents by fluorescence titration of mixed solutions of **1** and **2**, in dichloromethane with aqueous solutions of NH_4NO_3 . The results obtained from distribution experiments showed fluorescence enhancements upon contact with ammonium nitrate solutions. The control experiments with KNO_3 , NaNO_3 , NaCl and KCl gave negligible responses. NH_4NO_3 in aqueous media exists as hydrated ions. In organic media however ion pairing is maintained because of the low dielectric constant of the solvent and electrostatic attraction between cations and anions. Thus, intermolecular effects like FRET, give unique responses for the ion pair compared to the individual ions. We have now demonstrated a unique extraction-based ion pair sensing method using FRET for the first time. This novel ion-pair sensing paradigm paves the way for future sensitive and selective ion-pair sensing methods based on organophilic polymers or other materials of low polarity that can potentially be optimized for on-field detection use.

3.5 Experimental

3.5.1 Materials and methods

All materials (purchased from Aldrich Chemical Company or Acros Organics) were standard reagent grade and were used without further purification. Compound **1** was synthesized as previously reported. $^1\text{H-NMR}$ spectra were recorded on a 400 MHz Bruker NMR spectrometer and were referenced to the residual solvent resonance. All chemical shifts, δ , are reported in ppm.

3.5.2. Synthesis of 1,3,5-Tris-(5-dimethylamino-1-naphthalenesulfonamido)methyl]-2,4,6-triethylbenzene (2).

Triethylamine (0.062 mL, 0.465 mmol) was used to deprotonate 1,3,5-tris(aminomethyl)-2,4,6-triethylbenzene (0.039 g, 0.155 mmol) in 2 mL of anhydrous 1,2-DCE for 30 mins at room temperature. Dansyl chloride (0.12 g, 0.46 mmol) dissolved in 6 mL of dichloroethane, was slowly added to the solution. The reaction mixture was left to stir under nitrogen for 4h. After the 4h elapsed, ethyl acetate (0.1 M in water) was used to quench the reaction. The resulting solution was extracted with CH₃Cl. The organic layer was collected and dried with anhydrous sodium sulfate. This solution was concentrated and hexanes was added dropwise. The yellow precipitate that was formed was purified by column chromatography (90:10 CH₂Cl₂/ EtOAc) and dried under vacuum yielding **2** (0.12 g, 85% yield): mp 218-220 °C; ¹H NMR (CDCl₃, 400 MHz), 0.45 (9H, t, J = 7.4 Hz), 1.86 (6H, q, J = 7.4 Hz), 2.93 (18H, s), 3.66 (6H, d, J = 5.2 Hz), 4.01 (3H, s), 7.56 (6H, m, J = 3.9 Hz), 8.22 (3H, d, J = 8.6 Hz), 8.26 (3H, d, J = 7.2 Hz), 8.58 (3H, d, J = 8.2 Hz); ¹³C{¹H} NMR (CDCl₃, 400 MHz) δ 15.6, 21.8, 40.8, 45.4, 115.4, 118.4, 123.0, 128.5, 129.6, 129.7, 129.8, 130.2, 130.7, 133.4, 144.3, 152.0.

3.5.3 ¹H NMR Titrations of **2** with (*n*-Bu)₄N⁺X⁻.

The association constants for the formation of anion-receptor complexes were determined by titration of solutions of **2** (2.0 x 10⁻³ M) in CDCl₃ (solution A) with 1 x 10⁻¹ M solutions of (*n*-Bu)₄N⁺NO₃⁻ prepared by dilution with solution A, thus keeping a constant concentration of **2** (solution B). In a typical experiment solution A (0.700 mL) was placed in an NMR tube. Solution B was added in increments until a total of 1000 μl was added. The chemical shift changes for the N-H proton were monitored and the results

were plotted and fitted to the 1:1 binding isotherm (Eq.1) using non-linear regression analysis.

$$\Delta\delta = \delta_{\text{obs}} - \delta_2 = ([\mathbf{R}]_t + [\mathbf{X}]_t + K_a^{-1} - ((([\mathbf{R}]_t + [\mathbf{X}]_t + K_a^{-1})^2 - 4[\mathbf{X}]_t [\mathbf{R}]_t)^{1/2}))\Delta\delta_{\text{max}} / (2[\mathbf{R}]_t) \quad (\text{Eq.1})$$

3.5.4 Fluorescence Titrations of **2** with (*n*-Bu)₄N⁺NO₃⁻

Fluorescence emission was measured using an excitation wavelength of 352 nm, a measurement increment of 0.5 nm, and integration time of 0.1 s, excitation slit width of 10 nm, emission slit width of 5 nm, and an emission wavelength of 505.5 nm. Experiments were run using solutions of **2** (1.0 x 10⁻⁶ M) in CH₂Cl₂ (solution A) which were titrated with solutions of (*n*-Bu)₄N⁺NO₃⁻ (1.0 x 10⁻³ M) and **2** (1.0 x 10⁻⁶ M) in CH₂Cl₂ (solution B). 2.0 mL of solution A was added to the fluorescence cuvette and solution B was added in increments until a total of 1000 μL was added. The fluorescence intensity at 505.5 nm was monitored and recorded.

3.5.5 Fluorescence titrations of solutions of **1** & **2** with NH₄PF₆ and (*n*-Bu)₄N⁺NO₃⁻

Fluorescence titration experiments were performed using receptors **1** and **2** in an organic solvent to extract NH₄NO₃ in an aqueous medium. Extraction experiments were performed using receptors **1** and **2** with NH₄PF₆ with (*n*-Bu)₄N⁺NO₃⁻ in CH₃OH/CH₂Cl₂ (2:8). Experiments were run using solutions of **1** and **2** (5 x 10⁻⁵ M) in CH₃OH/CH₂Cl₂ (2:8) (solution A) which were titrated with solutions of NH₄⁺PF₆⁻ and (*n*-Bu)₄N⁺NO₃⁻ (5.0 x 10⁻³ M) and **1** and **2** (5.0 x 10⁻⁵ M) in CH₃OH/CH₂Cl₂ (2:8) (solution B). 2.0 mL of solution A was added to the fluorescence cuvette and solution B was added in increments until a total of 1000 μL was added. The fluorescence intensity at 505.5 nm was monitored.

3.5.6 Extraction Titrations and Controls.

Extraction experiments were performed using receptors **1** and **2** in an organic solvent to extract NH_4NO_3 in an aqueous medium. For all steps, aqueous phase to organic phase volume ratios were 1:1. All aqueous phases were prepared in deionized water, and all organic phases used spectroscopic grade CH_2Cl_2 as the solvent. NH_4NO_3 extractions were performed in initial aqueous concentration range of 1.0×10^{-5} M to 1.0×10^{-4} M. The organic phases contained 5.0×10^{-5} M of **1** and **2** in CH_2Cl_2 . In a typical experiment, 5.0 mL of both aqueous and organic phases were used. Extraction took place over 4 h, with the organic layer being separated from the aqueous layer thereafter. The fluorescence of the organic layer was recorded. The same procedure was repeated for NaNO_3 , KNO_3 , NH_4Cl , NaCl , and KCl .

3.6. References

- (1) Cafeo, G.; Gattuso, G.; Kohnke, F. H.; Notti, A.; Occhipinti, S.; Pappalardo, S.; Parisi, M. F. Remarkable Boosting of the Binding of Ion-Paired Organic Salts by Binary Host Systems. *Angew. Chemie - Int. Ed.* **2002**, *41*, 2122-2126.
- (2) McConnell, A. J.; Beer, P. D. Heteroditopic Receptors for Ion-Pair Recognition. *Angew. Chemie - Int. Ed.* **2012**, *51*, 5052-5061.
- (3) Beer, P. D.; Bernhardt, P. V. A ferrocene functionalised macrocyclic receptor for cations and anions.. *J. Chem. Soc., Dalt. Trans.* **2001**, 1428-1431.
- (4) Beer, P. D.; Drew, M. G. B.; Knubley, R. J.; Ogden, M. I. Synthesis and coordination chemistry of a novel bis(benzo crown ether) substituted calix[4]arene that can simultaneously complex cations and anions. *J. Chem. Soc., Dalt. Trans.* **1995**, 3117-3123.
- (5) Cooper, J. B.; Drew, M. G. B.; Beer, P. D. Heteroditopic rhenium(I) and ruthenium(II) bipyridyl calix[4]arene receptors for binding cation–anion ion pairs. *J. Chem. Soc., Dalt. Trans.* **2001**, 392-401.
- (6) Cooper, J. B.; Drew, M. G. B.; Beer, P. D. Alkali metal cation cooperative anion recognition by heteroditopic bis(calix[4]arene) rhenium(I) bipyridyl and ferrocene receptor molecules. *J. Chem. Soc., Dalt. Trans.* **2000**, 2721-2728.

- (7) Rudkevich, D. M.; Mercer-Chalmers, J. D.; Verboom, W.; Ungaro, R.; de Jong, F.; Reinhoudt, D. N. Bifunctional Recognition: Simultaneous Transport of Cations and Anions through a Supported Liquid Membrane. *J. Am. Chem. Soc.* **1995**, *117*, 6124-6125.
- (8) Reetz, M. T.; Niemeyer, C. M.; Harms, K. Crown Ethers with a Lewis Acidic Center: A New Class of Heterotopic Host Molecules. *Angew. Chemie Int. Ed. English* **1991**, *30*, 1472-1474.
- (9) D. Beer, P.; K. Hopkins, P.; D. McKinney, J. Cooperative Halide, Perrhenate Anion-Sodium Cation Binding and Pertechnetate Extraction and Transport by a Novel Tripodal Tris(amido Benzo-15-Crown-5) Ligand. *Chem. Commun.* **1999**, 1253-1254.
- (10) Kavallieratos, K.; Danby, A.; Berkel, G. J. Van; Kelly, M. a; Sachleben, R. a; Moyer, B. a; Bowman-james, K. Enhancement of CsNO₃ Extraction in 1,2-Dichloroethane by Tris (2-Aminoethyl) Amine Triamide Derivatives via a Dual-Host Strategy. **2008**, *72*, 5258-5264.
- (11) Kavallieratos, K.; Sachleben, R. A.; Van Berkel, G. J.; Moyer, B. A. Novel Dual-Host Approach in Ion Pair Extraction: A Simple Tripodal Nitrate Host Facilitates CsNO₃ Transfer to 1,2-Dichloroethane by a Large Crown Ether. *Chem. Commun.* **2000**, 187-188.
- (12) Ravikumar, I.; Saha, S.; Ghosh, P. Dual-Host Approach for Liquid-Liquid Extraction of Potassium Fluoride/chloride via Formation of an Integrated 1-D Polymeric Complex. *Chem. Commun.* **2011**, *47*, 4721-4723.
- (13) Chutia, R.; Dey, S. K.; Das, G. A Supramolecular Dual-Host Based Ion-Pair Induced Formation of 1D Coordination Polymer. *CrystEngComm* **2013**, *15*, 9641-9647.
- (14) Chin, J.; Walsdorff, C.; Stranix, B.; Oh, J.; Chung, H. J.; Park, S. M.; Kim, K. A Rational Approach to Selective Recognition of NH₄⁺ over K⁺. *Angew. Chemie - Int. Ed.* **1999**, *38*, 2756-2759.
- (15) (a) Ahn, K. H.; Ku, H. Y.; Kim, Y.; Kim, S. G.; Kim, Y. K.; Son, H. S.; Ku, J. K. Fluorescence Sensing of Ammonium and Organoammonium Ions with Tripodal Oxazoline Receptors. *Org. Lett.* **2003**, *5*, 1419-1422. (b) Currie, R. Spectroscopic, Electrochemical and Mass Spectrometric Investigation of Anion Binding by Tripodal Molecular Receptors. Florida International University, 2005.
- (16) Ahn, K. H.; Kim, S. G.; Jung, J. Y.; Kim, K. H.; Kim, J.; Chin, J.; Kim, K. Selective Recognition of NH₄⁺ over K⁺ with Tripodal Oxazoline Receptors. *Chem. Lett.* **2000**, 170-171.
- (17) Rueda-zubiaurre, A.; Herrero-garcía, N. Rational Design of a Nonbasic Molecular Receptor for Selective NH₄⁺ / K⁺ Complexation in the Gas Phase. *Chem. Eur. J.* **2012**, *1*, 16884-16889.
- (18) Jon, S. Y.; Kim, J.; Kim, M.; Park, S.; Jeon, W. S.; Heo, J.; Kim, K. A Rationally

- Designed NH_4^+ Receptor Based on Cation– π Interaction and Hydrogen Bonding .
Angew. Chemie **2001**, *113*, 2174-2177.
- (19) Kim; Ahn. Novel Artificial Receptors for Alkylammonium Ions with Remarkable Selectivity and Affinity. *Chemistry* **2000**, *6* , 3399-3403.
- (20) Jon, S. Y.; Kim, J.; Kim, M.; Park, S.; Jeon, W. S.; Heo, J.; Kim, K. A Rationally Designed NH_4^+ Receptor Based on Cation– π Interaction and Hydrogen Bonding .
Angew. Chemie Int. Ed. **2001**, *40*, 2116-2119.
- (21) KaleidaGraph, Version 3.0.2. Synergy Software (PCS Inc.), Reading, PA 19606.
Developed by Abelbeck Software Inc.
- (22) Kilway, K. V; Siegel, J. S. Control of Functional Group Proximity and Direction by Conformational Networks: Synthesis and Stereodynamics of Persubstituted Arenes.
Tetrahedron **2001**, *57*, 3615-3627.

CHAPTER IV

Tripodal pyrazole ligands and analogs for selective lanthanide sensing

Tosin M. Jonah, Logesh Mathivathanan, Gabriel Flores, Raphael G. Raptis, Konstantinos

Kavallieratos*

Department of Chemistry & Biochemistry, Florida International University, Miami, FL,

United States.

4.1 Abstract

Actinide removal from alkaline high-level waste (HLW) stored in underground tanks at the Hanford & Savannah River sites is of great concern. Furthermore, selectively separating actinides (An) from lanthanides (Ln) in used nuclear fuel presents an important challenge in closing the nuclear fuel cycle. Tripodal ligand frameworks based on 1,3,5-trisubstituted-2,4,6 triethylbenzene provide a highly pre-organized cavity for binding of cations, such as NH_4^+ , Ln(III) and An(III). Previous work by our group and others have shown the potential of such frameworks for binding NH_4^+ (Chapter 2). Herein, we compare three tris-pyrazole frameworks for Ln(III) extraction and sensing, with the further goal of eventually developing selective An(III)/Ln(III) separation processes and combined Cs(I) and An(III) separation and extraction from High-Level Waste. The proposed ligands are based on the 1,3,5-tris(pyrazolyl)-2,4,6-triethyl benzene frameworks. Binding of Ln(III) in organic solvents by these ligands is confirmed by fluorescence, and NMR titration experiments. Chemical shift changes for all proton resonances were observed, indicating cation binding. Fluorescence titrations of 1×10^{-4} M of 1,3,5-tris(3,5-dimethylpyrazolyl)-2,4,6-triethyl benzene with $\text{La}(\text{NO}_3)_3 \cdot 6\text{H}_2\text{O}$ also showed evidence of binding. The binding affinity was determined by ^1H -NMR titrations with La^{3+} in acetone- d_6 . Non-linear regression analysis of the binding isotherms gave a 1-1 complexation ratio, with an association constant K_a of 155 M^{-1} for La^{3+} .

4.2 Introduction

The processing and removal of high heat emitters from nuclear waste streams continuously poses a serious concern. These streams usually contain long-lived radiotoxic minor actinides and fission products.¹⁻³ The radiotoxicity and high heat generator in these

nuclear waste streams are the actinides.³⁻⁹ There is a continuous effort in generating ligands that can separate these high heat emitters from the nuclear fuel waste. Selectively separating minor actinides (An) from lanthanides (Ln) in used nuclear fuel presents an important challenge in closing the nuclear fuel cycle. This is because of the chemical similarities between the actinides and lanthanides in their ionic radii and identical oxidation states. There has been continuous effort in looking for ligands to successfully separate the trivalent actinides from lanthanides, and fission products. Gullu et al¹⁰ synthesized macrocyclic receptors based on the lactam ionophore to investigate the complexation pattern of this class of ligands towards Ln(III). The observed changes in the emission and absorption spectra of these compounds upon contact with Ln(III) were attributed to intramolecular energy transfer process. A fluorescent sensor bearing a diazostilbenzene and benzo-15-crown ether moiety capable of detecting lanthanide ions with high sensitivity and resolution has also been reported.¹¹ Detectable fluorescence signals were observed when equimolar concentrations of the ligands and Ln(III) were used in THF. A cyclen-based fluorescent ligand capable of detecting micromolar concentrations of Y³⁺ and La³⁺ ions in water was reported by Aoki et al.¹² Preorganized tripodal ligands¹³⁻¹⁵ have recently been explored for Ln(III) sensing: The tripodal fluoroionophore reported by Das et al.¹³ shows selective fluorescence enhancement with addition of Ce(III) in dry THF. The tris-(2-benzimidazolymethyl) amine showed strong intramolecular π - π interactions and gave 2:1 ligand to metal ratios upon complexation with Ln(III).¹⁴

Herein, we report the complexation behavior of Ln(III) (La³⁺, Nd³⁺, Lu³⁺, Ce³⁺, Eu³⁺ and Sm³⁺) with three pyrazole receptors, based on the 1,3,5-triethylbenzene framework. We have undertaken a systematic study of the effects of pyrazole substitution on the Ln(III)

binding properties by NMR and fluorescence spectroscopy, with remarkably similar conclusions on the effects of solvation and ion pairing, as in our study described earlier on NH_4^+ (Chapter 2). The binding affinity of these ligands towards Ln(III) were determined by ^1H -NMR titrations in acetone- d_6 as well as from analysis of the fluorescence spectra.

4.3 Results and discussion

The three receptors used in this work were prepared by modifications of previously reported methods.¹⁶ NaOH was used to deprotonate the corresponding pyrazole in DMF. The resulting solution was then let to react with tris-1,3,5-(bromomethyl)-2,4,6-triethylbenzene at 70 °C for 48 h. The fluorescence emission intensity of the free receptors is shown in Figures 4.1 and 4.2. The emission intensities in the presence of Ln(III) (La^{3+} , Nd^{3+} , Lu^{3+} , Ce^{3+} , Eu^{3+} and Sm^{3+}) are shown in Figures 4.3-4.5.

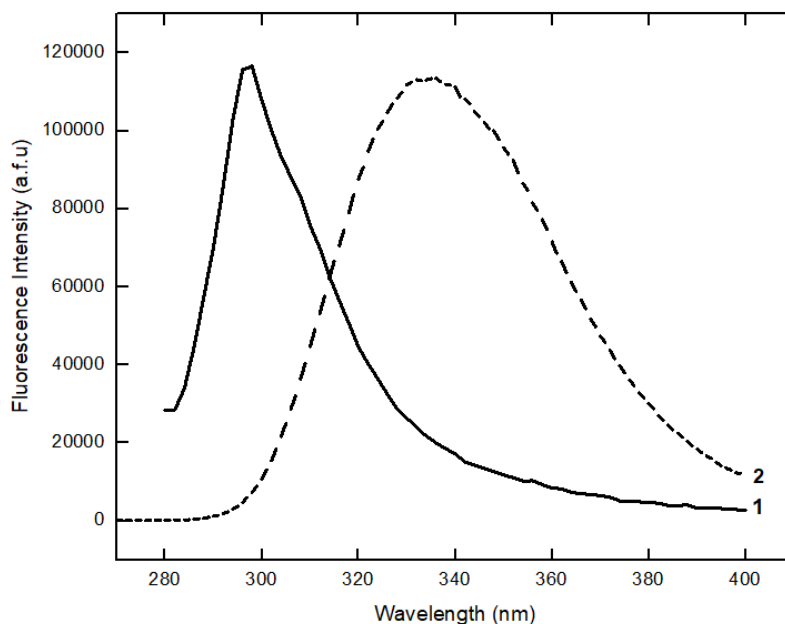


Figure 4.1 Fluorescence emission for receptor **1** ($\lambda_{\text{exc}} = 272 \text{ nm}$) and **2** ($\lambda_{\text{exc}} = 262 \text{ nm}$) in $\text{CH}_3\text{CN}/\text{CH}_2\text{Cl}_2$ (1:1).

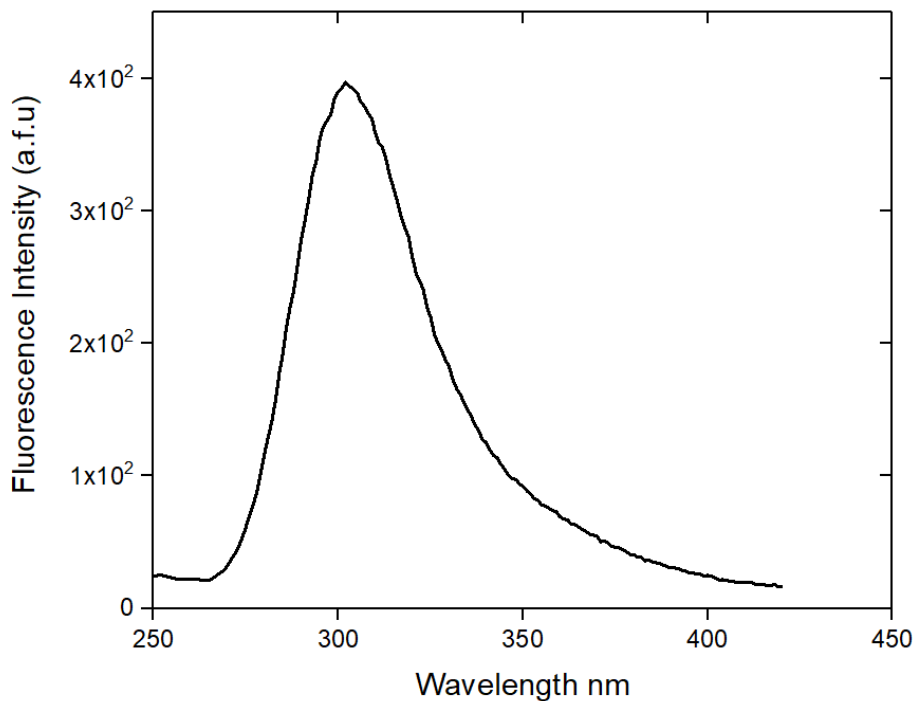


Figure 4.2 Fluorescence emission of receptor **3** in CH₃CN at λ_{exc} = 230 nm

Fluorescence titrations of the three receptors with Ln(III) salts were carried out at constant receptor concentration (1.0×10^{-4} M) in CH₃CN (λ_{exc} = 272 nm; λ_{em} = 298 nm for **1**, and λ_{exc} = 262 nm; λ_{em} = 335 nm for **2** and λ_{exc} = 230 nm; λ_{em} = 304 nm for **3**). In the case of receptor **1**, the addition of Sm³⁺, Eu³⁺, La³⁺, Nd³⁺, Lu³⁺ to solution of **1**, resulted in enhancement in intensity at the maximum emission at 298 nm, with the receptor reaching saturation at 1:1 ratio (Figures 4.3-4.8). When Ce³⁺ was added to a solution of **1**, two phenomena were observed: An increase in fluorescence followed by a sharp quenching, a trend different from the other Ln (III). The results from the titration curves indicate that pyrazoles are indeed a family that can be used for Ln(III) sensing. When the pyrazole substitution pattern changes from dimethyl in **1** to diphenyl in **2**, the results show that the diphenyl receptor **2** does not appreciably bind to Ln(III). The fluorescence intensity

changes observed with the addition of Sm^{3+} , La^{3+} , Nd^{3+} , Lu^{3+} to a solution of **2** in acetonitrile showed only small changes and no particular trend (Figure 4.3-4.8) except for Ce^{3+} that showed slight, but consistent quenching. For the unsubstituted pyrazole **3**, addition of lanthanide salts in acetonitrile, led to consistent fluorescence quenching without any considerable shift in the emission maximum, indicating Ln(III) binding.

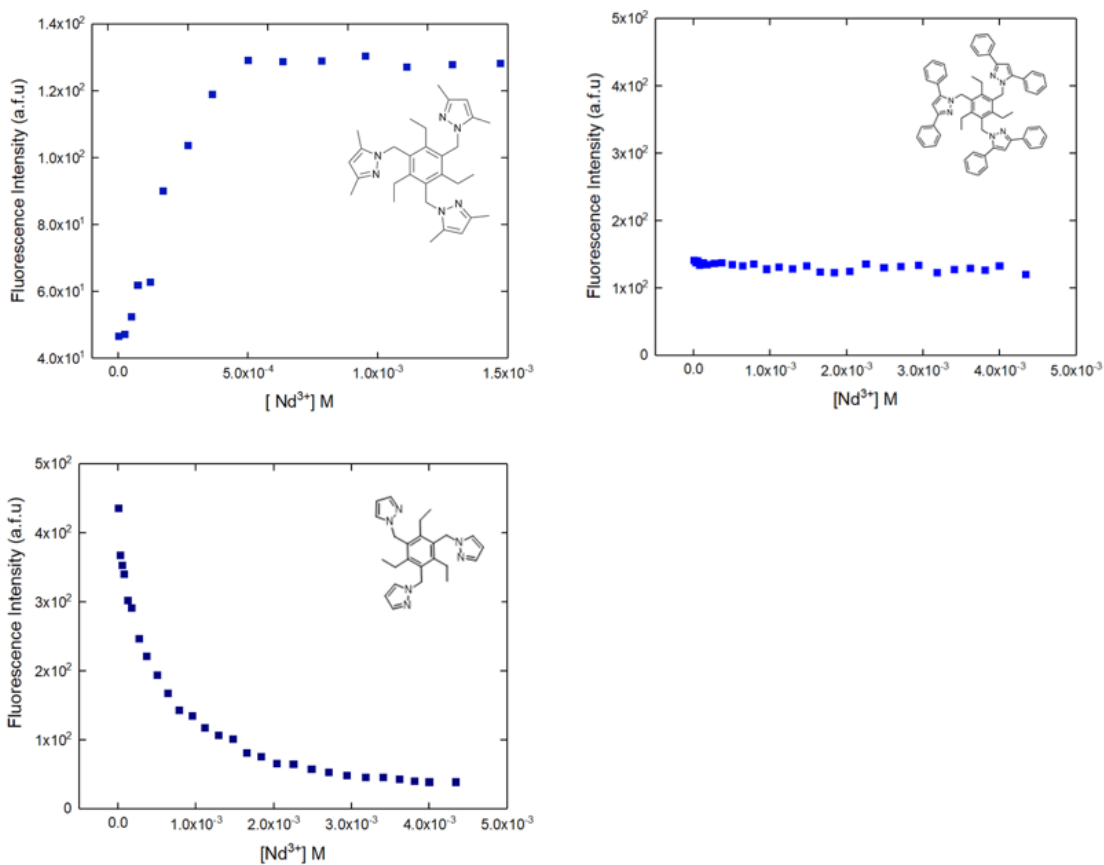


Figure 4.3. Fluorescence titrations of **1**, **2** and **3** (1.0×10^{-4} M) with $\text{Nd}(\text{NO}_3)_3$ in CH_3CN .

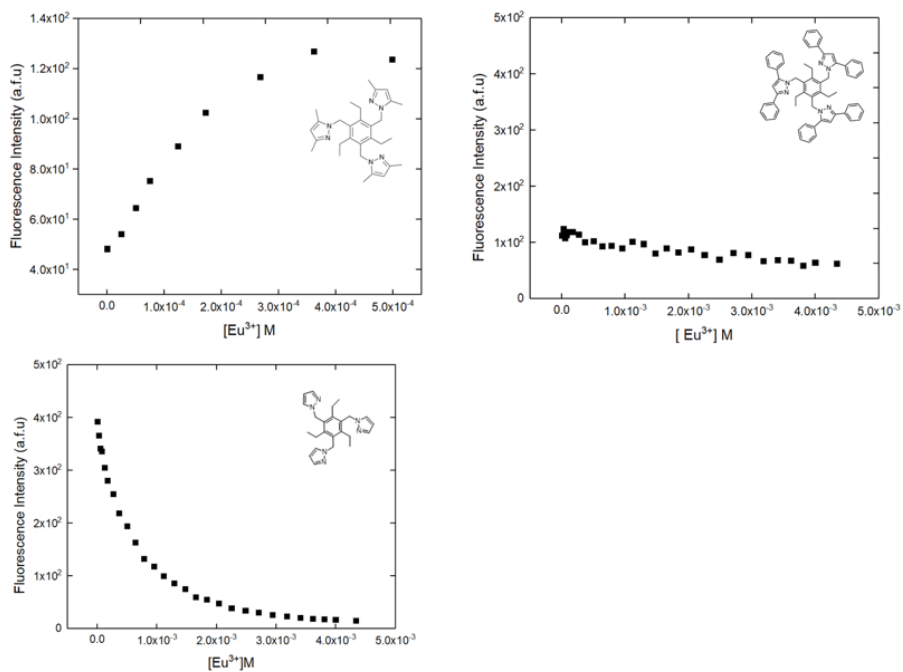


Figure 4.4. Fluorescence titrations of **1**, **2** and **3** (1.0×10^{-4} M) with $\text{Eu}(\text{NO}_3)_3$ in CH_3CN .

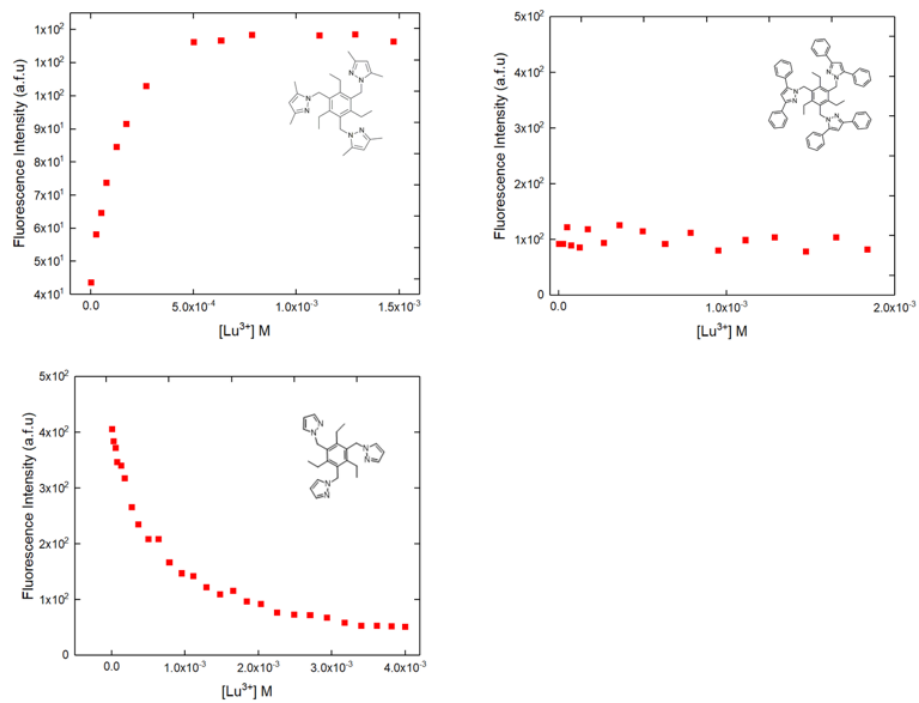


Figure 4.5. Fluorescence titrations of **1**, **2** and **3** (1.0×10^{-4} M) with $\text{Lu}(\text{NO}_3)_3$ in CH_3CN .

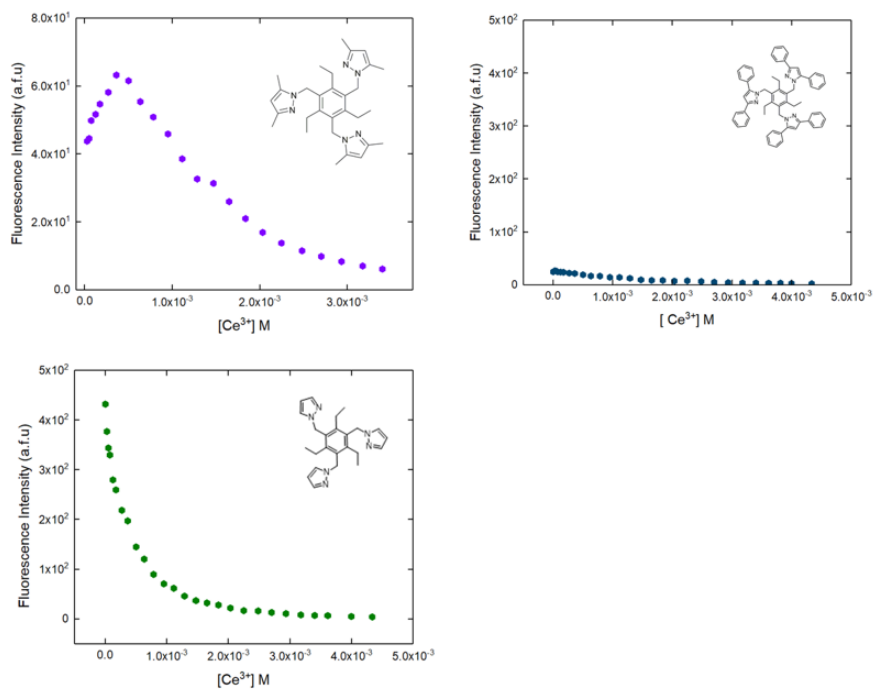


Figure 4.6. Fluorescence titrations of **1**, **2** and **3** (1.0×10^{-4} M) with $\text{Ce}(\text{NO}_3)_3$ in CH_3CN .

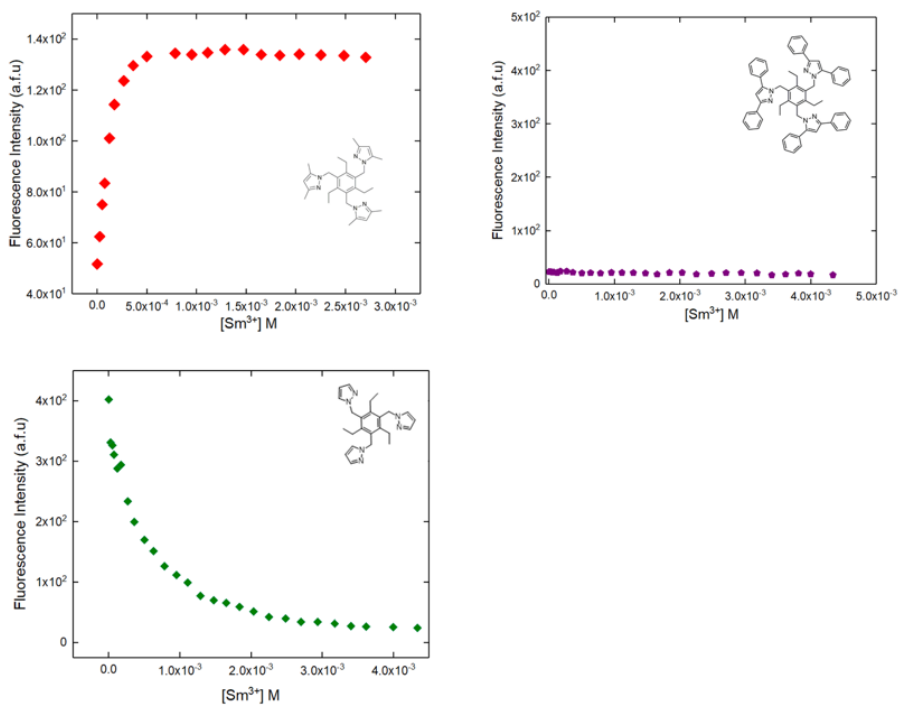


Figure 4.7. Fluorescence titrations of **1**, **2** and **3** (1.0×10^{-4} M) with $\text{Sm}(\text{NO}_3)_3$ in CH_3CN .

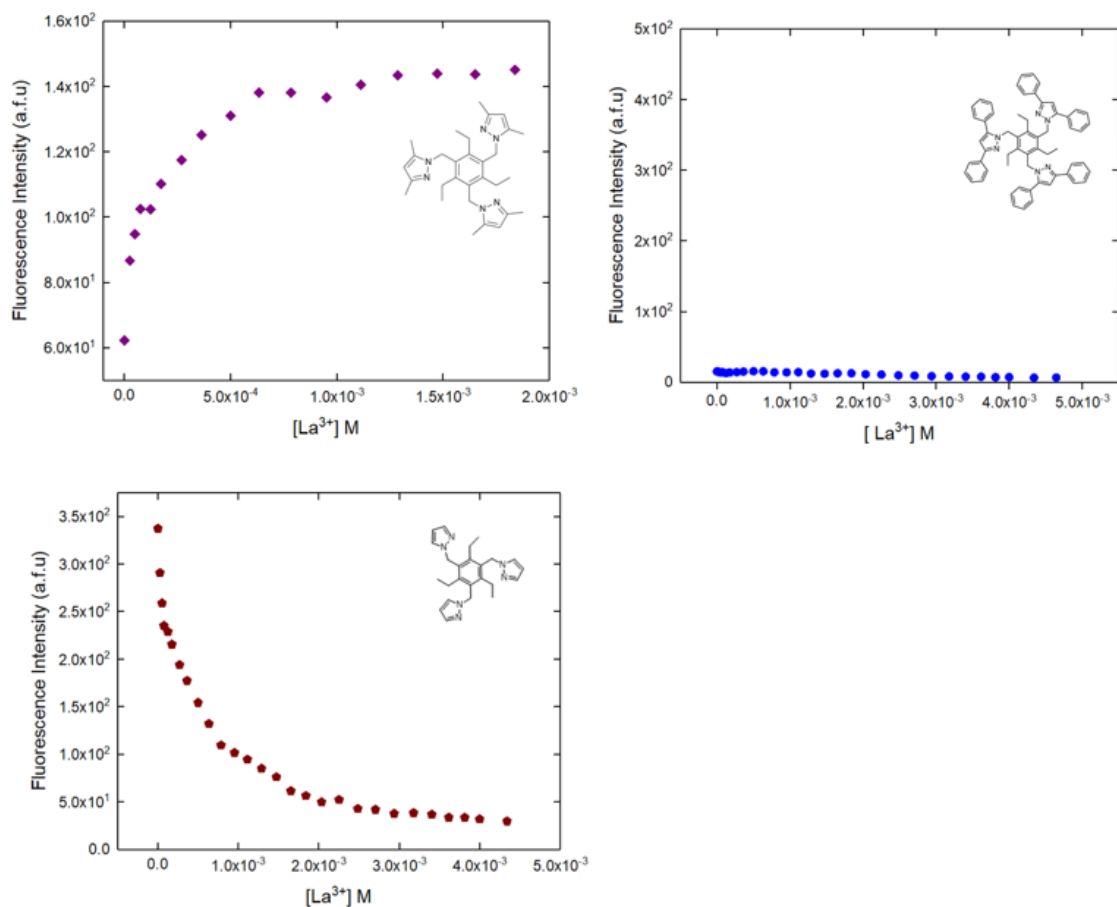


Figure 4.8. Fluorescence titrations of **1**, **2** and **3** (1.0×10^{-4} M) with $\text{La}(\text{NO}_3)_3$ in CH_3CN .

The observed fluorescence enhancements were fitted to the Benesi-Hildebrand equation:

$$I_0/I - I_0 = b/(a - b)[1/K[M] + 1] \text{ -----eq. 4.1}$$

where I_0 is the fluorescence intensity of the sensor in the absence of guest $\text{Ln}(\text{III})$; I is the fluorescence intensity of the sensor in the presence of guest; $[M]$ is the concentration of the substrates; and K is the association constant between the sensor and the substrates. In the equation, a and b are constants. The value of $b/(a-b)$ is the intercept of the plot of $I_0/(I-I_0)$

against the inverse of the concentration term, M^{-1} . I_0 and I are found out experimentally. The association constant of **1** with La^{3+} was $2.5 \times 10^4 M^{-1}$, and for **1** with Sm^{3+} was $2020 M^{-1}$ (Figure 4.9 & 4.10) as derived from the Benesi-Hildebrand equation.

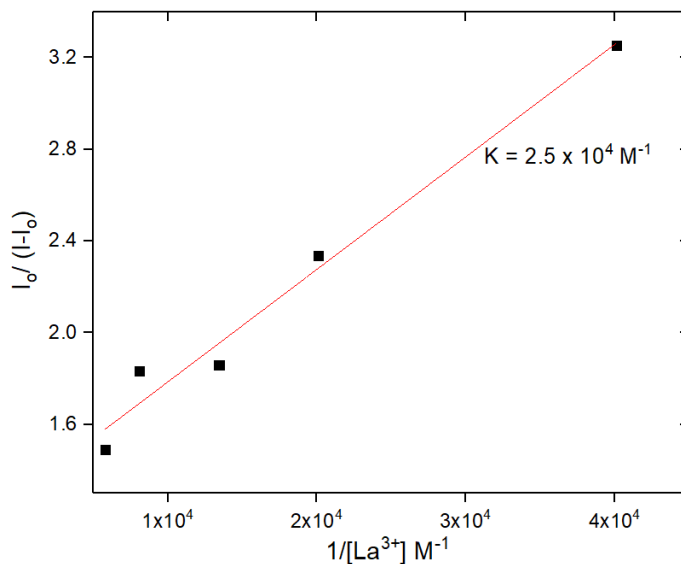


Figure 4.9. Benesi-Hildebrand plot of receptor **1** in acetonitrile in the presence of La^{3+} .

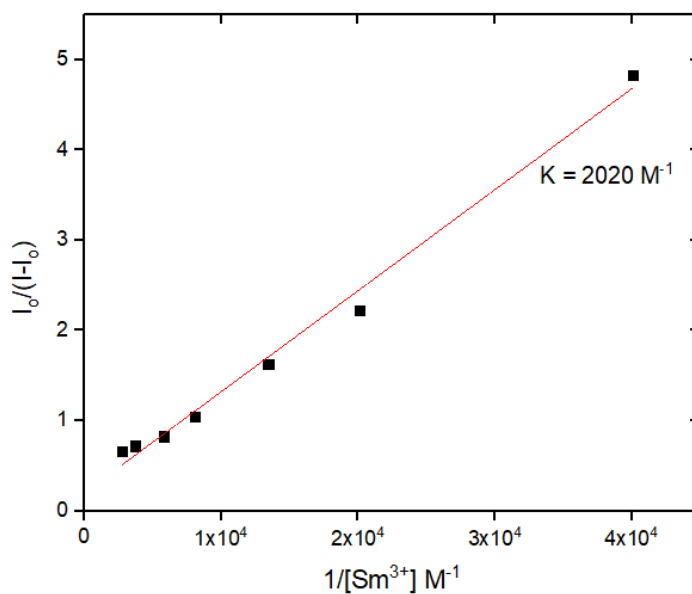


Figure 4.10. Benesi-Hildebrand plot of receptor **1** in acetonitrile in the presence of Sm^{3+} .

The observed fluorescence quenching upon titration of unsubstituted pyrazole receptor **3** with Ln(III) was fitted to the Stern-Volmer equation (eq. 4.2) where, the quencher concentration is [Q], the Stern-Volmer constant is K_{sv} , I_0 is the measured fluorescence intensity without quencher present, and I is the measured fluorescence intensity with [Q] present.

$$I_0/I = 1 + K_{sv}[Q] \dots\dots\dots \text{Eq. 4.2}$$

At lower concentrations of Ln(III), a plot of I_0/I vs [Ln] is linear, and the Stern-Volmer constant (K_{sv}) for fluorescence quenching is 1900 M^{-1} for Sm^{3+} , 4000 M^{-1} for Ce^{3+} , 2400 M^{-1} for La^{3+} , 2600 M^{-1} , for Nd^{3+} and 1500 M^{-1} for Lu^{3+} . The Stern-Volmer constant K_{sv} showed that **3** binds stronger to Ce^{3+} compared to the other Ln(III) ions studied. The Stern-Volmer plot for **3** with Sm^{3+} , Lu^{3+} , and Nd^{3+} are shown in Figures 4.11-4.13. From the fluorescence titration results, we can conclude that **1** and **3** can be utilized as sensors for Ln(III) ions while **2** does not show any appreciable trend in fluorescence to conclude that it binds Ln(III). These results are consistent with the conclusions on the effects of pyrazole substitution to solvation and ion pairing, from our NH_4^+ complexation study (Chapter 2).

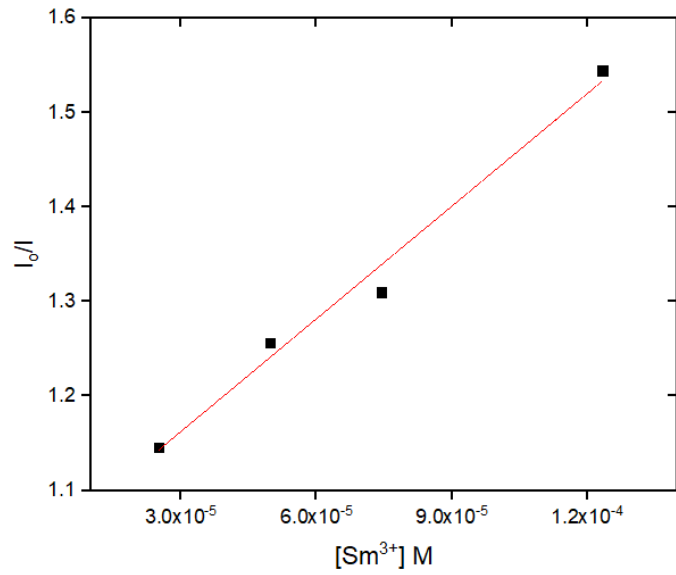


Figure 4.11. Stern-Volmer plot of **3** (1.0×10^{-4} M) with low concentration of $\text{Sm}(\text{NO}_3)_3$ in CH_3CN .

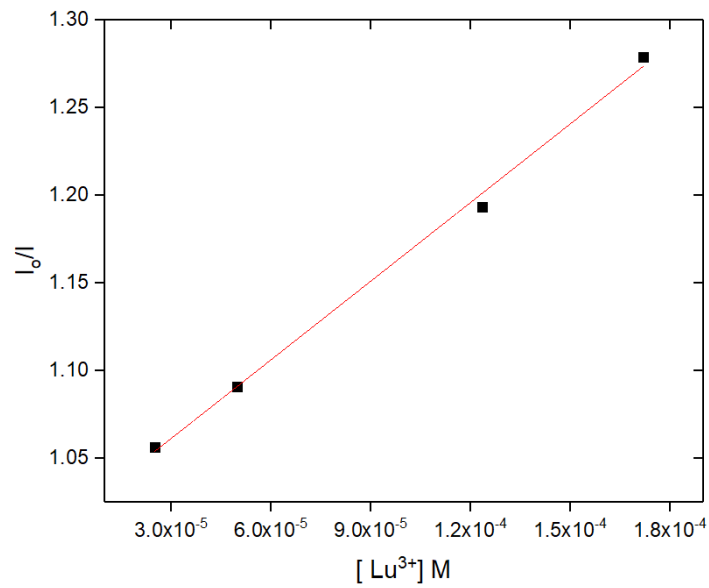


Figure 4.12. Stern- Volmer plot of **3** (1.0×10^{-4} M) with low concentration of $\text{Lu}(\text{NO}_3)_3$ in CH_3CN .

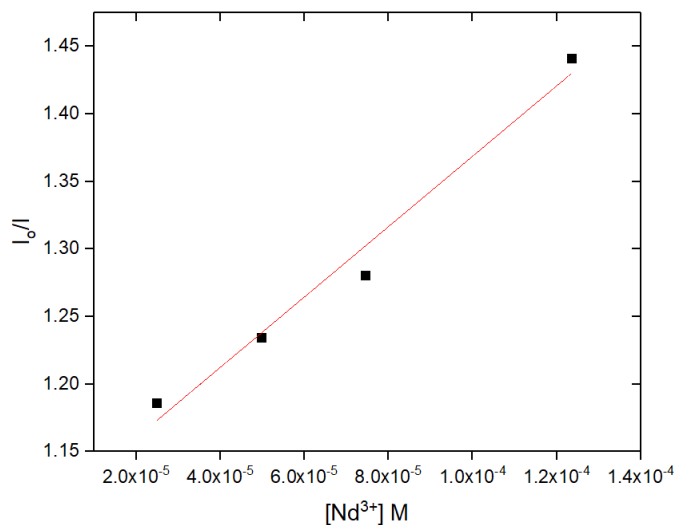


Figure 4.13. Stern-Volmer plot of **3** (1.0×10^{-4} M) with low concentration of $\text{Nd}(\text{NO}_3)_3$ in CH_3CN .

The cation binding properties of **1-3** with $\text{La}(\text{NO}_3)_3$ were determined in acetone- d_6 for **1** and **2**, and $\text{CD}_3\text{CN}-d_3$ for **3** by $^1\text{H-NMR}$ titrations with M^+NO_3^- ($\text{M}^+ = \text{La}^{3+}$). The association constants for the formation of a 1:1 complex, K_a , were determined by non-linear regression analysis using the 1:1 binding isotherm (Eq. 4.3):

$$\Delta\delta = \delta_{\text{obs}} - \delta_2 = ([\mathbf{R}]_t + [\text{X}^-]_t + K_a^{-1} - ((([\mathbf{R}]_t + [\text{X}^-]_t + K_a^{-1})^2 - 4[\text{X}^-]_t [\mathbf{R}]_t)^{1/2})) \Delta\delta_{\text{max}} / (2[\mathbf{R}]_t) \quad \text{eqn. 4.3}$$

For **1**, downfield shifts of all the pyrazolyl proton resonances were observed upon cation addition. The CH_2 protons of the ethyl showed slight upfield shifts, instead. Non-linear regression analysis of the binding isotherms obtained from the downfield chemical shift changes for the C–H, resonances gave a 1:1 association constant K_a of 155 M^{-1} for the formation of **1**· $[\text{La}^{3+}]$ (Figure 4.14).

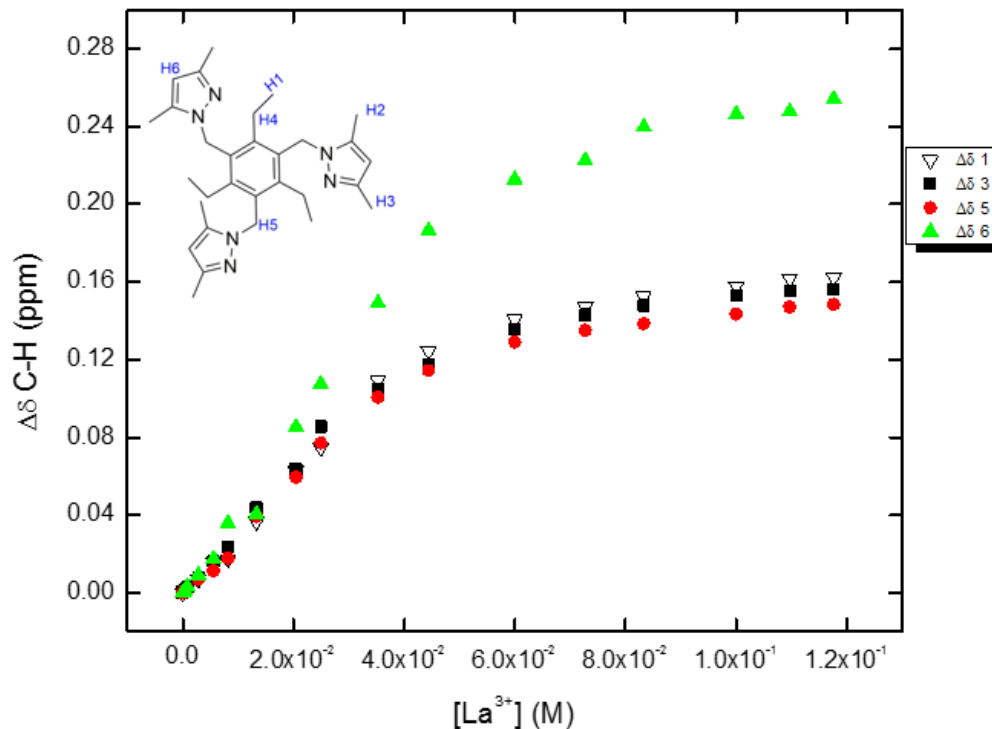


Figure 4.14. $^1\text{H-NMR}$ titration plot of **1** with $\text{La}(\text{NO}_3)_3 \cdot 6\text{H}_2\text{O}$ in acetone- d_6 . The concentration of **1** was kept constant at 2 mM.

In the case of the diphenyl substituted pyrazole **2**, downfield shift of the proton was observed when titrated with $\text{La}(\text{NO}_3)_3 \cdot 6\text{H}_2\text{O}$. However, the spectrum did not show appreciable shifts large enough to determine the association constant K_a . For **3**, the CH_2 protons of the ethyl group shift upfield upon addition of $\text{La}(\text{NO}_3)_3 \cdot 6\text{H}_2\text{O}$ while two of the protons (H_5 and H_6) on the pyrazolyl ring both moved downfield and the third (H_4) moved upfield (Figure 4.15).

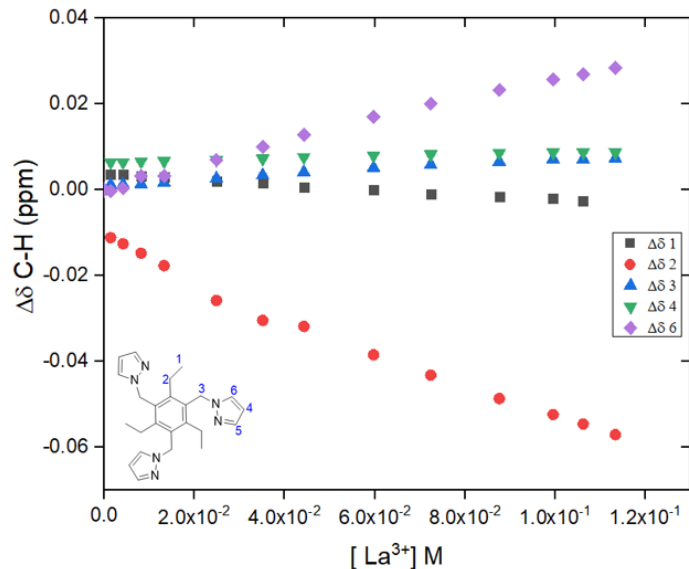


Figure 4.15. ¹H-NMR titration plot of **3** with La(NO₃)₃·6H₂O in acetonitrile-d₃. The concentration of **3** was kept constant at 2 mM.

4.4 Conclusion

In conclusion, selective ammonium binding and fluorescence sensing by tripodal pyrazolyl receptors was demonstrated. Fluorescence and ¹H-NMR provide evidence of Ln(III) binding, with differences on pyrazole substitution greatly affecting binding and fluorescence effects. This is consistent with the NH₄⁺ binding study (Chapter 2), where the role of ion-pairing plays a major role in the binding affinities. Theoretical DFT calculations and structural and spectroscopic investigations are expected to provide comparisons with An(III) binding and further understanding of observed selectivities.

4.5 Experimental

4.5.1 Materials and methods

All commercial reagents and solvents were purchased from Fisher Scientific or Sigma Aldrich and were used without further purification. 1,3,5-Tris(bromomethyl)benzene was

either purchased from Sigma Aldrich or synthesized according to published literature procedures. $^1\text{H-NMR}$ spectra were recorded on a 400 MHz Bruker NMR spectrometer and were referenced using the residual solvent resonances. All chemical shifts, δ , are reported in ppm. Fluorescence spectra were recorded on an Agilent technologies Cary Eclipse fluorimeter.

4.5.2 $^1\text{H-NMR}$ Titrations

The association constants for the formation of cation-receptor complexes were determined by titration of solutions of 2.0×10^{-3} M of **1** or **2** in acetone- d_6 (or acetonitrile- d_3 for **3**) (solution A) with 0.2 M of $\text{La}(\text{NO}_3)_3 \cdot 6\text{H}_2\text{O}$ (solution B). Solution B was prepared by dilutions with solution A, thus keeping a constant concentration of **1** or **2** upon titration of solution A with solution B. In a typical experiment, solution A (0.700 mL for La^{3+}) was placed in an NMR tube. Solution B was added in increments until a total of 950 μL was added. The changes of chemical shifts were monitored, with the results plotted and fitted to the 1:1 binding isotherm (Eq. 1), using non-linear regression analysis.

4.5.3 Fluorescence Titration of **1**, **2** or **3** with $\text{Ln}(\text{NO}_3)_3 \cdot 6\text{H}_2\text{O}$

Fluorescence emissions were measured using an excitation wavelength of 272 nm for receptor **1**, 262 nm for receptor **2**, or 230 nm for receptor **3**, a measurement increment of 0.5 nm, and integration time of 0.1 s, excitation slit width of 10 nm, emission slit width of 5 nm. Experiments were run using receptor solutions of R (R = **1**, **2**, **3**, 1.0×10^{-4} M) in CH_3CN (solution A), which were titrated with solutions of $\text{Ln}(\text{NO}_3)_3 \cdot 6\text{H}_2\text{O}$ (Ln = La^{3+} , Nd^{3+} , Lu^{3+} , Ce^{3+} , Eu^{3+} and Sm^{3+} , 1.0×10^{-2} M) and R (R = **1**, **2**, **3**) (1.0×10^{-4} M) in CH_3CN (solution B). 2000 μL of solution A was added to the fluorescence cuvette and solution B

was added in increments until a total of 1000 μL was added. The fluorescence intensity at emission maxima was monitored.

4.6. References

- (1) Hudson, M. J.; Harwood, L. M.; Laventine, D. M.; Lewis, F. W. Use of Soft Heterocyclic N-Donor Ligands To Separate Actinides and Lanthanides. *Inorg. Chem.* **2013**, *52*, 3414-3428.
- (2) Bhattacharyya, A.; Mohapatra P. K.; Manchanda, V. K. Separation of Americium(III) and Europium(III) from Nitrate Medium Using a Binary Mixture of Cyanex-301 with N-donor Ligands. *Solvent Extr. Ion Exch.* **2006**, *24*, 1-17.
- (3) Salvatores, M.; Palmiotti, G. Radioactive Waste Partitioning and Transmutation within Advanced Fuel Cycles: Achievements and Challenges. *Prog. Part. Nucl. Phys.* **2011**, *66*, 144-166.
- (4) Panak, P. J.; Geist, A. Complexation and Extraction of Trivalent Actinides and Lanthanides by Triazinylpyridine N-Donor Ligands. *Chem. Rev.* **2013**, *113*, 1199-1236.
- (5) Demir, S.; Brune, N. K.; Van Humbeck, J. F.; Mason, J. A.; Plakhova, T. V.; Wang, S.; Tian, G.; Minasian, S. G.; Tyliczszak, T.; Yaita, T.; Kobayashi, T.; Kalmykov, S. N.; Shiwaku, H.; Shuh, D. K.; Long, J. R. Extraction of Lanthanide and Actinide Ions from Aqueous Mixtures Using a Carboxylic Acid-Functionalized Porous Aromatic Framework. *ACS Cent. Sci.* **2016**, *2*, 253-265.
- (6) Edwards, A. C.; Wagner, C.; Geist, A.; Burton, N. A.; Sharrad, C. A.; Adams, R. W.; Pritchard, R. G.; Panak, P. J.; Whitehead, R. C.; Harwood, L. M. Exploring Electronic Effects on the Partitioning of actinides(III) from lanthanides(III) Using Functionalised Bis-Triazinyl Phenanthroline Ligands. *Dalton Trans.* **2016**, *45*, 18102-18112.
- (7) Macerata, E.; Mossini, E.; Scaravaggi, S.; Mariani, M.; Mele, A.; Panzeri, W.; Boubals, N.; Berthon, L.; Charbonnel, M.-C.; Sansone, F.; Arduini, A.; Casnati, A. Hydrophilic Clicked 2,6-Bis-Triazolyl-Pyridines Endowed with High Actinide Selectivity and Radiochemical Stability: Toward a Closed Nuclear Fuel Cycle. *J. Am. Chem. Soc.* **2016**, *138*, 7232-7235.
- (8) Geist, A.; Müllich, U.; Magnusson, D.; Kaden, P.; Modolo, G.; Wilden, A.; Zevaco, T. Actinide(III)/Lanthanide(III) Separation Via Selective Aqueous Complexation of Actinides(III) Using a Hydrophilic 2,6-Bis(1,2,4-Triazin-3-Yl)-Pyridine in Nitric Acid. *Solvent Extr. Ion Exch.* **2012**, *30*, 433-444.

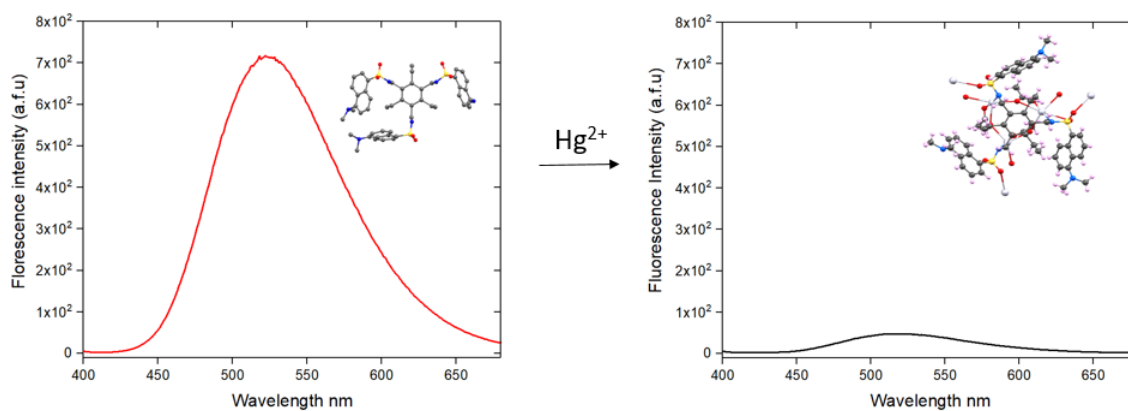
- (9) Zalupski, P. R.; Nash, K. L.; Martin, L. R. Thermodynamic Features of the Complexation of Neodymium(III) and Americium(III) by Lactate in Trifluoromethanesulfonate Media. *J. Solut. Chem.* **2010**, *39*, 1213-1229.
- (10) Güllü, F.; Bayrakçı, M.; Kursunlu, A. N.; Yiğiter, Ş.; Ertul, Ş. Synthesis and Trivalent Lanthanide Ion Complexation Studies of New Macrocyclic Receptors Based Lactam Ionophores. *J. Incl. Phenom. Macrocycl. Chem.* **2014**, *80*, 303-312.
- (11) Bekiari, V.; Judeinstein, P.; Lianos, P. A Sensitive Fluorescent Sensor of Lanthanide Ions. *J. Lumin.* **2003**, *104*, 13-15.
- (12) Aoki, S.; Kawatani, H.; Goto, T.; Kimura, E.; Shiro, M. A Double-Functionalized Cyclen with Carbamoyl and Dansyl Groups (Cyclen = 1,4,7,10-Tetraazacyclododecane): A Selective Fluorescent Probe for Y³⁺ and La³⁺. *J. Am. Chem. Soc.* **2001**, *123*, 1123-1132.
- (13) Ghosh, P.; Shukla, A. D.; Das, A. Cerium Ion-Induced Fluorescence Enhancement of a Tripodal Fluoroionophore. *Tetrahedron Lett.* **2002**, *43*, 7419-7422.
- (14) Wietzke, R.; Mazzanti, M. Strong Intramolecular [π]-[π] Interactions Favor the Formation of 2:1 (L:M) Lanthanide Complexes of tris(2-Benzimidazolylmethyl)amine. *Chem. Commun.* **1999**, 209-210.
- (15) Badr El Aroussi, B.E.; Dupont, N.; Bernardinelli, G.; Hamacek, J. Unsymmetrical Tripodal Ligand for Lanthanide Complexation: Structural, Thermodynamic, and Photophysical Studies. *Inorganic Chemistry.* **2010**, *49*, 606-615.
41. (16) Chin, J.; Walsdorff, C.; Stranix, B.; Oh, J.; Chung, H. J.; Park, S. M.; Kim, K. A Rational Approach to Selective Recognition of NH₄⁺ over K⁺. *Angew. Chemie - Int. Ed.* **1999**, *38*, 2756-2759.

CHAPTER V

Hg(II) complexation and sensing by a tris-dansylamide derivative of 1,3,5-Tris(2-aminomethyl) -2,4,6-triethylbenzene.

Tosin M. Jonah, Logesh Mathivathanan, Gabriel Flores, Raphael G. Raptis, Konstantinos Kavallieratos

Department of Chemistry and Biochemistry and the Biomolecular Sciences Institute,
Florida International University, 11200 SW 8th St, Miami, FL 33199, USA.



5.1 Abstract

A new tripodal fluorescent receptor **LH₃** based on dansyl fluorophore for Hg(II) was developed. The receptor showed selectivity towards Hg(II). The X-ray crystal structure obtained from the complex formed between **LH₃** and Hg(CH₃COO)₂ shows that one molecule of **LH₃** binds three molecules of Hg²⁺, while the analogous structure obtained for **LH₃** and HgCl₂ revealed that just one of the sulfonamide groups in **LH₃** is deprotonated and two molecules of **LH₃** bind to a single Hg(II).

5.2 Introduction

Over the last few decades, much research effort has been dedicated to the design and synthesis of selective Hg(II) receptors and sensors. This effort arises from the toxic nature of mercury to both the human health and the environment.^{1,2} Mercury is ranked among the priority metals that are of public health significance.³ These metallic elements are considered systemic toxicants that are known to induce multiple organ damage, even at lower levels of exposure. The pollution has been shown to originate from both natural and anthropogenic sources. Minamata diseases⁴ and prenatal brain damage are some of the hazardous effects that arise from mercury exposure in humans.⁵⁻⁹

In recent years, numerous methods have been employed in the detection of Hg(II), including colorimetric sensing techniques, atomic absorption, X-ray fluorescence spectroscopy and electrochemical sensing. The use of colorimetric and fluorescence sensors for Hg(II) detection stems from the low cost, operational simplicity and high selectivity. An example is the highly selective and sensitive colorimetric method based on gold nanoparticles that utilizes gold amalgamation and grown Au nanoparticles for rapid

Hg(II) detection.¹⁰⁻¹³ Moreover, a number of fluorescence chemosensors have been reported in the literature for Hg(II) detection. Che et al. reported a fluorescent 5-bromoindole-3-carboxaldehyde ethylthiosemicarbazone receptor that can detect and remove Hg(II) from water by extraction.¹⁴ This ligand coordinates directly to Hg(II) through its N and S atoms. It also showed good selectivity towards Hg(II), with a detection limit of 1.31×10^{-7} M. Compounds containing the rhodamine fluorophore¹⁵⁻¹⁹ have found many uses due to their emissive performance²⁰ and emission turn-on effect, which is caused by Hg(II) ions. The dansylamide fluorophore has also found uses as fluorescent probe because it possesses high fluorescence quantum yield and large Stokes shifts. A few dansyl-based receptors have been reported for Hg(II) detection.²¹⁻²⁵

In this work, we combined the optical properties of dansyl fluorophore and its N-donor atoms in the synthesis of a tripodal receptor **LH₃**, based on the same successful 1,3,5-triethylbenzene framework used for the NH₄⁺ and Ln(III) sensing work (Chapters 2-4), by incorporating three dansyl groups that can bind to Hg(II) when deprotonated, while maintaining the fluorescence sensing capacity of the dansyl group. The dansylated receptor **LH₃** can be synthesized in good yields, in only a few synthetic steps (Chapter 3).

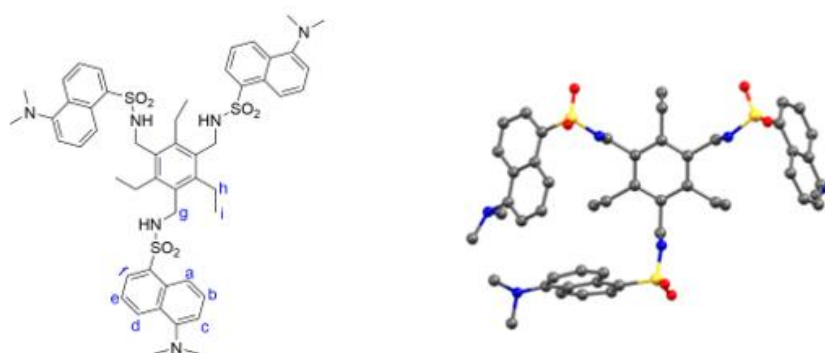


Figure 5.1. Chemical and crystal structures of receptor **LH₃**.

5.3 Results and Discussion

Compound **LH₃** was prepared as previously reported (Chapter 3) by adding a solution of 1,3,5-tris(aminomethyl)-2,4,6-triethylbenzene²⁶ and triethylamine in anhydrous 1,2-DCE to a stirring solution of dansyl chloride dissolved in 1,2-DCE. The mercury binding and sensing properties were investigated by ¹H-NMR and fluorescence spectroscopy. The fluorescence emission intensity of the free receptor **LH₃** and the changes in the emission intensity in the presence of the mercury (added as Hg(CH₃COO)₂ or HgCl₂) are shown in figure 5.2 and 5.3. Fluorescence titrations of **LH₃** with Hg(CH₃COO)₂ and HgCl₂ at constant receptor concentration of 1 μM were carried out in CH₃OH (λ_{exc} = 350 nm). The fluorescence titration results showed that the fluorescence emission intensity at 522 nm decreased with the addition of Hg(II) without any considerable shift in the emission maximum. By the time the titration was finished, the fluorescence intensity of **LH₃** was almost completely quenched by the addition of Hg (CH₃COO)₂. Fluorescence quenching is measured quantitatively with the Stern-Volmer equation (eqn. 5.1) where, the quencher concentration is [Q], the Stern-Volmer constant is K_{sv}, I₀ is the measured fluorescence intensity without quencher present, and I is the measured fluorescence intensity with [Q] present.

$$I_0/I = 1 + K_{sv}[Q] \dots \dots \dots \text{eqn. 5.1}$$

At lower concentrations of Hg(II), a plot of I₀/I vs [Hg(II)] is linear, (figure 5.4) and the slope obtained gives the Stern-Volmer constants (K_{sv}) as 4.3 x 10⁴ and 2.3 x 10⁵ M⁻¹ for **LH₃** with Hg(CH₃COO)₂ and HgCl₂, respectively.

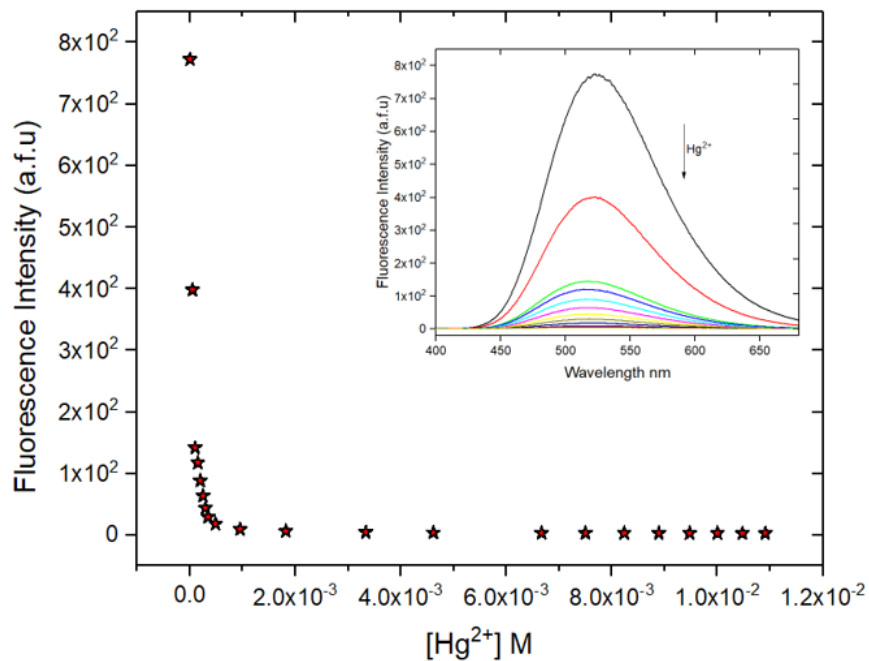


Figure 5.2. Fluorescence titration of LH_3 (1.0×10^{-6} M) with $\text{Hg}(\text{CH}_3\text{COO})_2$ in methanol.

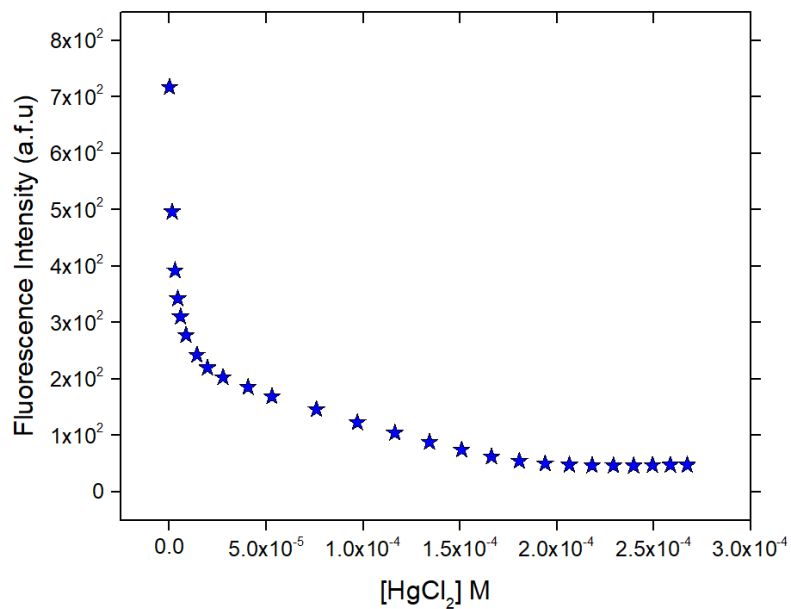


Figure 5.3. Fluorescence titration of LH_3 (1.0×10^{-6} M) with HgCl_2 in methanol.

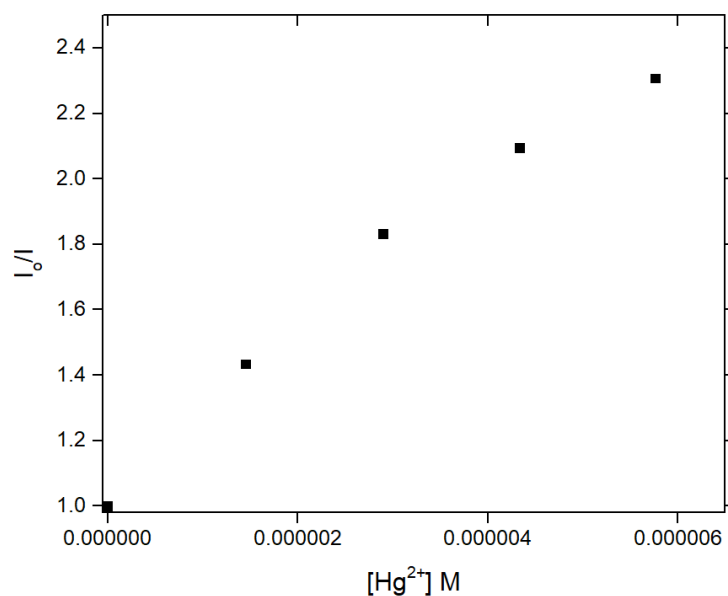


Figure 5.4. Stern- Volmer plot of **LH₃** (1.0×10^{-6} M) with low concentration of **HgCl₂** in methanol.

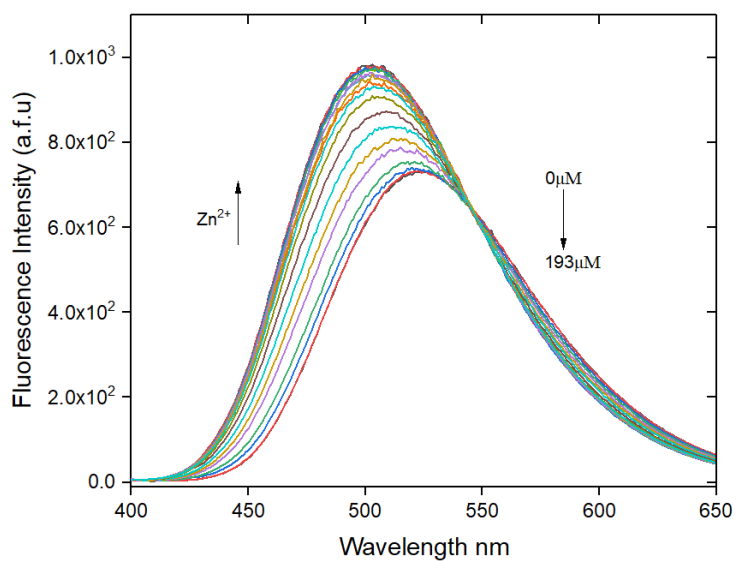


Figure 5.5 Fluorescence titration of **LH₃** (1.0×10^{-6} M) with **ZnCl₂** in **CH₃OH**.

Selectivity studies were also carried out on **LH₃** in methanol solution monitoring the changes in fluorescence emission intensity of **LH₃** with addition of other cations, such as

Ag^+ , Co^{2+} , Ca^{2+} , Cu^{2+} , Zn^{2+} and Cd^{2+} . The fluorescence emission of LH_3 with addition of these cations showed little to no change, except for Zn^{2+} which showed fluorescence enhancement. When Zn^{2+} was added to solution of LH_3 in methanol, the emission maximum at 522 nm was blue-shifted by 31 nm with an increase in the fluorescence intensity (figure 5.5). The fluorescence results showed that LH_3 is selective for Hg^{2+} (Figure 5.6) compared to the other cations used in the selectivity studies.

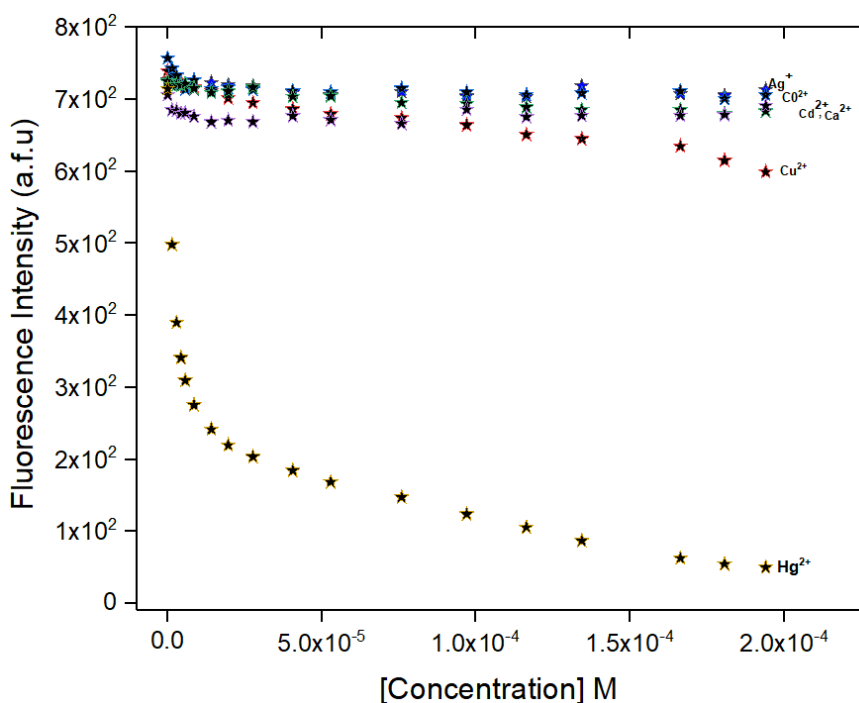


Figure 5.6. Fluorescence titration of LH_3 ($\lambda_{\text{exc}} = 350 \text{ nm}$, $1 \mu\text{M}$) with Hg^{2+} , Ag^+ , Co^{2+} , Ca^{2+} , Cu^{2+} and Cd^{2+} ($500 \mu\text{M}$) in CH_3OH .

Competitive experiments were also performed in order to determine the sensing performance of LH_3 for $\text{Hg}(\text{II})$ in the presence of competing cations. The fluorescence changes for formation of the complex of LH_3 with $\text{Hg}(\text{II})$ were systematically examined in the presence of excess concentration of competing cations, such as Ag^+ , Ca^{2+} , and Co^{2+} . From the titration results, the fluorescence quenching observed was substantial in the

presence of Ca(II) and even a mix of several competing cations, yet smaller than when LH_3 was titrated with HgCl_2 in the absence of those ions (Figure 5.7). It can be inferred from the results that the cations used in the competitive studies interact with LH_3 , but weaker than Hg, and that LH_3 can still be utilized as a receptor for Hg(II) even in the presence of higher backgrounds background Ag^+ , Co^{2+} and Ca^{2+} .

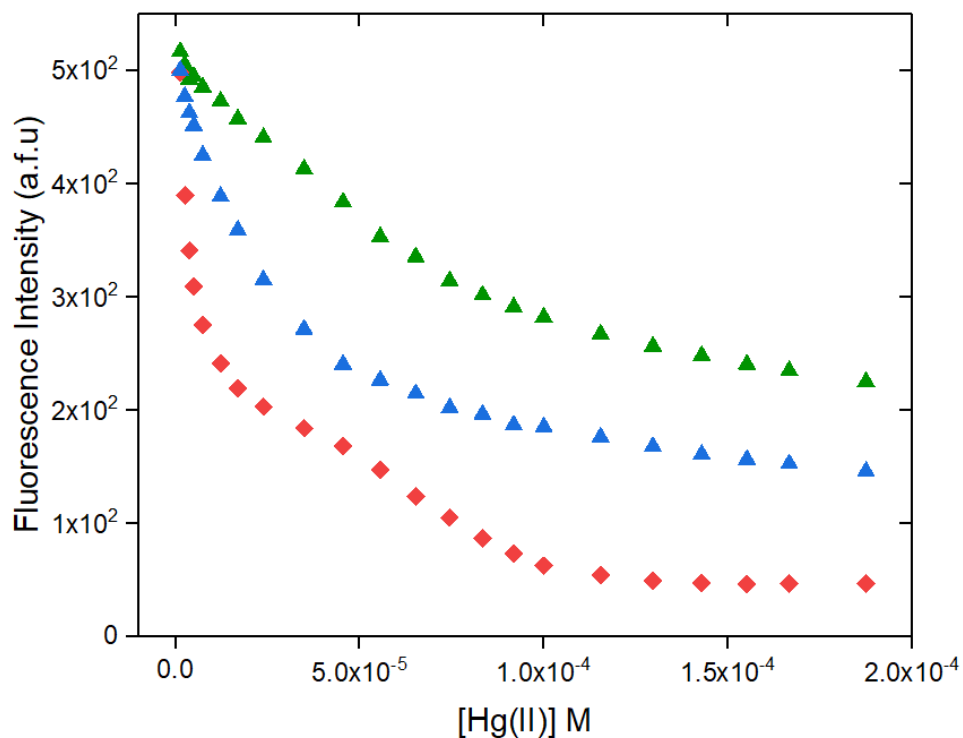


Figure 5.7 Fluorescence titrations of LH_3 (1 μM) and Et_3N (3 μM) with Hg(II) in the presence of other cations in methanol ($\lambda_{\text{exc}} = 350 \text{ nm}$). The concentration of LH_3 was stable at all experiments (1 μM). Titration with Hg(II) in the absence of competing ions (red rhombus) in constant concentration of Ca(II) at 10 μM , (blue triangles), and in constant concentration (10 μM) each of Ag^+ , Co^{2+} , and Ca^{2+} (green triangles).

The Hg(II) binding properties of receptor LH_3 were determined in DMSO-d_6 by ^1H -NMR titration experiments of LH_3 (deprotonated with trimethylamine) with HgCl_2 . Hg(II) binds to LH_3 through the nitrogen atoms of the sulfonamide group, which was also evident

through the change in the chemical shifts of the naphthalene rings (downfield movements) present in LH_3 .

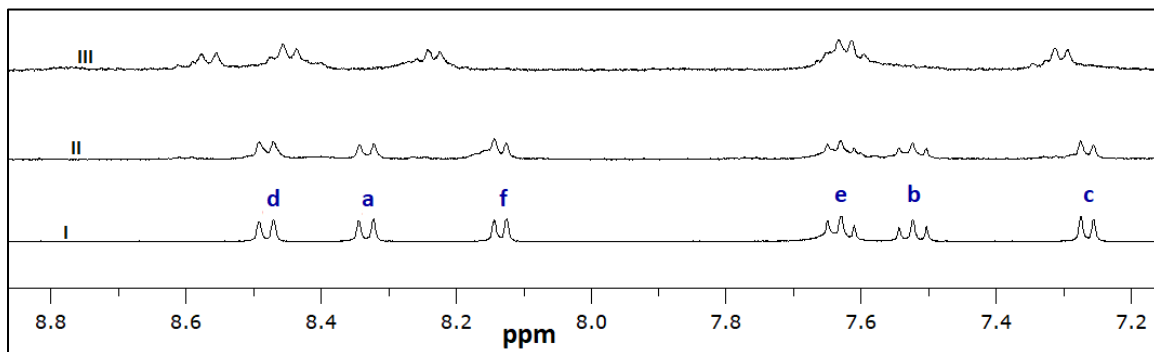


Figure 5.8: ^1H -NMR titration experiments of LH_3 with HgCl_2 (deprotonated with 3 equivalents of triethylamine) in DMSO-d_6 . (i) LH_3 ; (ii) LH_3 with 1 equivalent of Hg(II) ; (iii) LH_3 with 18 equivalent of Hg(II)

Crystals suitable for X-ray structural analysis for $\text{Hg}_3(\text{L})(\text{CH}_3\text{COO})_3$ were obtained by slow evaporation of solutions of LH_3 and $\text{Hg}(\text{CH}_3\text{COO})_2$ in methanol/acetone solution (1:1 mol ratio). Crystals suitable for X-ray structural analysis for $[\text{Hg}(\text{L.H}_2)_2(\text{H}_2\text{O})]$ was obtained from the slow evaporation of solutions of LH_3 , HgCl_2 , and trimethylamine.

Compound $\text{Hg}_3(\text{L})(\text{CH}_3\text{COO})_3$ crystallizes in a triclinic space group, with the whole molecule present in the asymmetric unit. The crystallographic data is presented in Table 1. The ligand LH_3 has three secondary amine nitrogen atoms that on deprotonation bind a $[\text{Hg}(\text{OAc})]^-$ unit each. Hg^{2+} ions are present in a nearly linear geometry (are $176.9(4)^\circ$, $176.3(4)^\circ$ and $175.4(3)^\circ$) and $\text{Hg}-\text{N}$ distances: 2.037(9), 2.049(10) and 2.042(10) Å, and $\text{Hg}-\text{O}$ distances: 2.064(8), 2.049(10) and 2.061(9) Å. All three Hg -ions have weak interactions with acetate ions bound to adjacent Hg -atoms ($\text{Hg}-\text{O}$ distances larger than 2.5 Å). One of the Hg ions also has a weak interaction with a solvent methanol present in the crystal structure. The Hg atoms in a triangular arrangement are quite far from each

other, at 4.8752(7), 5.1186(7) and 5.0750(7) Å. However, the weak interactions with acetate O-atoms form an interesting chair-like structure as shown in the figure 5.9 below.

Compounds containing the dansyl fluorophore have been extensively studied as sensors for various metal ions. However, only 31 hits were obtained for a dansylamide-M query in CSD (as of Sep 5, 2017, where M is any metal), and only one Hg-compound. This is the first time a tripodal ligand has been used to bind three Hg-atoms at once.

The compound with the molecular formula, [Hg(L.H₂)₂(H₂O)] crystallizes in the monoclinic C2/c space group with one half of the molecule in the asymmetric unit (Figure 5.11). One of the three sulfonamide protons from each treb ligand is bound to the Hg cation forming a linear N-Hg-N arrangement (N—Hg 2.366(1) Å, ∠NHgN 174.0(1)°). A water molecule coordinates to Hg (O—Hg 2.6579(2) Å), forming a T-shaped coordination geometry around mercury. The coordinated water molecule is disordered around a two-fold axis and was refined with PARTS. The ethyl groups on the phenyl ring of treb face the direction opposite to the Hg cation, enabling a weak Hg-π interaction (3.576(2) Å). The oxygen atoms from the sulfonamide groups involve in weak H-bonding interactions. One of the naphthyl rings from a dansyl group shows an intermolecular π-π-stacking interaction (centroid-centroid distance 3.861 Å) (Figure 5.12).

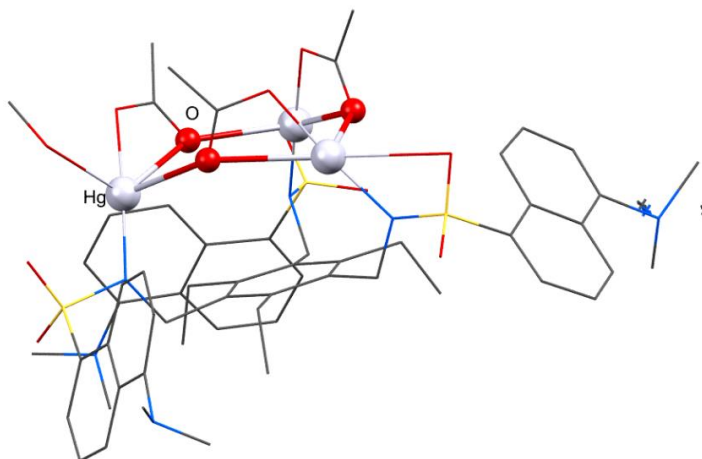


Figure 5.9. X-ray crystal structure of $\text{Hg}_3(\text{L})(\text{CH}_3\text{COO})_3$ highlighting the chair conformation of the Hg_3O_3 unit.

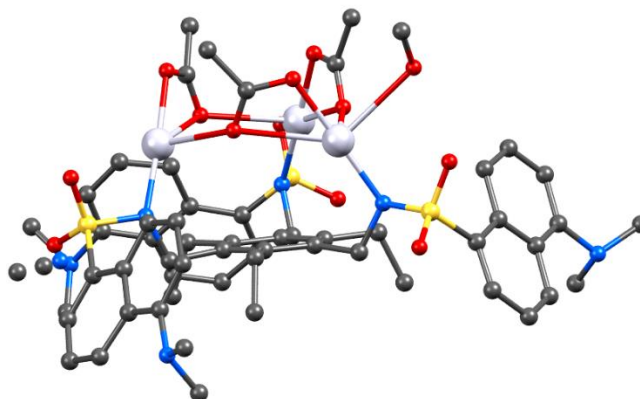


Figure 5.10. X-ray crystal structure of $\text{Hg}_3(\text{L})(\text{CH}_3\text{COO})_3$. Hydrogen atoms are not shown for clarity. Color coding: silver, Hg; red, O; yellow, S; blue, N; dark gray, C

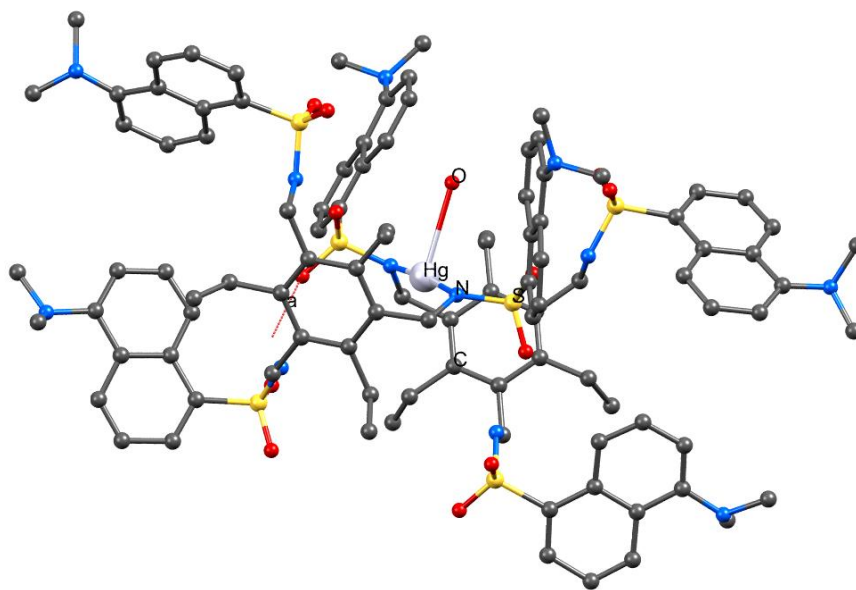


Figure 5.11. X-ray crystal structure of [Hg(L.H₂)₂(H₂O)], Hydrogen atoms are not shown for clarity. Color coding: silver, Hg; red, O; yellow, S; blue, N; dark gray, C

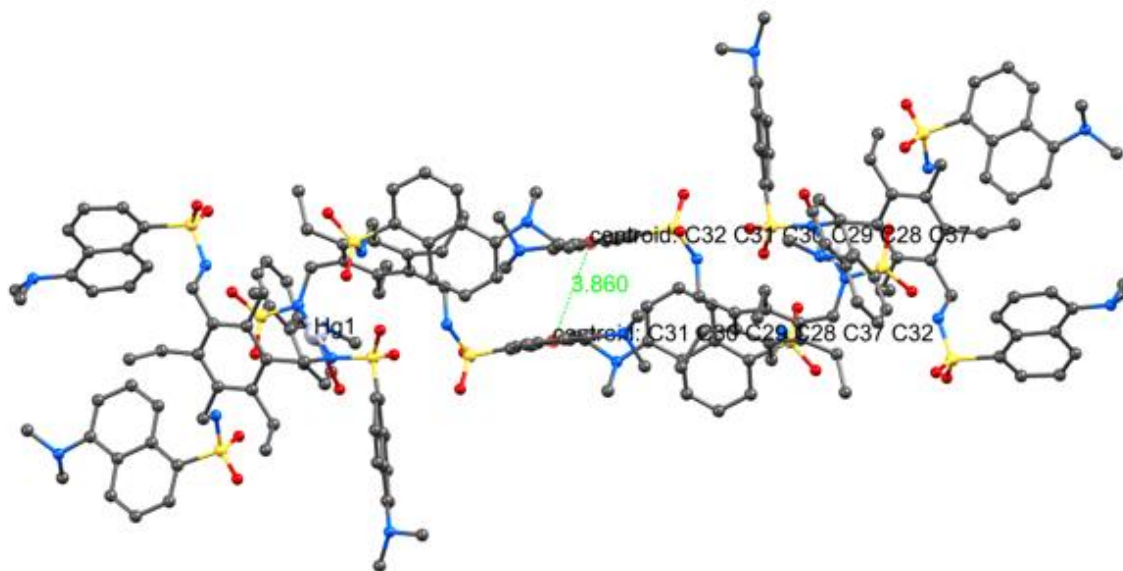


Figure 5.12. Ball and stick representation showing intermolecular π - π interaction between two centroids.

FT-IR spectroscopy was performed on the both the receptor **LH₃** (Figure 5.13) and the crystals of complex derived from **LH₃** with HgCl₂ (Figure 5.15) or **LH₃** with Hg(CH₃COO)₂ (Figure 5.14). The FT-IR spectrum of **1** shows the N-H peak at 3272 cm⁻¹. Upon complexation with mercury in Hg(II), the NH stretch at 3272 cm⁻¹ has disappeared indicating that the sulfonamide ligand is deprotonated in the **L.Hg(II)** complex. Another noticeable difference in the structures is the shift of the symmetric stretch of sulfonyl bands from 1142 cm⁻¹ in the IR spectrum of **LH₃** to a lower frequency 1125cm⁻¹ in the Hg₃(**L**)(CH₃COO)₃ complex. In the crystal structure of the complex derived from **LH₃** with HgCl₂, the sulfonyl band at 1142 cm⁻¹ is now split into two bands appearing at 1163 cm⁻¹ and 1127 cm⁻¹. This shift indicates that the sulfonamide groups of **LH₃** are involved in coordination with Hg(II). Figure 5.16 shows an overlay between **LH₃** and the [Hg(**LH₂)₂(H₂O)] complex formed between **LH₃** and HgCl₂.**

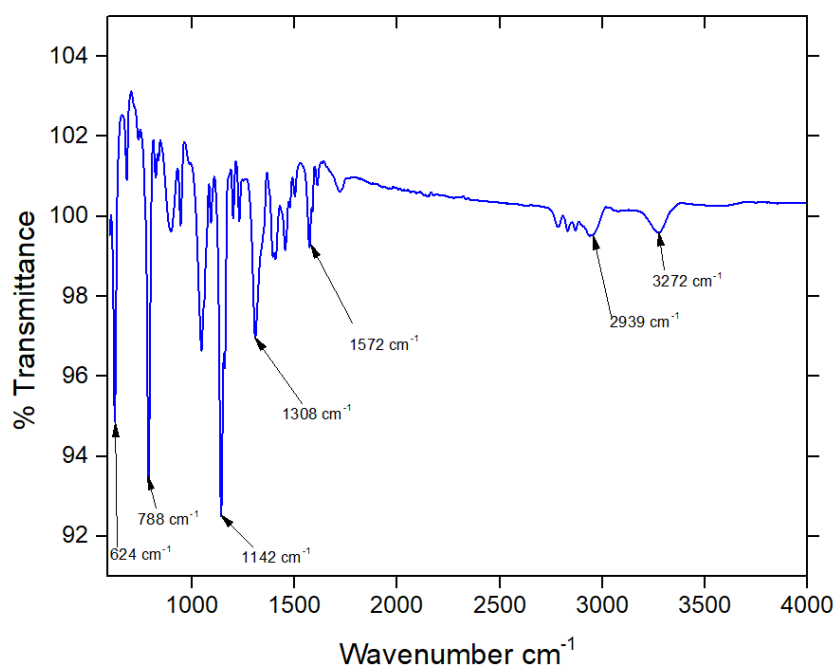


Figure 5.13. FT-IR spectrum of **LH₃**

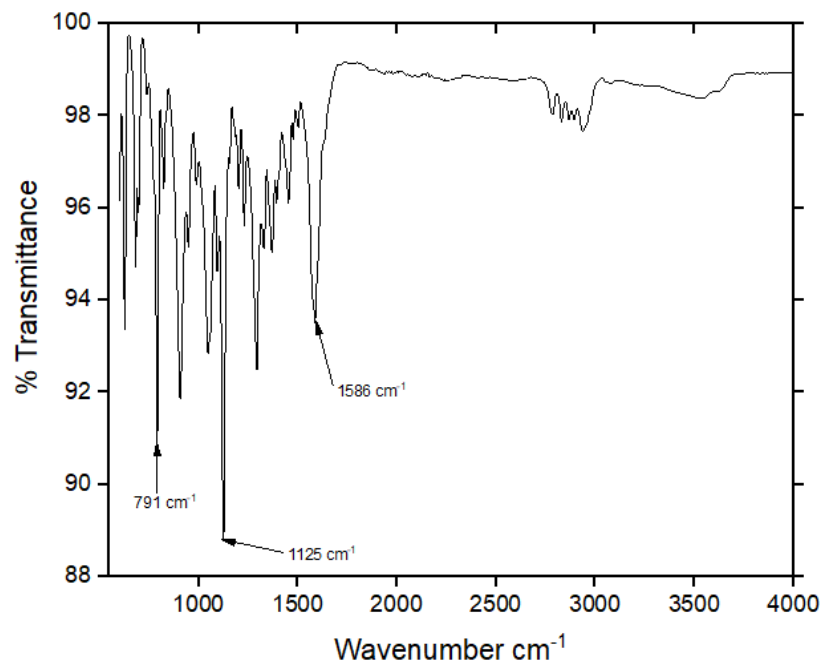


Figure 5.14. FT-IR spectrum of crystals of $\text{Hg}_3(\text{L})(\text{CH}_3\text{COO})_3$.

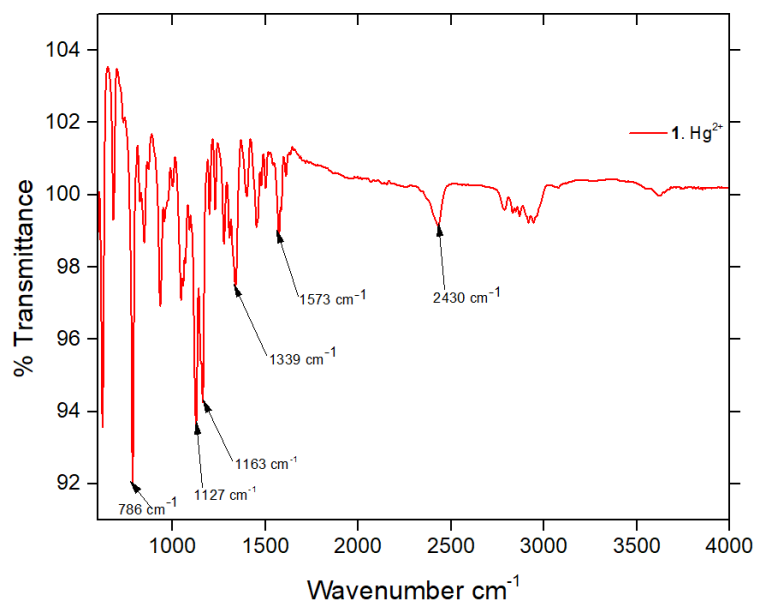


Figure 5.15. FT-IR spectrum of crystals of $[\text{Hg}(\text{L.H}_2)_2(\text{H}_2\text{O})]$.

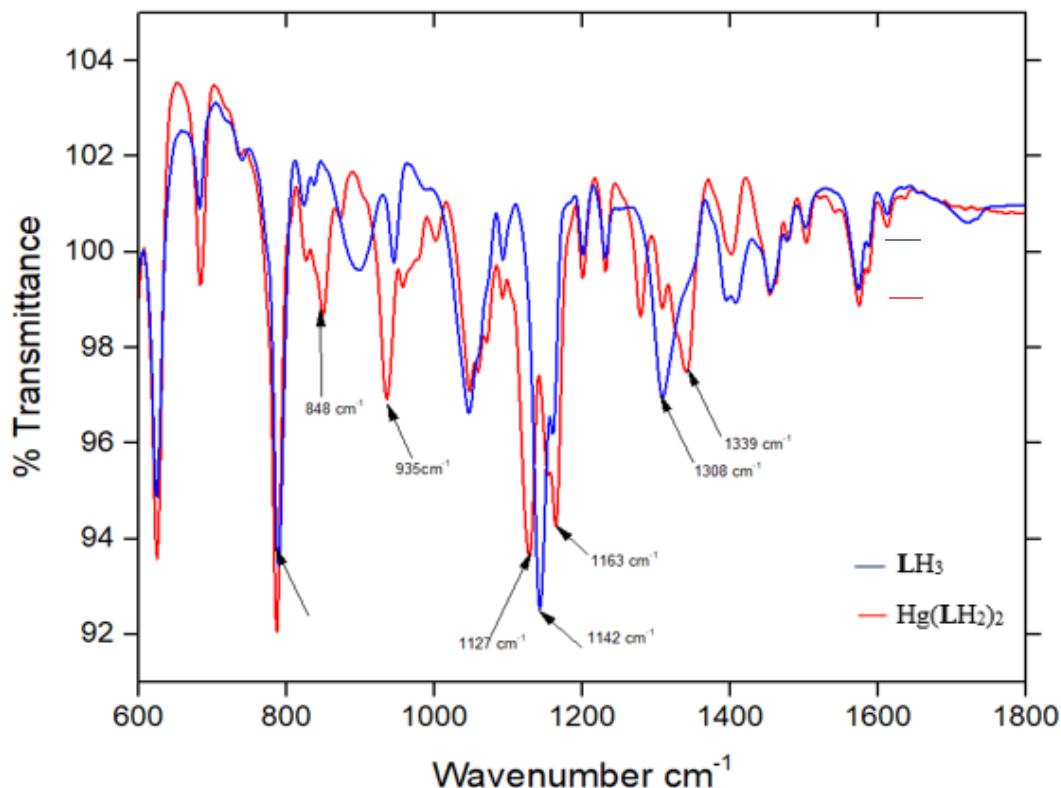


Figure 5.16. Overlay of the FT-IR spectra (crystals) of $[\text{Hg}(\text{L.H}_2)_2(\text{H}_2\text{O})]$ and LH_3

5.4 Conclusion

In conclusion, we have studied a fluorescence receptor LH_3 that possesses high selectivity for $\text{Hg}(\text{II})$, even in the presence of competing ions. The fluorescence of LH_3 was almost completely quenched by the addition of HgCl_2 or $\text{Hg}(\text{CH}_3\text{COO})_2$. The crystal structure of the complexes formed between LH_3 and $\text{Hg}(\text{CH}_3\text{COO})_2$ shows that one molecule of LH_3 binds three $\text{Hg}(\text{II})$ while the complexed obtained from LH_3 and HgCl_2 revealed that just one of the sulfonamide N-H in LH_3 was deprotonated and two molecules of LH_3 bind to one $\text{Hg}(\text{II})$.

5.5 Experimental

5.5.1 Materials and methods

All commercial reagents and solvents were purchased from Fisher Scientific or Sigma Aldrich and were used without further purification. 1,3,5-Tris(aminomethyl)-2,4,6-triethylbenzene was synthesized as previously reported.²⁶ ¹H and ¹³C-NMR spectra were recorded on a 400 MHz Bruker NMR spectrometer and were referenced, using the residual solvent resonances. All chemical shifts, δ , are reported in ppm. FT-IR spectra were recorded on a Agilent Technologies Cary 600 series FT-IR Spectrometer. Fluorescence spectra were recorded on a Agilent Technologies Cary Eclipse fluorescence spectrophotometer. X-ray diffraction data were collected from single crystals mounted atop a glass fiber with a Bruker AXS SMART 1K CCD area detector with graphite monochromated Mo K α radiation ($\lambda = 0.71073 \text{ \AA}$) using the program SMART-NT³ and processed by SAINT-NT.⁴ An empirical absorption correction was applied by the program SADABS. The structures were solved by intrinsic phase method and refined by full matrix least-squares methods on F².⁵ All non-hydrogen atoms were refined anisotropically, while H-atoms were placed in calculated positions with their thermal parameters riding on those of their C atoms.

5.5.2 ¹H-NMR Titrations of 1,3,5-Tris-(5-dimethylamino-1 naphthalenesulfonamido)methyl]-2,4,6-triethylbenzene with HgCl₂

The association constants for the formation of cation-receptor complexes were determined by titration of solution of $2 \times 10^{-3} \text{ M}$ of the ligand in DMSO-d₆ (solution A) with 0.1 M of HgCl₂ (solution B). Solution B was prepared by dilutions with solution A, thus keeping a constant concentration of LH₃ upon titration of solution A with solution B.

6.0 x 10⁻³ M trimethylamine was added into the stock solution A to deprotonate the ligand. In a typical experiment, solution A (0.700 ml) was placed in an NMR tube. Solution B was added in increments until a total of 950 µl was added. The changes of chemical shifts were monitored, with the results plotted and fitted to the 1:1 binding isotherm (Eq.1) using non-linear regression analysis:

$$\Delta\delta = \delta_{\text{obs}} - \delta_2 = ([\mathbf{R}]_t + [\mathbf{X}^-]_t + K_a^{-1} - ((([\mathbf{R}]_t + [\mathbf{X}^-]_t + K_a^{-1})^2 - 4[\mathbf{X}^-]_t [\mathbf{R}]_t)^{1/2})) \Delta\delta_{\text{max}} / (2[\mathbf{R}]_t)$$

(Eq.1)

5.5.4 Fluorescence Titration of 1 with HgCl₂ and Hg (CH₃COO)₂

Fluorescence emission was measured using an excitation wavelength of 350 nm for receptor LH₃, a measurement increment of 0.5 nm, and integration time of 0.1 s, excitation slit width of 10 nm, and emission slit width of 10 nm. 3 x 10⁻⁶ M trimethylamine was added into the stock solution of LH₃ to deprotonate the ligand when titrating with HgCl₂. Experiments were run using solutions of LH₃ (1.0 x 10⁻⁶ M) in CH₃OH (solution A) which were titrated with solutions of HgCl₂ or Hg(CH₃COO)₂ (5.0 x 10⁻⁴ M) and LH₃ (1.0 x 10⁻⁶ M) in CH₃OH (solution B). 2000 µL of solution A was added to the fluorescence cuvette and solution B was added in increments until a total of 1000 µL was added. The fluorescence intensity at λ_{max} of 522 nm was monitored.

5.5.5 Fluorescence Titration of LH₃ with CaCl₂, CdCl₂, CoCl₂, CuSO₄ and AgCl₂

Fluorescence emission was measured using an excitation wavelength of 350 nm for receptor LH₃, a measurement increment of 0.5 nm, and integration time of 0.1 s, excitation slit width of 10 nm, and emission slit width of 10 nm. 3 x 10⁻⁶ M trimethylamine was added into the stock solution of LH₃ to deprotonate the ligand when titrating with HgCl₂.

Experiments were run using solutions of LH_3 (1.0×10^{-6} M) in CH_3OH (solution A) which were titrated with solutions of Ca^{2+} , Cd^{2+} , Cu^{2+} , Ag^+ , and Zn^{2+} (5×10^{-4} M) and LH_3 (1.0×10^{-6} M) in CH_3OH (solution B). 2000 μL of solution A was added to the fluorescence cuvette and solution B was added in increments until a total of 1000 μL was added. The fluorescence intensity at λ_{max} of 522 nm was monitored.

5.5.6. Competitive Experiments

Fluorescence emission was measured using an excitation wavelength of 350 nm for receptor LH_3 , a measurement increment of 0.5 nm, and integration time of 0.1 s, excitation slit width of 10 nm, and emission slit width of 10 nm. Experiments were run using solutions of LH_3 (1.0×10^{-6} M), trimethylamine (3×10^{-6} M) and CaCl_2 or (Ag^+ , Co^{2+} , and Ca^{2+}) in CH_3OH (solution A) which were titrated with solutions B prepared from $\text{Hg}(\text{II})$ (5.0×10^{-4} M) dissolved in solution A. 2000 μL of solution A was added to the fluorescence cuvette and solution B was added in incrementally. The fluorescence intensity at λ_{max} of 522 nm was monitored.

5.5.7. FTIR complexation studies of LH_3 with $\text{Hg}(\text{CH}_3\text{COO})_2$ or HgCl_2

The FTIR of the crystal of ligand LH_3 and of the crystal of $\text{Hg}(\text{LH}_2)_2$ were collected using the Agilent Technologies Cary 600 series FTIR spectrometer.

5.5.8. Crystallographic data

Single yellow prism-shaped crystals of $\text{Hg}_3(\text{L})(\text{CH}_3\text{COO})_3$ were obtained by recrystallization from an acetone solution of LH_3 and $\text{Hg}(\text{CH}_3\text{COO})_2$, while colorless crystals of $[\text{Hg}(\text{LH}_2)_2(\text{H}_2\text{O})]$ were obtained by slow evaporation of a mixture of LH_3 ,

HgCl₂ and triethylamine in a EtOH solution of the compound. A suitable crystal of Hg₃(L)(CH₃COO)₃ (0.07×0.07×0.05) mm³ was selected and mounted on a Bruker D8 Quest CMOS diffractometer. The crystal was kept at $T = 150(2)$ K during data collection. Using **APEX3**²⁷, the structure was solved with the **ShelXT**²⁸ structure solution program, using the Intrinsic Phasing solution method. The model was refined with version 2016/6 of **ShelXL**²⁹ using Least Squares minimization embedded in Olex2.³⁰

Crystal Data. C₅₈H₇₀Hg₃N₆O₁₃S₃, $M_r = 1757.15$, triclinic, P-1 (No. 2), $a = 12.9492(7)$ Å, $b = 15.2503(8)$ Å, $c = 17.6699(10)$ Å, $\alpha = 71.328(2)^\circ$, $\beta = 73.826(2)^\circ$, $\gamma = 85.263(2)^\circ$, $V = 3174.9(3)$ Å³, $T = 150(2)$ K, $Z = 2$, $Z' = 1$, $\mu(\text{MoK}\alpha) = 7.399$, 58037 reflections measured, 13210 unique ($R_{int} = 0.1066$) which were used in all calculations. The final wR_2 was 0.1347 (all data) and R_I was 0.0634 ($I > 2(I)$).

Table 5.1. Crystallographic data for Hg₃(L)(CH₃COO)₃

Compound	Hg ₃ (L)(CH ₃ COO) ₃
Formula	C ₅₈ H ₇₀ Hg ₃ N ₆ O ₁₃ S ₃
$D_{calc.}/\text{g cm}^{-3}$	1.838
μ/mm^{-1}	7.399
Formula Weight	1757.15
Colour	yellow
Shape	prism
Size/mm ³	0.07×0.07×0.05
T/K	150(2)
Crystal System	triclinic
Space Group	P-1
$a/\text{Å}$	12.9492(7)
$b/\text{Å}$	15.2503(8)
$c/\text{Å}$	17.6699(10)
$\alpha/^\circ$	71.328(2)
$\beta/^\circ$	73.826(2)

$\gamma/^\circ$	85.263(2)
$V/\text{\AA}^3$	3174.9(3)
Z	2
Z'	1
Wavelength/ \AA	0.710760
Radiation type	MoK α
$\Theta_{min}/^\circ$	2.917
$\Theta_{max}/^\circ$	26.573
Measured Refl.	58037
Independent Refl.	13210
Reflections Used	7514
R_{int}	0.1066
Parameters	792
Restraints	96
Largest Peak	2.405
Deepest Hole	-2.009
Goof	1.015
wR_2 (all data)	0.1347
wR_2	0.1124
R_1 (all data)	0.1464
R_1	0.0634

Reflections:	d min (Mo) 0.79	I/σ 10.6	R_{int} 10.66%	complete 100%
Refinement:	Shift -0.001	Max Peak 2.4	Min Peak -2.0	Goof 1.015

Structure Quality Indicators

A yellow prism-shaped crystal with dimensions $0.07 \times 0.07 \times 0.05$ mm³ was mounted on X-ray diffraction data were collected using a Bruker D8 Quest CMOS diffractometer equipped with a Oxford Cryostream low-temperature device, operating at $T = 150(2)$ K. Data were measured using ϕ and ω scans of 0.50° per frame for 150.00 s using MoK α radiation (50 kV, 30 mA). The total number of runs and images was based on the strategy calculation from the program APEX3. The maximum resolution achieved was $\Theta = 26.573^\circ$.

Cell parameters were retrieved using the **SAINT** (Bruker, V8.37A, after 2013) software and refined using **SAINT** (Bruker, V8.37A, after 2013) on 9916 reflections, 17 % of the observed reflections. Data reduction was performed using the **SAINT** (Bruker, V8.37A, after 2013) software which corrects for Lorentz polarisation. The final completeness is 99.80% out to 26.573° in θ . A numerical absorption correction was performed using SADABS-2016/2 (Bruker,2016/2) was used for absorption correction. $wR_2(\text{int})$ was 0.0673 before and 0.0567 after correction. The ratio of minimum to maximum transmission is 0.8384. The $\lambda/2$ correction factor is not present. The absorption coefficient μ of this material is 7.399 mm^{-1} at this wavelength ($\lambda = 0.71073 \text{ \AA}$) and the minimum and maximum transmissions are 0.6609 and 0.7883. The structure was solved in the space group P-1 (# 2) by intrinsic phasing using the **ShelXT** (Sheldrick, 2015) structure solution program and refined by Least Squares using version 2016/6 of **ShelXL** (Sheldrick, 2015). All non-hydrogen atoms were refined anisotropically. Hydrogen atom positions were calculated geometrically and refined using the riding model. Exptl absorption process details: SADABS-2016/2 (Bruker,2016/2) was used for absorption correction. $wR_2(\text{int})$ was 0.0673 before and 0.0567 after correction. The Ratio of minimum to maximum transmission is 0.8384. The $\lambda/2$ correction factor is not present. There is a single molecule in the asymmetric unit, which is represented by the reported sum formula. In other words: Z is 2 and Z' is 1.

Table 5.2. Fractional Atomic Coordinates ($\times 10^4$) and Equivalent Isotropic Displacement Parameters ($\text{\AA}^2 \times 10^3$) for $\text{Hg}_3(\mathbf{L})(\text{CH}_3\text{COO})_3$. U_{eq} is defined as 1/3 of the trace of the orthogonalised U_{ij} .

Atom	x	y	z	U_{eq}
Hg1	2087.4(3)	4329.3(3)	4499.2(3)	32.78(13)
Hg2	4478.5(4)	4747.9(4)	1734.1(3)	48.38(16)
Hg3	5011.6(4)	1967.4(3)	4145.5(3)	47.22(16)
S1	-95(2)	3540.5(18)	5645.7(18)	38.5(8)
S2	3453(2)	5419(2)	273.4(19)	48.8(9)
S3	5467(2)	130(2)	3719.4(18)	46.1(9)
O1	336(7)	3898(5)	6161(5)	50(2)
O2	-926(6)	4073(5)	5310(5)	51(2)
O3	4032(7)	6193(6)	236(6)	74(3)
O4	3866(7)	4968(7)	-346(5)	74(3)
O5	6478(6)	326(6)	3826(5)	55(2)
O6	4835(6)	-624(5)	4349(5)	61(3)
O7	3522(8)	3085(6)	4839(7)	79(3)
O8	5199(7)	2792(6)	4823(6)	63(3)
O9	3229(6)	5362(5)	4100(5)	48(2)
O10	3063(7)	5314(7)	2918(5)	67(3)
O11	5457(9)	3404(7)	2761(7)	103(4)
O12	5703(7)	4897(6)	2210(5)	64(3)
N1	915(7)	3342(6)	4940(5)	34(2)
N2	3279(7)	4706(7)	1203(5)	40(2)
N3	4813(6)	1078(6)	3541(5)	40(3)
C1	1601(7)	2792(7)	3721(6)	23(2)
C2	2263(8)	2033(7)	3894(6)	27(2)
C3	3099(7)	1866(7)	3249(6)	28(3)
C4	3277(8)	2451(7)	2433(6)	33(3)
C5	2599(8)	3239(7)	2268(6)	26(2)
C6	1768(7)	3400(7)	2900(6)	24(2)
C7	638(8)	2926(7)	4386(6)	34(3)
C8	1051(8)	4231(7)	2715(6)	30(3)
C9	49(8)	4025(8)	2494(7)	42(3)
C10	2735(9)	3823(8)	1385(6)	39(3)
C11	4196(9)	2276(8)	1754(7)	42(3)
C12	3878(11)	1677(10)	1305(8)	73(5)
C13	3734(8)	965(7)	3437(7)	35(3)
C14	2077(8)	1366(7)	4775(6)	31(3)
C15	1318(9)	575(8)	4993(7)	42(3)
C16	-669(8)	2427(7)	6205(6)	33(3)
C17	-1699(9)	2284(8)	6228(6)	41(3)

Atom	x	y	z	U_{eq}
C18	-2215(9)	1421(8)	6666(7)	43(3)
C19	-1645(9)	716(8)	7042(7)	41(3)
C20	-563(8)	805(7)	7023(6)	32(3)
C21	-61(8)	1691(7)	6631(6)	31(3)
C22	981(8)	1803(7)	6683(7)	36(3)
C23	1484(9)	1065(8)	7096(7)	47(3)
C24	1017(9)	190(7)	7462(7)	44(3)
C25	8(9)	49(7)	7416(7)	40(3)
C28	2141(10)	5783(8)	179(7)	43(3)
C029	42(19)	7113(12)	1692(14)	100(7)
C29	1836(10)	5635(9)	-444(8)	52(3)
C30	820(13)	5942(9)	-577(9)	61(4)
C31	158(12)	6338(10)	-72(11)	72(5)
C32	415(11)	6506(8)	603(10)	57(4)
C33	1456(10)	6244(7)	704(7)	43(3)
C34	1757(12)	6451(8)	1350(8)	57(4)
C35	1031(17)	6882(10)	1825(10)	78(5)
C36	-270(18)	6926(12)	1137(14)	102(7)
C39	5719(8)	-158(8)	2795(7)	42(3)
C40	6328(8)	421(7)	2007(7)	33(3)
C41	6511(9)	127(8)	1304(8)	40(3)
C42	6033(11)	-720(9)	1399(9)	60(4)
C43	5466(10)	-1259(9)	2150(9)	55(4)
C44	5300(9)	-984(10)	2849(9)	63(4)
C45	6804(8)	1283(7)	1901(7)	34(3)
C46	7432(9)	1765(8)	1160(7)	42(3)
C47	7593(11)	1463(8)	493(8)	58(4)
C48	7126(10)	676(9)	529(8)	51(3)
C51	5938(11)	4105(12)	2642(9)	81(5)
C52	6868(13)	4101(14)	2995(12)	146(10)
C53	3437(10)	5671(8)	3306(9)	51(4)
C54	4139(12)	6518(9)	2887(9)	81(5)
C55	4311(13)	3184(9)	5036(10)	66(4)
C56	4288(14)	3777(11)	5587(12)	103(6)
O13	7230(8)	1870(8)	3898(6)	87(3)
C57	7597(11)	1926(11)	4562(9)	78(5)
N1_1	-490(8)	-853(6)	7755(7)	56(2)
C1_1	-66(11)	-1543(8)	8387(8)	67(3)
C2_1	-555(11)	-1243(8)	7119(8)	58(3)
N1_2	-1260(50)	7240(40)	850(30)	164(13)
C1_2	-1380(40)	8280(30)	820(30)	164(13)
C2_2	-1980(30)	6550(30)	1120(30)	167(13)
N1_3	-1360(50)	7160(50)	1180(30)	110(14)
C1_3	-2160(30)	7060(30)	1960(30)	109(15)

Atom	x	y	z	U_{eq}
C2_3	-1740(40)	7830(40)	590(30)	112(15)
N1_4	7287(12)	302(10)	-152(9)	94(3)
C1_4	6484(14)	627(12)	-564(11)	101(4)
C2_4	8350(14)	480(12)	-758(10)	99(4)

Table 5.3. Anisotropic Displacement Parameters ($\times 10^4$) $\text{Hg}_3(\text{L})(\text{CH}_3\text{COO})_3$. The anisotropic displacement factor exponent takes the form: $-2\pi^2[h^2a^{*2} \times U_{11} + \dots + 2hka^* \times b^* \times U_{12}]$

Atom	U_{11}	U_{22}	U_{33}	U_{23}	U_{13}	U_{12}
Hg1	35.4(3)	26.4(2)	31.7(3)	-2.39(19)	-7.6(2)	-5.77(19)
Hg2	34.3(3)	62.8(4)	30.8(3)	13.1(2)	-9.6(2)	-13.9(2)
Hg3	31.3(3)	46.2(3)	46.7(3)	17.0(2)	-18.0(2)	-5.5(2)
S1	43.7(18)	17.5(15)	37.5(17)	2.7(13)	2.6(14)	-0.6(13)
S2	34.0(17)	60(2)	30.7(18)	16.2(16)	-7.4(14)	-7.4(16)
S3	25.8(16)	47.5(19)	36.5(18)	18.9(14)	-3.7(13)	10.3(14)
O1	73(6)	23(4)	44(5)	-9(4)	1(5)	-11(4)
O2	48(5)	29(5)	49(5)	5(4)	5(4)	8(4)
O3	59(6)	70(7)	68(7)	27(5)	-30(5)	-24(5)
O4	57(6)	112(8)	26(5)	-1(5)	3(4)	11(6)
O5	30(4)	75(6)	41(5)	5(4)	-14(4)	18(4)
O6	38(5)	55(6)	45(5)	31(4)	-1(4)	9(4)
O7	73(7)	55(6)	147(10)	-44(6)	-79(7)	18(5)
O8	54(6)	49(6)	89(7)	-1(5)	-46(5)	-12(5)
O9	60(6)	35(5)	46(5)	-3(4)	-15(4)	-15(4)
O10	62(6)	83(7)	48(6)	-1(5)	-15(5)	-40(5)
O11	99(8)	75(7)	114(9)	58(7)	-83(7)	-47(7)
O12	56(6)	69(6)	55(6)	14(5)	-29(5)	-13(5)
N1	40(5)	25(5)	26(5)	2(4)	-2(4)	-2(4)
N2	29(5)	54(7)	24(5)	5(5)	-8(4)	-1(5)
N3	20(5)	49(6)	28(5)	16(4)	-5(4)	5(4)
C1	11(5)	28(6)	21(5)	3(5)	4(4)	-11(4)
C2	19(5)	23(6)	29(6)	5(5)	-5(5)	-9(4)
C3	17(5)	28(6)	29(6)	6(5)	-7(5)	5(5)
C4	21(6)	40(7)	26(6)	4(5)	-5(5)	-2(5)
C5	22(5)	22(6)	27(6)	3(5)	-8(5)	-3(4)
C6	12(5)	29(6)	27(6)	-4(5)	-4(4)	-2(4)
C7	40(7)	30(6)	24(6)	7(5)	-9(5)	-6(5)
C8	25(6)	39(7)	18(6)	-1(5)	-4(5)	-2(5)
C9	32(6)	55(8)	37(7)	-7(6)	-19(5)	15(6)
C10	33(6)	53(8)	24(6)	-3(6)	-8(5)	10(6)

Atom	U_{11}	U_{22}	U_{33}	U_{23}	U_{13}	U_{12}
C11	36(7)	52(8)	25(6)	-1(6)	-1(5)	13(6)
C12	79(11)	77(11)	52(9)	-18(8)	-9(8)	36(9)
C13	25(6)	33(7)	36(7)	3(5)	-9(5)	6(5)
C14	28(6)	20(6)	31(6)	6(5)	-1(5)	-5(5)
C15	36(7)	44(7)	33(7)	-2(6)	-1(5)	-2(6)
C16	32(6)	23(6)	31(6)	4(5)	-2(5)	0(5)
C17	40(7)	40(7)	26(6)	1(5)	0(5)	12(6)
C18	32(7)	33(7)	57(8)	0(6)	-18(6)	1(5)
C19	38(7)	27(6)	42(7)	4(5)	-4(6)	-7(5)
C20	26(6)	29(6)	29(6)	0(5)	4(5)	-6(5)
C21	29(6)	28(6)	24(6)	3(5)	1(5)	-11(5)
C22	32(6)	21(6)	47(7)	-2(5)	-5(6)	-5(5)
C23	39(7)	46(8)	52(8)	-11(7)	-12(6)	9(6)
C24	49(8)	19(6)	48(8)	10(5)	-16(6)	9(6)
C25	43(7)	30(7)	36(7)	2(5)	-6(6)	-4(6)
C28	52(8)	37(7)	30(7)	10(6)	-11(6)	-18(6)
C029	122(19)	49(11)	118(18)	-56(12)	14(15)	12(11)
C29	57(9)	53(8)	38(8)	4(6)	-16(7)	-20(7)
C30	82(11)	52(9)	61(10)	1(8)	-53(9)	-17(8)
C31	63(10)	44(9)	86(12)	20(8)	-34(10)	11(8)
C32	57(9)	27(7)	67(10)	15(7)	-21(8)	-2(7)
C33	66(9)	23(7)	26(7)	8(5)	-7(6)	-6(6)
C34	82(10)	37(8)	34(8)	8(6)	-8(8)	-7(7)
C35	120(15)	55(11)	50(10)	-15(8)	-13(11)	8(11)
C36	119(18)	47(11)	115(18)	-24(11)	-2(15)	30(11)
C39	9(5)	44(8)	48(8)	17(6)	-6(5)	6(5)
C40	18(5)	30(7)	42(7)	3(5)	-7(5)	-3(5)
C41	33(7)	26(7)	56(8)	-11(6)	-8(6)	-2(5)
C42	68(10)	44(8)	59(9)	-9(7)	-9(8)	-7(7)
C43	39(8)	30(7)	74(11)	1(7)	2(7)	-7(6)
C44	25(7)	57(10)	70(11)	14(8)	6(7)	4(7)
C45	28(6)	29(7)	39(7)	-8(5)	-3(5)	3(5)
C46	60(8)	37(7)	22(6)	-4(6)	-2(6)	-7(6)
C47	79(10)	38(8)	32(8)	13(6)	2(7)	-23(7)
C48	59(9)	46(8)	38(8)	-4(6)	1(6)	-20(7)
C51	63(10)	98(13)	59(10)	40(9)	-45(8)	-41(9)
C52	80(13)	156(18)	151(19)	78(15)	-79(13)	-66(12)
C53	42(8)	33(7)	67(10)	7(7)	-17(7)	-23(6)
C54	84(11)	62(10)	86(12)	-2(9)	-20(9)	-33(9)
C55	73(11)	32(8)	103(13)	-3(8)	-62(10)	4(8)
C56	107(14)	85(13)	145(17)	-32(13)	-87(14)	8(11)
O13	66(7)	122(10)	67(7)	-3(7)	-35(6)	-9(6)
C57	52(9)	89(12)	83(12)	-1(9)	-33(9)	4(8)
N1_1	65(5)	28(5)	68(6)	7(4)	-30(5)	-6(4)

Atom	U_{11}	U_{22}	U_{33}	U_{23}	U_{13}	U_{12}
C1_1	76(6)	36(6)	76(6)	13(5)	-33(5)	-3(5)
C2_1	65(6)	28(5)	72(6)	2(4)	-23(5)	-8(5)
N1_2	160(30)	160(20)	220(30)	-90(20)	-100(20)	107(19)
C1_2	160(30)	160(20)	220(30)	-100(20)	-100(20)	107(19)
C2_2	160(30)	160(20)	220(30)	-90(20)	-100(20)	105(19)
N1_3	80(20)	120(30)	80(20)	8(18)	6(15)	42(18)
C1_3	80(20)	120(30)	80(20)	7(18)	6(15)	43(18)
C2_3	80(20)	120(30)	80(20)	10(18)	6(15)	41(18)
N1_4	116(9)	93(7)	75(8)	-31(7)	-19(6)	-14(7)
C1_4	123(9)	104(8)	80(9)	-33(7)	-23(6)	-9(8)
C2_4	121(9)	94(8)	78(9)	-31(7)	-13(6)	-8(8)

Table 5.4. Bond Lengths in Å for Hg₃(L)(CH₃COO)₃.

Atom	Atom	Length/Å
Hg1	O7	2.593(8)
Hg1	O9	2.064(7)
Hg1	N1	2.036(8)
Hg1	C53	2.731(12)
Hg2	O12	2.049(8)
Hg2	N2	2.041(9)
Hg2	C51	2.735(12)
Hg3	O8	2.061(9)
Hg3	N3	2.045(10)
Hg3	C55	2.746(17)
S1	O1	1.445(8)
S1	O2	1.439(8)
S1	N1	1.620(9)
S1	C16	1.771(10)
S2	O3	1.425(9)
S2	O4	1.432(10)
S2	N2	1.619(9)
S2	C28	1.779(12)
S3	O5	1.441(8)
S3	O6	1.435(8)
S3	N3	1.602(9)
S3	C39	1.762(13)
O7	C55	1.202(14)
O8	C55	1.270(16)
O9	C53	1.284(15)
O10	C53	1.212(14)
O11	C51	1.212(16)

O12	C51	1.269(16)
N1	C7	1.456(13)
N2	C10	1.473(14)
N3	C13	1.490(12)
C1	C2	1.387(13)
C1	C6	1.417(13)
C1	C7	1.507(13)
C2	C3	1.410(14)
C2	C14	1.529(13)
C3	C4	1.397(13)
C3	C13	1.533(13)
C4	C5	1.429(13)
C4	C11	1.511(14)
C5	C6	1.389(13)
C5	C10	1.496(13)
C6	C8	1.511(13)
C8	C9	1.537(13)
C11	C12	1.530(17)
C14	C15	1.503(13)
C16	C17	1.356(14)
C16	C21	1.446(14)
C17	C18	1.408(14)
C18	C19	1.352(14)
C19	C20	1.408(14)
C20	C21	1.422(13)
C20	C25	1.411(14)
C21	C22	1.406(14)
C22	C23	1.357(14)
C23	C24	1.388(15)
C24	C25	1.369(15)
C25	N1_1	1.439(13)
C28	C29	1.354(16)
C28	C33	1.413(16)
C029	C35	1.36(2)
C029	C36	1.27(3)
C29	C30	1.417(18)
C30	C31	1.315(19)
C31	C32	1.43(2)
C32	C33	1.417(17)
C32	C36	1.38(2)
C33	C34	1.432(17)
C34	C35	1.354(19)
C36	N1_2	1.50(5)
C36	N1_3	1.41(7)
C39	C40	1.434(14)

C39	C44	1.378(17)
C40	C41	1.405(15)
C40	C45	1.434(14)
C41	C42	1.420(16)
C41	C48	1.406(15)
C42	C43	1.355(17)
C43	C44	1.385(18)
C45	C46	1.344(14)
C46	C47	1.357(16)
C47	C48	1.364(16)
C48	N1_4	1.448(17)
C51	C52	1.501(18)
C53	C54	1.500(16)
C55	C56	1.52(2)
O13	C57	1.411(15)
N1_1	C1_1	1.466(14)
N1_1	C2_1	1.453(15)
N1_2	C1_2	1.56(7)
N1_2	C2_2	1.34(7)
N1_3	C1_3	1.44(6)
N1_3	C2_3	1.38(8)
N1_4	C1_4	1.402(19)
N1_4	C2_4	1.473(19)

Table 5.5. Bond Angles in $^{\circ}$ for $\text{Hg}_3(\text{L})(\text{CH}_3\text{COO})_3$

Atom	Atom	Atom	Angle/ $^{\circ}$
O7	Hg1	C53	98.0(4)
O9	Hg1	O7	90.5(3)
O9	Hg1	C53	26.7(4)
N1	Hg1	O7	91.1(3)
N1	Hg1	O9	176.9(3)
N1	Hg1	C53	155.3(4)
O12	Hg2	C51	26.1(4)
N2	Hg2	O12	175.5(4)
N2	Hg2	C51	158.4(4)
O8	Hg3	C55	26.0(3)
N3	Hg3	O8	176.3(3)
N3	Hg3	C55	154.3(4)
O1	S1	N1	107.2(5)
O1	S1	C16	110.8(5)
O2	S1	O1	116.9(5)
O2	S1	N1	112.9(5)

Atom	Atom	Atom	Angle/°
O2	S1	C16	105.0(5)
N1	S1	C16	103.2(5)
O3	S2	O4	118.2(6)
O3	S2	N2	106.6(5)
O3	S2	C28	108.8(6)
O4	S2	N2	112.2(5)
O4	S2	C28	104.8(6)
N2	S2	C28	105.5(5)
O5	S3	N3	107.7(5)
O5	S3	C39	108.7(5)
O6	S3	O5	117.4(5)
O6	S3	N3	113.0(4)
O6	S3	C39	105.2(6)
N3	S3	C39	104.0(5)
C55	O7	Hg1	126.4(9)
C55	O8	Hg3	108.7(8)
C53	O9	Hg1	107.0(7)
C51	O12	Hg2	108.7(8)
S1	N1	Hg1	113.0(5)
C7	N1	Hg1	120.6(6)
C7	N1	S1	115.1(7)
S2	N2	Hg2	113.9(5)
C10	N2	Hg2	119.9(6)
C10	N2	S2	116.9(7)
S3	N3	Hg3	115.8(5)
C13	N3	Hg3	119.9(7)
C13	N3	S3	113.1(7)
C2	C1	C6	120.1(9)
C2	C1	C7	120.3(8)
C6	C1	C7	119.4(8)
C1	C2	C3	119.8(9)
C1	C2	C14	120.3(9)
C3	C2	C14	119.9(9)
C2	C3	C13	118.6(9)
C4	C3	C2	121.3(9)
C4	C3	C13	119.7(9)
C3	C4	C5	118.2(9)
C3	C4	C11	120.5(9)
C5	C4	C11	121.2(9)
C4	C5	C10	118.1(9)
C6	C5	C4	120.6(9)
C6	C5	C10	121.0(9)
C1	C6	C8	120.0(9)
C5	C6	C1	120.0(9)

Atom	Atom	Atom	Angle/°
C5	C6	C8	120.0(9)
N1	C7	C1	112.9(8)
C6	C8	C9	113.2(9)
N2	C10	C5	111.6(9)
C4	C11	C12	113.4(10)
N3	C13	C3	114.2(9)
C15	C14	C2	115.5(9)
C17	C16	S1	118.2(8)
C17	C16	C21	120.7(9)
C21	C16	S1	121.1(8)
C16	C17	C18	121.6(10)
C19	C18	C17	118.4(10)
C18	C19	C20	123.2(10)
C19	C20	C21	118.6(9)
C19	C20	C25	121.5(10)
C25	C20	C21	119.8(10)
C20	C21	C16	117.2(9)
C22	C21	C16	124.0(9)
C22	C21	C20	118.8(9)
C23	C22	C21	119.3(10)
C22	C23	C24	122.6(11)
C25	C24	C23	119.9(10)
C20	C25	N1_1	118.6(10)
C24	C25	C20	119.5(10)
C24	C25	N1_1	121.9(10)
C29	C28	S2	117.1(11)
C29	C28	C33	120.8(12)
C33	C28	S2	122.0(9)
C36	C029	C35	123(2)
C28	C29	C30	120.2(14)
C31	C30	C29	119.6(13)
C30	C31	C32	123.4(14)
C33	C32	C31	116.6(14)
C36	C32	C31	124.1(17)
C36	C32	C33	119.3(16)
C28	C33	C32	119.2(13)
C28	C33	C34	123.0(12)
C32	C33	C34	117.7(13)
C35	C34	C33	118.1(14)
C34	C35	C029	120.9(17)
C029	C36	C32	121(2)
C029	C36	N1_2	129(3)
C029	C36	N1_3	112(4)
C32	C36	N1_2	110(3)

Atom	Atom	Atom	Angle/°
C32	C36	N1_3	128(4)
C40	C39	S3	123.3(10)
C44	C39	S3	117.1(10)
C44	C39	C40	119.6(12)
C39	C40	C45	122.9(11)
C41	C40	C39	119.5(11)
C41	C40	C45	117.5(10)
C40	C41	C42	118.0(11)
C40	C41	C48	120.4(11)
C48	C41	C42	121.6(12)
C43	C42	C41	121.5(13)
C42	C43	C44	120.8(13)
C39	C44	C43	120.5(12)
C46	C45	C40	120.4(11)
C45	C46	C47	120.7(12)
C46	C47	C48	122.7(11)
C41	C48	N1_4	116.1(12)
C47	C48	C41	118.2(12)
C47	C48	N1_4	125.5(12)
O11	C51	Hg2	78.0(7)
O11	C51	O12	123.1(12)
O11	C51	C52	122.2(14)
O12	C51	Hg2	45.2(6)
O12	C51	C52	114.7(14)
C52	C51	Hg2	159.7(12)
O9	C53	Hg1	46.3(5)
O9	C53	C54	116.3(13)
O10	C53	Hg1	75.9(7)
O10	C53	O9	122.0(11)
O10	C53	C54	121.7(13)
C54	C53	Hg1	161.3(11)
O7	C55	Hg3	78.0(9)
O7	C55	O8	123.3(15)
O7	C55	C56	121.1(15)
O8	C55	Hg3	45.3(7)
O8	C55	C56	115.6(13)
C56	C55	Hg3	160.7(10)
C25	N1_1	C1_1	116.8(10)
C25	N1_1	C2_1	112.8(10)
C2_1	N1_1	C1_1	110.0(10)
C36	N1_2	C1_2	105(4)
C2_2	N1_2	C36	111(4)
C2_2	N1_2	C1_2	132(5)
C36	N1_3	C1_3	123(5)

Atom	Atom	Atom	Angle/°
C2_3	N1_3	C36	126(4)
C2_3	N1_3	C1_3	106(5)
C48	N1_4	C2_4	115.8(13)
C1_4	N1_4	C48	109.6(14)
C1_4	N1_4	C2_4	109.4(14)

Table 5.6. Hydrogen Fractional Atomic Coordinates ($\times 10^4$) and Equivalent Isotropic Displacement Parameters ($\text{\AA}^2 \times 10^3$) $\text{Hg}_3(\mathbf{L})(\text{CH}_3\text{COO})_3$. U_{eq} is defined as 1/3 of the trace of the orthogonalised U_{ij} .

Atom	x	y	z	U_{eq}
H7A	113.05	3326	4120.83	41
H7B	288.46	2318.33	4715.66	41
H8A	1470.61	4734.84	2246.98	36
H8B	819.51	4453.49	3204.51	36
H9A	259.66	3684.01	2089.62	63
H9B	-290.63	4607.96	2255.33	63
H9C	-461.34	3650.71	2995.8	63
H10A	3161.09	3479.2	1014.02	47
H10B	2019.99	3948.5	1274.19	47
H11A	4783.74	1966.33	1998.28	51
H11B	4476.82	2877.01	1345.05	51
H12A	4487.15	1634.81	842.87	110
H12B	3265.63	1957.93	1092.43	110
H12C	3677.28	1056.01	1692.8	110
H13A	3308.06	517.27	3950.09	42
H13B	3827.07	698.01	2979.69	42
H14A	2779.13	1108.64	4856.85	37
H14B	1794.82	1722.99	5168.71	37
H15A	1604.58	194.4	4628.38	63
H15B	614.46	817.86	4922.04	63
H15C	1238.83	196.07	5570.9	63
H17	-2081.44	2778.59	5942.48	49
H18	-2945.45	1336.43	6696.1	51
H19	-1990.82	132.54	7334.14	49
H22	1329.93	2389.75	6431.75	43
H23	2182.99	1149.92	7136.23	56
H24	1397.19	-310.13	7743.38	53
H029	-439.14	7427.82	2029.83	119
H29	2305.02	5324.28	-791.76	63
H30	618.16	5862.96	-1028.58	73
H31	-528.76	6521.61	-161.8	86

H34	2446.76	6290.94	1441.42	68
H35	1213.28	7026	2256.83	94
H42	6113.21	-912.53	925.23	72
H43	5177.96	-1833.78	2197.38	67
H44	4893.55	-1367.76	3370.03	75
H45	6675.49	1515.05	2358.22	41
H46	7765.68	2323.5	1102.14	51
H47	8050.58	1813.95	-20.69	69
H52A	7241.03	4699.88	2733.71	175
H52B	7367.11	3608.29	2888.65	175
H52C	6601.46	3991.1	3594.49	175
H54A	4078.91	6868.21	3275.49	97
H54B	3908.03	6905.95	2402.85	97
H54C	4887.6	6333.45	2709.08	97
H56A	4068.12	3396.07	6169.59	123
H56B	3774.81	4282.31	5484.2	123
H56C	5006.36	4036.3	5461.8	123
H13	7587.32	2237.47	3451.77	131
H57A	8376.56	1831.06	4441.19	94
H57B	7239.41	1448.49	5071.38	94
H57C	7431.45	2538.37	4632.92	94
H1A_1	647.24	-1739.29	8126.1	81
H1B_1	-551.65	-2080.08	8649.39	81
H1C_1	-10.77	-1271.07	8806.8	81
H2A_1	-777.26	-762.37	6673.8	69
H2B_1	-1083.1	-1750.18	7361.46	69
H2C_1	150.51	-1480.22	6892.03	69
H1A_2	-1517.56	8325.93	1376.33	197
H1B_2	-1984.95	8551.16	586.55	197
H1C_2	-718.43	8617.6	462.55	197
H2A_2	-1613.67	5995.45	1008.65	200
H2B_2	-2541.96	6729.39	829.29	200
H2C_2	-2297.93	6414.16	1717.27	200
H1A_3	-1954.35	6545.4	2394.06	130
H1B_3	-2854.88	6919.53	1906.94	130
H1C_3	-2199.8	7629.88	2100.6	130
H2A_3	-1864.76	8399.16	745.8	134
H2B_3	-2412.08	7614.56	560.61	134
H2C_3	-1205.34	7946.78	53.87	134
H1A_4	5783.01	575.98	-155.74	122
H1B_4	6476.51	255.38	-923.88	122
H1C_4	6629.5	1275.86	-899.78	122
H2A_4	8426.37	1142.38	-1067.23	119
H2B_4	8415.73	125.97	-1144.27	119
H2C_4	8913.53	291.92	-467.25	119

Table 5.7. Atomic occupancies for all atoms that are not fully occupied in $\text{Hg}_3(\text{L})(\text{CH}_3\text{COO})_3$

Atom	Occupancy
N1_2	0.61(3)
C1_2	0.61(3)
H1A_2	0.61(3)
H1B_2	0.61(3)
H1C_2	0.61(3)
C2_2	0.61(3)
H2A_2	0.61(3)
H2B_2	0.61(3)
H2C_2	0.61(3)
N1_3	0.39(3)
C1_3	0.39(3)
H1A_3	0.39(3)
H1B_3	0.39(3)
H1C_3	0.39(3)
C2_3	0.39(3)
H2A_3	0.39(3)
H2B_3	0.39(3)
H2C_3	0.39(3)

Table 5.8. Crystal data and structure refinement for [Hg(L.H₂)₂(H₂O)]

Identification code	[Hg(L.H ₂) ₂ (H ₂ O)]
Empirical formula	C ₅₁ H ₆₂ Hg _{0.5} N ₆ O _{7.5} S ₃
Formula weight	1075.54
Temperature/K	296.06
Crystal system	monoclinic
Space group	C2/c
a/Å	35.824(3)
b/Å	12.9928(9)
c/Å	23.3652(17)
α/°	90
β/°	105.892(2)
γ/°	90
Volume/Å ³	10459.8(13)
Z	8
ρ _{calc} /cm ³	1.366
μ/mm ⁻¹	1.658
F(000)	4464.0
Crystal size/mm ³	0.122 × 0.116 × 0.075
Radiation	MoKα (λ = 0.71076)
2θ range for data collection/°	6.106 to 53.018
Index ranges	-44 ≤ h ≤ 44, -16 ≤ k ≤ 16, -29 ≤ l ≤ 29
Reflections collected	68747
Independent reflections	10793 [R _{int} = 0.2651, R _{sigma} = 0.2443]
Data/restraints/parameters	10793/0/632
Goodness-of-fit on F ²	0.910
Final R indexes [I >= 2σ (I)]	R ₁ = 0.0795, wR ₂ = 0.1416
Final R indexes [all data]	R ₁ = 0.2226, wR ₂ = 0.1936
Largest diff. peak/hole / e Å ⁻³	0.72/-0.76

Table 5.9. Bond Lengths for [Hg(L.H₂)₂(H₂O)]

Atom	Atom	Length/Å	Atom	Atom	Length/Å
Hg1	N1 ¹	2.037 (6)	C7	C8	1.528 (11)
Hg1	N1	2.037 (6)	C8	C9	1.514 (12)
Hg1	O10A	2.66 (4)	C10	C11	1.536 (13)
S1	O1	1.427 (6)	C13	C14	1.517 (12)
S1	O2	1.425 (6)	C16	C17	1.350 (11)
S1	N1	1.588 (6)	C16	C27	1.379 (11)
S1	C16	1.798 (9)	C17	C18	1.393 (12)
S2	O3	1.424 (8)	C18	C19	1.325 (13)
S2	O4	1.430 (8)	C19	C20	1.441 (13)
S2	N2	1.606 (7)	C20	C21	1.425 (13)
S2	C28	1.750 (9)	C20	C27	1.434 (12)
S3	O5	1.418 (7)	C21	C22	1.370 (16)
S3	O6	1.430 (7)	C22	C23	1.393 (18)
S3	N3	1.601 (7)	C23	C24	1.379 (15)
S3	C40	1.762 (10)	C24	C27	1.431 (13)
N1	C1	1.477 (9)	C28	C29	1.385 (12)
N2	C12	1.456 (10)	C28	C37	1.421 (12)
N3	C15	1.457 (10)	C29	C30	1.393 (13)
N4	C21	1.409 (14)	C30	C31	1.342 (13)
N4	C25	1.439 (14)	C31	C32	1.425 (13)
N4	C26	1.449 (14)	C32	C33	1.448 (13)
N5	C33	1.380 (13)	C32	C37	1.433 (13)
N5	C38	1.465 (15)	C33	C34	1.368 (14)
N5	C39	1.436 (14)	C34	C35	1.385 (15)
N6	C49	1.426 (12)	C35	C36	1.347 (14)
N6	C50	1.446 (16)	C36	C37	1.393 (12)
N6	C51	1.468 (15)	C40	C41	1.365 (13)
C1	C2	1.506 (10)	C40	C45	1.435 (12)
C2	C3	1.400 (11)	C41	C42	1.432 (17)
C2	C7	1.408 (11)	C42	C43	1.325 (17)
C3	C4	1.399 (10)	C43	C44	1.401 (14)
C3	C10	1.502 (11)	C44	C45	1.428 (12)
C4	C5	1.394 (10)	C44	C49	1.439 (14)
C4	C12	1.507 (10)	C45	C46	1.391 (12)
C5	C6	1.412 (10)	C46	C47	1.357 (12)
C5	C13	1.519 (10)	C47	C48	1.391 (13)
C6	C7	1.390 (10)	C48	C49	1.339 (13)
C6	C15	1.499 (11)	O10	O10A	0.96 (10)

¹1-X,+Y,1/2-Z

Table 5.10. Bond Angles for [Hg(L.H₂)₂(H₂O)]

Atom	Atom	Atom	Angle/°	Atom	Atom	Atom	Angle/°
N1 ¹	Hg1	N1	174.1 (4)	C14	C13	C5	113.7 (7)
N1	Hg1	O10A	89.8 (9)	N3	C15	C6	108.9 (7)
N1 ¹	Hg1	O10A	95.7 (9)	C17	C16	S1	115.6 (7)
O1	S1	N1	112.6 (4)	C17	C16	C27	121.4 (9)
O1	S1	C16	104.2 (4)	C27	C16	S1	122.5 (8)
O2	S1	O1	116.1 (4)	C16	C17	C18	120.9 (9)
O2	S1	N1	107.1 (4)	C19	C18	C17	120.8 (10)
O2	S1	C16	112.7 (4)	C18	C19	C20	120.3 (9)
N1	S1	C16	103.5 (4)	C21	C20	C19	119.7 (10)
O3	S2	O4	119.2 (6)	C21	C20	C27	122.3 (10)
O3	S2	N2	109.5 (5)	C27	C20	C19	117.8 (8)
O3	S2	C28	106.4 (5)	N4	C21	C20	119.7 (12)
O4	S2	N2	105.3 (5)	C22	C21	N4	123.6 (12)
O4	S2	C28	108.6 (5)	C22	C21	C20	116.7 (12)
N2	S2	C28	107.3 (4)	C21	C22	C23	122.5 (12)
O5	S3	O6	119.8 (5)	C24	C23	C22	122.1 (13)
O5	S3	N3	107.0 (4)	C23	C24	C27	118.7 (12)
O5	S3	C40	109.9 (4)	C16	C27	C20	118.4 (9)
O6	S3	N3	106.9 (4)	C16	C27	C24	124.0 (10)
O6	S3	C40	105.7 (5)	C24	C27	C20	117.7 (9)
N3	S3	C40	106.8 (4)	C29	C28	S2	116.7 (8)
S1	N1	Hg1	119.8 (4)	C29	C28	C37	120.2 (9)
C1	N1	Hg1	119.3 (5)	C37	C28	S2	123.0 (7)
C1	N1	S1	116.1 (5)	C28	C29	C30	121.3 (10)
C12	N2	S2	122.8 (6)	C31	C30	C29	119.7 (10)
C15	N3	S3	121.9 (6)	C30	C31	C32	122.3 (10)
C21	N4	C25	116.0 (10)	C31	C32	C33	121.6 (10)
C21	N4	C26	115.9 (11)	C31	C32	C37	118.4 (9)
C25	N4	C26	112.1 (9)	C37	C32	C33	120.1 (10)
C33	N5	C38	113.9 (10)	N5	C33	C32	116.9 (11)
C33	N5	C39	114.7 (11)	C34	C33	N5	126.5 (11)
C39	N5	C38	111.8 (10)	C34	C33	C32	116.5 (10)
C49	N6	C50	113.9 (10)	C33	C34	C35	122.3 (11)
C49	N6	C51	114.7 (11)	C36	C35	C34	121.9 (11)
C50	N6	C51	112.5 (12)	C35	C36	C37	120.2 (11)
N1	C1	C2	109.6 (6)	C28	C37	C32	118.0 (9)
C3	C2	C1	118.4 (7)	C36	C37	C28	123.2 (10)
C3	C2	C7	120.5 (7)	C36	C37	C32	118.7 (10)

C7	C2	C1	121.0 (8)	C41	C40	S3	117.3 (8)
C2	C3	C10	119.5 (7)	C41	C40	C45	120.6 (10)
C4	C3	C2	119.1 (8)	C45	C40	S3	122.1 (7)
C4	C3	C10	121.4 (8)	C40	C41	C42	119.6 (11)
C3	C4	C12	119.3 (7)	C43	C42	C41	119.9 (11)
C5	C4	C3	120.8 (7)	C42	C43	C44	123.2 (12)
C5	C4	C12	119.7 (7)	C43	C44	C45	118.0 (11)
C4	C5	C6	119.8 (7)	C43	C44	C49	122.8 (11)
C4	C5	C13	120.8 (7)	C45	C44	C49	118.9 (9)
C6	C5	C13	119.4 (7)	C44	C45	C40	118.1 (9)
C5	C6	C15	120.3 (7)	C46	C45	C40	123.5 (9)
C7	C6	C5	119.8 (7)	C46	C45	C44	118.4 (9)
C7	C6	C15	119.8 (8)	C47	C46	C45	120.4 (8)
C2	C7	C8	120.5 (7)	C46	C47	C48	121.8 (9)
C6	C7	C2	119.9 (8)	C49	C48	C47	120.6 (10)
C6	C7	C8	119.6 (8)	N6	C49	C44	116.7 (11)
C9	C8	C7	113.5 (7)	C48	C49	N6	123.6 (11)
C3	C10	C11	113.0 (8)	C48	C49	C44	119.7 (9)
N2	C12	C4	108.5 (7)	O10	O10AHg1		85 (4)

5.6 References

- (1) Renzoni, A.; Zino, F.; Franchi, E. Mercury Levels along the Food Chain and Risk for Exposed Populations. *Environ. Res.* **1998**, *77*, 68-72.
- (2) Harris, H. H.; Pickering, I. J.; George, G. N. The Chemical Form of Mercury in Fish. *Science*, **2003**, *301*, 1203 LP-1203.
- (3) Tchounwou, P. B.; Yedjou, C. G.; Patlolla, A. K.; Sutton, D. J. Heavy Metals Toxicity and the Environment. *EXS* **2012**, *101*, 133-164.
- (4) Akagi, H.; Grandjean, P.; Takizawa, Y.; Weihe, P. Methylmercury Dose Estimation from Umbilical Cord Concentrations in Patients with Minamata Disease. *Environ. Res.* **1998**, *77*, 98-103.
- (5) Cavalleri, A.; Gobba, F. Reversible Color Vision Loss in Occupational Exposure to Metallic Mercury. *Environ. Res.* **1998**, *77*, 173-177.
- (6) Grandjean, P.; Weihe, P.; White, R. F.; Debes, F. Cognitive Performance of Children Prenatally Exposed to "Safe" Levels of Methylmercury. *Environ. Res.* **1998**, *77*, 165-172.
- (7) Henriksson, J.; Tjälve, H. Uptake of Inorganic Mercury in the Olfactory Bulbs via Olfactory Pathways in Rats. *Environ. Res.* **1998**, *77*, 130-140.

- (8) Mahaffey, K. R.; Mergler, D. Blood Levels of Total and Organic Mercury in Residents of the Upper St. Lawrence River Basin, Québec: Association with Age, Gender, and Fish Consumption. *Environ. Res.* **1998**, *77*, 104-114.
- (9) Shenker, B. J.; Guo, T. L.; Shapiro, I. M. Low-Level Methylmercury Exposure Causes Human T-Cells to Undergo Apoptosis: Evidence of Mitochondrial Dysfunction. *Environ. Res.* **1998**, *77*, 149-159.
- (10) Zhou, Y.; Ma, Z. Colorimetric Detection of Hg (II) by Au Nanoparticles Formed by H₂O₂ Reduction of HAuCl₄ Using Au Nanoclusters as the Catalyst. *Sensors Actuators B Chem.* **2017**, *241*, 1063-1068.
- (11) Tan, L.; Zhang, Y.; Qiang, H.; Li, Y.; Sun, J.; Hu, L.; Chen, Z. A Sensitive Hg(II) Colorimetric Sensor Based on Synergistic Catalytic Effect of Gold Nanoparticles and Hg. *Sensors Actuators B Chem.* **2016**, *229*, 686-691.
- (12) Zhao, Y.; Gui, L.; Chen, Z. Colorimetric Detection of Hg (II) Based on Target-Mediated Growth of Gold Nanoparticles. *Sensors Actuators B Chem.* **2017**, *241*, 262-267.
- (13) Tian, K.; Siegel, G.; Tiwari, A. A Simple and Selective Colorimetric Mercury (II) Sensing System Based on Chitosan Stabilized Gold Nanoparticles and 2,6-Pyridinedicarboxylic Acid. *Mater. Sci. Eng. C* **2017**, *71*, 195-199.
- (14) Che, Y.; Wu, D.; Deng, C.; Liu, L.; Jia, D. 5-Bromoindole-3-Carboxaldehyde Ethylthiosemicarbazone for Hg(II) Sensing and Removal. *Chem. Phys. Lett.* **2016**, *644*, 171-175.
- (15) Angupillai, S.; Hwang, J.-Y.; Lee, J.-Y.; Rao, B. A.; Son, Y.-A. Efficient Rhodamine-Thiosemicarbazide-Based Colorimetric/fluorescent “Turn-On” Chemodosimeters for the Detection of Hg(II) in Aqueous Samples. *Sensors Actuators B Chem.* **2015**, *214*, 101-110.
- (16) Song, K.; Mo, J.; Lu, C. Hg(II) Sensing Platforms with Improved Photostability: The Combination of Rhodamine Derived Chemosensors and up-Conversion Nanocrystals. *Spectrochim. Acta Part A Mol. Biomol. Spectrosc.* **2017**, *179*, 125-131.
- (17) Wan, D.; Li, Y.; Zhu, P. A Series of Emission “turn-On” Probes Derived from Rhodamine for Hg(II) Recognition and Sensing: Synthesis, Characterization and Performance. *Sensors Actuators B Chem.* **2015**, *221*, 1271-1278.
- (18) Nutiu, R.; Li, Y. Structure-Switching Signaling Aptamers. *J. Am. Chem. Soc.* **2003**, *125*, 4771.
- (19) Jun, W.; Kai, R.; Beijing, H. Synthesis and Sensing Behavior of Fluorescence “turn-On” Chemosensors Based on Rhodamine for Hg(II) Detection. *Sensors Actuators B Chem.* **2016**, *224*, 465-477.

- (20) Ramette, R. W.; Sandell, E. B. Rhodamine B Equilibria. *J. Am. Chem. Soc.* **1956**, *78*, 4872-4878.
- (21) Zhou, S.; Zhou, Z.-Q.; Zhao, X.-X.; Xiao, Y.-H.; Xi, G.; Liu, J.-T.; Zhao, B.-X. A Dansyl Based Fluorescence Chemosensor for Hg(II) and Its Application in the Complicated Environment Samples. *Spectrochim. Acta Part A Mol. Biomol. Spectrosc.* **2015**, *148*, 348-354.
- (22) Srivastava, P.; Ali, R.; Razi, S. S.; Shahid, M.; Patnaik, S.; Misra, A. A Simple Blue Fluorescent Probe to Detect Hg(II) in Semiaqueous Environment by Intramolecular Charge Transfer Mechanism. *Tetrahedron Lett.* **2013**, *54*, 3688-3693.
- (23) Wanichacheva, N.; Kumsorn, P.; Sangsuwan, R.; Kamkaew, A.; Lee, V. S.; Grudpan, K. A New Fluorescent Sensor Bearing Three Dansyl Fluorophores for Highly Sensitive and Selective Detection of Hg(II) Ions. *Tetrahedron Lett.* **2011**, *52*, 6133-6136.
- (24) Li, H.-W.; Wang, B.; Dang, Y.-Q.; Li, L.; Wu, Y. A Highly Selective Fluorescent Sensor for Mercury Ions in Aqueous Solution: Detection Based on Target-Induced Aggregation. *Sensors Actuators B Chem.* **2010**, *148*, 49-53.
- (25) Métivier, R.; Leray, I.; Valeur, B. Lead and Mercury Sensing by Calixarene-Based Fluoroionophores Bearing Two or Four Dansyl Fluorophores. *Chem.- A Eur. J.* **2004**, *10*, 4480-4490.
- (26) Kilway, K. V; Siegel, J. S. Control of Functional Group Proximity and Direction by Conformational Networks: Synthesis and Stereodynamics of Persubstituted Arenes. *Tetrahedron* **2001**, *57*, 3615-3627.
- (27) Software for the Integration of CCD Detector System Bruker Analytical X-ray Systems, Bruker axs, Madison, WI , 2013
- (28) Sheldrick, G.M., Crystal structure refinement with ShelXL, *Acta Cryst.*, **2015**, *C27*, 3-8.
- (29) Sheldrick, G.M., ShelXT-Integrated space-group and crystal-structure determination, *Acta Cryst.*, **2015**, *A71*, 3-8.
- (30) O. V. Dolomanov and L. J. Bourhis and R. J. Gildea and J. A. K. Howard and H. Puschmann, Olex 2: A complete structure solution, refinement and analysis program, *J. Appl. Cryst.*, **2009**, *42*, 339-341.

CHAPTER VI

General Conclusions

In this work we have showed the role of ion pairing on the binding and sensing selectivity for different species by tris-pyrazole and tris-dansyl ion receptors, derived from 1,3,5-triethylbenzene. In Chapter II, we reported two tris-pyrazole fluorescent sensors for NH_4^+ based on 1,3,5-triethylbenzene that show binding and sensing selectivity for NH_4^+ vs. K^+ . Non-linear regression analysis of the binding isotherms obtained gave a 1:1 association constant K_a of 74000 (\pm 900) M^{-1} for the formation of $\mathbf{1}\cdot\text{NH}_4^+$ and a K_a of 15 M^{-1} for the formation of $\mathbf{2}\cdot\text{NH}_4^+$ which is almost four orders of magnitude lower than those of the dimethyl analog $\mathbf{1}$. This difference in binding cannot be simply explained by electronic and steric effects, as the cavity of the tris(diphenyl)pyrazole can comfortably accommodate the NH_4^+ (unlike for $\mathbf{1}$) The role of ion pairing and solvation was revealed by X-ray and theoretical DFT studies. The X-ray structure of $\mathbf{2}\cdot\text{NH}_4^+$ and DFT calculations for $\mathbf{1}$, $\mathbf{2}$ and their corresponding NH_4^+ complexes provide consistent information related to the lack of ion pairing of NH_4^+ with the PF_6^- counteranion for $\mathbf{2}$.

In Chapter III, we demonstrated a unique dual-host extraction-based ion-pair sensing paradigm using Förster Resonance Energy Transfer (FRET), showing selectivity for NH_4NO_3 . The fluorescence emission of the NH_4^+ sensor tris-(3,5-dimethyl)pyrazole (305-340 nm), is compatible with the excitation wavelength of the dansyl fluorophore of the nitrate sensor 1,3,5-tris-(5-dimethylamino-1-naphthalenesulfonamido)methyl]-2,4,6-triethylbenzene, thus resulting in FRET emission upon combined use of these two sensors for the NH_4NO_3 ion pair. Contact

of dichloromethane solutions containing the two hosts with aqueous solutions of NH_4NO_3 (1.0×10^{-5} M to 1.0×10^{-4} M), resulted in FRET fluorescence enhancements at 510 nm, with increasing concentrations of NH_4NO_3 , while NaNO_3 , KNO_3 , NaCl and KCl showed only minimal fluorescence responses, under identical conditions. In Chapter IV, we exploited the ability of the tris-pyrazole to bind Ln(III) ions. Investigations of binding and sensing of different Ln(III) via fluorescence and $^1\text{H-NMR}$ showed the same dependence of fluorescence responses on pyrazole substitution patterns that had been observed for NH_4^+ , indicating the significant role of ion pairing for Ln(III) binding and fluorescence sensing. In Chapter V, the trisdansyl nitrate receptor LH_3 , was found to be an efficient Hg(II) fluorescent sensor. An X-ray crystal structure showed the ability of the trianionic version of this receptor to bind three Hg(II) atoms, also containing three CH_3COO^- counteranions. The X-ray crystal structure of the same receptor with HgCl_2 showed a 2:1 complexation pattern, with one Hg atom complexed by two bis-deprotonated receptor molecules.

APPENDIX A

Ammonium Fluorescence Sensing by 1,3,5-Tris(4-methyl-2-oxazolinylmethyl)-2,4,6-triethylbenzene (1)

Tosin M. Jonah and Konstantinos Kavallieratos

Department of Chemistry and Biochemistry and the Biomolecular Sciences Institute,
Florida International University, 11200 SW 8th St, Miami, FL 33199, USA.

A.1. Introduction

The design and synthesis of selective ammonium receptors and sensors is of biological and environmental importance. Synthetic receptors for NH_4^+ have found uses in measuring the urea and creatine levels and in environmental applications.¹⁻³ NH_4^+ over K^+ selectivity is always a challenge due to the similarity in ionic radii between these ions (286 vs. 266 pm for NH_4^+ vs K^+ , respectively). Several ammonium receptors have been reported⁴⁻⁷ that bind to ammonium via hydrogen bonding, including derivatives of crown ethers and nonactin.⁸ A highly sensitive and selective cage-type NH_4^+ receptor based on cation- π interaction and hydrogen bonding.^{9,14} This receptor is comparable to nonactin in terms of selectivity and sensitivity. Tripodal oxazolines have been shown to bind ammonium through hydrogen bonding and cation- π interactions.^{9,10} These include a trimethyl oxazoline analog derived from 1,3,5-trimethylbenzene^{8,12,13} that showed selective fluorescence response at the 305-340 nm range ($\lambda_{\text{exc}} = 272$ nm), for ammonium over K^+ , Na^+ , and Mg^{2+} .

Herein, we report a new oxazoline (**1**) receptor, based on the 1,3,5-triethylbenzene framework. The tris-oxazoline **1**, is selective for NH_4^+ over K^+ . The binding constants by NMR titrations reveal remarkable binding strength and selectivity for NH_4^+ over K^+ for **1**.

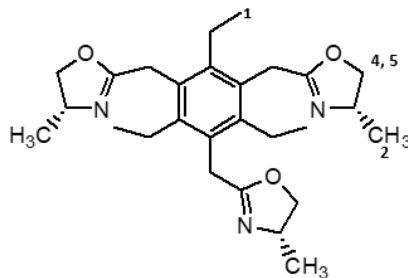
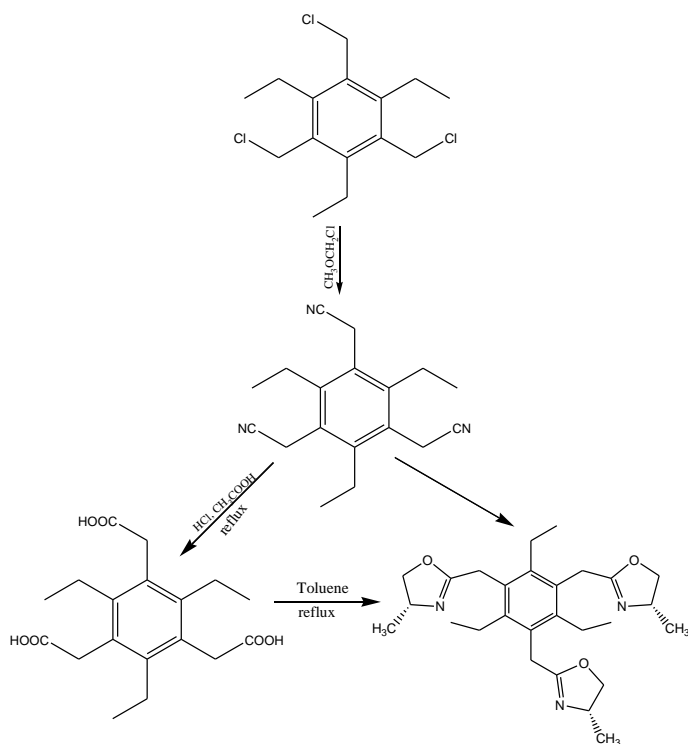


Figure A.1. Chemical structure of receptor **1**

A.2 Results and Discussion

Compound **1** was prepared by modifications of previously reported methods.^{11,15} Fluorescence titrations of receptors with NH_4PF_6 at constant receptor concentration (1.0×10^{-4} M) were carried out in CH_3OH for **1** (1:1) for **2** and **3** ($\lambda_{\text{exc}} = 272$ nm). The results for tris-oxazoline **1** were comparable to the trimethyl analog reported in the literature with increase in fluorescence higher for NH_4^+ vs. K^+ and Na^+ .¹³ The tris-(oxazoline) ammonium sensor **1** was prepared in good yields using modified versions of reported⁸ procedures for the trimethylbenzene analog (Scheme 1).



Scheme A. 1: Synthetic scheme for preparation of tris-(oxazoline) ammonium sensor **1**.

Fluorescence titrations of **1** with $\text{NH}_4^+\text{PF}_6^-$ and K^+PF_6^- were carried out. Emission was measured using an excitation wavelength of 272 nm. The fluorescence intensity increased gradually with increase in the amount of NH_4^+ added (Figure A.2 and A.3) while a decrease in fluorescence intensity (quenching) was observed when **1** was titrated with K^+PF_6^- (figure A.4).

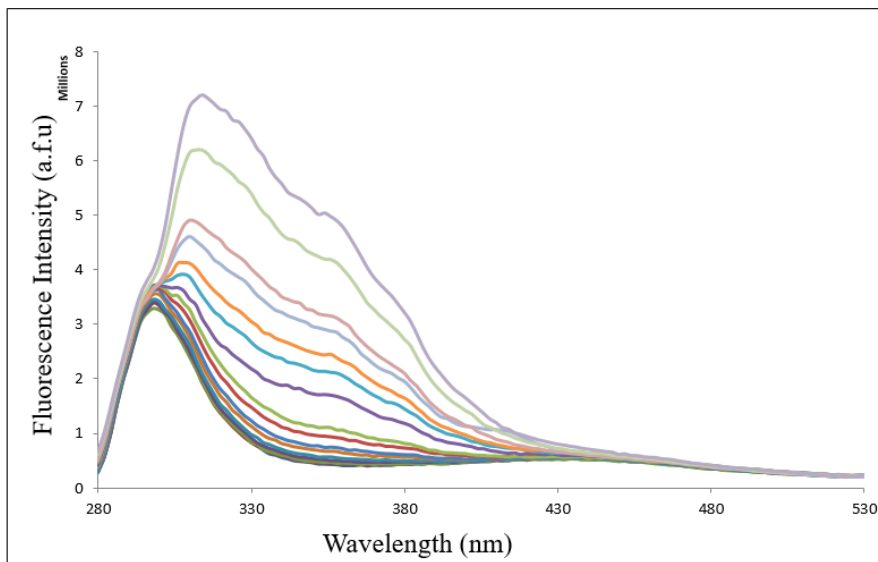


Figure A.2: Fluorescence Titration of **1** with $\text{NH}_4^+\text{PF}_6^-$ in CD_3OD ($\lambda_{\text{exc}} = 272 \text{ nm}$).

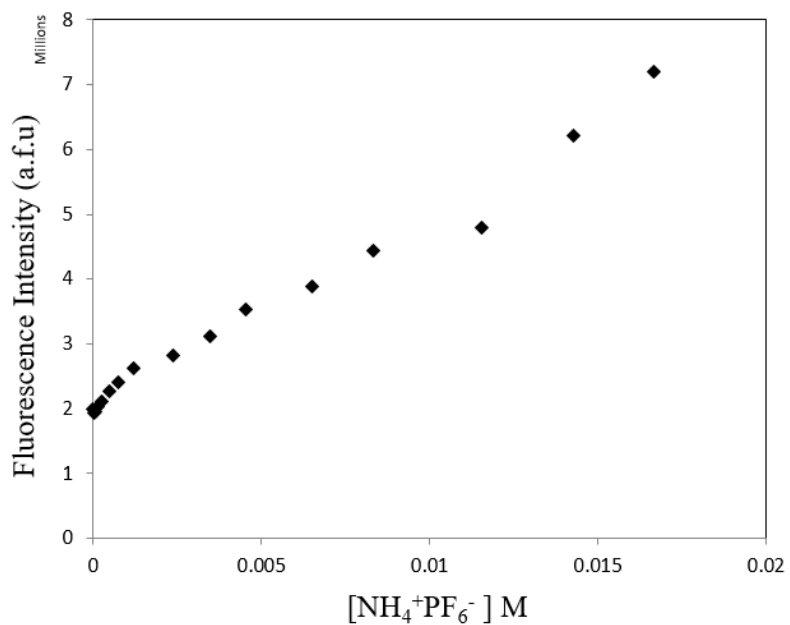


Figure A.3: Fluorescence Titration curve of **1** with $\text{NH}_4^+\text{PF}_6^-$ ($\lambda_{\text{exc}} = 272 \text{ nm}$)

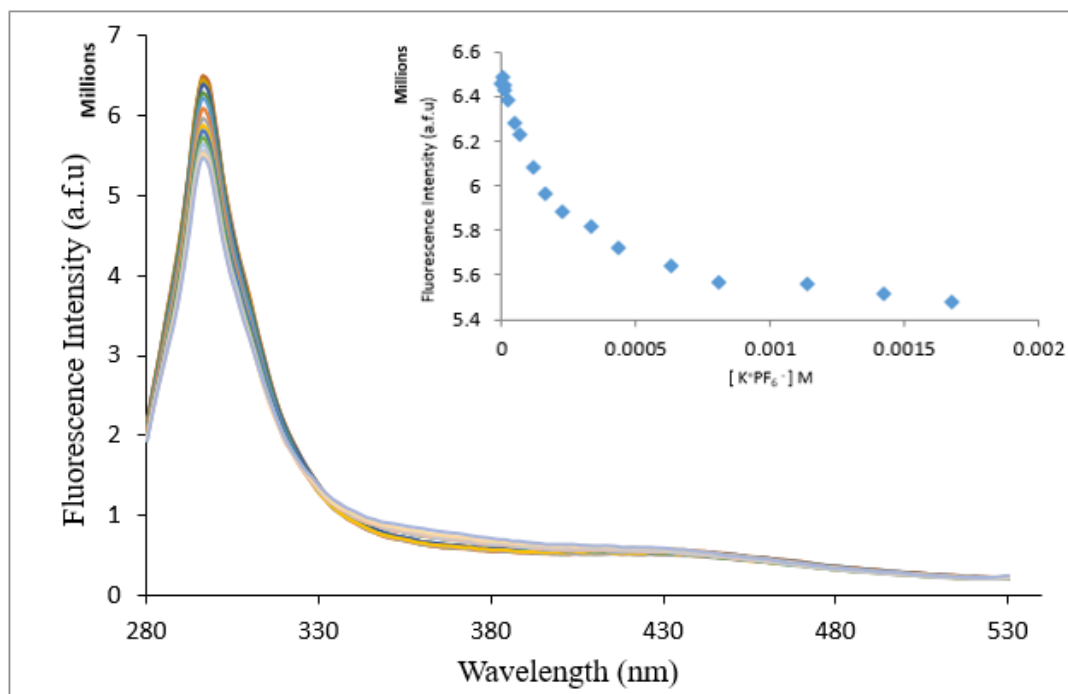


Figure A.4: Fluorescence titration curve of **1** with K^+PF_6^- ($\lambda_{\text{exc}} = 272 \text{ nm}$).

The NH_4^+ binding properties of receptor **1** were investigated by ^1H -NMR titrations in CD_3OD by with $\text{NH}_4^+\text{PF}_6^-$. Downfield shifts of the oxazolinyl proton resonance were observed, indicating cation binding via hydrogen bonding (Figure A.5). The electron cloud above and below the plane of the ring circulates in reaction to the external field so as to generate an opposing field at the center of the ring and a supporting field at the edge of the ring. Regions in which the induced field supports or adds to the external field are said to be deshielded, because a slightly weaker external field will bring about resonance for nuclei in such areas. While regions in which the induced field opposes the external field are termed shielded because an increase in the applied field is needed for resonance.

The benzylic CH₃ and CH₂ also showed some slight observable upfield shifts. This upfield shield seen in the benzylic CH₃ and CH₂ may be because the cation- π interactions disturb the delocalization of the benzene π electrons which subsequently results to a decrease in their deshielding effects. Association constants for the formation of 1:1 complexes, K_a , were determined by non-linear regression analysis using the 1:1 binding isotherm (Eq. 1), to be 737 M⁻¹ for **1**.NH₄⁺ while a K_a of 72 M⁻¹ was obtained for **1**.K⁺. The continuous variation method (Job Plot) by ¹H-NMR gave a 1:1 binding stoichiometry for **1**.NH₄⁺ (Figure A.7).

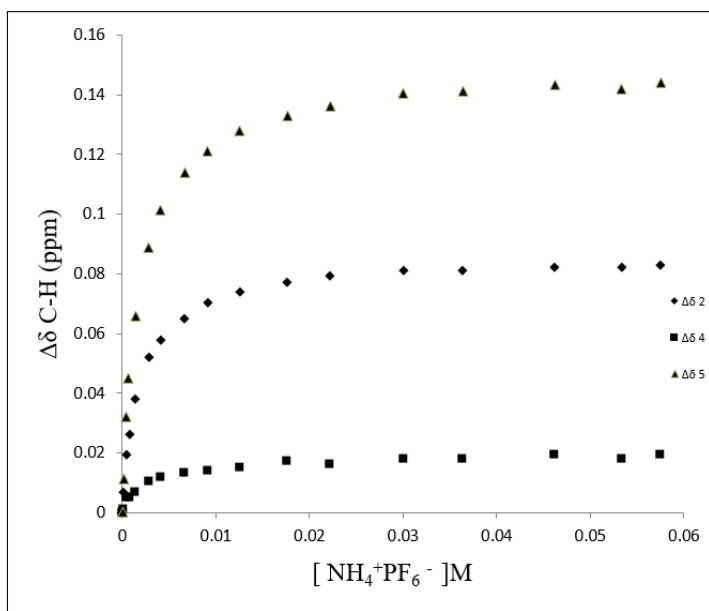


Figure A.5. ¹H-NMR titration plot of **1** with NH₄⁺PF₆⁻ in CD₃OD. The concentration of **1** was kept constant at 2 mM.

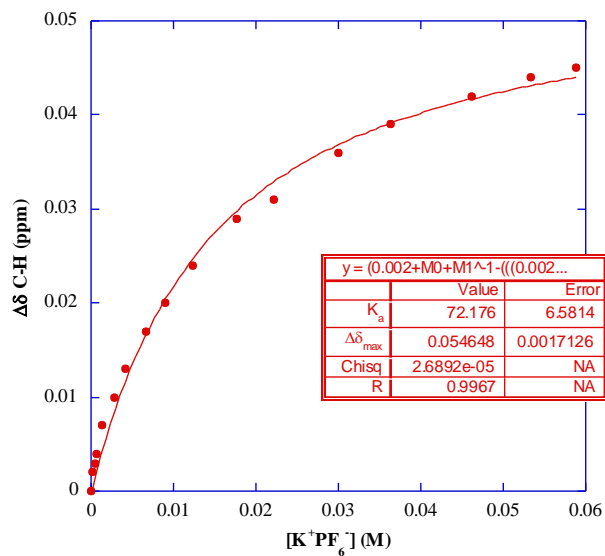


Figure A.6. ^1H -NMR titration plot of **1** with K^+PF_6^- in CD_3OD . The concentration of **1** was kept constant at 2 mM.

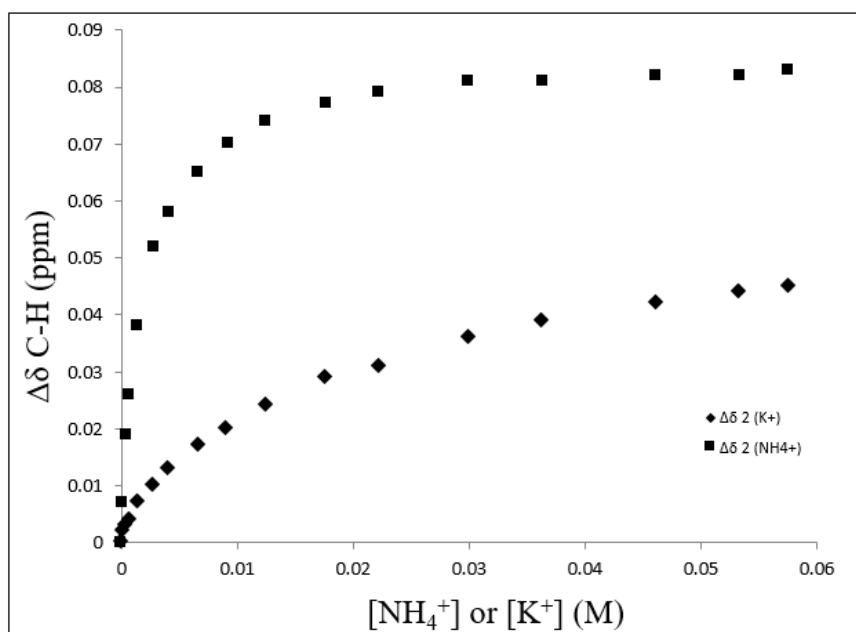


Figure A.7. ^1H -NMR titration plot showing the binding of NH_4^+ over K^+ by **1** in CD_3OD

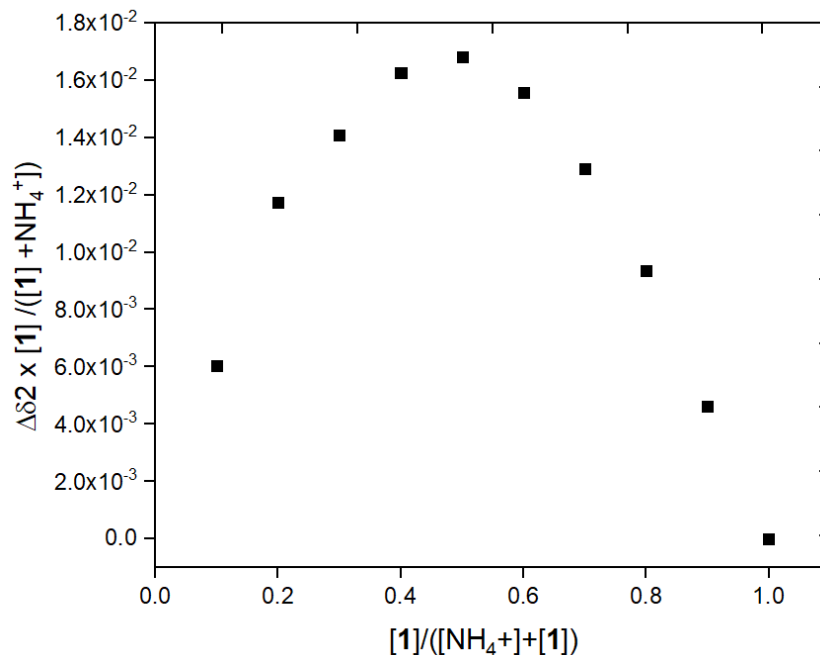


Figure A.8. Job plot of **1** with $\text{NH}_4^+\text{PF}_6^-$ in CD_3OD . 0.002 M Stock solutions of **1** and $\text{NH}_4^+\text{PF}_6^-$ were used.

In an effort to obtain single crystals of the complex between 1,3,5-Tris(4-methyl-2-oxazolinylmethyl)-2,4,6-triethylbenzene (**1**) and NH_4PF_6 , we instead obtained **RGR534_a**, a doubly deprotonated 2,4,6-triethylbenzene-1,3,5-triacetic acid bound to an ammonium cation at the carboxylate end and a protonated alaninol (protonated at the amine nitrogen), forming two H-bonds to the carboxylate oxygen atoms (Figure A.9). The triacetic acid is doubly deprotonated to compensate the two positive charges imposed by the ammonium and alaninol. The strong interaction between the cations and the acid is indicated by the numerous strong H-bonds as shown in table A1. The ammonium cation is also bound by a cation- π interaction, (N-H... π -centroid 3.150(6) Å) (Figure A.9)

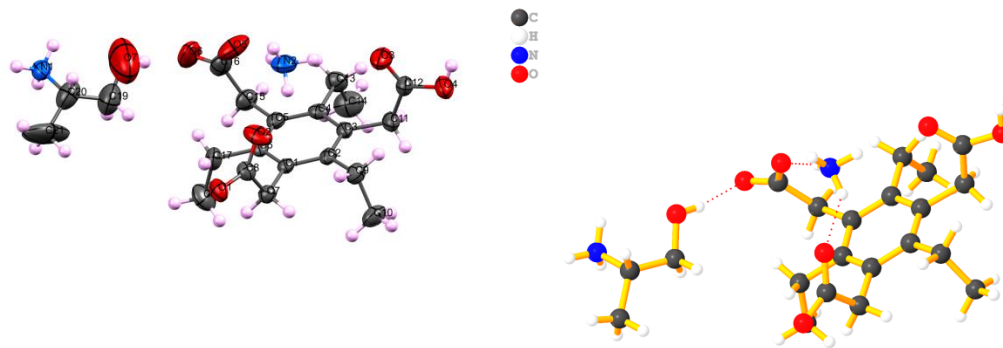


Figure A.9: 50% probability ORTEP Thermoellipsoid (left) and PLATO (right) representation of the crystal structure of 2,4,6-triethylbenzene-1,3,5-triacetic acid, with NH_4^+ and alaninol, showing the NH_4^+ binding to tricarboxylic acid interactions via H-bonding and cation- π interactions.

As it can be seen in Figure A.10, a supramolecular network of alternate hydrophilic and hydrophobic layers is formed through a series of hydrogen bonds, cation- π interactions and hydrophobic interactions.

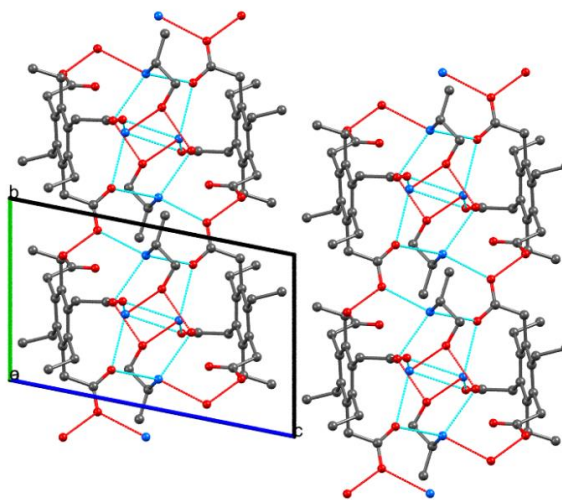


Figure A.10: Packing diagram of the crystal structure of the alaninol/ NH_4^+ /2,4,6-triethylbenzene-1,3,5-triacetic acid, showing alternate layers of hydrophilic H-bonding networks and organic networks stabilized by hydrophobic interactions and crystal packing

Table A.1: Hydrogen Bond information for **RGR534_a**.

Compound	RGR534_a
Formula	C ₂₁ H ₃₆ N ₂ O ₇
<i>D</i> _{calc.} / g cm ⁻³	1.239
μ /mm ⁻¹	0.092
Formula Weight	428.52
Color	colorless
Shape	plate
Size/mm ³	0.14×0.12×0.02
<i>T</i> /K	298(2)
Crystal System	triclinic
Space Group	P-1
<i>a</i> /Å	9.4528(5)
<i>b</i> /Å	9.9700(6)
<i>c</i> /Å	14.0679(8)
α /°	99.453(2)
β /°	90.982(2)
γ /°	117.938(2)
<i>V</i> /Å ³	1148.64(11)
<i>Z</i>	2
<i>Z</i> '	1
Wavelength/Å	0.710760
Radiation type	MoK α
θ _{min} /°	2.953
θ _{max} /°	26.421
Measured Refl.	25721
Independent Refl.	4710
Reflections Used	2751
<i>R</i> _{int}	0.0592
Parameters	294
Restraints	1
Largest Peak	0.689
Deepest Hole	-0.465
Goof	1.038
<i>wR</i> ₂ (all data)	0.2844
<i>wR</i> ₂	0.2494
<i>R</i> ₁ (all data)	0.1753
<i>R</i> ₁	0.1081

D	H	A	d(D-H)/Å	d(H-A)/Å	d(D-A)/Å	D-H-A/deg
O4	H4	O1 ¹	0.82	1.80	2.594(5)	163.4
N2	H2A	O2	0.91(8)	2.08(7)	2.839(7)	140(6)
N2	H2D	O5	0.81(2)	2.02(2)	2.823(9)	172(7)
N1	H1C	O1 ²	0.89	1.911	2.747(5)	155.7
N1	H1B	O1 ³	0.889	2.013	2.827(7)	

A.3. EXPERIMENTAL SECTION

A.3.1. Material and Methods

All materials (purchased from Aldrich Chemical Co., ACROS Organics, or Alfa Aesar) were standard reagent grade and were used without further purification. ¹H and ¹³C NMR spectra were recorded on a 400 Bruker NMR spectrometer and were referenced, using the residual solvent resonances. All chemical shifts, δ , are reported in ppm.

A.3.2. Synthesis of 1,3,5- Tris (4-methyl-2- oxazolinylmethyl)-2,4,6 triethylbenzene.(1)

380 mg of 2,4,6-triethylbenzene-1,3,5-triacetic acid was dissolved in 40 mL of anhydrous toluene and the system was purged with nitrogen and solution heated to reflux. After 5mins, a solution of 240 mg of alaninol in 5 mL toluene was added. The solution was left to reflux for 48h. After 48 h, the reaction was allowed to cool and the solvent was evaporated to give a cream colored solid (0.49g, 1.1 mmol, 40%). ¹H NMR (CH₃OD) δ , 1.13 (9H, t, $J=7.6$ Hz), 1.16 (9H, d), 2.59 (6H, q, $J=7.6$ Hz), 3.73 (1H, m), 3.45 (3H, d), 3.56 (3H, d), 3.66 (3H, s).

A.3.3. Fluorescence Spectroscopy

The fluorescence emission was measured using an excitation wavelength of 272 nm, a measurement increment of 0.5 nm, and integration time of 0.1 s, excitation slit width

of 10 nm and emission slit width of 5 nm. Experiments were run using solutions of (5×10^{-5} M) in CH₃OH/CH₂Cl₂ 1:10 (solution A) which were titrated with solutions of NH₄⁺PF₆⁻ (5×10^{-3} M) and (5×10^{-5} M) in CH₃OH/CH₂Cl₂ 1:10 (solution B). In a typical experiment, 2.5 mL of solution A was added to the fluorescence cuvette and solution B was added in increments until a total of 1000 μL was added. The fluorescence intensity at 298 nm was monitored and recorded. The same procedure was repeated for K⁺PF₆⁻ and Na⁺PF₆⁻.

A.3.4. ¹H-NMR Titrations of **1** with NH₄⁺PF₆⁻ and K⁺PF₆⁻.

The association constants for the formation of cation-receptor complexes were determined by titration of solutions of **1** (2×10^{-3} M) in CD₃OD (solution A) with 1×10^{-1} M of NH₄⁺PF₆⁻ (solution B). Solution B was prepared by dilutions with solution A, thus keeping a constant concentration of **1** upon titration of solution A with solution B. In a typical experiment, solution A (0.700 mL) was placed in an NMR tube. Solution B was added in increments until a total of 950 μL was added. The chemical shift changes were monitored, with the results plotted and fitted to the 1:1 binding isotherm (Eq.1) using non-linear regression analysis:

$$\Delta\delta = \delta_{\text{obs}} - \delta_2 = ([\mathbf{R}]_t + [\mathbf{X}^-]_t + K_a^{-1} - ((([\mathbf{R}]_t + [\mathbf{X}^-]_t + K_a^{-1})^2 - 4[\mathbf{X}^-]_t [\mathbf{R}]_t)^{1/2}))\Delta\delta_{\text{max}} / (2[\mathbf{R}]_t) \quad (\text{Eq.1})$$

A.3.5. Continuous Variation Method (Jobs plots):

Stock solutions of the receptors **1** (0.002 M) and NH₄⁺PF₆⁻ (0.002 M) in CD₃OD were prepared. Ten NMR tubes were filled with 500 μl solutions of the host and guest in the following volume ratios (in μl).500:0, 450:50, 400:100, 350:150, 300:200, 250:250, 200:300,150:350, 100:400, 50:450. ¹H-NMR spectra were recorded and jobs plot was obtained

by plotting $\frac{[L]}{[NH_4^+] + [L]}$ against $\frac{[L]}{[NH_4^+] + [L]}$ (where **L** is receptor **1**). Jobs plot curve maxima at mol. fraction of 0.5 were observed for host:guest indicating a 1:1 complex stoichiometry.

A.4. Conclusion

We have synthesized 1,3,5-Tris(4-methyl-2-oxazolinylmethyl)-2,4,6-triethylbenzene (**1**) that is selective for NH_4^+ over K^+ . The binding constants by NMR titrations reveal remarkable binding strength and selectivity for NH_4^+ over K^+ for **1**.

A.5. References

1. Munshi, M. K.; Gade S. M.; Rane V. H. ; Kelkar A. A. : *RSC Advances*, **2014**, *4*, 32127-32133.
2. Bianchi, A; Browman-James, K; Garcia-Espania, E. *Supramolecular Chemistry of Anions*, Wiley, New York, **1997**.
3. Evans, N. H.; Rahman, H.; Davis, J. J.; Beer, P. D. *Anal. Bioanal. Chem.* **2012**, *402*, 1739 -1748.
4. Cafeo, G.; Gattuso, G.; Kohnke, F. H.; Notti, A.; Occhipinti, S.; Pappalardo, S.; Parisi, M. F *Angew. Chem. Int. Ed.* **2002**, *41*, 2122-2126.
5. Mc Connell, A.J.; Beer, P.D. *Angew. Chem. Int. Ed.*, **2012**, *51*, 5050-5061.
6. Kim, S. K.; Sessler, J. L. *Chem. Soc. Rev.* **2010**, *39*, 3784-3809.
7. Cort, A. D. *Supramolecular chemistry: From Molecules to Nanomaterials*, Wiley, New York, **2012**.
8. Ahn, K.H., Kim, S.G., Jung, J., Kim, K.H., Kim, J., Chin, J., & Kim, K. *Chem. Lett.*, **2000**, *29*, 170-171.
9. Wanichacheva, N., Kumsorn, P., Sangsuwan, R., Kamkaew, A., Lee, V. S., & Grudpan, K. *Tetrahedron. Lett.*, **2011**, *52*, 6133-6136.
10. Bhatt, K. D., Gupte, H. S., Makwana, B. A., Vyas, D. J., Maity, D., & Jain, V. K. *J. Fluoresc.*, **2012**, *22*, 1493-1500.
11. Currie, R. Spectroscopic, Electrochemical and Mass Spectrometric Investigation of

Anion Binding by Tripodal Molecular Receptors. Florida International University, 2005.

12. Currie, R., Pau A., Espetia O. D., and Kavallieratos K., Anion Binding Properties and Extraction effects of Fluorescent Dansylamide Receptors derived from Tris(2-aminoethyl)amine and 1,3,5-Tris(aminomethyl)-2,4,6-triethylbenzene. *Manuscript in preparation.*
13. Caygill, J. S., et. al., Current Trends in Explosive Detection Techniques. *Talanta* **2012**, 15.

VITA

TOSIN MOBOLAJI JONAH

Born in Ile-Ife, Nigeria

- Fall 2008 B.S. in Biochemistry
Ladoke Akintola University, Ogbomosho, Oyo State, Nigeria.
- Fall 2016 M.Sc. in Forensic Science
Florida International University, Miami, FL, USA
- Fall 2017 PhD Candidate (expected graduation Dec 2017)
Florida International University, Miami, FL, USA
Dissertation title: SELECTIVE SENSING OF IONS AND ION
PAIRS OF ENVIRONMENTAL AND FORENSIC
SIGNIFICANCE
Advisor: Konstantinos Kavallieratos, Ph.D.
- 2016 Doctoral Acquisition Award
Florida International University, Miami, FL

PUBLICATIONS AND PRESENTATIONS

Tosin M. Jonah, Logesh Mathivathanan, Raphael G. Raptis, Konstantinos Kavallieratos. Remarkably Selective NH_4^+ Binding and Fluorescence Sensing by Tripodal Tris(pyrazolyl) Receptors Derived from 1,3,5-Triethylbenzene; Structural and Theoretical Insights on the Role of Ion Pairing, *New Journal of Chemistry*, **2017**, *41*, 14835-14838.

Konstantinos Kavallieratos, Evgen V. Govor, Megan Twomey, Vasileios A. Anagnostopoulos, Tosin M. Jonah, Alexander N. Morozov, Alexander M. Mebel, Raphael G. Raptis: Tripodal Sulfonamide and Pyrazolyl Ligands for Extraction and Sensing of Lanthanides and Actinides. Proceedings of GLOBAL 2017 September 24-29, 2017 – Seoul (Korea).

Tosin M. Jonah, Logesh Mathivathanan, Shambhu Kandel, Raphael G. Raptis, Konstantinos Kavallieratos: Tripodal pyrazole ligands and analogs for selective ammonium and actinide extraction and sensing. 253rd ACS National Meeting & Exposition, San Francisco, California, April, 2017.

Tosin M. Jonah; Richild Currie; Konstantinos Kavallieratos: Towards selective ion-pair sensing based on anion and cation complexation and co-extraction: Dual-host combinations of fluorescent sensors for ammonium and nitrate. 251st ACS National Meeting & Exposition, San Diego, California, March, 2016.

Konstantinos Kavallieratos, Evgen V. Govor, Tosin M. Jonah, Shambhu Kandel, Raphael G. Raptis: Tripodal Sulfonamides and Pyrazoles for An(III) Coordination and Extraction. Separation Science and Technology Conference, Gatlinburg, TN, October, 2016

Tosin M. Jonah; Cynthia Cortes; Richild Currie; Konstantinos Kavallieratos: Dual-host combinations of fluorescent sensors for ammonium and nitrate based on anion and cation complexation and co-extraction for selective ion-pair sensing. Florida Annual Meeting and Exposition, May, 2016.

Jessica S. Duchene; Amanda M. Howett; Tosin M. Jonah; Konstantinos Kavallieratos; Towards a dual-host approach for sensing of ammonium nitrate and other explosive salts: Intermolecular interactions between the dansyl fluorophore and anions lead to fluorescence enhancements. 247th National spring meeting of American Chemical Society, Vol, 247, 2014